Design and Development of Optical and Electrical Transducers based on π-Conjugated Polymers

A thesis submitted by

Nehal Zehra

Roll No. 166122044

to

Indian Institute of Technology Guwahati

for the award of the degree of

Doctor of Philosophy

Department of Chemistry
Indian Institute of Technology Guwahati
Guwahati - 781039
India

October-2022

Dedicated To My Family

INDIAN INSTITUTE OF TECHNOLOGY GUWAHATI
Department of Chemistry

STATEMENT

I do hereby declare that the work contained in the thesis entitled **"Design and Development of Optical and Electrical Transducers based on π-Conjugated Polymers"** is the result of investigations carried out by me in the Department of Chemistry, Indian Institute of Technology Guwahati, Guwahati, Assam India under the supervision of Prof. Parameswar Krishnan Iyer, Professor, Department of Chemistry, Indian Institute of Technology Guwahati, Guwahati, Assam, India. This work has not been submitted elsewhere for the award of any degree.

Nehal Zehra

October, 2022 **Nehal Zehra**

IIT Guwahati

INDIAN INSTITUTE OF TECHNOLOGY GUWAHATI
Department of Chemistry

CERTIFICATE

This is to certify that the work contained in the thesis entitled **"Design and Development of Optical and Electrical Transducers based on π-Conjugated Polymers"** by **Nehal Zehra**, a Ph.D. student of Department of Chemistry, Indian Institute of Technology Guwahati, for the award of degree of Doctor of Philosophy has been carried out under my supervision and this work has not been submitted elsewhere for any degree.

October, 2022
Guwahati

Prof. Parameswar Krishnan Iyer
Thesis Supervisor
Department of Chemistry
Indian Institute of Technology Guwahati
Guwahati – 781039
Assam, India.

Acknowledgements

First and foremost, I am grateful to Almighty Allah for the countless bounties he has showered on me, which have enabled me to write the closing note of my research journey. Completion of my thesis work is not possible without the endless support and motivation of several people who have played an integral role throughout my intellectual journey. Words fall short of expressing how thankful I am to those people around me who made this thesis possible.

I am incredibly grateful to my thesis supervisor, Prof. Parameswar Krishnan Iyer for his expert guidance, scholarly inputs, and prudent suggestions during my research work. His approach to transforming serendipitous observations into new possibilities has always encouraged me to keep pursuing my research interest and has always served as a beacon for me in the future. I earnestly thank him for his expert supervision, consistent encouragement, and inspiration in this academic journey and life in general.

I offer my sincere gratitude to my doctoral committee members, Prof. Bhisma Kumar Patel, Prof. Siddhartha Sankar Ghosh, and Dr. Uttam Manna, for periodically evaluating my work and providing insightful suggestions and comments that incited me a lot to improve my research work. I express my sincere thanks to Prof. Siddhartha Sankar Ghosh for providing an opportunity to work in an interdisciplinary area through collaboration and for his valuable suggestions and advice, which further engaged me to widen my research perspectives.

I am grateful to all faculty members of the Department of Chemistry, IIT Guwahati for their help and encouragement and also the non-teaching staff of the Department for their technical support. I am thankful to the Central Instruments Facility (CIF), IIT Guwahati for various characterization facilities.

I gratefully acknowledge all my teachers at AMU, especially Prof. Anees Ahmad, Prof. Mehtab Parveen, Prof. Zeba N. Siddiqui**,** Dr. Zain Khan. Mr. Wasi-ur-rahman, Dr. Md. Musawwer Khan, Dr. Shahab Ali Asghar Nami, and Dr. Anamika Gupta for their excellent teachings, proper guidance, and treasurable advices, which undoubtedly greatly influence my decision to pursue doctoral research.

I convey my special thanks to Sameer Hussain, Akhtar Hussain Malik, and Anamika Kalita for their support, continuing encouragement, crucial advices, and assistance in my thesis

work. I am fortunate to have such wonderful seniors who always stepped up to assist when needed.

It is a pleasure to convey my heartfelt thanks to all my dear labmates Sameer Bhai, Akhtar Bhai, Adil Bhai, Radha Bhai, Anamika Kalita Di, Bhim Bhai, Suresh Bhai, Niranjan Bhai, Ramesh Bhai, Priyanka Di, Himani Di Subrata Bhai, Maimur Bhai, Muzaffer Bhai, Anamika Dey Di, Ekta Di, Ashish Bhai, Dipjyoti Bhai, Arvin Bhai, Sayan Bhai, Gopi Bhai, Rahul Bhai, Raman Bhai, Nystha, Indrani, Ravinder, Rithesh, Debasish, Retwik, Anita, Tapashi, Kavita, Debika, Raj, Priyam, Mayur, Sushant, Geetmani Bhai, Nasima, Biki, Tamal, Somulaya, Hirak, Sayantani, Anwesha, Paromita, Himangshu, Ramkrishna, Deepak for providing a friendly environment in the lab and making the journey memorable. I always found discussions and suggestions with them to be insightful.

I am grateful to my friends from AMU and IITG Sayfa, Zeba, Ruhena, Sana, Farha, Anjali, Jinat, Sana Ghaffar, Akhtar Alam, Simra, Musfica, Hani, Deepanjalee Di, Anita, Elina Di, Ishani Di, Zainab Api, Nusrat Api, for providing moral support and for being with me in thick and thin of my life. I will always cherish the wonderful moments we had together.

Finally, my PhD endeavour could not be completed without the everlasting love, unconditional support, tolerance, and blessings of my family. I would like to express my sincere gratitude with great honour to my family members who gave me lots of love, strength, kind support and blessings which made me to complete this journey. I am fortunate and blessed enough to have such caring and supportive parents Mr Kamal Haider Zaidi and Mrs. Iqbal Zehra, it is because of their prayers, sacrifice and struggle that I am able to live my dream to pursue doctoral research from IIT Guwahati, a renowned institute. I am grateful to my younger sister Misbahuz Zehra for her eternal love, cooperation and emotional support which are immensely needed throughout this journey.

Finally, once again I would like to thank Almighty Allah, for continuously showering his blessings and for providing me a talented supervisor cum mentor, a loving and supporting family, and amazing friends who have helped me to complete my research journey.

Nehal Zehra

Synopsis

The content of this synopsis report entitled **"Design and Development of Optical and Electrical Transducers based on π-Conjugated Polymers"** is divided into five chapters. Chapter 1 gives a brief introduction about the respective research area where the scope and significance of the subsequent chapters are discussed. Chapter 2 describes the synthesis of cationic conjugated polyelectrolyte PFBT-MI which is applied for ratiometric detection and wash-free imaging of bacteria, and explored its antibacterial applications. Chapter 3 discusses the synthesis of an amine-functionalized conjugated polymer PFPDA and its application in the detection of lethal nerve agent vapor by developing a low-cost electrical sensor. Chapter 3 also highlights the development of an electronic model for rapid onsite detection of nerve agent mimic vapor by bright visual alerts from a light-emitting diode (LED) and a loud alarm signal. Chapter 4 discusses the synthesis of anionic conjugated polyelectrolyte PFPS for rapid and point-of-care testing of the neurotransmitter serotonin in physiological conditions using a smartphone-based system. Chapter 5 describes the synthesis of AIEE active conjugated polyelectrolyte PFTT-D and its application in the detection of multicolor artificial food dyes in solution.

Chapter 1: Introduction

Conjugated Polymers (CPs) have attained immense popularity after the discovery of making insulating plastics into electrically conductive by three eminent scientists Hideki Shirakawa, Alan MacDiarmid, and Alan Heeger in 1977, which led to the Noble Prize in Chemistry twenty-three years later. Since then, the revolutionary applications of π-conjugated polymers have been witnessed in cross-disciplinary areas of material, chemical, and biological science. Specifically, these materials combine the light-harvesting features with semiconducting properties, making them useful for the development of various optoelectronic devices such as polymer solar cells, organic field-effect transistors (OFETs), plastics lasers, light-emitting electrochemical cells (LECs). Moreover, they appeared as the most promising materials in the field of sensing due to their high sensitivity, low detection limits, superior optical and electrical properties, facile solution processibility, and room temperature operation. The extended delocalized electronic structure of CPs allows efficient exciton or charge carrier transport which endorses them with remarkable photoluminescence efficiency, good electrical conductivity, and ultra-sensitivity compared with small molecule probes. CP-based sensors with signal amplification features can be implemented into a variety of transduction schemes depending on the need or requirement. CP with diverse type of backbone structures have been extensively explored; the most

prominent type includes poly(p-phenylene) (PPP), poly(p-phenylene vinylene) (PPV), polythiophene (PT), polyfluorene (PF), polypyrrole (PPy), poly(para-phenylene ethynylene) (PPE), etc. **(Figure 1)**. The incorporation of functional groups at the side chain of the CP backbone imparts solubility in a high dielectric solvent such as water while tuning the chemical interaction with the analyte of interest.

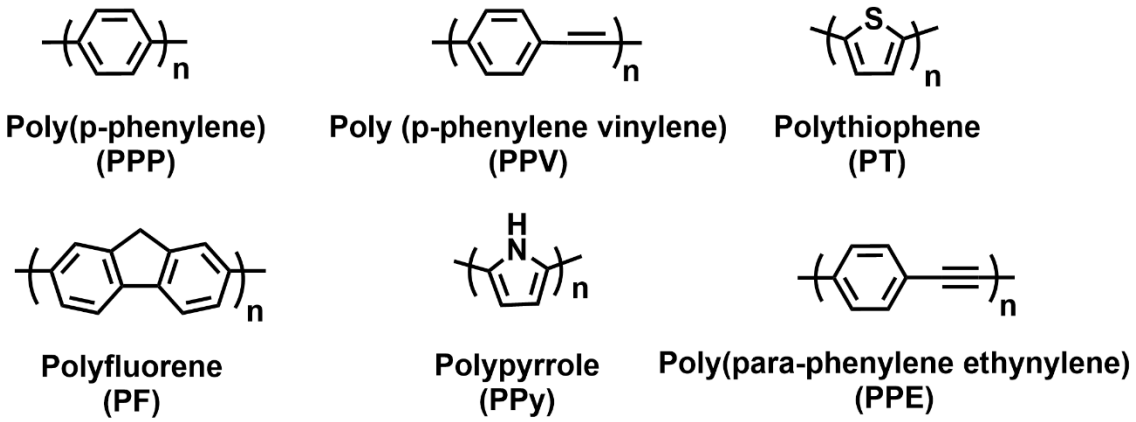

Figure 1. Structures of some well-known conjugated polymer systems.

CP as Transducer

CP-based sensors can be categorized into two main groups i.e., optical and electrical sensors. In optical transduction, the signal generation is related to the transfer of excitons (excited state) to electron acceptor/low energy sites in solution or interpolymer chain exciton transport in the aggregate or solid-state resulting change in the fluorescence property of CP. On the other hand, CP based electrical sensor is based on variations in electrical modulations of CP film during analyte receptor interaction. The change in electrical properties of CP could be brought about by various factors such as physical adsorption of analyte molecule (or swelling of CP film), partial charge transfer between analyte molecule and polymer, intermolecular interaction (dipole-charge or dipole-dipole), and chemical doping, etc. Generally, the non-covalent reciprocity between the CP and target analyte brings them close enough to each other to produce a change in the transduction signal. This can be achieved by tailoring the molecular structure of CP based on the chemical nature of the analyte of interest.

CP-based sensors are superior over small molecule probes in terms of sensitivity, selectivity, detection limit, stability, and room temperature operation. One of the most fascinating features of CP-based sensors that has attracted significant attention is their ability to transduce recognition events into amplified signals. The signal amplification

characteristics of CP are the result of the collective response of several conjugated units. When an analyte molecule binds to the receptor attached to a small molecule probe, the conducting property of a single molecule is affected. However, in the case of CP, the conducting properties of the entire backbone or several absorbing units are collectively affected by a single binding event of analyte molecule to receptor resulting in the amplified response. This signal amplification process was termed the "Molecular wire effect" by Swager and co-workers in 1995. This could be understood by considering CP as a 1-dimensional wire which allows exciton or charge carrier to migrate along the conjugated backbone, however, in case of a binding event, small perturbation at a single receptor is interrogated to multiple conjugated units by exciton or charge carrier resulting in the amplified signal response **(Figure 2)**.

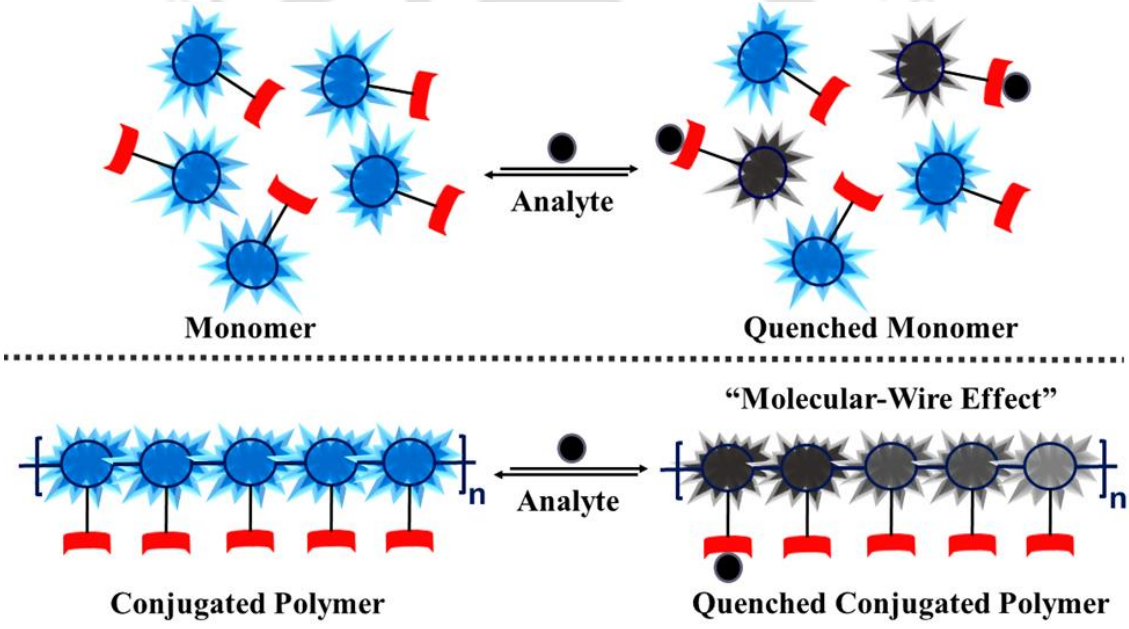

Figure 2. Pictorial representation of fluorescence quenching in monomer and polymer by analyte molecules.

Applications of conjugate polymers as sensors

In recent years CPs with different conjugated structures and side-chain functionalities have been tremendously explored as sensory materials for various chemical and biological species such as metal ions, explosives, small biomolecules, proteins, DNA, etc. CP-based sensors are implemented into a variety of signal transduction such as fluorometric sensors, colorimetric, conductometric, potentiometric, and amperometric sensors, etc. Due to amplified response, the CP-based sensor device exhibits a low detection limit in the range of ppb to ppt level. The enthralling properties such as transport of charge, rate of energy

migration, and electrical conductivity make the CPs, very attractive for chemo and bio-sensing applications.

Chapter 2: Fluorescence Resonance Energy Transfer-Based Wash-Free Imaging and Antibacterial Application Using a Cationic Conjugated Polyelectrolyte

Chapter 2 discusses the synthesis of a water-soluble cationic conjugated polyelectrolyte [9,9-bis(6′-methylimidazoliumbromide)hexyl)-fluorene-co-4,7-(2,1,3benzothiadiazole)] (PFBTMI) that displays dual emission in solution and aggregate state due to intermolecular FRET (**Figure 3**). The pendant cationic imidazolium group is strategically attached to the PFBT polymer backbone to impart water solubility as well as to bind with negatively charged bacterial membranes via electrostatic and hydrophobic interactions. The PFBT-MI undergo intermolecular FRET with substantial color change from blue to yellow under UV light upon binding with negatively charged bacterial membrane allowing very convenient detection as well as wash-free imaging of bacteria. Moreover, the antibacterial activity of PFBT-MI is explored against *S. aureus* and *E. coli*, as a representative of Gram-positive and Gram-negative bacteria with a minimum inhibitory concentration (MIC) and minimum bactericidal concentration (MBC) value of (23.7 μg/mL) and (47.7 μg/mL) for *S. aureus* and *E. coli* (47.7 μg/mL) and (79 μg/mL), respectively. The antibacterial activity of PFBT-MI is attributed to the membrane disintegration of bacterial cells and thereby leakage of intracellular components as revealed by FESEM analysis as well as protein and nucleic acid leakage studies (**Figure 4**). Besides, antibacterial activity the PFBT-MI shows less cytotoxicity against mammalian cells and thus it holds great potential for biomedical applications.

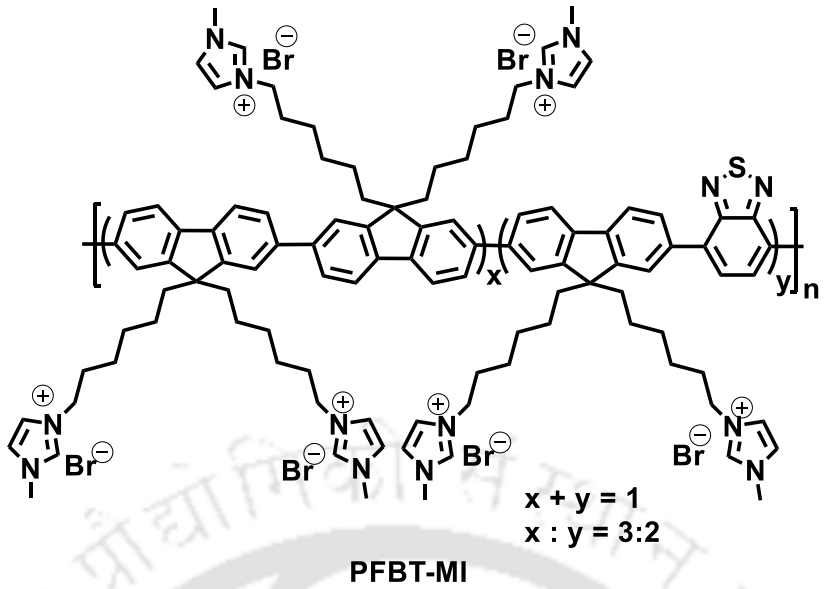

Figure 3. Structure of poly [9,9-bis(6′-methyl imidazolium bromide)hexyl)fluorene-co-4,7-(2,1,3-benzothiadiazole)] (PFBT-MI).

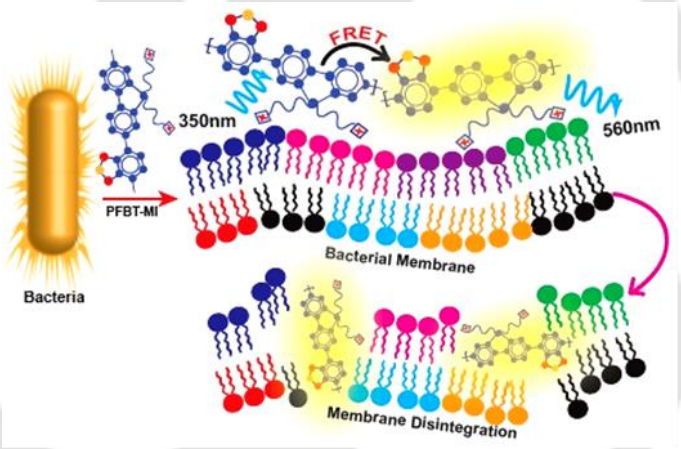

Figure 4. Schematic representation of bacterial imaging and its killing using cationic conjugated polyelectrolyte PFBT-MI.

Chapter 3: Conjugated Polymer-Based Electrical Sensor for Ultratrace Vapor-Phase Detection of Nerve Agent Mimics.

Chapter 3 describes the synthesis of amine-functionalized conjugated polymer poly(3-(9,9-dioctyl-9H-fluoren-2-yl)benzene-1,2-diamine) (PFPDA) (**Figure 5**) *via* Suzuki coupling reaction for low-cost onsite field detection of Diethyl chlorophosphate (DCP), a nerve agent mimic. A two-terminal electrical chemiresistor is fabricated on a low-cost glass substrate with PFPS as sensory channel material over a pair of Al electrodes. The PFPDA fabricated electrical sensor displayed a 100-fold increase in current intensity on DCP vapor exposure

with a detection limit of 5.8 ppb under ambient conditions. The highly selective and sensitive response of the PFPDA fabricated device for DCP is attributed to the redox interaction between p-type CP and electron-deficient DCP molecule facilitated by H-bond formation. To validate the sensing mechanism, a control experiment was performed using P0 CP (without amine groups) which displayed negligible current response on DCP exposure reflecting that the presence of amine groups at conjugated backbone is vital for redox interaction with organophosphate DCP molecule. Finally, the low-cost chemiresistor is integrated with an electronic circuit for onsite field detection of nerve agent vapors by a loud alarm signal and bright visual LED alerts without employing sophisticated instrumentation as shown in **Figure 6**. Moreover, a portable device is feasible for repeated multiple uses as it produces reproducible ON/OFF responses with DCP vapors.

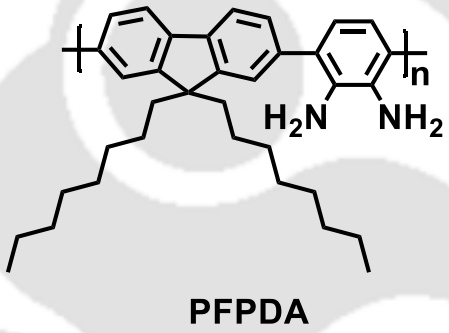

Figure 5. Structure of poly(3-(9,9-dioctyl-9H-fluoren-2-yl)benzene-1,2-diamine) (PFPDA).

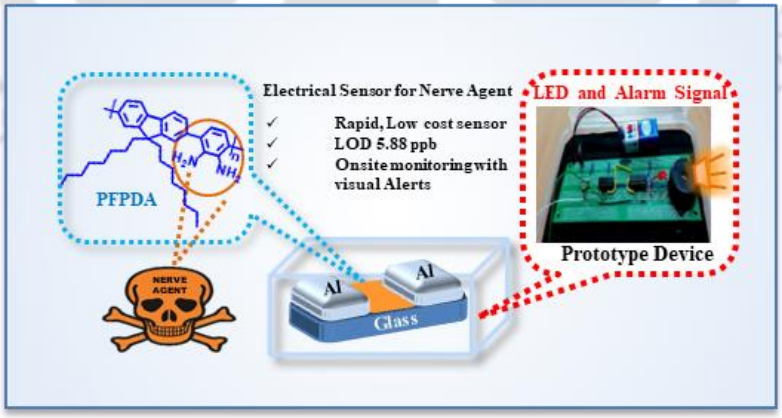

Figure 6. Schematic representation for the detection of Nerve agent mimic (DCP) using PFPDA fabricated low-cost electronic model.

Chapter 4: A Portable Conjugated Polymer based Smartphone Platform for Sensitive Detection of Monoamine Neurotransmitter

This chapter discusses the synthesis of rationally designed anionic conjugated polyelectrolyte (CPE) Poly[(9,9-bis(4'-sulfonatobutyl)fluorene-co-alt-1,4-phenylene) sodium], PFPS (**Figure 7)** *via* Suzuki cross-coupling polymerization without employing post functionalization step. The PFPS CP display a turn-off fluorescence response towards monoamine neurotransmitter-serotonin (5-HT) with evident visual color fading under UV light. An exceptionally high Stern Volmer constant (K_{sv}) of 1.14×10^5 M^{-1} and a very low LOD of 35 nM/7.65ppb are obtained for 5-HT in 100% aqueous solution is 100 times lower than the clinical range (0.5-1.4μM) present in blood plasma. A portable smartphone-enabled strategy is then realized for onsite real-time detection of 5-HT in blood plasma. The visual fluorescence response of PFPS by UV light irradiation is quantified into RGB intensities using color scanning android application, representing a low-cost instrument-free analytical approach for point-of-care testing of 5-HT. The mechanism insight reveals that excited state electron transfer and intermolecular π-stacked polymer aggregation are responsible for the remarkable sensitivity and selectivity of PFPS for 5-HT even in presence of other interfering neurochemicals as shown in **Figure 8.**

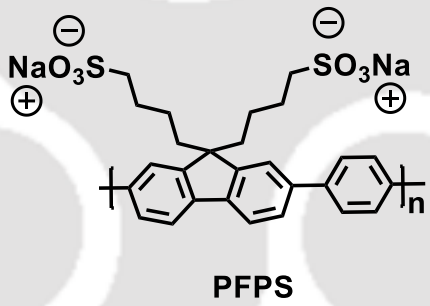

Figure 7. Structure of Poly[(9,9-bis(4'-sulfonatobutyl)fluorene-co-alt-1,4-phenylene) sodium], PFPS.

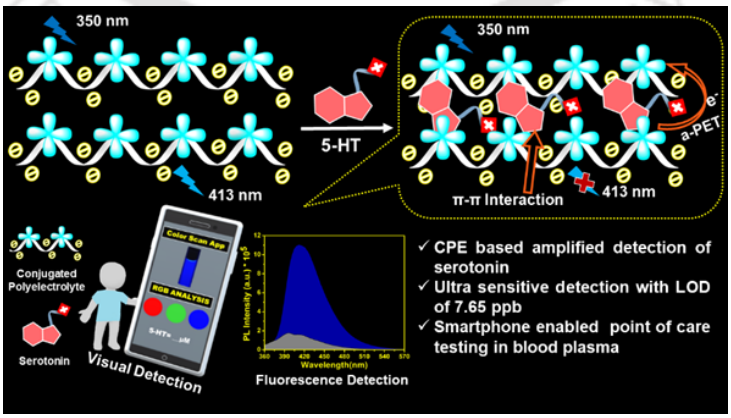

Figure 8. Schematic representation for the detection of the neurotransmitter serotonin by anionic conjugated polyelectrolyte PFPS.

Chapter 5: An AIEE active Conjugated Polyelectrolyte for Ultrasensitive Detection of Multicolor Artificial Food Dyes

This chapter describes the synthesis of newly developed AIEE active conjugated polyelectrolyte PFTT-D (**Figure 9**) *via* Suzuki cross-coupling polymerization reaction and successfully applied for the rapid, and highly sensitive detection of multicolor artificial food dyes in solution. The PFTT-D polymer forms a high emissive macro-aggregate in THF/water fraction and unveils remarkable sensitivity towards various food color dyes with detection limits in the range of 5.1-7.1nM. A very high quenching efficiencies with Ksv values of 6.4-4*10^5 M^{-1} were obtained for the first time which can be attributed to Inner filter effect(IFE), ground state, and excited state complexation. Moreover, the PFTT-D probe is also applied for the rapid detection of food dyes in various processed food samples representing great potential application in screening dyes levels in various food products with high precision (**Figure 10**).

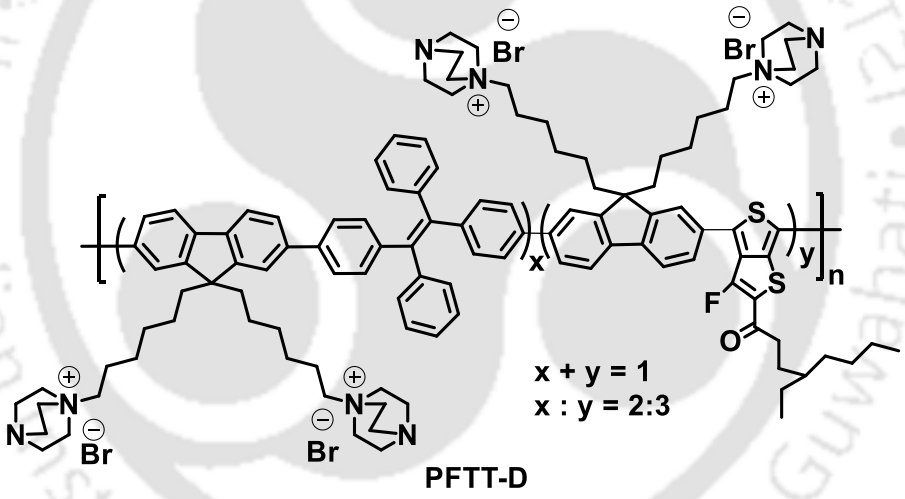

Figure 9. Structure of AIEE active conjugated polyelectrolyte PFTT-D.

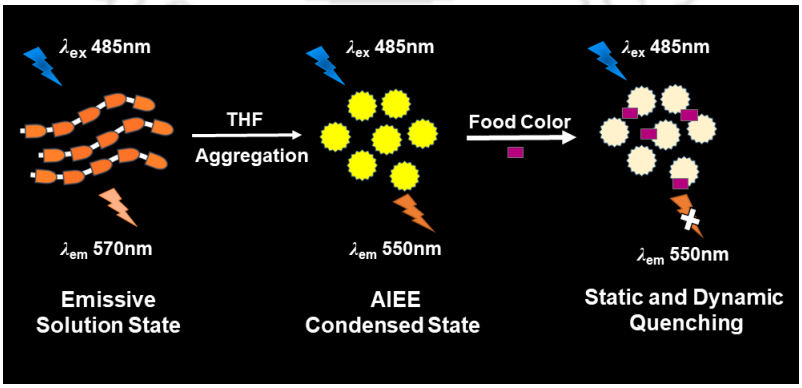

Figure 10. Schematic representation for the detection of artificial food color dyes by AIEE active Conjugate polyelectrolyte PFTT-D.

Conclusion and thesis overview

In conclusion, various novel conjugated polymers are rationally designed and synthesized *via* Suzuki cross coupling polymerization reaction followed by purification technique. The as designed CPs are successfully applied for detection of several chemical and biological analytes such as bacteria, lethal nerve agent vapor, biomarker serotonin, and artificial food color dyes.

Contents

Chapter 1

Introduction

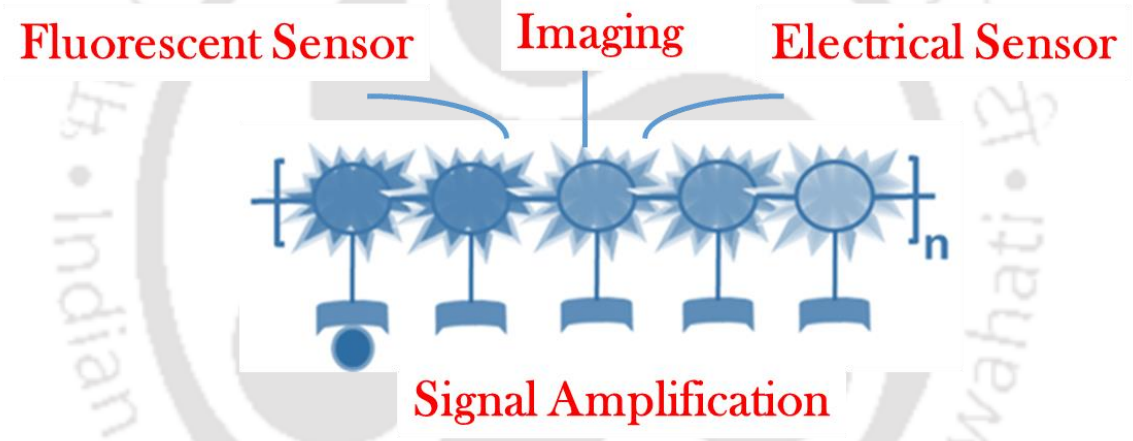

1.1 Introduction

Conjugated Polymers (CPs) are typical organic macromolecules that consist of alternative single and double bonds in their backbone chains. The extended delocalized electronic framework along the CP backbone imparts characteristics optoelectronic properties such as absorption or emission of light and transport of electrical charge.[1] The interest in π-conjugated polymer sparked in the 1970s when three renowned scientists, Alan MacDiarmid, Hideki Shirakawa, and Alan Heeger, discovered for the first time that the electrical conductivity of polyacetylene is increased by 10 million times upon electrochemical doping.[2] This breakthrough research in making plastics electrically conductive led them to win the 2000 Nobel Prize in Chemistry. Since then, CP has become the preferred material choice in the arena of photonics and plastic electronics such as light emitting diode (LED), field effect transistor (FET), photovoltaic cells, and sensors.[3-7] Moreover, they are also explored in the sensing field as novel and promising materials due to their unique electrochemical and optical properties, good processability, photo/thermal stability, and signal amplification features.[8,9]

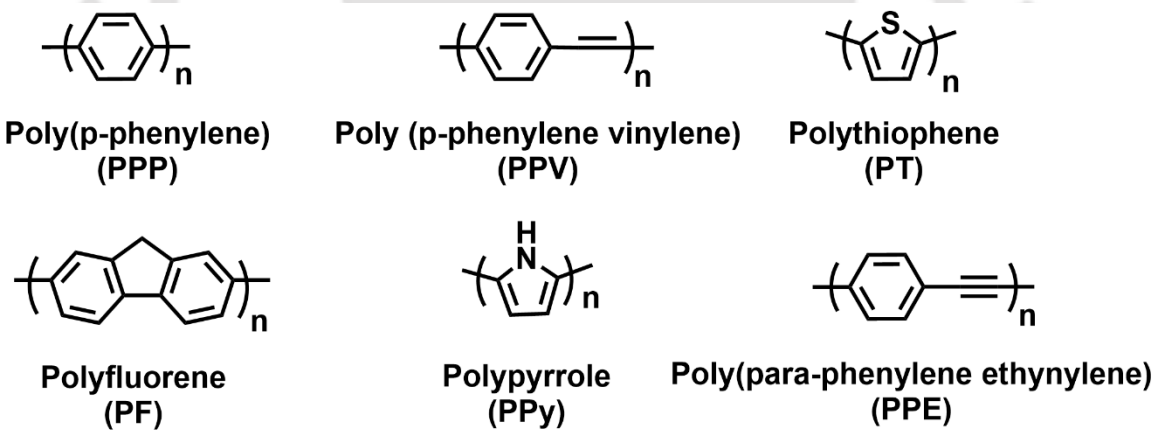

Figure 1.1: Structure of some well-known conjugated polymers.

In the past few years, several CPs with different backbone structures have been designed and developed. The most prominent types include poly(p-phenylene) (PPP), poly(p-phenylene vinylene) (PPV), polythiophene (PT), polyfluorene (PF), polypyrrole (PPy), poly(para-phenylene ethynylene) (PPE), etc as shown in **Figure 1.1**. Depending upon the application, these conjugated backbones can be further modified with different donor-acceptor monomers, alkyl side chains, and pendant functional groups to attain desirable optical or electrical properties as well as solubility and processibility.[10]

1.2 Sensor

A sensor can be defined as an analytical device that converts physical or chemical information into measurable output signals. Typically, a sensor consists of two main components i.e., recognition unit (receptor) and signaling or transducing unit. The recognition unit detects or responds to the external stimulus via chemical or physical interaction while the transducer unit converts such physical or chemical events into a useful output signal. There is great demand for highly sensitive and selective sensors in various fields such as environmental monitoring, food safety, public health, medical and healthcare products, agriculture industry, and cyber and national security. Although sensors can be classed into various schemes, however, depending on the transduction mechanism, sensors can be categorized into several types such as optical, electrical, magnetic thermometric, electrochemical and gravimetric, etc. In the case of an optical and electrical sensor, the transducer unit converts physical or chemical response with foreign substance into optical (absorbance or photoluminescence) and electrical signal (conductivity or resistivity) respectively. In the same manner, gravimetric, magnetic, electrochemical, and gravimetric sensors respond to the external stimulus and convert it into the change in the mass, magnetic, thermal, and electrochemical properties of the material, respectively.[11-13] Among various types, optical and electrical sensors are widely explored due to their low cost, high sensitivity, rapid response, and portable features. Moreover, while designing chemo or biosensors, various parameter needs to be considered, such as sensitivity, selectivity, stability, response time, portability and water solubility, etc., depending upon its implementation and application field. In the diverse sensing field, various materials such as metal oxides, carbon nanoparticles, small organic molecules, and polymers are designed and explored for the selective and sensitive detection of environmental and biological species. However, CPs represent promising sensing material due to their outstanding photophysical properties, chemical and thermal stabilities, biocompatibility, and amplified signal generation.

The basic design strategy for developing a CP-based chemo/biosensor is to connect the recognition element (receptor) with the signaling or transducer unit (conjugated backbone) such that these two components communicate with each other. The analyte triggers variation in measurable properties of the material during the binding event and is quantified as an amplified signal response. Therefore, the functionalization of a conjugated backbone

with a specific receptor not only tunes the desired physical property but also improves the solubility, specificity, and sensitivity of CP towards the analyte of interest.[14,15]

1.3 Signal amplification in CP

A key feature of CP that has received significant attention as a transducer is its ability to transform an analyte-binding event into an amplified optical or electrical signal. This unique signal amplification feature is derived from the efficient migration of charge carriers or exciton throughout the conjugated backbone after analyte receptor chemical interaction.[16] The conceptual model of signal amplification was termed as "Molecular Wire Effect" by Swager and coworkers while demonstrating paraquat sensing using cyclophane functionalized poly(phenylene ethynylene), PPE CP.

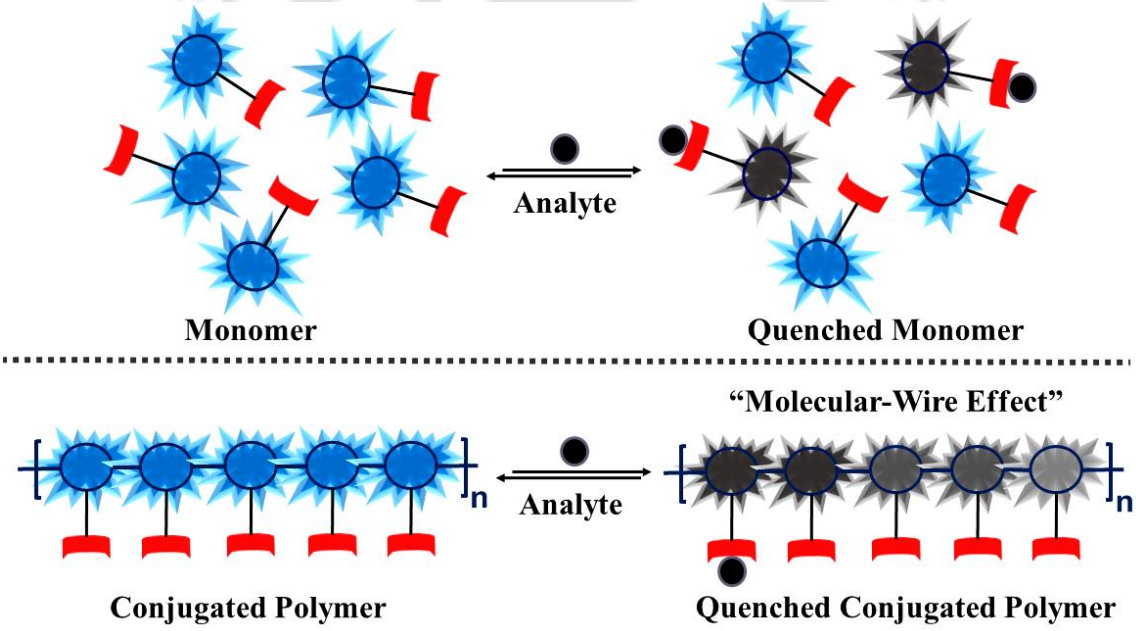

Figure 1.2: Pictorial representation of monomer and polymer's emission quenching by analyte molecules. The figure is reprinted (adapted) with permission from Ref. 13. Copyright 2017 Elsevier.

The paraquat is a well-known electron acceptor that efficiently quenches the PPE CP fluorescence via the formation of a rotaxane complex. To evaluate amplify binding event, an analogous small molecule containing cyclophane receptor was also synthesized and the role of exciton transport was convoluted in a single isolated polymer chain. The study reveals that exciton could ramp around 65 receptors thereby generating 65-fold signal enhancement compared to the model compound containing a single receptor.[17] Therefore, CP in solution behaves as a 1-dimensional wire such that the influence of a single analyte

binding event is interrogated to multiple receptors (conjugated units) via efficient charge carrier or exciton transport resulting in the extraordinary signal enhancement. Such a unique recognition process eventually leads to an amplified signal compared to a small molecule probe where the change in fluorescence occurs due to a single binding event (**Figure 1.2**).

1.4 Conjugated polymer as a fluorescent sensor

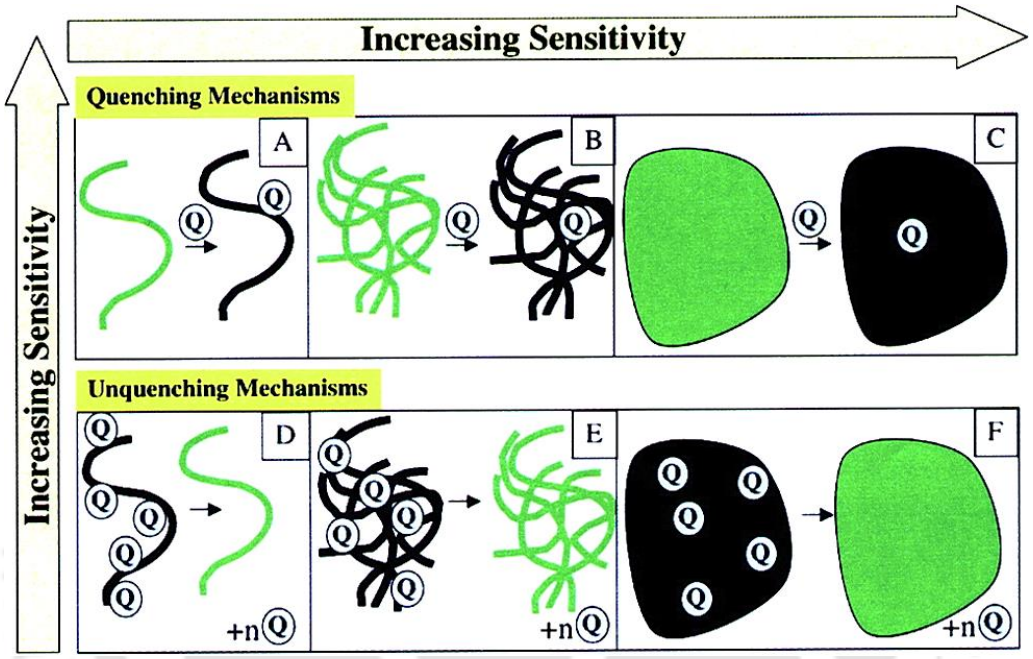

Figure 1.3: Effect of dimensionality on the sensitivity of CPs in quenching and de-quenching scheme. The figure is reprinted (adapted) with permission from Ref. 8. Copyright 2007 American Chemical Society.

Due to CP's unique optical properties, such as high fluorescence quantum yield, remarkable sensitivity, good photo and thermal stability, and thin-film ability, it is widely explored as an optical probe for various environmental and biological species. The fluorescence signal of CP can be implemented into two different sensing approaches, i.e., turn-on (dequenching) or turn-off (quenching) process.[18] Generally, the fluorescence lifetime and emission intensity of fluorophore are monitored in fluorescence mode detection. During the turn-on scheme, enhancement in CP emission is observed due to conformational change of the polymer chain or generation of low/high energy fluorophore after interaction with the target molecule.[19] While in the turn-off sensor approach, CP fluorescence is quenched by non-radiative relaxation processes such as electron transfer, Förster resonance energy transfer, inner filter effect, or analyte-induced polymer aggregation.[20] The level of signal

acquisition is highly dependent on the physical state of CP. For instance, the quenching of CP in solution is commonly less sensitive than in thin film as exciton transport in one-dimension results in revisiting the same receptor site multiple times. However, in the case of polymer's aggregates or thin film, the signal gain is much more pronounced due to the vectorial transport of exciton in three-dimension. In addition, the turn-on sensor is less sensitive than the turn-off sensor, because removing a quencher molecule does not guarantee signal enhancement as another quencher's influence may overlap with the same quenching volume (**Figure 1.3**). Thus, for trace analyte detection in a competing environment, a turn-off or quenching scheme is most appropriate.[8,21]

1.4.1 Stern Volmer theory for fluorescence quenching

Fluorescence quenching is the deactivation process of fluorescence which proceed with the decrease in fluorescence intensity or the lifetime of a fluorophore (X) after interaction with a quencher (Q) molecule. Generally, fluorescence quenching occurs through two primary quenching mechanisms i.e., ground state complex formation (static quenching) or collisional quenching (dynamic quenching).

In static quenching, a fluorophore forms a non-radiative complex with a quencher molecule before the excitation process.

Static or ground state complexation

$$X + Q \underset{}{\overset{K_a}{\rightleftharpoons}} [X,Q] \xrightarrow{h\nu} [X^*,Q] \longrightarrow X + Q$$

While dynamic quenching occurs when the excited state fluorophore (X*) encounters collision with the quencher molecule resulting radiation less decay to the ground state.[13]

Dynamic or collisional quenching

$$X^* + Q \longrightarrow X + Q$$

The static and dynamic quenching can be differentiated by recording fluorophore lifetime with quencher concentration as well as monitoring quenching efficiency at different temperatures. Moreover, it could also be possible that both these processes are present in the system. Therefore, to define fluorescence quenching by these two limiting mechanisms, the Stern-Volmer equation is used.

$$I_0/I = 1 + K_{sv}[Q] \qquad 1.1$$

Where I_0 and I represent the emission intensity of fluorophore without and with a quencher. Equation 1.1 is known as the Stern-Volmer equation and K_{sv} is Stern-Volmer constant or quenching constant. In the limits, when quenching exclusively involve a dynamic process, $K_{sv} = K_q\tau_0$, where 'K_q' and 'τ_0' represents the bimolecular quenching constant and fluorescence lifetime of fluorophore X* respectively. As a result, the Stern-Volmer equation can be modified to;

$$\tau_0/\tau = I_0/I = 1 + K_q\tau_0[Q] \qquad 1.2$$

On the other hand, if quenching exclusively involves a static mechanism, $K_{sv} = K_a$, where 'Ka' denotes the dissociation constant for the ground state complex.[22] In such case, the Stern-Volmer can be represented as,

$$I_0/I = 1 + K_D[Q] \qquad 1.3$$

Thus, if quenching is dominated by a static or dynamic process, the S-V curve should be linear.

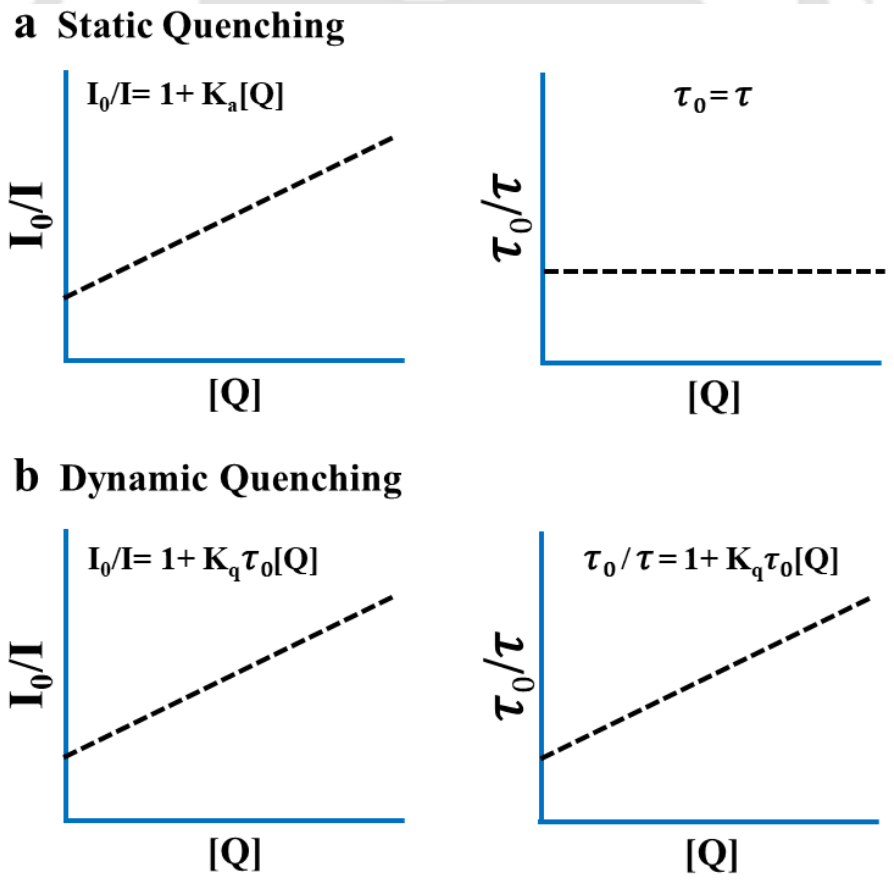

Figure 1.4: Fluorescence intensity (I) and decay lifetime (τ) vs Quencher concentration plots in static and dynamic quenching.

Moreover, the fluorophore lifetime should vary with quencher concentration in case of dynamic process and no change in fluorescence lifetime would be observed in static quenching (**Figure 1.4**). However, in several systems, S-V plot displayed non-linearity indicating the presence of multiple mechanisms such as fluorophore aggregation, reabsorption process, mixed dynamic and static mechanism, etc.[23]

1.4.2 Selected examples of CP-based fluorescent sensor

In recent years CPs with different conjugated structures and side-chain functionalities have been tremendously explored as fluorescent sensory materials for various chemical and biological species such as toxic chemicals, environmental pollutants, metal ions, explosives, biomarkers, etc. Some of these examples are discussed below.[24-30]

The most successful applications of CP-based sensors are the detection of explosives, especially picric acid (PA), 2,4,6-trinitrotoluene (TNT), trinitrobenzene (TNB), which are critically important to detect in the context of homeland security from the chemical threat.[31] In this regard, Scherf and co-workers reported microwave synthesis of two Polycarbazole AIE active CP (**P1** & **P2**) via nickel-catalyzed Yamamoto coupling (**Figure 1.5)**. Interestingly both the polymers display the electron-donor nature of polycarbazole and the AIE character of TPE moiety attached at the side chain. The polymers show the amplified response for trinitrobenzene with the quenching constant of 2.14 * 10^5 M^{-1}. The reason for the amplified response is the polymer's topology that forms a twisted 3D structure in a nano aggregates state leading to efficient inter-chain exciton diffusion. The polymer-coated Whatman test strip shows fluorescence quenching on the addition of both the TNB vapor and solution demonstrating the potential application in the solid-state gas sensors.

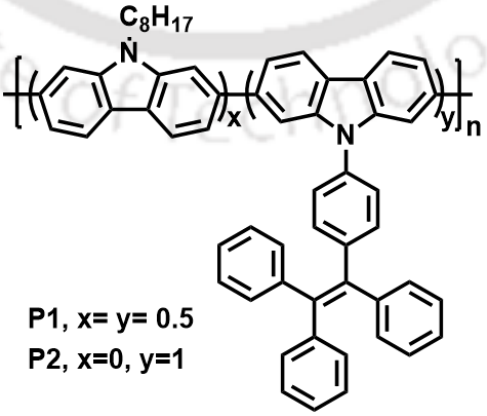

Figure 1.5: Structures of **P1** and **P2** CP.

Later on, Seung Lee and coworker designed a Donor-Acceptor (D-A) type **P3** CP, using fluorene as donor and quinoxaline as an acceptor (**Figure 1.6**).[32] The polymer was explored as a photoacid generator and a probe for nerve gas mimics. The thin film of the polymer acts as a reversible photoacid generator as it exhibits concentration and pH-dependent emission. Since the quinoxaline unit has a nucleophilic property; thus, it acts as a reactive site for electron-deficient organophosphates. The probe showed ultra-sensitivity for nerve gas vapor with a detection limit of 14.9 μM. The system can be useful for real-time monitoring of toxic nerve gas using low-cost portable paper strips.

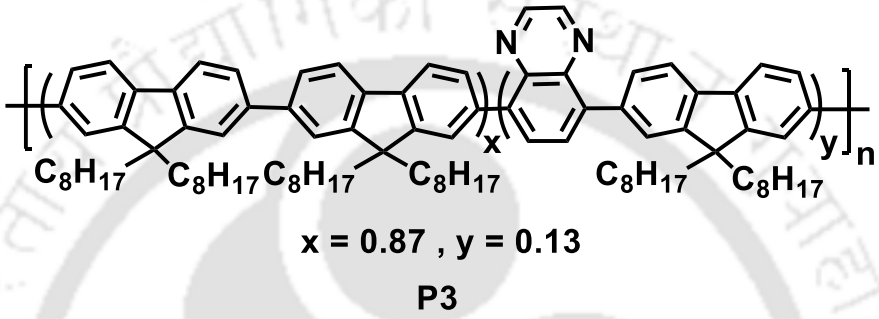

Figure 1.6: Structure of **P3** CP.

Fan and coworker synthesized fluorescent CP **P4** with carboxylic acid as pendant group attached at the side chain via Sonogashira coupling reaction (**Figure 1.7)**.[33] The polymer exhibits a discriminatory response in the presence of aliphatic and aromatic amines. The pendant carboxylic group is involved in acid-base interaction with the organic amines resulting in fluorescence quenching ("turn-off") by the aromatic amines and fluorescence enhancement ("turn-on") in the case of aliphatic amines. The turn-on response for aliphatic amines may be originated from polymer chain conformation, whereas aromatic π-π stacking with the aromatic amines causes fluorescence quenching of the polymer.

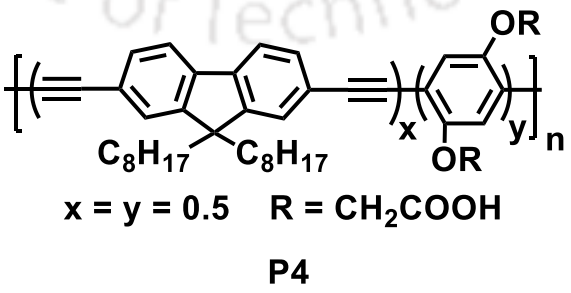

Figure 1.7: Structure of **P4** CP.

Similarly, Li and co-workers designed a color-tunable water-soluble conjugated polyelectrolyte **P5** using the Suzuki-coupling reaction (**Figure 1.8**).[34] The cationic bisimidazoium groups are attached to the side chains of **P5** as binding sites for the negatively charged phosphate group in the ATP molecule. Moreover, oligo (ethylene glycol) units were incorporated at the end of the side chain to increase the water solubility and inhibit the polymer's self-aggregation. The polymer emits purple fluorescence in the well-dissolved state due to inefficient intramolecular FRET from fluorene donor to 1,4-di thienyl benzothiadiazole (DBT) acceptor. When ATP was introduced into the system, a robust electrostatic complexation occurred between the cationic imidazolium units of the **P5** and phosphate group of ATP resulting in aggregation-induced intermolecular-FRET with the red-shifted fluorescence emission from the DBT unit. Thus, by designing donor-acceptor type CP with a specific recognition structure, the ultra-sensitive ratiometric sensing of a biologically relevant analyte, ATP, was achieved.

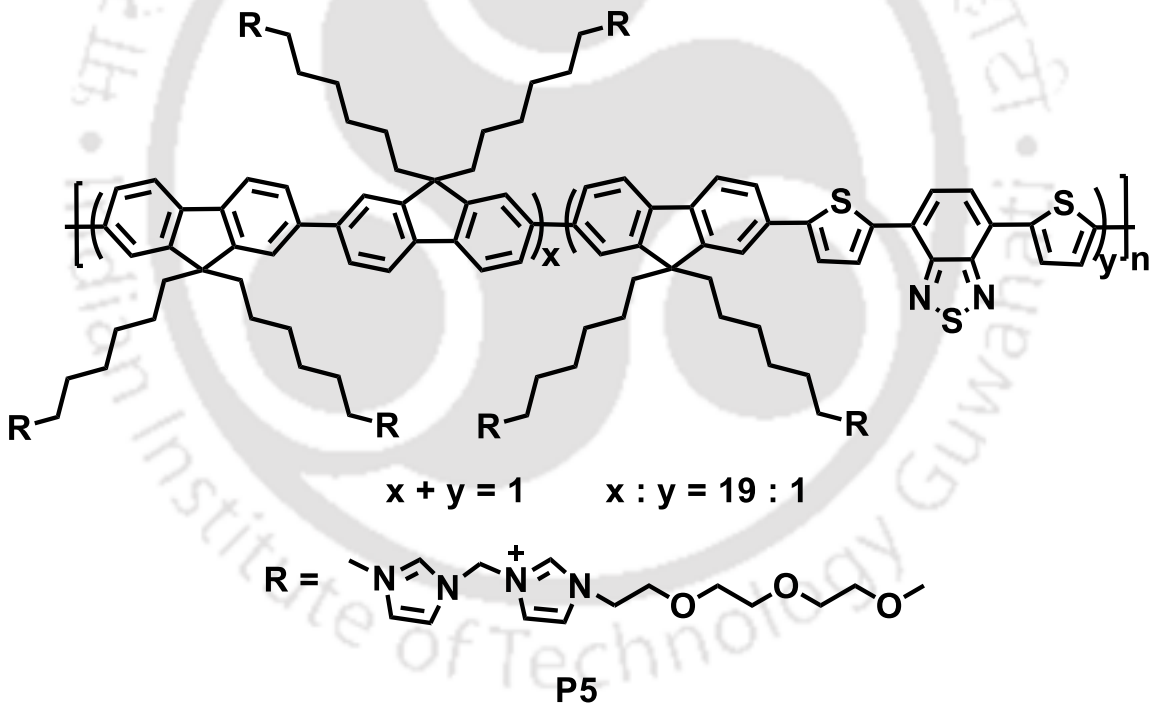

P5

Figure 1.8: Structure of **P5** CP.

Similarly, Shu Wang and coworkers developed a new strategy to discriminate against the fungi (*C. albicans*), Gram-positive (*B. subtilis*), and Gram-negative bacteria (*E. coli*) using cationic **P6** CP **(Figure 1.9).**[35] The three species were differentiated by their unique fluorescence microscopic images recorded after staining with **P6** in the PBS solution of different ionic strengths. Each species showed a unique imaging trend in different ionic

strength PBS solutions due to differences in their cell wall component. The isothermal titration reveals that the binding of **P6** to *C. albicans* and *E. coli* is dominated by electrostatic interactions, while hydrophobic interactions for PPV-NMe^{3+} and *B. subtilis*. The method for detection of microbial pathogens was much more straightforward and very rapid as it requires less than 3 h to complete the analysis.

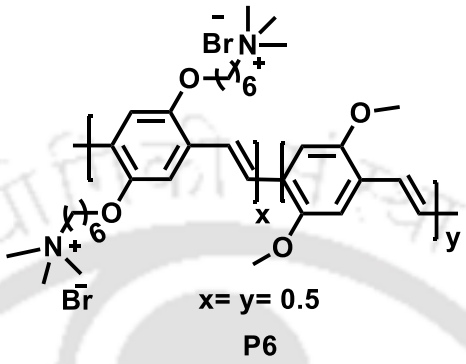

Figure 1.9: Structure of **P6** CP.

Later on, Tang and coworker designed a novel CP based strategy for the detection of Nitroreductase, an enzyme overexpressed in hypoxia tumors.[36] In **P7** CP, the aromatic nitro group was incorporated as a reactive site for NTR, which gives rise to low fluorescence signal of the probe due to excited state electron transfer (PET) from the conjugated backbone to the nitro group-containing side chains **(Figure 1.10)**. The NTR catalyzed the reduction of a *p*-nitrophenyl group into a *p*-aminophenyl group, which resulted in the blocking of PET with strong fluorescence emission from **P7**. The probe was also used for hypoxic tumor cells as well as NTR-expressed bacteria (*E. coli*) demonstrating the unique method for hypoxia diagnosis and bacterial imaging.

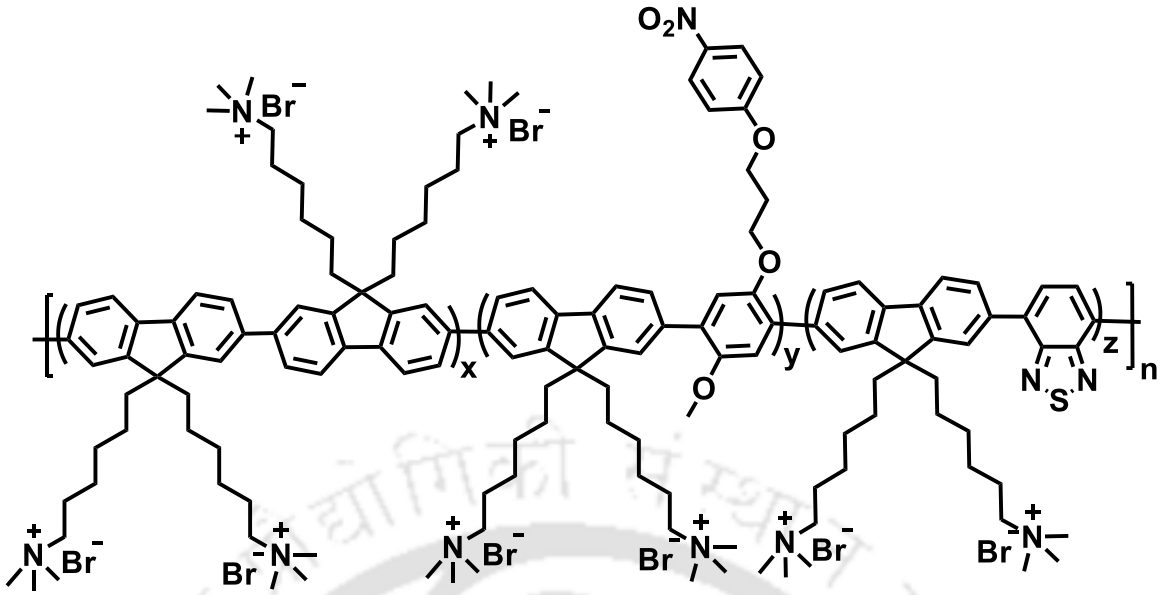

Figure 1.10: Structure of **P7** CP.

In 2019, Iyer and coworkers developed a water-soluble anionic CPE, **P8** for the detection and removal of broad spectrum antibiotic, Tetracycline (Tc) as shown in **Figure 1.11**.[37] An anionic moiety, 5-hydroxyisophthalate were installed at the side chain of the precursor polymer to augment the electrostatic interaction with the positively charged Tc resulting in efficient photo-induced electron transfer from LUMO of the CPE to the LUMO of the Tc, and eventually the amplified fluorescence quenching of **P8** CPE. The lowest detection limit of 6.80 ppb and quenching constant K_{sv} of 1.57×10^5 M^{-1} were obtained without any interference from competing analytes, reflecting the highly effective CPE-based biosensor. Furthermore, a polymer-doped chitosan fluorescent membrane was fabricated for Tc removal from antibiotic-infested wastewater with a phenomenal absorption capacity of 3.12 mg/g.

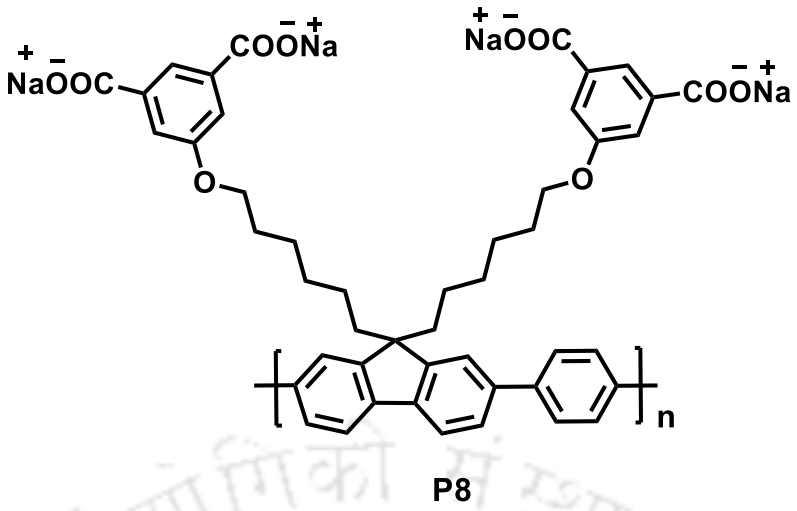

P8

Figure 1.11: Structure of **P8** CP.

1.5 Conjugated polymer for electrical sensor

To meet the rising demands of portable and wearable sensor for environmental or healthcare monitoring, flexible electronic devices has emerged as one of the most promising technologies that can be used for several applications, such as wireless hazardous gas monitoring, point-of-care devices, on-field explosive sensor, and implantable biomedical devices.[38] Semiconducting polymers are the preferred choice of material in organic electronics due to their tunable optoelectrical properties, facile solution processability, high flexibility, thermal stability, and thin-film forming properties. Moreover, the π-electron distribution of conducting polymer is highly sensitive to the immediate polarization effect caused by proximate molecules or atom.[39] This characteristic feature is particularly useful for the development of highly sensitive electrical sensors which transduce chemical interaction into an electrical signal. Generally, electrically conducting polymers are formulated into a variety of transduction schemes/sensor modes such as potentiometric, amperometry, and chemiresistive (conductometric) schemes. However, chemiresistive are most rigorously explored due to their superior sensitivity, ease of fabrication, and faster response time. A chemiresistive sensor typically consists of an organic semiconductor (OSC) as channel material that forms an electrical contact with two or more electrodes deposited on an insulating substrate such as plastic or glass and the analyte of interest is detected based on variation in electrical conductivity or resistivity of organic semiconductor **(Figure 1.12a)**.[40,41] The advantage of chemiresistive sensors over optical or electrochemical-based sensors is their ability to deliver label-free responses using

a simple electronic circuit that can be further miniatured into smart portable or wearable systems.

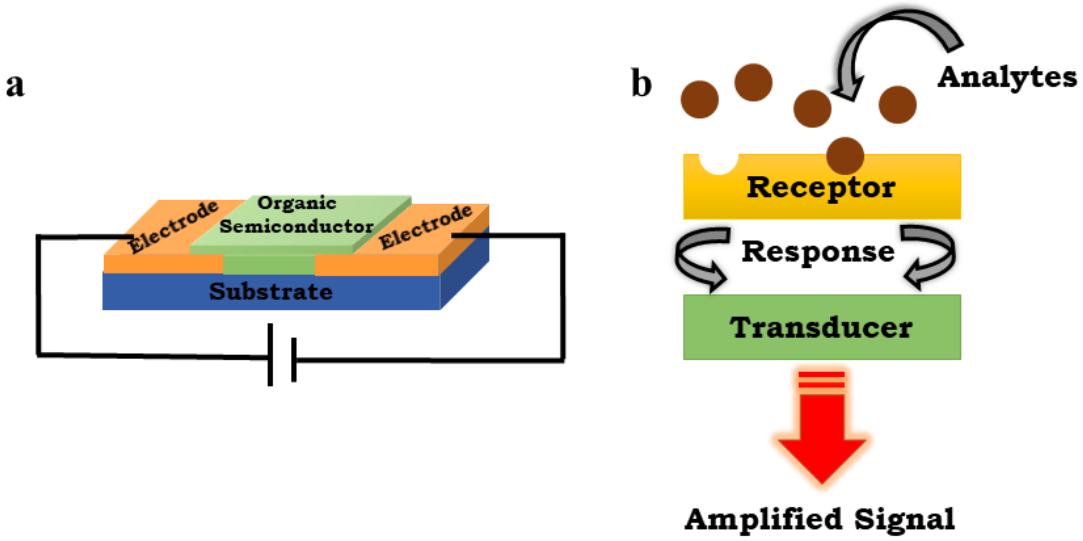

Figure 1.12: (a) Schematic representation of typical chemiresistive sensor, (b) working principle of CP based chemiresistive sensor.

1.5.1 Working principle of chemiresistive sensor

As discussed above, chemiresistive sensor is the simplest form of electrical sensor that integrates organic semiconductor as an active transport layer between a pair of the metal electrode. The sensing response of such a device is greatly related to the change in electrical properties of organic semiconductors after chemical interaction with analyte molecules. The analyte-induced conductivity change can be brought through direct chemical interaction between the semiconductor and analyte such as dipole–dipole, acid–base, hydrogen bonding, coulombic, etc. with the partial transfer of electronic charges between them leading to the variation in density or mobility of charge carriers of semiconductor. Moreover, the adsorption or diffusion of analyte molecules at the surface of organic semiconductors can also result in the trapping of charge carriers at the grain boundaries or an increase in intergrain charge transport resistance and subsequently variation in device current.[42]

In the case of CP fabricated chemiresistive sensor, the chemical binding event between the analyte and recognition unit (receptor group) is converted into an amplified change in conductivity/ resistivity by the transducer unit (conjugated backbone), **Figure 1.12b**. The amplified signal is a collective response of several conjugated units which allow the efficient transport of charges and any molecular level hindrance in the charge carrier path

by external stimuli can obstruct bulk mobility, resulting in higher sensitivity than the small-molecule probe.[43,44]

1.5.2 Parameters of electrical sensor

The important analytical parameters that define the performance of electrical gas sensor are discussed below.[45-48] These analytical parameters are needed to be assessed prior to practical applications.

a) **Sensitivity:** The sensitivity is defined as the ability to distinguish small differences in mass or concentration of the target analyte and is generally calculated from the slope of the calibration curve. So, the high sensitivity of the sensor corresponds to the large change in output signal by the presence of a very small amount of analyte.

b) **Selectivity:** Selectivity refers to the capability of the sensor to discriminate the test analyte from other competing or interfering compounds. It is quite difficult to achieve 100% selectivity however, to achieve selective detection, specific receptor groups should be incorporated while designing the molecular structure of organic semiconductors. The selectivity of the sensor is generally expressed as a percentage of variation in output signal in presence of various interfering analytes.

c) **Response and recovery time:** The response time is referred to the time taken by the gas sensor to reach 90% of the maximum output signal. Whereas, recovery time is defined as the time needed by a gas sensor to return back from 90% of signal change to its original value after the removal of the target gas.

d) **Repeatability:** Repeatability refers to the ability of a sensor to generate the same measurement (or response) repeatedly at the same concentration of target analyte under identical conditions.

e) **Limit of detection:** The limit of detection (LOD) or detection limit is defined as the minimum concentration of test analyte that can be detected; however, it may not necessarily be determined as an exact value. The LOD can be calculated by the equation as shown below

$$LOD = \frac{3\sigma}{k}$$

Where 'σ' corresponds to the standard deviation of output signal of sensor measured at 'n' time without analyte and 'k' is the slope of a calibration curve.

1.5.3 Selected examples of CP based electrical sensor

Mostly, CP-fabricated chemiresistor sensor is utilized for the detection of volatile organic chemicals, explosive chemicals and toxic gases. Some recent progress in CP-based electrical sensors is discussed below.

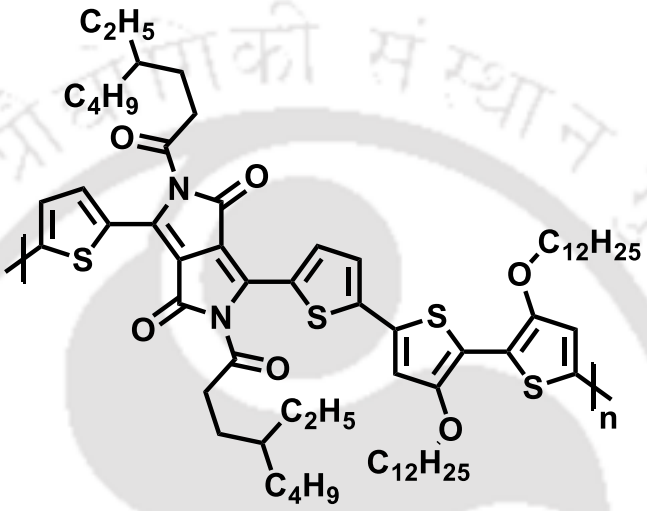

P9

Figure 1.13: Structure of **P9** CP.

Jenner *et al.* designed a donor-acceptor type low band gap **P9** CP for low power driven two electrode chemresistive sensor by taking 3,3′-bis(dodecyloxy)-2,2′-bithiophene as electron donor and diketopyrrolopyrrole (DPP) as electron accepting building block respectively (**Figure 1.13)**.[49] A thermally labile carbamate group was inserted into the DPP unit to form solvent-resistant CP film for the construction of robust chemiresistor sensor devices. The HCl doped **P9** CP fabricated two electrode chemiresistor was then tested against various volatile organic liquids *viz*, chloroform, hexane, acetone, diethyl ether, acetonitrile, alcohol, esters, etc. Each volatile organic liquid displayed a distinct current versus time signature profile depending upon the strength and nature of molecular interaction with **P9** CP as well as its volatility and diffusion rates. Importantly, HCl doped **P9** fabricated sensor can be reused several times without affecting its output characteristics demonstrating its long-term operational and environmental stability.

In 2008, Swager and coworkers have reported hexafluoroisopropanol substituted polythiophene, **P10** based chemiresistive sensor for the detection of nerve gas mimic, DMMP (Dimethyl methyl phosphate) as shown in **Figure 1.14**.[50] The polymer was blended with the carbon nanotube to improve the performance and sensitivity of the sensor. The polymer dispersed CNT fabricated chemiresistor displayed a highly sensitive response on exposure to very low DMMP vapor concentration with a detection limit in ppb level. The hexafluoroisopropanol group was strategically incorporated into the polymer framework to promote the H-binding interaction with DMMP vapors resulting in 9 times sensitivity increase compared to unfunctionalized polythiophene/CNT film. The decrease in conductivity of polymer/CN film on DMMP vapor exposure was attributed to the formation of scattering sites and the charge transfer process.

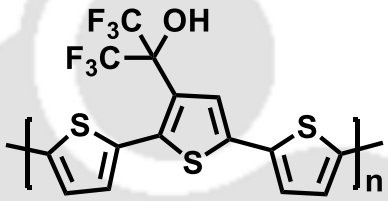

P10

Figure 1.14: Structure of **P10** CP.

Park *et al.* demonstrate the sensing of NO_2 gas by designing a series of high molecular weight n-type conjugated polymers with good mechanical strength (**Figure 1.15)**.[51] The n-type naphthalene diimide (NDI) **P11** CP was modified with a different fraction of phenylene bis[1-(2-thienyl)methenamine group to enhance the redox interaction with NO_2 gas. Furthermore, to achieve operational stability and high electrical signal, n-type CP were doped with electron-rich poly(ethyleneimine) polymer. The PNDIT2/IM-0.1 and PEI fabricated chemiresistor sensor shows excellent sensing operation with high selectivity and sensitivity towards NO_2 gas. The sensing mechanism is related to the weakening of conjugation in the CP chain by redox interaction between the electron-donating imine bond of CP and the electron-deficient NO_2 molecule.

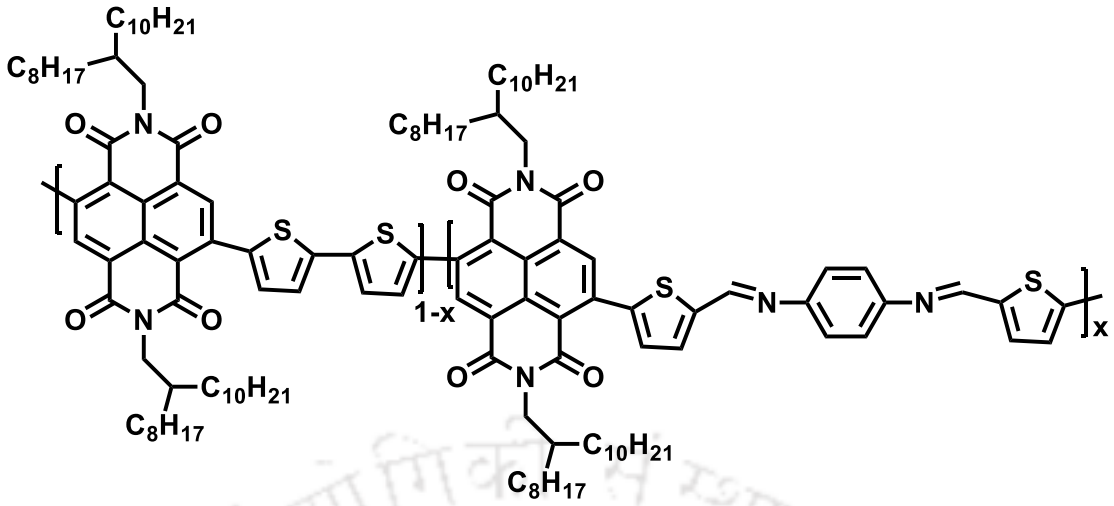

P11

Figure 1.15: Structure of **P11** CP.

Later on, Limbu *et al.* reported low voltage operated, **P12** CP fabricated chemiresistive sensor for VOC detection and discrimination (**Figure 1.16)**.[52] The bare polymer was unresponsive to VOCs due to its weak signal below the noise level. However, the electrical conductivity and sensitivity were improved by increasing charge carrier density in the CP film through ionic liquid (IL) doping. The IL-doped CP fabricated device was then tested for VOCs, showing superior and discriminatory electrical response towards polar and non-polar VOCs. For instance, on non-polar toluene vapor exposure, a turn-on response was observed, while a turn-off response was obtained in the case of polar acetone vapor. This sensing behavior was clearly understood by considering specific intermolecular interactions associated with polar and non-polar VOCs. The polar acetone molecule can electrostatically interact with IL resulting in the weakening of electrostatic interaction between IL and **P12** polymer and ultimately decreasing the π-electron density of IL doped polymer film. In contrast, non-polar toluene cannot form electrostatic interaction with either of them; however, it can be adsorbed and cause swelling of the film, which may result in the augmentation of electronic coupling between polymer and IL.

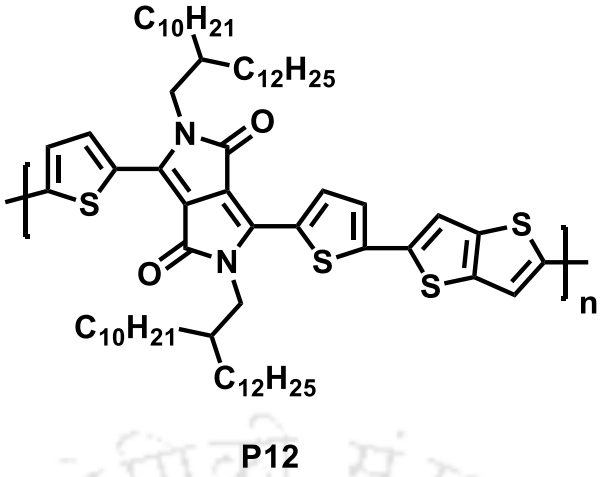

P12

Figure 1.16: Structure of **P12** CP.

Zhang *et al.* developed DPP-bithiophene polymer, **P13** based chemiresistor in OFET configuration for the detection of ammonia gas (**Figure 1.17)**.[53] The polymer was decorated with tert-butoxycarboxyl groups at the side chain to achieve desired selectivity and solution processibility. The *tert*-butoxycarboxyl group is thermally liable and converted into the reactive COOH group with the elimination of isobutylene after annealing of CP film at 240 ˚C. The **P13** fabricated device shows a turn-off current response on exposure to ammonia vapor. This could be attributed to the formation of ammonium carboxylate by the reaction of COOH functionalized polymer and ammonia molecule resulting in the loss of hole mobility via charge carrier trapping.

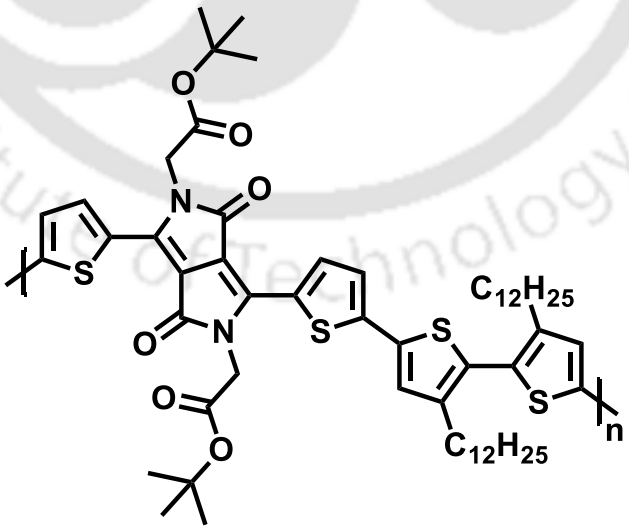

P13

Figure 1.17: Structure of **P13** CP.

1.6 Objectives and conclusion of the thesis work

The primary focus of the present thesis work was to design and develop CP-based sensors for highly sensitive and selective detection of various biological and environmental important analytes with the major aim of overcoming the problem and challenges associated with existing sensing systems. Various novel CPs are rationally designed and successfully implemented as rapid, highly sensitive, and portable systems for on-field monitoring of toxic gases, food additives, disease biomarkers, and pathogens. The key objective and conclusion for each work are described below-

- The rapid emergence of pathogen infections with antibiotic resistance has become public health issue and puts immense pressure on healthcare systems across the globe. According to the report published by the Center for Disease Control and Prevention (CDCP), the number of people affected by multidrug-resistant bacterial infections annually is around 2 lakhs, and by 2050 average death rate would be 10 million. Therefore, there is an urgent need to develop novel resistance-free antibacterial materials. Chapter II discussed the synthesis of dual emissive cationic conjugated polyelectrolyte for ratiometric detection of bacteria and explored its antibacterial application.
- Organophosphorous nerve agents are extremely toxic chemicals, easily manufactured on a large scale and regarded as weapons of mass destruction. They are colorless and odorless, volatile liquids and can enter the human body through skin or inhalation. The volatile agents inhibit the neuroenzyme acetylcolinesterase, thereby disturbing nerve impulse transmission and finally causing paralysis or death of the victim. Chapter III describes the design and synthesis of amine-functionalized CP for vapor phase detection of nerve agent mimic, i.e., diethyl chlorophosphate (DCP) using a low-cost portable chemiresistive sensing platform.
- Serotonin is an important signaling molecule of CNS that regulates several fundamental aspects of behavior and physiology including mood, sleep, pain sensation, platelet coagulation, gastrointestinal motility. The aberration in serotonin neurotransmission results in multiple neurological disorders such as anxiety, schizophrenia, depression, bipolar disorder, and autism. Moreover, it has been reported that the elevated level of serotonin in blood plasma is associated with neuroendocrine tumors or carcinoid tumors. Chapter IV discusses the

synthesis and characterization of an anionic conjugated polyelectrolyte for the rapid visual detection and real-time monitoring of serotonin in real blood sample using smartphone application.

- Artificial food colorants are synthetic dyes that are readily available and extensively used in food items to restore or enhance the natural color of food, lost during processing or storage. However, the indiscriminate use of food colorants raises concerns for public health, food security, and environmental monitoring. Therefore, several international organization and governing agencies, including WHO and U.S.-FDA, has set strict regulations on the usage, purity, and permissible limit of food colorants. Most of the existing detection methods for food colorant rely on conventional techniques liquid chromatography (LC) or mass spectroscopy which are time-consuming, require complex instrumentation, yet present lower selectivity and sensitivity than required. Chapter V describes the design and development of AIE active conjugated polyelectrolyte for the detection of various food colorants ranging from blue to red with ultralow detection limits in the nanomolar range.

References

(1) Heeger, A. J. Semiconducting polymers: the Third Generation. *Chem. Soc. Rev.* **2010**, *39*, 2354-2371.

(2) Quade, D. T. M.; Pullen, A. E.; Swager, T. M. Conjugated Polymer-Based Chemical Sensors. *Chem. Rev.* **2000**, *100*, 2537-2574.

(3) Facchetti**,** A. π-Conjugated Polymers for Organic Electronics and Photovoltaic Cell Applications. *Chem. Mater*. **2011**, *23*, 733-758.

(4) Gunes, S.; Neugebauer, H.; Sariciftci, N. S. Conjugated Polymer-Based Organic Solar Cells. *Chem. Rev.* **2007**, *107*, 1324-1338.

(5) Kraft, A.; Grimsdale, A. C.; Holmes, A. B. Electroluminescent Conjugated Polymers—Seeing Polymers in a New Light. *Angew. Chem., Int. Ed*. **1998**, *37*, 402-428.

(6) Torsi, L.; Dodabalapur, A.; Rothberg, L. J.; Fung, A. W. P.; Katz, H. E. Intrinsic Transport Properties and Performance Limits of Organic Field-Effect Transistors. *Science* **1996**, *272*, 1462-1464.

(7) Sirringhaus, H. Device Physics of Solution-Processed Organic Field-Effect Transistors. *Adv. Mater.* **2005**, *17*, 2411-2425.

(8) Thomas, S. W.; Joly, G. D.; Swager, T. M. Chemical Sensors Based on Amplifying Fluorescent Conjugated Polymers. *Chem. Rev.* **2007**, *107*, 1339-1386.

(9) Duarte, A.; Pu, K. Y.; Liu, B.; Bazan, G. C. Recent Advances in Conjugated Polyelectrolytes for Emerging Optoelectronic Applications. *Chem. Mater.* **2011**, *23*, 501-515.

(10) Cui, Q.; Bazan, G. C. Narrow Band Gap Conjugated Polyelectrolytes. *Acc. Chem. Res*. **2018**, *51*, 202-211.

(11) Padvi, M. N.; Moholkar, A. V.; Prasad, S. R.; Prasad N. R. A Critical Review on Design and Development of Gas Sensing Materials. *Eng. Sci*., **2021**, *15*, 20-37.

(12) Lin. P.; Yan, F. Organic Thin-Film Transistors for Chemical and Biological Sensing. *Adv. Mater.* **2012**, *24*, 34-51.

(13) Fan, L. J.; Zhang, Y.; Murphy, C. B.; Angell, S. E.; Parker, M. F.; Flynn, B. R.; Jones Jr, W. E. Fluorescent Conjugated Polymer Molecular Wire Chemosensors for Transition Metal Ion Recognition and Signaling. *Coordination Chemistry Reviews* **2009,** *253*,410-422.

(14) Zhu, C.; Liu, L.; Yang, Q.; Lv, F.; Wang, S. Water-Soluble Conjugated Polymers for Imaging, Diagnosis, and Therapy. *Chem. Rev.* **2012**, *112*, 4687-4735.

(15) Gopalan, A-I.; Komathi, S.; Muthuchamy, N.; Lee, K-P.; Whitcombe, M.J.; Dhana, L.; Anand, G. S. Functionalized Conjugated Polymers for Sensing and Molecular Imprinting Applications. *Prog. Polym. Sci.* **2019**, *88*, 1-29.

(16) Liu, Y.; Ogawa, K.; Schanze, K. S. Conjugated Polyelectrolytes as Fluorescent Sensors. *Photochem. Photobiol. C: Photochem. Rev.* **2009**, *10*, 173-190.

(17) Swager, T.M. The Molecular Wire Approach to Sensory Signal Amplification**.** *Acc. Chem. Res.* **1998**, *31*, 201-207.

(18) Rochat, S.; Swager, T. M. Conjugated Amplifying Polymers for Optical Sensing Applications. *ACS Appl. Mater. Interfaces* **2013**, *5*, 4488-4502.

(19) Wang, C-H.; Nesterov, E. E. Amplifying Fluorescent Conjugated Polymer Sensor for Singlet Oxygen Detection. *Chem. Commun.* **2019**, *55*, 8955-8958.

(20) Feng, X.; Liu, L.; Wang, S.; Zhu, D. Water-soluble Fluorescent Conjugated Polymers and their Interactions with Biomacromolecules for Sensitive Biosensors. *Chem. Soc. Rev.* **2010**, *39*, 2411-2419.

(21) Chen, X.; Sameer Hussain, S.; Hao, Y.; Tian, X.; Gao, R. Review-Recent Advances of Signal Amplified Smart Conjugated Polymers for Optical Detection on Solid Support. *ECS J. Solid State Sci. Technol.* **2021**, *10*, 037006.

(22) Tan, C; Atas, E.; Muller, J. G.; Pinto, M. R.; Kleiman, V. D.; Schanze, K. S. Amplified Quenching of a Conjugated Polyelectrolyte by Cyanine Dyes. *J. Am. Chem. Soc.* **2004**, *126*, 13685-13694.

(23) Tanwar, A. S.; Meher, N.; Adil, L. R.; Iyer, P. K. Stepwise Elucidation of Fluorescence-based Sensing Mechanisms Considering Picric Acid as a Model Analyte. *Analyst* **2020**, *145*, 4753-4767.

(24) Feng, X.; Tang, Y.; Duan, X.; Liu, L.; Wang, S. Lipid-Modified Conjugated Polymernanoparticles for Cell Imaging and Transfection. *J. Mater. Chem.*, **2010**, *20*, 1312-1316.

(25) Hussain, S.; Malik, A. H.; Afroz, M. A.; Iyer, P. K. Ultrasensitive Detection of Nitroexplosive – Picric Acid *via* a Conjugated Polyelectrolyte in Aqueous Media and Solid Support. *Chem. Commun.*, **2015**, *51*, 7207-7210.

(26) Senthilkumar, T.; Asha, S. K. Selective and Sensitive Sensing of Free Bilirubin in Human Serum Using Water-Soluble Polyfluorene as Fluorescent Probe**.** *Macromolecules* **2015**, *48*, 3449-3461.

(27) Li, Z.; Acharya, R.; Wang, S.; Schanze, K. S. Photophysics and Phosphate Fluorescence Sensing by Poly(phenylene ethynylene) Conjugated Polyelectrolytes with Branched Ammonium Side Groups. *J. Mater. Chem. C* **2018**, *6*, 3722-3730.

(28) Feng, L.; Liu, L.; Lv, F.; Bazan, G. C.; Wang, S. Preparation and Biofunctionalization of Multicolor Conjugated Polymer Nanoparticles for Imaging and Detection of Tumor Cells. *Adv. Mater.* **2014**, *26*, 3926-3930.

(29) Xie, D.; Parthasarathy, A.; Schanze, K. S. Aggregation-Induced Amplified Quenching in Conjugated Polyelectrolytes with Interrupted Conjugation. *Langmuir* **2011**, *27*, 11732-11736.

(30) An, L.; Tang, Y.; Feng, F.; He, F.; Wang, S. Water-Soluble Conjugated Polymers for Continuous and Sensitive Fluorescence Assays for Phosphatase And Peptidase. *J. Mater. Chem.*, **2007**, *17*, 4147-4152.

(31) Dong, W.; Fei, T.; Palma-Cando A.; Scherf, U. Aggregation Induced Emission and Amplified Explosive Detection of Tetraphenylethylene-Substituted Polycarbazoles. *Polym. Chem.* **2014**, *5*, 4048-4053.

(32) Jo, S.; Kim, D.; Son, S. H.; Kim, Y.; Lee, T. S. Conjugated Poly(fluorene-quinoxaline) for Fluorescence Imaging and Chemical Detection of Nerve Agents with Its Paper-Based Strip. *ACS Appl. Mater. Interfaces* **2014**, *6*, 1330-1336.

(33) Zhao, Y.-J.; Miao, K.; Zhu, Z.; Fan, L-. J. Fluorescent Light-Up Detection of Amine Vapors Based on Aggregation-Induced Emission. *ACS Sens.* **2017**, *2*, 842-847.

(34) Cui, Q.; Yang, Y.; Yao, C.; Liu, R.; Li, L. Aggregation-Induced Energy Transfer of Conjugated Polymer Materials for ATP Sensing. *ACS Appl. Mater. Interfaces* **2016**, *8*, 35578-35586.

(35) Yuan, H.; Liu, Z.; Liu, L.; Lv, F.; Wang, Y.; Wang, S. Cationic Conjugated Polymers for Discrimination of Microbial Pathogens. *Adv. Mater.* **2014**, *26*, 4333-4338.

(36) Zhang, X.; Zhao, Q.; Li, Y.; Duan, X.; Tang, Y. Multifunctional Probe Based on Cationic Conjugated Polymers for Nitroreductase-Related Analysis: Sensing, Hypoxia Diagnosis, and Imaging. *Anal. Chem.* **2017**, *89*, 5503-5510.

(37) Malik, A. H.; Iyer, P. K. Conjugated Polyelectrolyte Based Sensitive Detection and Removal of Antibiotics Tetracycline from Water. *ACS Appl. Mater. Interfaces* **2017**, *9*, 4433-4439.

(38) Zhang, C.; Chen, P.; Hu, W. Organic Field-Effect Transistor-Based Gas Sensors. *Chem. Soc. Rev.* **2015**, *44*, 2087-2107.

(39) Leclerc, M. Optical and Electrochemical Transducers Based on Functionalized Conjugated Polymers. *Adv. Mater.* **1999**, *11*, 1491-1498.

(40) Li, H.; Shi, W.; Song, J.; Jang, H-J.; Dailey, J.; Yu, J.; Katz, H. E. Chemical and Biomolecule Sensing with Organic Field-Effect Transistors. *Chem. Rev.* **2019**, *119*, 3-35.

(41) Koo, W-T. K.; Kim, Y.; Savagatrup, S.; Yoon, B.; Jeon, I.; Choi, S-J.; Kim, I-D.; Swager, T. M. Porous Ion Exchange Polymer Matrix for Ultrasmall Au Nanoparticle-Decorated Carbon Nanotube Chemiresistors. *Chem. Mater.* **2019**, *31*, 5413-5420.

(42) Roberts, M. E.; Sokolov, A. N.; Bao, Z. Material And Device Considerations for Organic Thin-Film Transistor Sensors. *J. Mater. Chem.* **2009**, *19*, 3351–3363.

(43) Sugiyasu, K.; Swager, T. M. Conducting-Polymer-Based Chemical Sensors: Transduction Mechanisms. *Bull. Chem. Soc. Jpn.* **2007**, 80, 2074-2083.

(44) Janata, J.; Josowicz, M. Conducting Polymers in Electronic Chemical Sensors. *Nature Mater* **2003**, *2*, 19–24.

(45) Malik, A. H.; Hussain, S.; Kalita, A.; Iyer, P. K. Conjugated Polymer Nanoparticles for the Amplified Detection of Nitro-explosive Picric Acid on Multiple Platforms. *ACS Appl. Mater. Inter.* **2015**, *7*, 26968-26976.

(46) Kalita, A.; Hussain, S.; Malik, A. H.; Subbarao, N. V. V.; Iyer, P. K. Vapor Phase Sensing of Ammonia at the sub-ppm Level using a Perylene Diimide Thin Film Device. *J. Mater. Chem. C* **2015**, *3*, 10767-10774**.**

(47) Torsi, L.; Magliulo, M.; Manoli, K.; Palazzo, G. Organic Field-Effect Transistor Sensors: A Tutorial Review. *Chem. Soc. Rev.* **2013**, *42*, 8612-8628.

(48) Kalita, A.; Hussain, S.; Malik, A. H.; Barman, U.; Goswami, N.; Iyer, P. K. Anion-Exchange Induced Strong π–π Interactions in Single Crystalline Naphthalene Diimide for Nitroexplosive Sensing: An Electronic Prototype for Visual on- Site Detection**.** A*CS Appl. Mater. Interfaces* **2016**, *8*, 25326-25336.

(49) Ngai, J. H. L.; Gao, X.; Kumar, P.; Polena, J.; Li, Y. A Highly Stable Diketopyrrolopyrrole (DPP) Polymer for Chemiresistive Sensors. *Adv. Electron. Mater.* **2021**, *7*, 2000935.

(50) Wang, F.; Gu, H.; Swager, T. M. Carbon Nanotube/Polythiophene Chemiresistive Sensors for Chemical Warfare Agents. *J. Am. Chem. Soc.* **2008**, *130*, 5392-5393.

(51) Park, H.; Kim, D-H.; Ma, B. S.; Shin, E.; Kim, Y.; Kim, T-S.; Kim, F. S.; Kim, I-D.; Kim, B. J. High-Performance, Flexible NO_2 Chemiresistors Achieved by Design of Imine-Incorporated n-Type Conjugated Polymers. *Adv. Sci.* **2022**, *9*, 2200270.

(52) Limbu, S.; Stewart, K.; Nightingale, J.; Yan, H.; Balamurugan, C.; Hong, S.; Kim, J.; Lee, K.; Kwon, S.; Kim, J-S. Solid-State Ionic Liquid: Key to Efficient Detection and Discrimination in Organic Semiconductor Gas Sensors. *ACS Appl. Electron. Mater*. **2021**, *3*, 2152-2163.

(53) Yang, Y.; Zhang, G.; Luo, H.; Yao, J.; Liu, Z.; Zhang, D. Highly Sensitive Thin-Film Field-Effect Transistor Sensor for Ammonia with the DPP-Bithiophene Conjugated Polymer Entailing Thermally Cleavable *tert*-Butoxy Groups in the Side Chains. *ACS Appl. Mater. Interfaces* **2016**, *8*, 3635-3643.

Chapter 2

Fluorescence Resonance Energy Transfer-Based Wash-Free Imaging and Antibacterial Application Using a Cationic Conjugated Polyelectrolyte

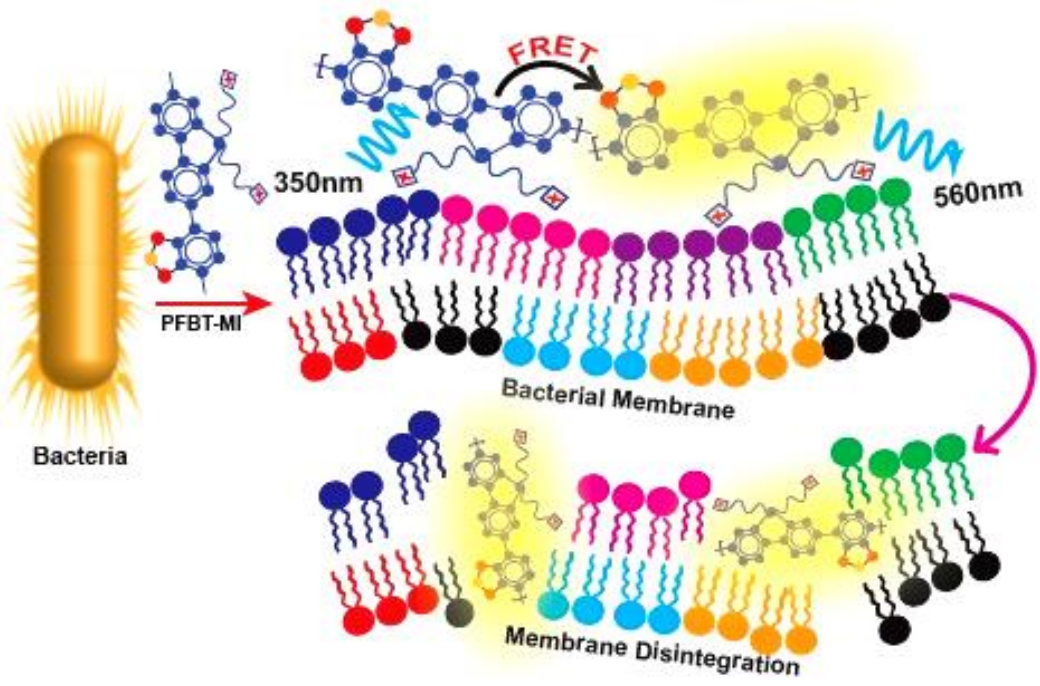

Zehra, N.; Dutta, D.; Malik, A. H.; Ghosh, S. S.; Iyer, P. K. Fluorescence Resonance Energy Transfer-Based Wash-Free Bacterial Imaging and Antibacterial Application Using a Cationic Conjugated Polyelectrolyte *ACS Appl. Mater. Interfaces* **2018**, *10*, 27603-27611.

Abstract

The increase in bacterial infection and antibiotic resistance has posed a severe threat to human health. This threat has warranted an imperative demand for the development of new and effective bactericidal material to eradicate antibiotic-resistant pathogenic bacteria. In this work, we report the wash-free imaging of both Gram-positive (*Staphylococcus aureus*) and Gram-negative (*Escherichia coli*) bacteria using cationic conjugated polyelectrolyte[9,9-bis(6′-methylimidazoliumbromide)hexyl)-fluorene-co-4,7-(2,1,3 benzothiadiazole)] (PFBT-MI) based on aggregation-induced fluorescence resonance energy transfer (FRET). Cationic imidazolium group strapped on the polymer side chain not only increases its solubility in water but also helps in binding with the negatively charged bacterial membrane via electrostatic interactions to turn on its bright yellow emission. The change in the fluorescence color of conjugated polyelectrolyte in presence of bacteria can be easily visualized by naked eye using UV lamp (365 nm). Furthermore, the antibacterial activity of PFBT-MI against *Staphylococcus aureus* and *Escherichia coli* are observed because of the amphiphilic nature of the conjugated polyelectrolyte which in turn is due to the presence of ionic functionality and conjugated polymer backbone that can intercalate very proficiently into the bacterial membrane, which disrupts the membrane integrity and thus results in toxicity. Morphologically, the membrane damage is perceived via FESEM images, which clearly indicated the disruption of cell membrane upon exposure to PFBT-MI. The PFBT-MI acts as an effective antibacterial agent, with an MIC and MBC value of (30 µM or 23.7 µg/mL) and (60 µM or 47.7 µg/mL) for *Staphylococcus aureus* and for *Escherichia coli* (60 µM or 47.7 µg/mL) and (100 µM or 79 µg/mL), respectively. Moreover, PFBT-MI shows less cytotoxicity against mammalian cells at concentration greater than MIC.

2.1 Introduction

In the past few decades, there has been a substantial emergence of bacterial infections which has engrossed attention of researchers owing to their close association with human illness and food security. Moreover, extensive and irrational use of antibiotics has led to the evolution of antibiotic-resistant bacteria that pose acute threat to the global health. Growing resistance of microorganisms towards newly developed drugs is a serious concern that should be addressed rationally.[1-3] A recent report published by Centre for Disease Control and Prevention (CDCP) states that the drug resistant bacteria affects the health of 2 million people annually and by 2050 antibiotic resistance would increase the average number of death to 10 million/year.[4]To address this globally precarious issue, efforts have been devoted by researchers worldwide to design probes with antimicrobial activity such as antibiotics, antimicrobial peptides, hydrogels, and inorganic nanoparticles. [5-14] Despite their individual effectiveness their clinical application remains elusive. Thus, there is urgent need, to develop a simple, sensitive and cost-effective technique for bacterial identification as well as bacterial killing to prevent the bacterial infections as well as outbreak of various epidemic diseases.

Fluorescence-based methods have gained much attention in the field of life sciences and biomedicine and are widely employed for cancer theranostics,[15,16]inflammatory disorders,[17] and antibacterial treatments.[18,19] Researchers have recently designed and used various fluorescent reporters for bacterial imaging and their killing such as nanomaterials (carbon nanotubes, carbon dots (CD), metal and metal oxides nanomaterials) and oligomers.[20] However, there are some challenges associated with them that avert their practical application.[21] For example, CD as a fluorescent probe at times, presents a weak fluorescent signal, unclear, and non-uniform bioimaging due to concentration-dependent aggregation-induced quenching (AIQ).[22] Similarly, the use of antibiotic-capped nanomaterials (Ag, Au, ZnO, MgO, TiO, WS_2) may lead to the growth of drug-resistant bacteria .[23] Recently, more advanced materials have been reported for bacterial identification, discrimination, and killing such as aggregation-induced emission (AIE) luminogens[24-26], conjugated oligomers[27-29] and polymers[30-33]. Among them, conjugated polymers are attractive fluorescence probes for bacterial imaging and killing.

Conjugated polyelectrolytes (CPE's) are organic macromolecules with ionic side chains that endow them with water solubility and facilitate numerous interactions towards

innumerable chemical and biological analytes. CPE's have emerged as outstanding materials in the interdisciplinary areas of optoelectronic devices, chemical, biological and medical science such as sensing, imaging, and theranostics because of their phenomenal attributes such as excellent photostability, high quantum efficiency, super sensitivity, amplified quenching effect and biocompatibility.[34-41] Recently, they have been explored as a novel light-activated antibacterial material with remarkable activity in dark as well. In addition, water-soluble CPEs with cationic head group offer efficient targeting and binding on charged cell membrane of bacteria. Moreover, cationic CPEs mainly target and disintegrate the bacterial cell membrane via electrostatic attraction and insertion into the lipid membrane. As a result of this, the bacterial cell membrane gets physically damaged and hence is difficult to repair. Therefore, restricting the potential development of bacterial resistance.[42-47] Remarkable advantages of using polymers with antibacterial property are their easily tailored structures and desired properties achieved by varying side chain cationic functionality and tuning the bandgap of the conjugated backbone. The former creates a difference in hydrophilic/hydrophobic interactions whereas the latter enhances singlet oxygen generation via increasing triplet state yield.[48]Schanze and co-workers reported a series of CPE's with different backbone structures and side chain functionalities for profound broad spectrum bacteria killing.[31,42,44,45,48-49] Similarly, Wang and co-workers develop a supramolecular approach based on cationic conjugated polymer for rapid discrimination and in-situ detection of pathogens.[50] However bacterial detection relying on a change in emission intensity at a single wavelength may result in various interference such as autofluorescence, instrument fluctuation, and environmental interventions. In this context, a ratiometric technique such as Förster resonance energy transfer (FRET) offers more accurate results and self-calibration by exterminating various environmental and instrument factors thereby opening up a new avenue to design dual-wavelength probes for real-time bacteria monitoring in aqueous media with high sensitivity and low background signal.[51-53] Furthermore, imaging bacteria without tedious wash-free steps is an important component for the success of antibacterial compounds. Wash-free-imaging reduces the time as well as bacterial loss during the bacterial imaging process [24,54] Considering the above challenges we designed a simple, cost-effective, multifunctional approach for efficient bacterial detection in aqueous media, along with wash-free bacterial imaging and also evaluated its antibacterial potential using conjugated polyelectrolyte with the cationic head group.

Herein, we report a water-soluble CPE Poly[9,9-bis(6′-methyl imidazolium bromide)hexyl) fluorene-*co*-4,7-(2,1,3-benzothiadiazole)] (PFBT-MI) for bacterial imaging based on aggregation-induced FRET and explored its antibacterial nature. Decorating the side chains with the imidazolium group provided electrostatic binding sites on the negatively charged bacterial membrane. Taking advantage of the FRET mechanism, the blue emitting polymer PFBT-MI displayed significant color change from blue to yellow as well as changes in its photophysical properties after interaction with bacterial membrane via electrostatic and hydrophilic interaction which resulted in a very convenient wash-free imaging of bacteria, at the same time demonstrating antibacterial activity as well. To the best of our knowledge, no FRET-based theranostics approach using a single fluorophore for wash-free imaging, and antibacterial activity has been reported to date.

2.2 Experimental

2.2.1 Materials and measurements: All the chemicals were purchased from Aldrich, Merck, Ranbaxy (India). Nutrient broth (NB), brain–heart infusion (BHI), Luria–Bertani (LB), and bacterial growth medium were obtained from Himedia.

The ^{1}H NMR (600 and 500 MHz) and ^{13}C NMR (150 and 125 MHz) spectra were collected on Bruker Ascend 600 and Bruker Avance Neo 500 spectrometers, respectively. GPC chromatogram was recorded on Waters Corporation, USA. Absorption and emission spectra were recorded on a Perkin Elmer Lambda-25 and Horiba Fluoromax-4 spectrofluorometer using 10 mm path length quartz curettes with a slit width of 3 nm at 298 K. Milli-Q water was used during experiments. Fluorescence lifetime studies were performed on Edinburgh Life Spec II instrument. Zeta sizer Nano ZS90, Model No. ZEN3690, Malvern was used to perform DLS based size and charge measurements. Morphological changes before and after incubation of Gram-positive and Gram-negative bacteria with PFBT-MI were observed with a Zeiss sigma field emission scanning electron microscope (FESEM) at an accelerating voltage of 2 kV.

2.2.2 Synthetic procedure

2.2.2a Synthesis of 2, 7-dibromo-9, 9-bis (6-bromohexyl)-9H-fluorene, M1:

The monomer M1 was prepared using the reported procedure.[55] 2, 7-dibromofluorene (1 g, 3.08 mmol), tetra butyl ammonium iodide (114 mg, 10 mol%) were placed in 50 mL round bottom flask. The mixture was degassed and 50% sodium hydroxide aq. the solution was added. The reaction vessel was then subjected to the freeze-thaw cycle for three times,

followed by addition of 1,6-Dibromohexane (4.5 g, 18.5 mmol). The mixture was stirred and heated at 70 ºC for 4h.

The reaction mixture was allowed to cool at room temperature and washed three times with chloroform/water. The resulting solution was concentrated under vacuum, followed by purification by silica gel column chromatography to obtain the pure product as colorless crystals (Yield=1.4 g, 70%).

^{1}H NMR (600 MHz, $CDCl_3$ δ ppm): 7.52 (d, 2H), 7.43 (dd, 4H), 3.29 (t, 4H), 1.92 (t, 4H), 1.69-1.64 (m, 4H), 1.22-1.17 (m, 4H), 1.11-1.06 (m, 4H), 0.61-0.55 (m, 4H).

^{13}C NMR (150 MHz, $CDCl_3$, δ ppm): 152.18, 139.09, 130.35, 126.10, 121.59, 121.26, 55.57, 40.07, 33.93, 32.63, 28.97, 27.78, 23.47.

2.2.2b Synthesis of 2,7-Bis[9,9′-bis(6″-bromohexyl) fluorenyl]-4,4,5,5-tetramethyl [1.3.2] dioxaborolane, M2: Monomer M1 (500 mg, 7.7 mmol), bis(pinacolato)diborane (292.4 mg, 23.1 mmol), potassium acetate (528.22 mg, 53.9 mmol) and dry dioxane (15 mL) were placed in 50ml round bottom flask under inert atmosphere. Afterward, catalyst $Pd(dppf)_2Cl_2$ (56.63 mg, 0.7 mmol) was introduced into flask and reaction mixture was refluxed overnight under inert atmosphere. The reaction mixture was then cooled and concentrated by rotary evaporation and residual solid was washed with dichloromethane and water thrice. The residue was purified by column chromatography using 4:1 hexane/ethyl acetate as eluent to yield M2 as white solid (350 mg, 61 %).

^{1}H NMR (600 MHz, $CDCl_3$, δ ppm): 7.80 (d, 2H), 7.73 (dd, 4H), 3.25 (t,4H), 2.02-1.99 (m,4H), 1.65-1.59(m,4H), 1.39 (s, 24H), 1.18-1.12 (m, 4H), 1.07-1.01 (m, 4H), 0.58-0.52 (m, 4H).

^{13}C NMR (150 MHz, $CDCl_3$, δ ppm): 150.10, 143.92, 133.82, 128.78, 119.49, 83.80, 55.07, 39.94, 33.94, 32.67, 29.71, 28.97, 27.74, 25.04, 24.97, 23.39

2.2.2c Synthesis of Poly[9,9-bis(6'-bromohexyl)fluorene-co-4,7-(2,1,3-benzothiadiazole)], PFBT: The monomer M1 (78 mg, 0.12 mmol), M2 (150 mg, 0.2 mmol), 4,7-dibromo-2,1,3-benzothiadiazole M3 (24 mg, 0.08 mmol), catalyst $[Pd(PPh_3)_4]$ (12mg) and K_2CO_3 (2M) were taken in 50ml RB fitted with condenser under argon. A water: THF (1:3) mixture was then added to the flask and degassed thrice via free thraw cycle to remove traces of oxygen. The reaction mixture was refluxed at 80 ºC for 36 h and extracted with chloroform. The resulting mixture was concentrated under vacuum followed by reprecipitation in methanol to get the dark brown coloured solid product (115 mg, 73%)

^{1}H NMR (500 MHz, $CDCl_3$, δ ppm): 8.06-8.04 (b, 0.5H), 7.95-7.86 (b, 2H), 7.72-7.68 (b, 4H), 3.31 (b, 4H), 2.16-2.04 (b, 4H), 1.71-1.68 (b, 4H), 1.28-1.26 (b, 8H), 1.18 (b, 4H), 0.88-0.84 (b, 4H).

GPC in THF, polystyrene standard: Mw= 2.93 × 10^4, PDI-1.28.

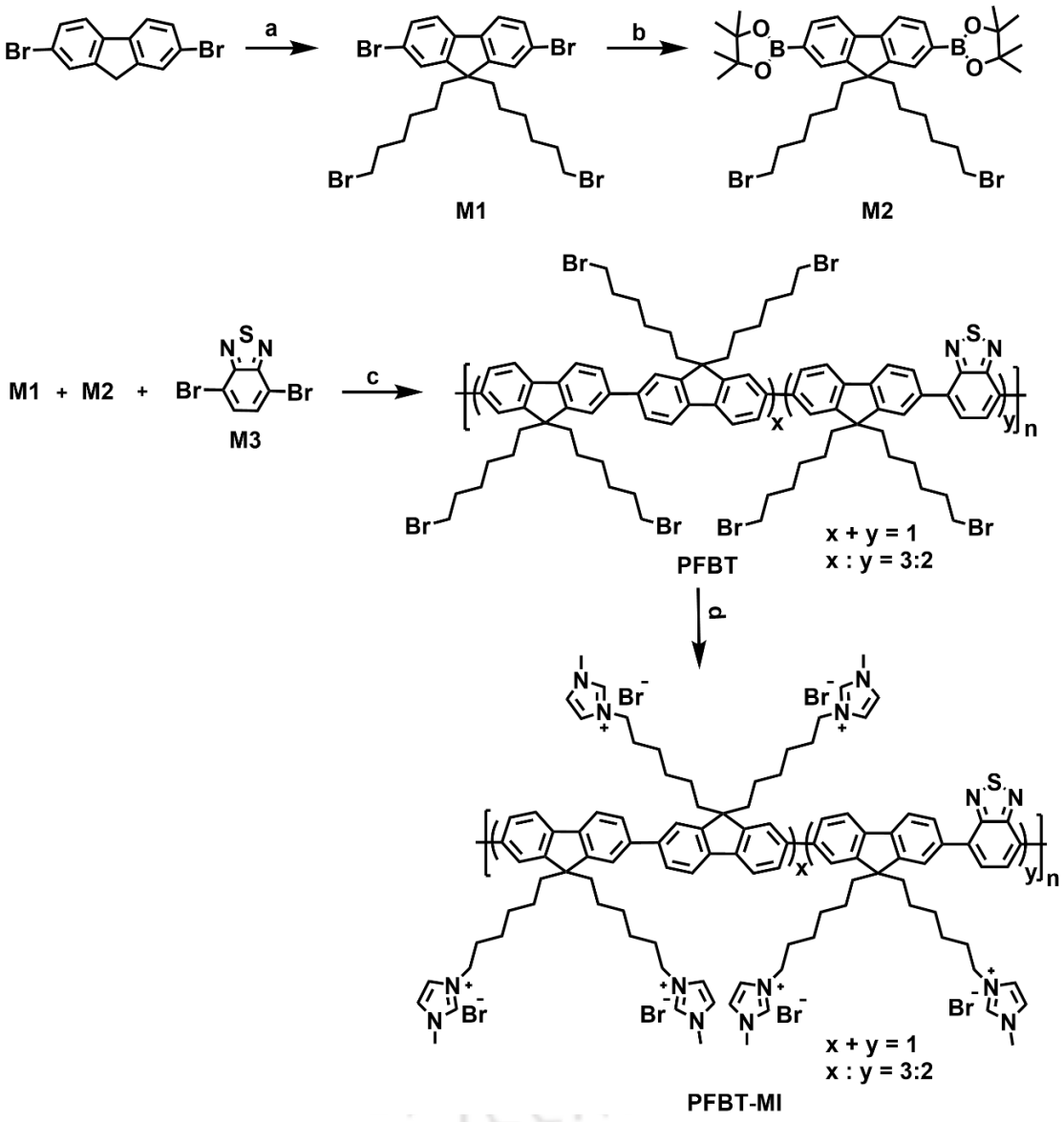

Scheme 2.1: Synthesis of PFBT-MI (a) 1,6-Dibromohexane, TBAI, 50% aq. NaOH, 70 °C, 4 h; (b) bis(pinacolato)diborane, KOAc, [Pd(dppf)Cl_2], dioxane, 85 °C, 24 h; (c)Pd(PPh_3)$_4$, 2M K_2CO_3 (aq), THF, reflux, 36 h; (d) 1-methyl imidazole, reflux, 24 h.

2.2.2d Synthesis of Poly [9,9-bis(6'-methyl imidazolium bromide)hexyl)fluorene-co-4,7-(2,1,3 benzothiadiazole)], PFBT-MI: A 25 ml round bottom flask was charged with polymer P1 (0.05 g, 0.031 mmol) in 2 mL of 1-methyl imidazole (excess) and was refluxed at 80 °C overnight. The reaction mixture was then poured into excess of chloroform to

afford yellow precipitate. The precipitate was redissolved in methanol and reprecipitated in chloroform 3 times and the final polymer PFBT-MI was obtained as yellow solid (43 g, 69%).

^{1}H NMR (600 MHz, CD_3OD-d4, δ ppm): 8.23-7.52 (b, 12.5H), 4.09 (b, 4H), 3.89 (b, 6H), 2.26-2.05 (b, 4H), 1.72 (b, 4H), 1.17 (b, 8H), 0.74 (b, 4H).

2.2.3 Imaging and detection of bacteria: For imaging, bacteria (10^8 CFU/mL) were treated with the polymer at the MIC concentration and incubated for 10min at 37 °C. After the treatment the bacteria was centrifuged at 10000 rpm for 1 min and dispersed in water. The samples were then drop casted on glass slides and sealed after mounting the cover slip. The samples were then observed under a Zeiss LSM 880 confocal microscope (405 nm excitation).

The stock solution for detection consists of 1mM of PFBT-MI was prepared in Milli-Q water. The bacteria (Gram-positive *Enterococcus faecalis* MTCC 439, *Staphylococcus aureus* MTCC96, *Bacillus subtilis* MTCC 1305 and Gram-negative *Pseudomonas aeruginosa* MTCC 2488, *Escherichia coli* MTCC 433, *Enterobacter aerogenes* MTCC 2822, *Escherichia coli* DH5α) were serially diluted (10^{-1}, 10^{-2}, 10^{-3} and 10^{-4}) and the fluorescence spectra of PFBT-MI were monitored by adding 1mL each of above mentioned serially diluted bacterial suspensions into the glass cuvette containing (0.3μM) solution. *Bacillus subtilis, Pseudomonas aeruginosa, Escherichia coli* 433 and *Enterobacter aerogenes* were grown in NB media at 37 °C for 12 h at 180 rpm. *Staphylococcus aureus, Enterococcus faecalis* was grown in BHI at 37 °C for 12 h at 180 rpm. *Escherichia coli DH5α* was grown in LB at 37 °C for 12 h at 180 rpm.

2.2.4 Antibacterial activity: In order to carry out assessment of antibacterial activity Gram positive bacteria (*Enterococcus faecalis* MTCC 439, *Staphylococcus aureus* MTCC 96, *Bacillus subtilis* MTCC 1305) and Gram-negative bacteria (*Pseudomonas aeruginosa* MTCC 2488, *Escherichia coli* MTCC 433, *Enterobacter aerogenes* MTCC 2822, *Escherichia coli* DH5α) were used. *Bacillus subtilis, Pseudomonas aeruginosa, Escherichia coli 433 and Enterobacter aerogenes* were grown in NB media at 37 °C for 12 h at 180 rpm. *Staphylococcus aureus, Enterococcus faecalis* was grown in BHI at 37 °C for 12 h at 180 rpm. *Escherichia coli* DH5αwas grown in LB at 37 °C for 12 h at 180 rpm. The bacteria (10^8 CFU/mol) were treated with different concentrations of the polymer (0.01mMor 10μM to 0.2mMor 200μM) for 12 hr. The minimum concentration where there

was no visual turbidity observed was taken as the MIC (minimum inhibitory concentration) value of the polymer. In order to determine the MBC (minimum bactericidal concentration), the treated bacterial cultures that did not show visual turbidity were re-inoculated in fresh media. MBC was taken as the minimum concentration that was bactericidal. The growth was monitored by recording the OD at 595 nm using the UV-visible spectrophotometer (Jasco V-630).

2.2.5 Protein leakage analysis: A standard Bradford assay was performed for both control and treated cells. In brief, *Escherichia coli* and *Staphylococcus aureus* cells were treated with MIC dose of polymer for 6 h at 37 °C. After centrifugation (6000 rpm for 15 min) supernatant was collected and to each 200 µl of the supernatant, 800 µl of the Bradford reagent was added. The optical density was measured at 595 nm after incubation in the dark for 10 min. Also, the absorbance of the supernatant was measured at 280 nm for protein (before adding Bradford).[56]

2.2.6 Nucleic acid leakage analysis: In brief, *Escherichia coli* and *Staphylococcus aureus* cells were treated with MIC dose of polymer for 6 h at 37 °C. After centrifugation (6000 rpm for 15 min) supernatant was collected and the absorbance of the supernatant was measured at 260 nm.[57]

2.2.7 Cell Culture: For cell culture studies, HEK 293T (human embryonic kidney) cells were procured from National Centre for Cell Sciences, Pune, India. For culturing cells, Dulbecco's modified Eagle's medium, supplemented with streptomycin (50 mg/mL), L-glutamine (4 mM), penicillin (50 units/mL), and 10% (v/v) fetal bovine serum (FBS; PAA Laboratories, Austria) was used and the cells were maintained in a 5% CO_2 humidified incubator at 37 °C.

2.2.8 MTT Assay: For evaluation of the cell viability, 1×10^4 HEK cells/well were seeded in a 96-well plate and cultured overnight at 37 °C in a 5% CO_2 incubator. The cells were treated with different concentrations of PBFT-MI for 12 h, followed by 3-(4,5-dimethylthiazolyl-2)-2,5-diphenyltetrazolium bromide (MTT) assay. MTT is reduced by living cells (mitochondria) into a colored formazan product. Thereafter, the absorbance at 570 nm is recorded which relates to the number of live or viable cells. The absorbance at 690 nm was subtracted a background interference. The percent of cell viability was calculated as

$$\% \text{ viable cell} = \frac{(\text{A570} - \text{A690})\text{of treated cells}}{(\text{A570} - \text{A690})\text{of control cells}} \times 100$$

2.3 Result and discussion

2.3.1 Synthesis and characterization of polymer PFBT-MI

The synthetic route of Poly[9,9-bis(6′-methylimidazoliumbromide)hexyl)-fluorene-co-4,7-(2,1,3-benzothiadiazole)] (PFBT-MI) is illustrated in **Scheme 2.1.** The neutral conjugated polymer PFBT was synthesized via Suzuki coupling reaction using fluorene as the donor and incorporating 20 mol% of benzothiadiazole as acceptor. The PFBT was then post-functionalized with N-methylimidazole to obtain cationic conjugated polyelectrolyte PFBT-MI (**Figure A2.1-2.7**). The cationic imidazolium group endows PFBT-MI with good solubility in a polar solvent like water, dimethyl sulfoxide, methanol and helps in binding with the negatively charged bacterial membrane. The zeta potential of PFBT-MI is found to be 15 mV (**Figure A2.8**). The PFBT-MI displays maximum absorption at 350 nm and a weak band ranging from 415-530 nm characteristic of fluorene and benzothiadiazole unit respectively. The emission spectra of PFBT-MI exhibit a strong fluorescence emission peak at 410 nm (ex. 350 nm) for fluorene unit (**Figure 2.1a**) and a weak emission band ranging from 520-560 nm (**Figure 2.1b**) corresponding to benzothiadiazole moiety, which indicates that PFBT-MI exhibits weak intra-chain FRET in dilute solution or non-aggregated state.

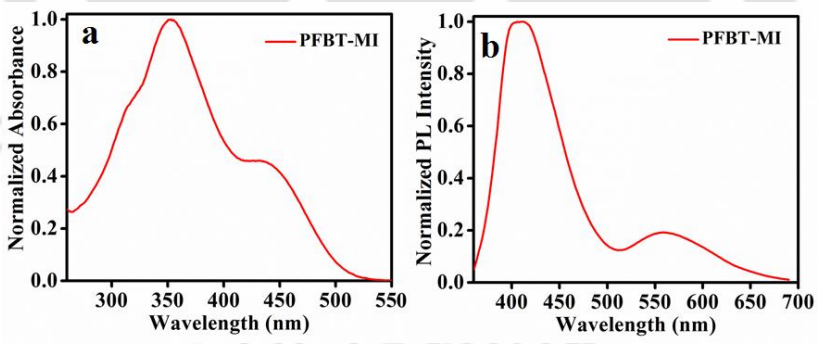

Figure 2.1: (a) UV-vis and **(b)** Fluorescence spectra of PFBT-MI in water.

The molecular state of PFBT-MI in water (good solvent) was studied by DLS that presents an observed distribution of ~12 nm which can be assigned to the hydrodynamic diameter of a single polymer chain. As the fraction of THF increased from 0 to 90%, the polymer chain starts to form large aggregates (**Figure 2.2a-e)**. This unimolecular state of polymer in water explains the presence of weak FRET efficiency from fluorene to the BT unit since inter-chain FRET is negligible as the molar ratio of the acceptor to donor moiety is low.

The initial emission peak at 560nm is increased gradually on adding increasing fraction of THF (poor solvent) to the PFBT-MI in water (**Figure 2.3a-b**). Interestingly, the colour of the solution changed from blue to yellow in water and water-THF mixture respectively that could be realized by the naked eye and under UV-light (lamp excitation-365 nm) (Inset of **Figure 2.3b**). The change in colour of PFBT-MI in water upon introducing the increasing fraction of THF indicates the appearance of an efficient inter-molecular FRET from fluorene (donor) to BT (acceptor) units of the polymer due to polymeric chain's self-aggregation which increases the local concentration of BT units.

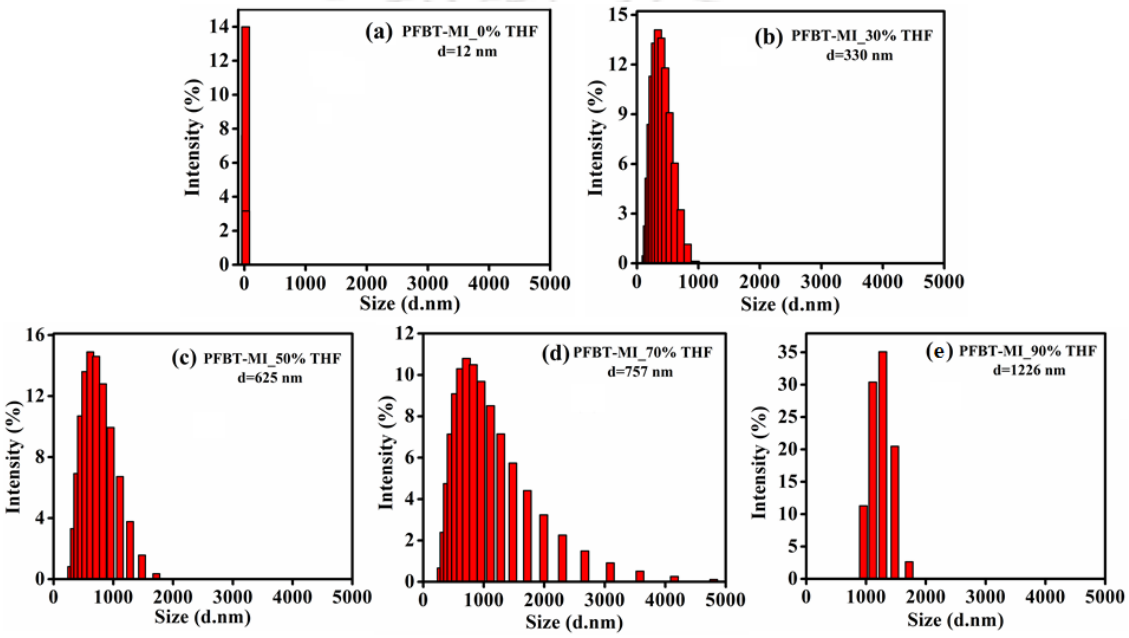

Figure 2.2: Aggregation study of PFBT-MI in (a) water and (b-d) water THF mixture.

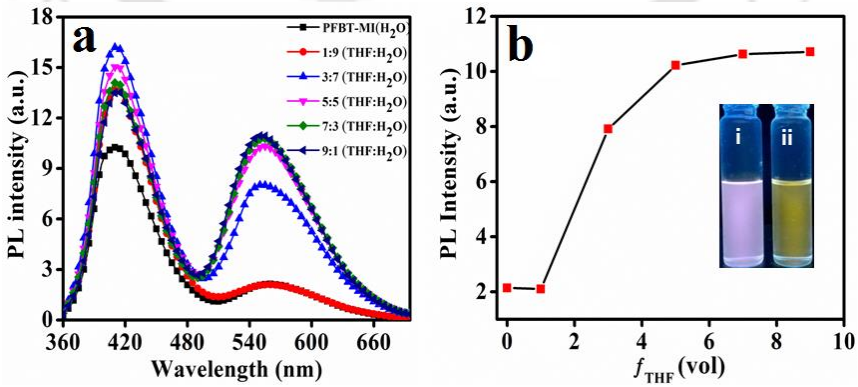

Figure 2.3: (a) Fluorescence emission spectra of PFBT-MI (10μM) with varying fraction of THF in water and **(b)** its corresponding plot showing the variation of emission intensity at 560 nm with increasing fraction of THF. Inset: Colour change of PFBT-MI in **(i)** water (blue) and **(ii)** water THF mixture (yellow).

Furthermore, there is a spectral overlap between the emission of the donor (fluorene) and absorption of the acceptor (BT), which is a prerequisite for the phenomenon of FRET to occur (**Figure 2.4a**). To confirm the phenomenon of FRET, the lifetime of the conjugated polyelectrolyte in water and water-THF mixture was examined and the decay curves for PFBT-MI at 410 nm and 560 nm has been fitted mono-exponentially and bi-exponentially respectively (**Figure A2.9**). Upon exciting by a laser pulse of 375 nm, the decay monitored for PFBT-MI at 410 nm in pure water (0.743 ns) shows a reduction in the lifetime after introducing a fraction of THF (0.636) (**Figure 2.4b**). Whereas the average lifetime of PFBT-MI observed at 560 nm in water THF mixture (2.63 ns) increases as compared to the polymer solution in pure water (0.29) (**Figure 2.4c**). Thus, the above investigation explains the occurrence of FRET from fluorene unit to BT moiety with the help of aggregation induced by increasing the fraction of poor solvent into a good solvent.

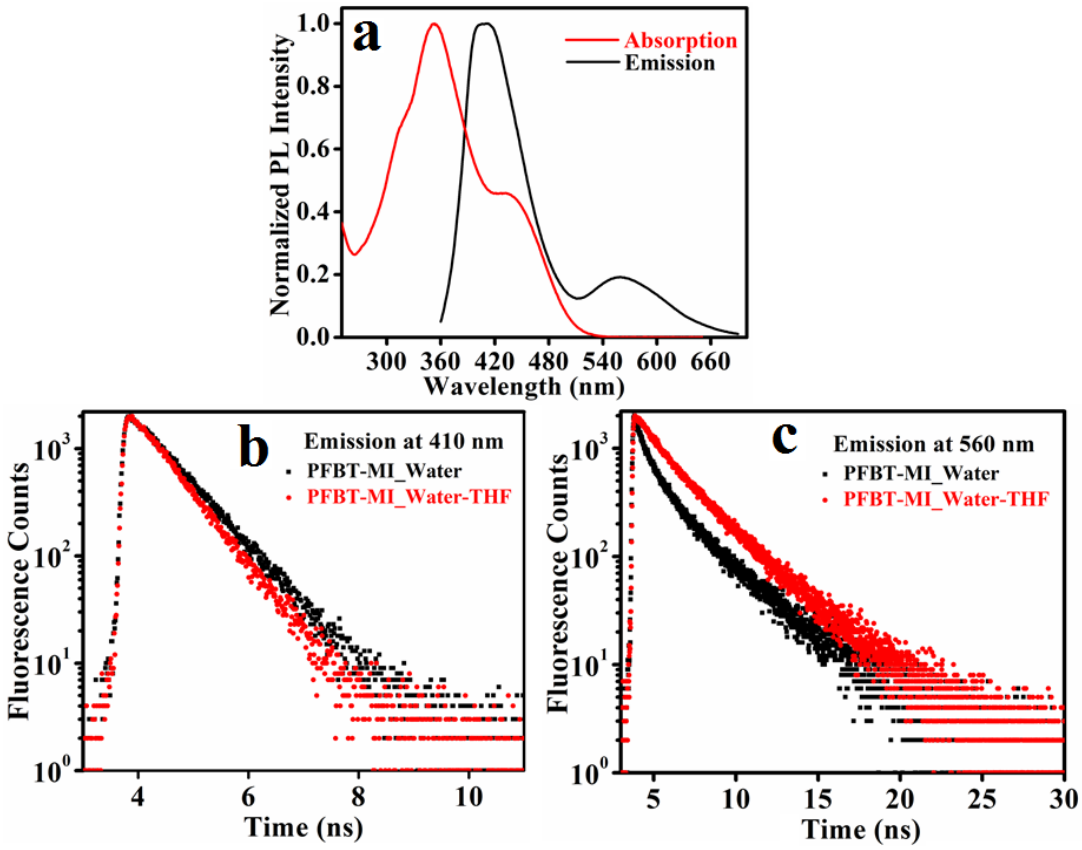

Figure 2.4: (a) Spectral overlap between emission of fluorene unit with the absorption of BT unit of PFBT-MI (10µM) in water. Time resolved photoluminescence of PFBT-MI (10µM) in water and water THF mixture observed at **(b)** 410 nm and **(c)** 560 nm using a laser excitation of 375 nm.

2.3.2 Imaging and Sensing of Bacteria

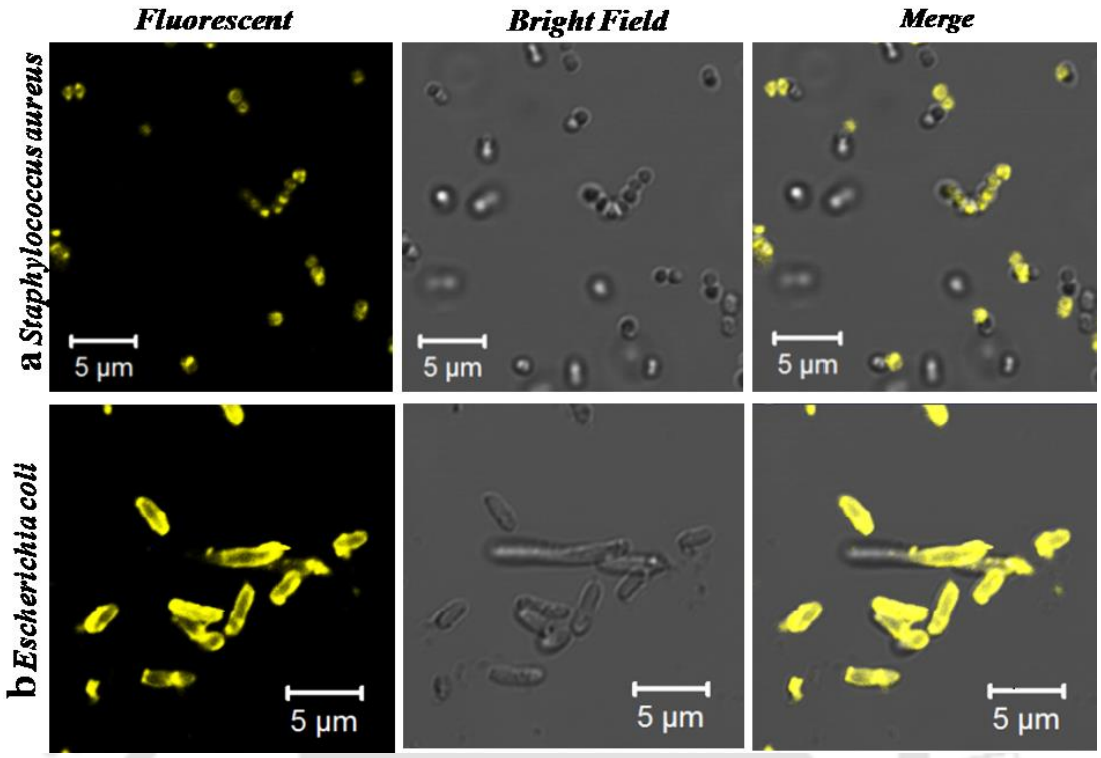

Figure 2.5: Confocal laser scanning fluorescence images (live) of **(a)** *Staphylococcus aureus* and **(b)** *Escherichia coli* after incubated with 10 mM of PFBT-MI for 10 min at 37°C.

To check the practicability of PFBT-MI for visualization of bacteria live confocal laser scanning microscopy (CLSM) is performed (**Figure 2.5a-b**). PFBT-MI successfully stained both Gram-positive bacteria and Gram-negative bacteria after incubation with 10 × 10^{-6} M of PFBT-MI for 10 min. The unbound PFBT-MI does not emit in the yellow channel (560 nm) which, as a unique outcome, prominently eliminates the background emission while as the polymer chains get attached to the bacterial membrane, it turns on the bright yellow emission. Adhesion of PFBT-MI to the bacterial membrane via electrostatic interactions between the cationic PFBT-MI and the negatively charged bacterial surface as well as the lyophilic interactions between PFBT-MI backbone and lipid membrane of the bacteria increases the concentration of the polymer on the bacterial membrane. Consequently, there is an increase in the local concentration of the acceptor moiety of the polymer around the donor units, which results in the efficient FRET from the fluorene (donor) to BT (acceptor) units thus PFBT-MI emits in the yellow channel. Using this easy approach, the bacteria could be visualized without involving any washing process via the

phenomenon of FRET thus, preventing loss of bacteria during washing and simplifying the process of imaging rapidly.

To gain further insight into bacterial quantification, the fluorescence response of PFBT-MI with different bacterial strains was recorded in aqueous media (HEPES buffer 10mM pH 7.4). The fluorescence emission signals are measured by adding serially diluted bacterial suspension (1mL) into the glass cuvette containing PFBT-MI (0.3 µM) solution. Initially, PFBT-MI solution emits at 410 nm (λ_{ex} 350 nm) and no significant peak appears in the higher wavelength region. Upon adding bacterial strains to the PFBT-MI solution, a new peak is observed at 560 nm while the diminishing of a peak at 410 nm reflects the process of energy transfer from the donor fluorene to the acceptor benzathiadiazole unit. This shift in the emission peak of PFBT-MI solution from 410 nm to 560 nm is evident from the colour change of the polymer solution observed on irradiating UV-light (lamp excitation 365 nm) upon adding bacteria as shown in **Figure 2.6a**. Furthermore, the FRET ratio I-Io/Io (where I= $I_{560}/I_{410}$for different bacterial strains and Io= I_{560}/I_{410} for the PFBT-MI only) of the polymer for different bacterial strain is calculated as shown in **Figure 2.6b.** It is observed that different signal responses are obtained with different strains of the same bacterial species although having the same charge, possibly because each strain possesses specific surface structures. This method thereby provides a simple, rapid technique for determining the presence of bacteria in a sample. The minimum concentration of bacteria that is able to shift the emission from blue to yellowish green is ~10^4 CFU/mL.

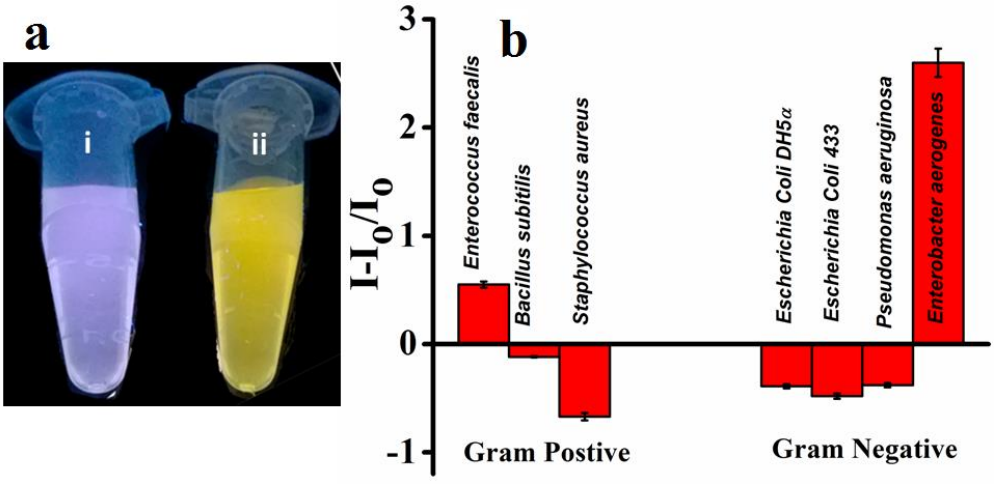

Figure 2.6: (a) Colour of PFBT-MI (0.3 µM) solution from **(i)** blue to **(ii)** yellow upon adding bacterial strain (10^{-1}). **(b)** FRET ratio of PFBT-MI (0.3 µM) with different bacterial strain.

2.3.3 Antibacterial Activity

The antibacterial activity of PFBT-MI is examined against both the *Staphylococcus aureus* and *Escherichia coli* as a representative of Gram-positive and Gram-negative bacteria respectively. The MIC and corresponding MBC value of polymer PFBT-MI for *Staphylococcus aureus* are (30µM or 23.7µg/mL) and (60µM or 47.7µg/mL) and for *Escherichia coli* are (60µM or47.7µg/mL) and (100µM or 79µg/mL), respectively (**Figure 2.7a-b & Table 2.1**). The growth curve was monitored up to 12 h. It was observed that the growth was inhibited at MIC concentration and no growth was observed in case of MBC (**Figure 2.8a-b)**. Furthermore, when compared to earlier reports the observed MIC values for the antibacterial polymer in the present context are much lower (**Table A2.1)**.

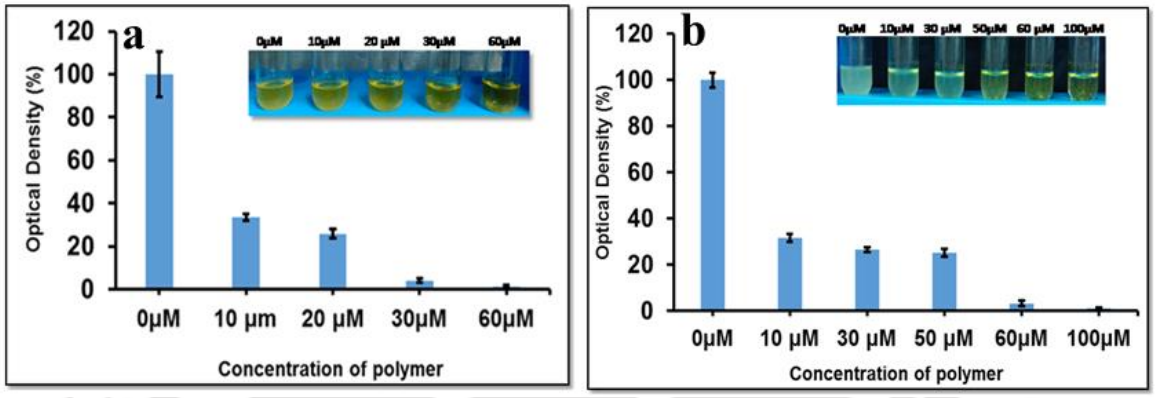

Figure 2.7: The Optical Density vs Concentration plot for (a) *Staphylococcus aureus* and (b) *Escherichia coli* treated with different concentrations of PFBT_MI (0µM, 10µM, 30µM, 50µM, 60µM, 100µM). Inset: (a) *Staphylococcus aureus and (b) Escherichia coli* treated with different concentrations of polymer from left to right. Clear solutions include no cell growth.

Table 2.1: MIC and MBC values of polymer PFBT-MI against *Staphylococcus aureus and Escherichia coli.*

Bacteria	**MIC (µg/mL)**	**MBC (µg/mL)**
Escherichia coli	47.7	79
Staphylococcus aureus	23.7	47.7

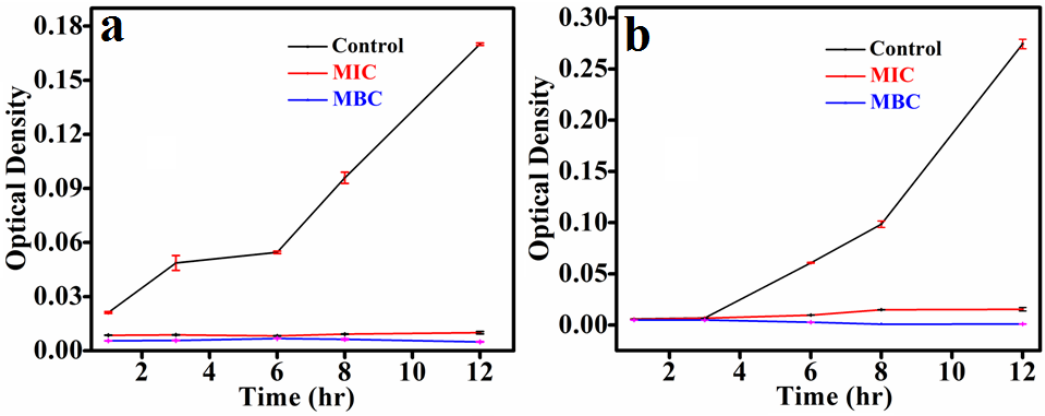

Figure 2.8: Growth curves of **(a)** *Staphylococcus aureus* and **(b)** *Escherichia coli* incubated with different concentration of PFBT-MI.

To validate the killing efficiency of PFBT-MI, the plating experiment was performed. Control samples lacking PFBT-MI have dense bacterial growth as shown in **Figure A2.10**. The growth of *Staphylococcus aureus* and *Escherichia coli* are appreciably suppressed on the treatment of these samples with polymer at respective MIC concentrations. However, at MBC concentrations of polymer, complete inhibition of bacterial growth is observed.

2.3.4 Mechanism of antibacterial activity

To investigate the mechanism of antibacterial activity of PFBT-MI, morphological changes of *Staphylococcus aureus* and *Escherichia coli* as models for Gram-positive and Gram-negative are examined before and after the treatment of conjugated polyelectrolyte by FESEM imaging at their respective MIC concentrations. For the control population of both (Escherichia coli and Staphylococcus aureus), the cell surface morphology appeared smooth and regular with clear edges indicating a viable state of the bacteria. On the other hand, in case of treated bacteria disintegration of the cell membrane was observed. It is concluded from FESEM results that PFBT-MI successfully caused bacterial cell death by disruption of the cell membrane as shown in **Figure 2.9 & 2.10.** It has been previously reported that imidazolium molecules and polymers can exhibit antibacterial activity towards Gram-positive and Gram-negative bacteria.[49]

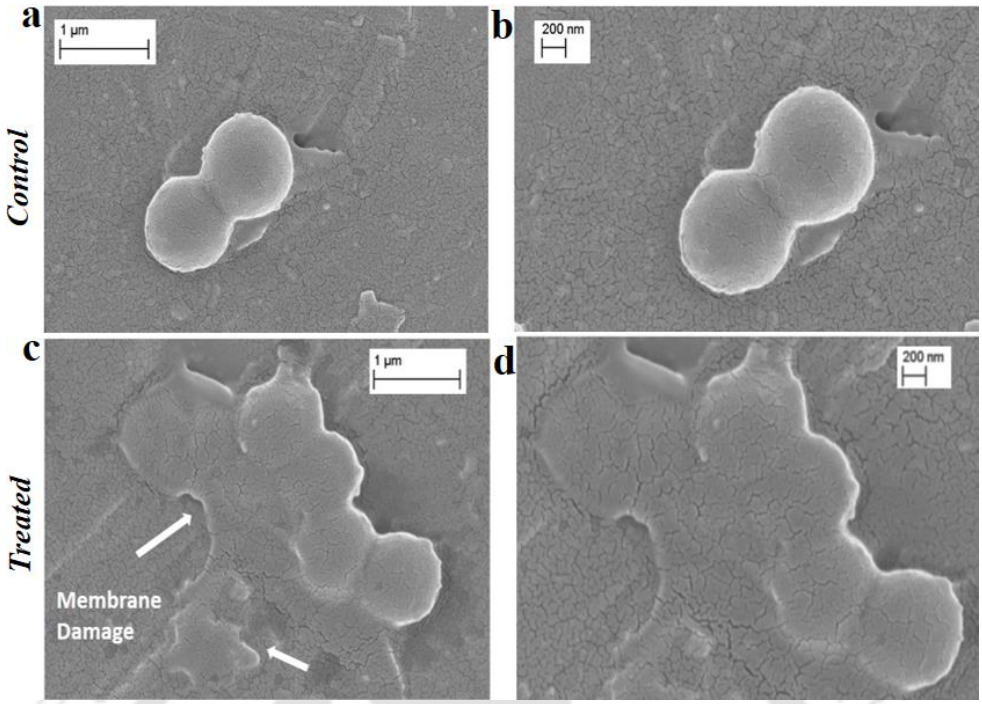

Figure 2.9: FESEM images of *Escherichia coli* (a, b) and *Escherichia coli* (c, d) incubation without and with PFBT-MI, respectively.

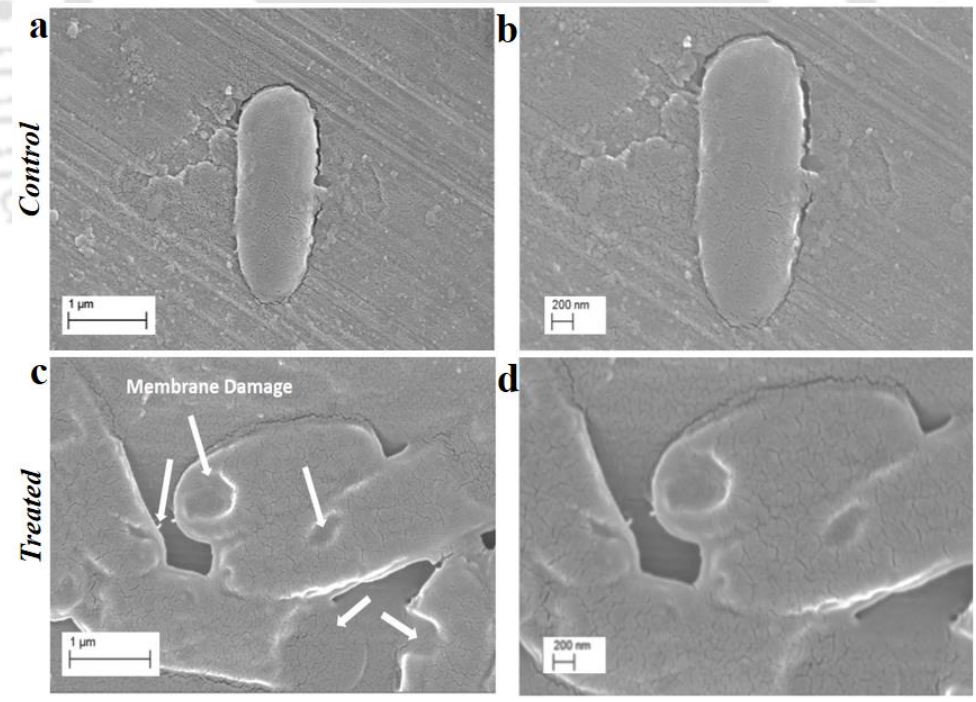

Figure 2.10: FESEM images of control *Staphylococcus aureus* (a, b) and treated *Staphylococcus aureus* (c, d) incubation without and with PFBT-MI, respectively.

Therefore, due to the cationic nature of the polymer, it is possible that it can interact with the bacteria's negatively charged cell membrane, leading to membrane disruption and leakage of intracellular constituents as presented in the schematic of **Figure 2.11**.

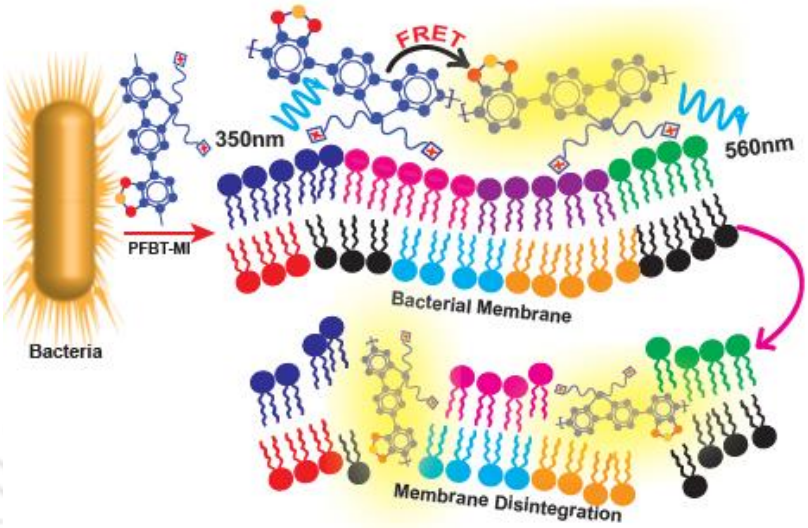

Figure 2.11: Proposed schematic representation of bacterial membrane with PFBT-MI and its antibacterial activity.

To get additional insight into the antibacterial mechanism, protein, and nucleic acid leakage studies have been carried out. In the protein leakage study, both Bradford and OD measurements at 280 nm (**Figure 2.12a-b**) nm suggested that there is an increased amount of protein present in the supernatant of the treated cells signifying membrane damage because of which proteins are released in the supernatant.

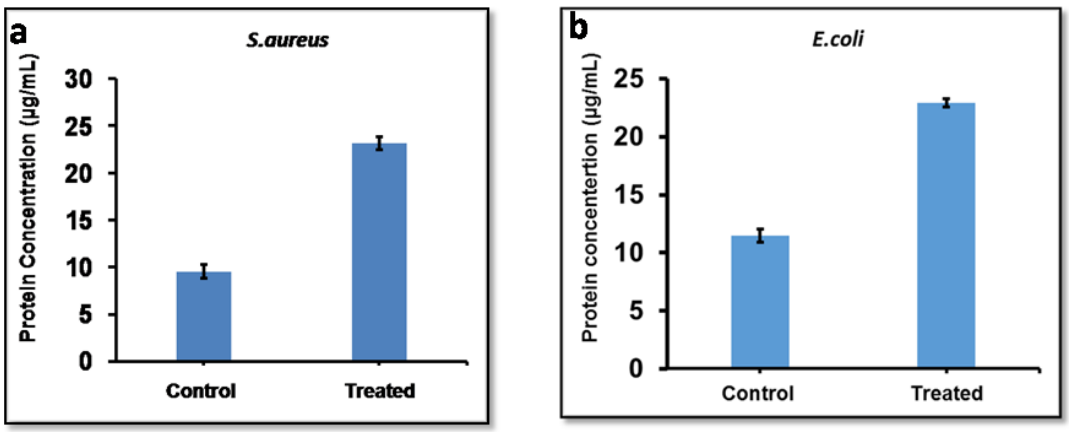

Figure 2.12: Protein Leakage analysis in (a) *Staphylococcus aureus* and (b) *Escherichia coli* cells by Bradford assay after 6h treatment.

Also, the nucleic acid leakage analysis showed increased OD at 260 nm in the case of the treated cells, indicating likely release of nucleic acid into the supernatant due to the damage of the membrane (**Figure 2.13a-b**). This data corroborates with the FESEM analysis which also suggested bacterial cell death due to membrane disruption.

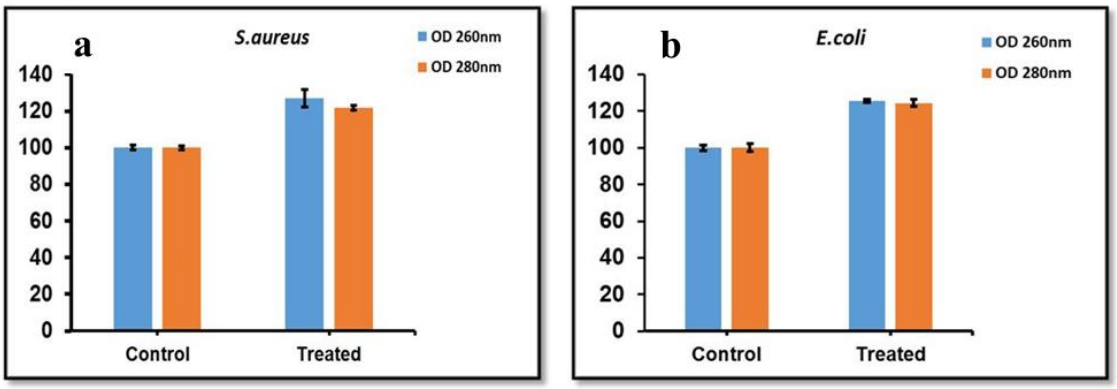

Figure 2.13: Nucleotide and Protein Leakage analysis in (a) *Staphylococcus aureus* and (b) *Escherichia coli* cells by OD measurement at 260 nm and 280 nm respectively after 6h treatment.

2.3.5 Cytotoxicity

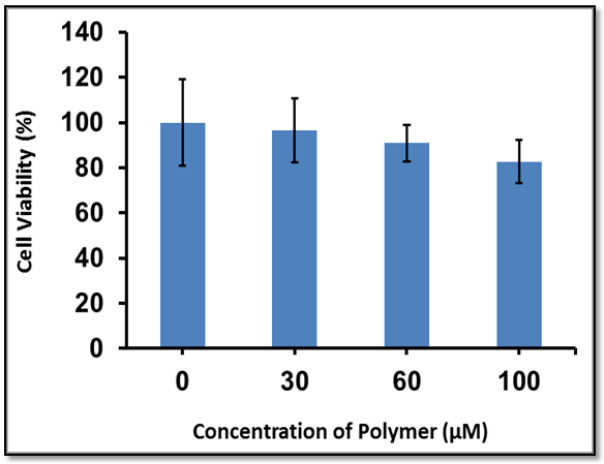

Figure 2.14: Cell Viability assay of HEK 293T with different concentrations of PBFT-MI for 12 h.

The use of the antibacterial agent for biomedical applications is gaining interest, as they selectively kill pathogenic bacteria over mammalian cells. Thus, they can be applied as an antibacterial coating or bactericidal surface for medical devices. In this regard, the cytotoxicity nature of PFBT-MI is examined by MTT assay. The cell viability assay of

PBFT-MI shows that approximately 80% of the cells is viable at the 100μM concentration (which is the maximum dose used in antibacterial studies) after 12 h of treatment **Figure 2.14**. This indicates that the polymer is less toxic in nature towards mammalian cells and shows pronounced killing activity towards bacterial cell.

2.4 Conclusion

In summary, we have developed and explored the potential application of cationic conjugated polyelectrolyte PFBT-MI in wash-free bacterial imaging as well as its antibacterial activity. The side chain strapped imidazolium group of PFBT-MI makes the solution phase quantification and imaging process simple. The imaging process is wash free as the PFBT-MI underwent aggregation-induced FRET from the fluorene unit to the BT on binding with the negatively charged bacterial surface. The PFBT-MI exhibits effective antibacterial activity against Gram-positive (*Staphylococcus aureus*) and Gram-negative (*Escherichia coli*) bacteria. The killing efficacy was higher for Gram-positive bacteria compared to Gram-negative one. The MIC value for Gram-positive and Gram-negative is found to be 23.7μg/mL and 47.7μg/mL respectively. The antibacterial action of PFBT-MI is due to the disintegration of cell membrane resulting in leakage of intracellular constituents and ultimately cell death. This conclusion is supported by FESEM analysis as well as by performing protein and nucleic acid leakage studies.

References

(1) Ivnitski, D.; Abdel-Hamid, I.; Atanasov, P.; Wilkins, E. D. Biosensors for Detection of Pathogenic Bacteria. *Biosens. Bioelectron.***1999**, *14*, 599–624.

(2) Daszak, P., Cunningham, A. A.; Hyatt, A. D. Emerging Infectious Diseases of Wildlife Threats to Biodiversity and Human Health. *Science* **2000**, *287*, 443–449.

(3) Hoffmann, J. A.; Kafatos, F. C.; Janeway, C. A.; Ezekowitz, R. Phylogenetic Perspectives in Innate Immunity. *Science* **1999**, *284*, 1313–1318.

(4) Mendoza, G.; Regiel-Futyra, A.; Andreu, V.; Sebastian, V.; Kyzioł, A.; Stochel, G.; Arruebo, M. Bactericidal Effect of Gold−Chitosan Nanocomposites in Coculture Models of Pathogenic Bacteria and Human Macrophages. ACS *Appl. Mater. Interfaces* **2017**, *9*, 17693–17701.

(5) Li, Q.; Wu, Y.; Lu, H.; Wu, X.; Chen, X.; Song, N.; Yang, Y.-W.; Gao, H. Construction of Supramolecular Nanoassembly for Responsive Bacterial Elimination and Effective Bacterial Detection. *ACS Appl. Mater. Interfaces* **2017**, *9*, 10180−10189.

(6) Liu, L.; Xu, K.; Wang, H.; Tan, P. J.; Fan, W.; Venkatraman, S. S.; Li, L.; Yang, Y.-Y. Self-Assembled Cationic Peptide Nanoparticles as an Efficient Antimicrobial Agent. *Nat. Nanotechnol***. 2009**, *4*, 457−463.

(7) Irwansyah, I.; Li, Y-Q.; Shi, W.; Qi, D.; Leow, W. R.; Tang, M. B. Y.; Li, S.; Chen, X. Gram-Positive Antimicrobial Activity of Amino Acid-Based Hydrogels. *Adv. Mater.* **2015**, *27*, 648–654.

(8) Chen, J.; Wang, F.; Liu, Q.; Du, J. Antibacterial Polymeric Nanostructures for Biomedical Applications. *Chem. Commun.* **2014**, *50*, 14482–14493.

(9) Guilhelmelli, F.; Vilela, N.; Albuquerque, P.; Derengowski, L. S.; Silva-Pereira, I.; Kyaw, C. M. Antibiotic Development Challenges: the Various Mechanisms of Action of Antimicrobial Peptides and of Bacterial Resistance. *Front Microbiol* **2013**, *4*, 353–365.

(10) Fernandez-Lopez, S.; Kim, H.-S.; Choi, E. C.; Delgado, M.; Granja, J. R.; Khasanov, A.; Kraehenbuehl, K.; Long, G.; Weinberger, D. A.; Wilcoxen, K. M.; Ghadiri, M. R. Antibacterial Agents Based on the Cyclic D, L-A-Peptide Architecture. *Nature* **2001**, *412*, 452−455.

(11) Yeaman, M. R.; Yount, N. Y. Mechanisms of Antimicrobial Peptide Action and Resistance. *Pharmacol Rev* **2003**, *55*, 27−55.

(12) Kenawy, E.-R.; Worley, S. D.; Broughton, R. The Chemistry and Applications of Antimicrobial Polymers: A State-of-the-Art Review. *Biomacromolecules* **2007**, *8*, 1359−1384.

(13) Brogden, K. A. Antimicrobial Peptides: Pore Formers or Metabolic Inhibitors in Bacteria? *Nat. Rev. Microbiol.* **2005**, *3*, 238−250.

(14) Zhou, C.; Wang, F.; Chen, H.; Li, M.; Qiao, F.; Liu, Z.; Hou, Y.; Wu, C.; Fan, Y.; Liu, L.; Wang, S.; Wang, Y. Selective Antimicrobial Activities and Action Mechanism of Micelles Self-Assembled by Cationic Oligomeric Surfactants. *ACS Appl. Mater. Interfaces* **2016**, *8*, 4242−4249.

(15) Gui, C.; Zhao, E.; Kwok, R. T. K.; Leung, A. C. S.; Lam, J. W. Y.; Jiang, M.; Deng, H.; Cai, Y.; Zhang, W.; Sub, H.; Tang, B. Z. AIE-active Theranostic System: Selective Staining and Killing of Cancer Cells. *Chem. Sci.* **2017**, *8*, 1822.

(16) Qian, C.; Yu, J.; Chen, Y.; Hub, Q.; Xiao, X.; Sun, W.; Wang, C.; Feng, P.; Shen, Q.-D.; Gu, Z. Light-Activated Hypoxia-Responsive Nanocarriers for Enhanced Anticancer Therapy. *Adv. Mater.* **2016**, *28*, 3313–3320.

(17) Sakamoto, F. H.; Torezan, L.; Anderson, R. R. Photodynamic Therapy for Acne Vulgaris: a Critical Review from Basics to Clinical Practice: Part II. Understanding Parameters for Acne Treatment with Photodynamic Therapy. *J. Am. Acad. Dermatol*. **2010**, *63*,195–211.

(18) Riduan, S. N.; Zhang, Y. G. Imidazolium Salts and Their Polymeric Materials for Biological Applications. *Chem. Soc. Rev.* **2013**, *42*, 9055−9070.

(19) Li, J.; Zhao, Q.; Shi, F.; Liu, C.; Tang, Y. NIR-Mediated Nanohybrids of Upconversion Nanophosphors and Fluorescent Conjugated Polymers for High-Efficiency Antibacterial Performance Based on Fluorescence Resonance Energy Transfer. *Adv. Healthcare Mater.* **2016**, *23*, 2967–2971.

(20) Liu, G-J.; Tian, S.-N.; Li, C.-Y.; Xing, G.-W.; Zhou, L. Aggregation-Induced-Emission Materials with Different Electric Charges as an Artificial Tongue: Design, Construction, and Assembly with Various Pathogenic Bacteria for Effective Bacterial Imaging and Discrimination. *ACS Appl. Mater. Interfaces* **2017**, *9*, 28331−28338.

(21) Dutta, D.; Sailapu, S. K.; Chattopadhyay, A.; Ghosh, S. S. Phenylboronic Acid Templated Gold Nanoclusters for Mucin Detection Using a Smartphone-Based Device and Targeted Cancer Cell Theranostics. *ACS Appl. Mater. Interfaces* **2018**, *10*, 3210−3218.

(22) Zhang, Y.; Li, C.; Fan, Y.; Wang, C.; Yang, R.; Liu, X.; Zhou, L. A Self-quenching-Resistant Carbon Nanodot Powder with Multicolored Solid-State Fluorescence for Ultra-

fast Staining of Various Representative Bacterial Species within One Minute. *Nanoscale* **2016**, *8*, 19744–19753.

(23) Jiang, Y.-W.; Gao, G.; Zhang, X.; Jia, H.-R.; Wu, F.-G. Antimicrobial Carbon Nanospheres. *Nanoscale* **2017**, *9*, 15786–15795.

(24) Zhao, E.; Chen, Y.; Chen, S.; Deng, H.; Gui, C.; Leung, C. W.; Hong, Y.; Lam, J. W.; Tang, B. Z. A Luminogen with Aggregation Induced Emission Characteristics for Wash-Free Bacterial Imaging, High-Throughput Antibiotics Screening and Bacterial Susceptibility Evaluation. *Adv. Mater.* **2015**, *27*, 493–4937.

(25) Zhao, E.; Chen, Y.; Wang, H.; Chen, S.; Lam, J.W. Y.; Leung, C.W. T.; Hong, Y.; Tang, B. Z. Light-Enhanced Bacterial Killing and Wash-Free Imaging Based on AIE Fluorogen. *ACS Appl. Mater. Interfaces* **2015**, *7*, 7180−7188.

(26) Feng, G.; Yuan, Y.; Fang, H.; Zhang, R.; Xing, B.; Zhang, G.; Zhang, D.; Liu, B. A Light-up Probe with Aggregation-induced Emission Characteristics (AIE) for Selective Imaging, Naked-eye Detection and Photodynamic Killing of Gram-positive Bacteria. *Chem. Commun.* **2015**, *51*, 12490–12493.

(27) Thomas, A.W.; Catania, C.; Garner, L.E.; Bazan, G. C. Pendant Ionic Groups of Conjugated Oligoelectrolytes Govern their Ability to Intercalate into Microbial Membranes. *Chem. Commun.* **2015**, *51*, 9294—9297.

(28) Yan, H.; Rengert, Z.D.; Thomas, A.W.; Rehermann, C.; Hinks, J.; Bazan, G. C. Influence of Molecular Structure on the Antimicrobial Function of phenylenevinylene Conjugated Oligoelectrolytes. *Chem. Sci.* **2016**, *7*, 5714–5722.

(29) Wang, B.; Wang, M.; Mikhailovsky, A.; Wang, S.; Bazan, G. C. A Membrane-Intercalating Conjugated Oligoelectrolyte with High-Efficiency Photodynamic Antimicrobial Activity. *Angew. Chem. Int. Ed.* **2017**, *56*, 5031–5034.

(30) Chen, H.; Li, M.; Liu, Z.; Hu, R.; Li, S.; Guo, Y.; Lv, F.; Liu, L.; Wang, Y.; Yi, Y.; Wang, S. Design of Antibacterial Peptide-like Conjugated Molecule with Broad Spectrum Antimicrobial Ability. *Sci. China Chem.* **2018**, *61*, 113-117.

(31) Ji, E.; Parthasarathy, A.; Corbitt, T. S.; Schanze, K. S.; Whitten, D. G. Antibacterial Activity of Conjugated Polyelectrolytes with Variable Chain Length. *Langmiur* **2011**, *27*, 10763–10769.

(32) Yang, Y.; Cai1, Z.; Huang, Z.; Tang, X.; Zhang, X. Antimicrobial Cationic Polymers: from Structural Design to Functional Control. *Polymer* **2018**, *50*, 33–44.

(33) Konai, M.M.; Bhattacharjee, B.; Ghosh, S.; Haldar, J. Recent Progress in Polymer Research to Tackle Infections and Antimicrobial Resistance. *Biomacromolecules* **2018**, *19*, 1888−1917.

(34) Henson, Z. B.; Zhang, Y.; Nguyen, T.-Q.; Seo, J. H.; Bazan, G. C. Synthesis and Properties of Two Cationic Narrow Band Gap Conjugated Polyelectrolytes. *J. Am. Chem. Soc.* **2013**, *135*, 4163–4166.

(35) Gaylord, B. S.; Heeger, A. J.; Bazan, G. C. DNA Hybridization Detection with Water-Soluble Conjugated Polymers and Chromophore-Labeled Single-Stranded DNA. *J. Am. Chem. Soc.* **2003**, *125*, 896–900.

(36) Liu, B.; Bazan, G. C. Homogeneous Fluorescence-Based DNA Detection with Water-Soluble Conjugated Polymers. *Chem. Mater.* **2004**, *16*, 4467–4476.

(37) Thomas, S. W., III; Joly, G. D.; Swager, T. M. Chemical Sensors Based on Amplifying Fluorescent Conjugated Polymers. *Chem. Rev.* **2007**, *107*, 1339–1386.

(38) Ho, H. A.; Najari, A.; Leclerc, M. Optical Detection of DNA and Proteins with Cationic Polythiophenes. *Acc. Chem. Res.* **2008**, *41*, 168–178.

(39) Zhu, C.; Liu, L.; Yang, Q.; Lv, F.; Wang, S. Water-Soluble Conjugated Polymers for Imaging, Diagnosis, and Therapy. *Chem. Rev.* **2012**, *112*, 4687–4735.

(40) McQuade, D. T.; Pullen, A. E.; Swager, T. M. Conjugated Polymer-Based Chemical Sensors. *Chem. Rev.* **2000**, *100*, 2537–2574.

(41) Liang, J.; Li, K.; Liu, B. Visual Sensing with Conjugated Polyelectrolytes. *Chem. Sci.* **2013**, *4*, 1377–1394.

(42) Wang, Y.; Jett, S. D.; Crum, J.; Schanze, K. S.; Chi, E. Y.; Whitten D. G. Understanding the Dark and Light-Enhanced Bactericidal Action of Cationic Conjugated Polyelectrolytes and Oligomers. *Langmuir* **2013**, *29*, 781–792.

(43) Zhou, C.; Wang, F.; Chen, H.; Li, M.; Qiao, F.; Liu, Z.; Hou, Y.; Wu, C.; Fan, Y.; Liu, L.; Wang, S.; Wang, Y. Selective Antimicrobial Activities and Action Mechanism of Micelles Self-Assembled by Cationic Oligomeric Surfactants. *ACS Appl. Mater. Interfaces* **2016**, *8*, 4242–4249.

(44) Wang Y.; Zhou Z.; Zhu J.; Tang Y.; Canady T. D.; Chi E. Y.; Schanze K. S.; Whitten D. G. Dark Antimicrobial Mechanisms of Cationic Phenylene Ethynylene Polymers and Oligomers against Escherichia coli. *Polymers* **2011**, *3*, 1199–1214.

(45) Wang, Y.; Corbitt, T. S.; Jett, S. D.; Tang, Y.; Schanze, K. S.; Chi, E. Y.; Whitten, D. G. Direct Visualization of Bactericidal Action of Cationic Conjugated Polyelectrolytes and Oligomers. *Langmuir* **2012**, *28*, 65−70.

(46) Sun, H.; Yin, B.; Ma, H.; Yuan, H.; Fu, B.; Liu. L. Synthesis of a Novel Quinoline Skeleton Introduced Cationic Polyfluorene Derivative for Multimodal Antimicrobial Application. *ACS Appl. Mater. Interfaces* **2015**, *7*, 25390−25395.

(47) Kenawy, El-R.; Worley, S. D.; Broughton, R. The Chemistry and Applications of Antimicrobial Polymers: A State-of-the-Art Review. *Biomacromolecules* **2007**, *8*, 1359−1384.

(48) Ji, E.; Corbitt, T. S.; Parthasarathy, A.; Schanze, K. S.; Whitten, D. G. Light and Dark-Activated Biocidal Activity of Conjugated Polyelectrolytes. *Appl. Mater. Interfaces* **2011**, *3*, 2820–2829.

(49) Parthasarathy, A.; Pappas, H. C.; Hill, E. H. ; Huang, Y.; Whitten, D. G.; Schanze K. S. Conjugated Polyelectrolytes with Imidazolium Solubilizing Groups. Properties and Application to Photodynamic Inactivation of Bacteria. *ACS Appl. Mater. Interfaces* **2015**, *7*, 28027–28034.

(50) Bai, H.; Chen, H.; Hu, R.; Li, M.; Lv, F.; Liu, L., Wang, S. Supramolecular Conjugated Polymer Materials for in Situ Pathogen Detection. *ACS Appl. Mater. Interfaces* **2016**, *8*, 31550−31557.

(51) Jares-Erijman, E. A.; Jovin, T. M. FRET Imaging. *Nat. Biotechnol.* **2003**, *21*, 1387–1395.

(52) Varghese, S. S; Zhu, Y.; Davis, T. J.; Trowell, S. C. FRET for Lab-on-a-chip Devices-Current Trends and Future Prospects. *Lab Chip* **2010**, *10*, 1355–1364.

(53) Hussain, S.; Malik, A. H.; Iyer, P. K. FRET-assisted Selective Detection of Flavins via Cationic Conjugated Polyelectrolyte under Physiological Conditions. *J. Mater. Chem. B* **2016**, *4*, 4439–4446.

(54) Shi, X.; Yu, C.Y. Y.; Su, H.; Kwok, R. T. K.; Jiang, M.; He, Z.; Lam, J. W. Y.; Tang, B. Z. A Red-Emissive Antibody–AIEgen Conjugate for Turn-on and Wash-free Imaging of Specific Cancer Cells. *Chem. Sci.* **2017**, *8, 7014–7024.*

(55) Malik A. H.; Hussain S.; Iyer, P. K. Aggregation-Induced FRET via Polymer−Surfactant Complexation: A New Strategy for the Detection of Spermine. *Anal. Chem.* **2016**, *88*, 7358–7364.

(56) Liu, L. H.; Huang, Y.; Riduan, S. N.; Gao, S. J.; Yang, Y. Y.; Fan, W. M.; Zhang, Y. G. Main-Chain Imidazolium Oligomer Material as a Selective Biomimetic Antimicrobial Agent. *Biomaterials* **2012**, *33*, 8625−8631.

(57) Riduan, S. N.; Zhang, Y. G. Imidazolium Salts and Their Polymeric Materials for Biological Applications. *Chem. Soc. Rev.* **2013**, *42*, 9055−9070.

(58) Nanda, S.S.; Yi, D.K.; Kim, K. Study of antibacterial mechanism of Graphene Oxide using Raman Spectroscopy. *Scientific Reports* **2016**, *6*, 28443.

(59) Reddy, L.S.; Nisha, M.M.; Joice, M.; Shilpa, P.N. Antimicrobial Activity of Zinc Oxide (ZnO) Nanoparticle Against Klebsiella pneumonia. *Pharmaceutical Biology*, **2014**, *52*, 1388-1397.

Appendix

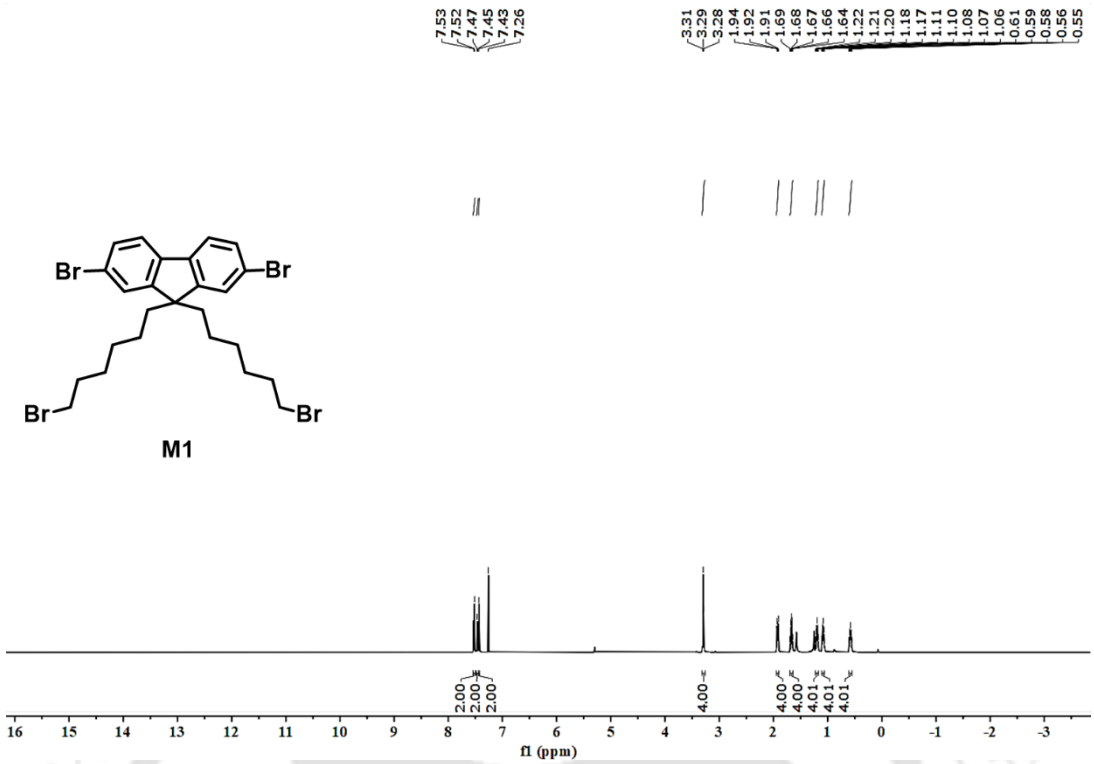

Figure A2.1 ^{1}H NMR spectra of M1.

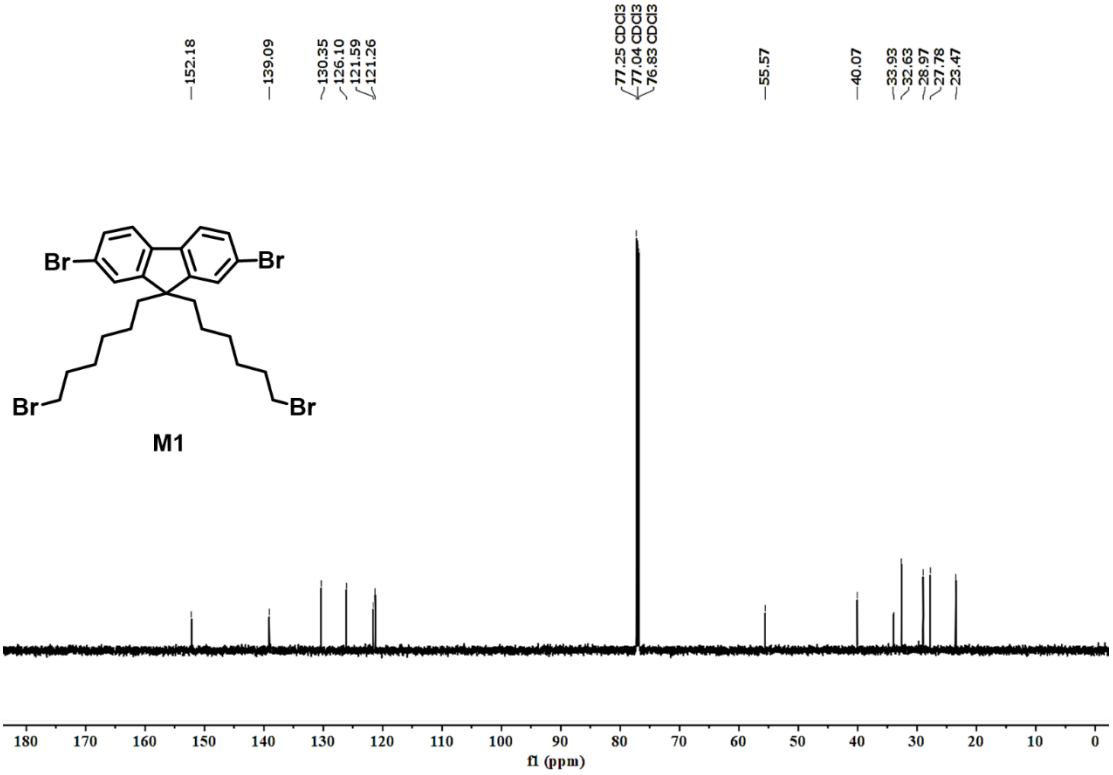

Figure A2.2 ^{13}C NMR spectra of M1.

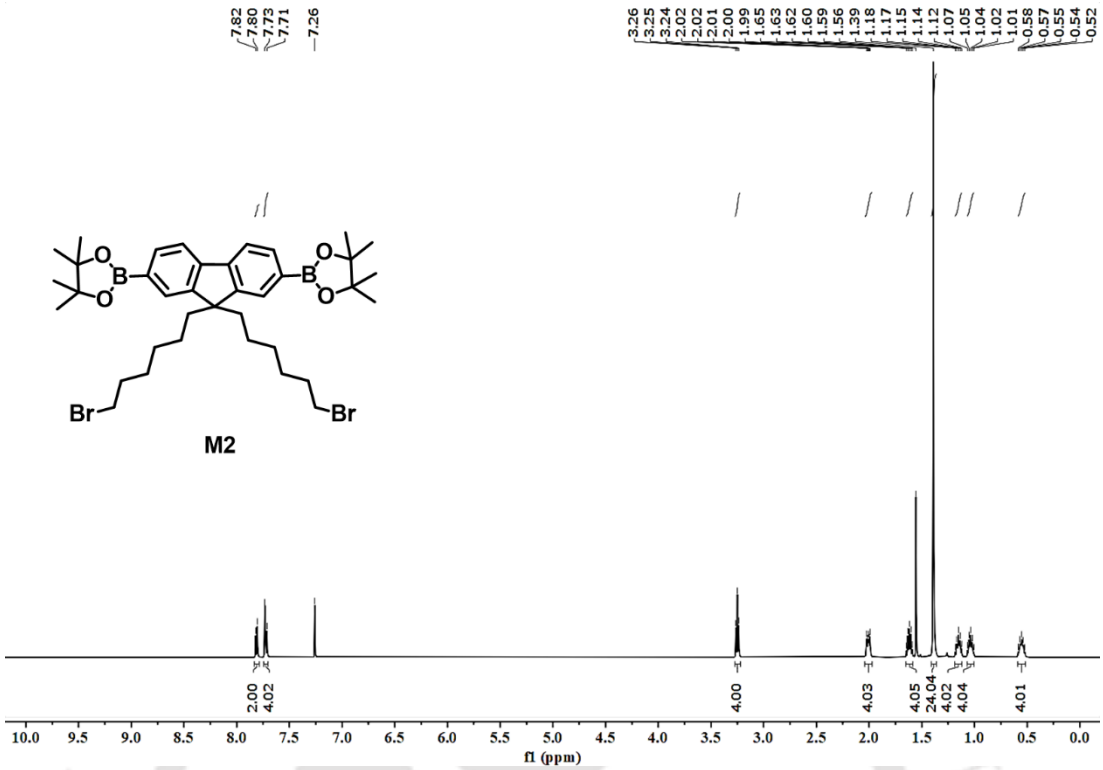

Figure A2.3 ^{1}H NMR spectra of M2.

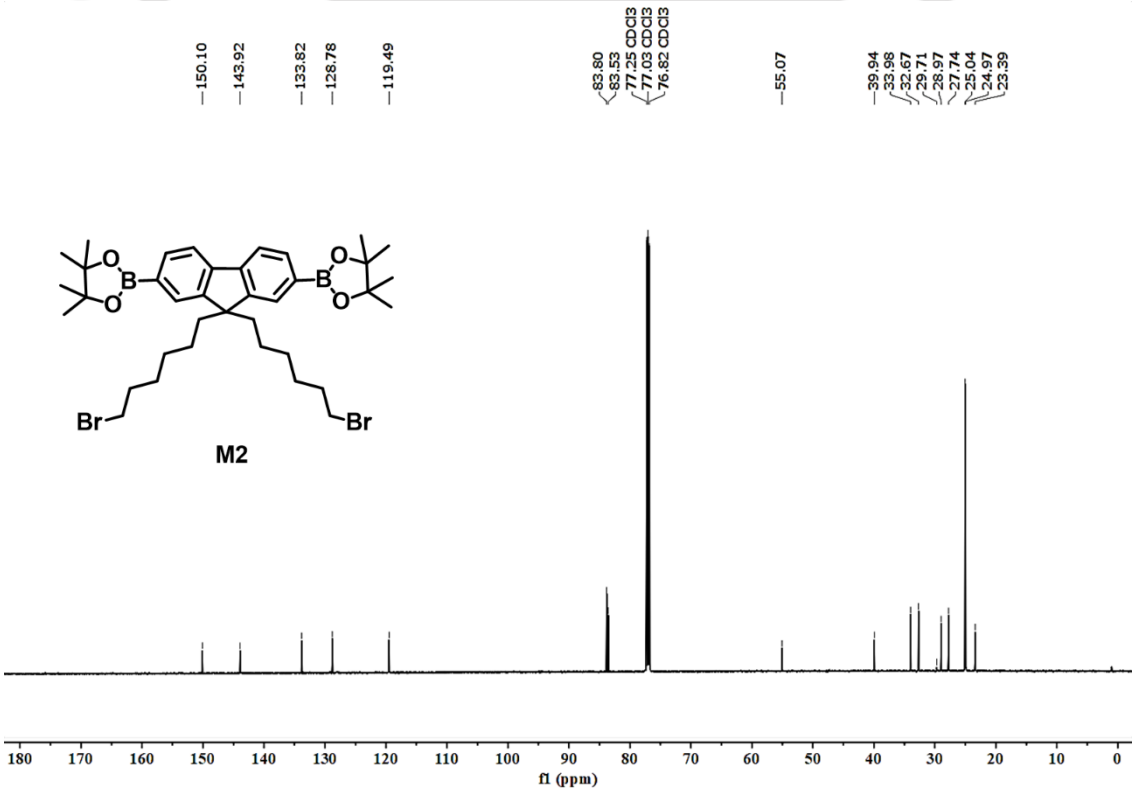

Figure A2.4 ^{13}C NMR spectrum of M2.

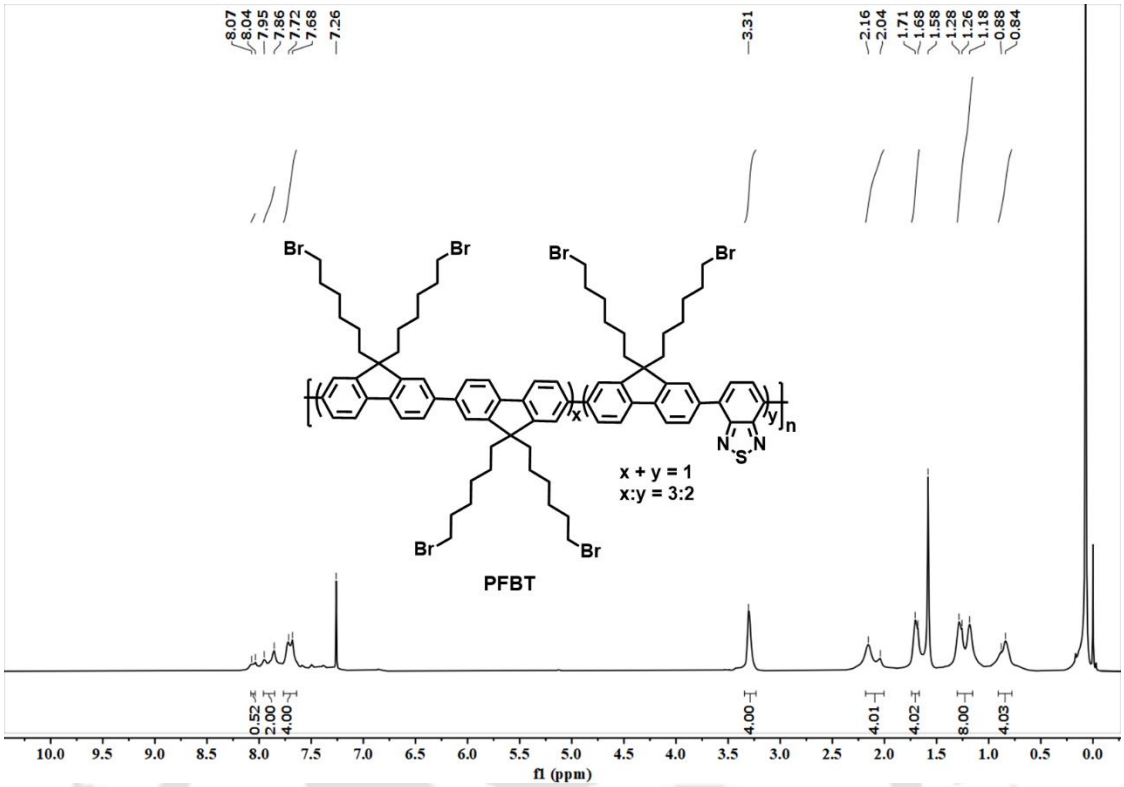

Figure A2.5 ^{1}H NMR spectra of PFBT.

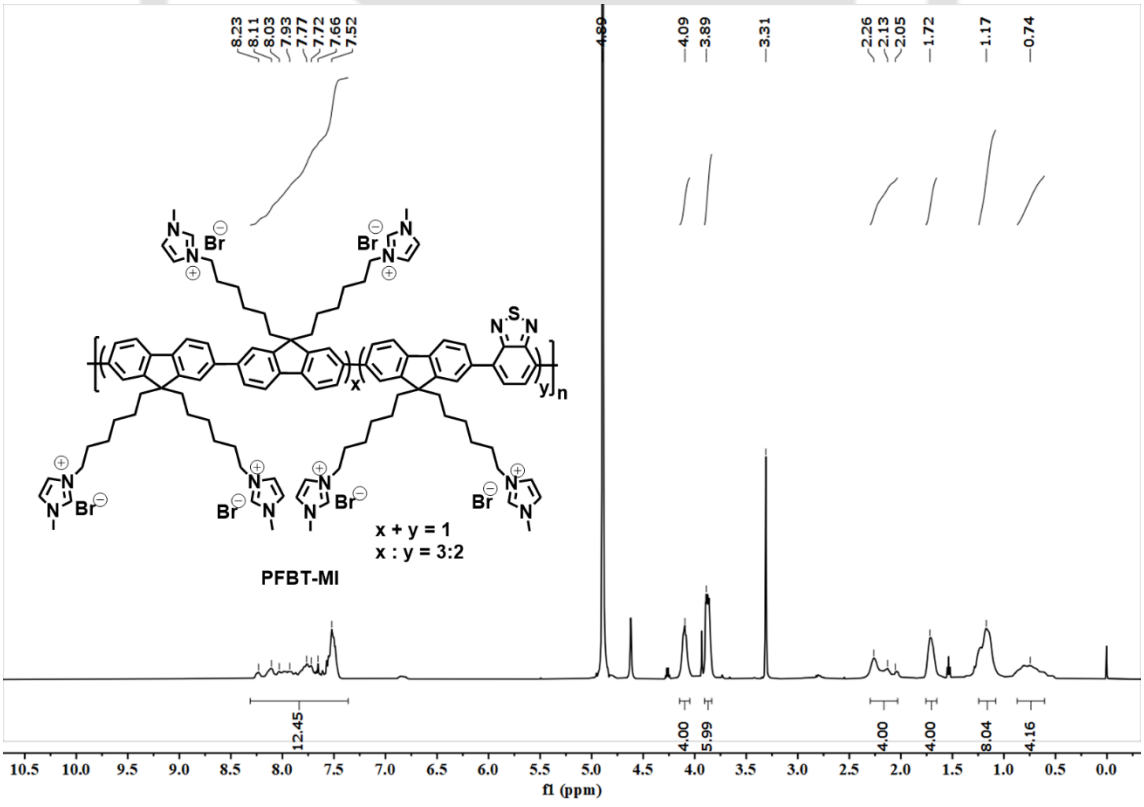

Figure A2.6 ^{1}H NMR spectrum of PFBT-MI.

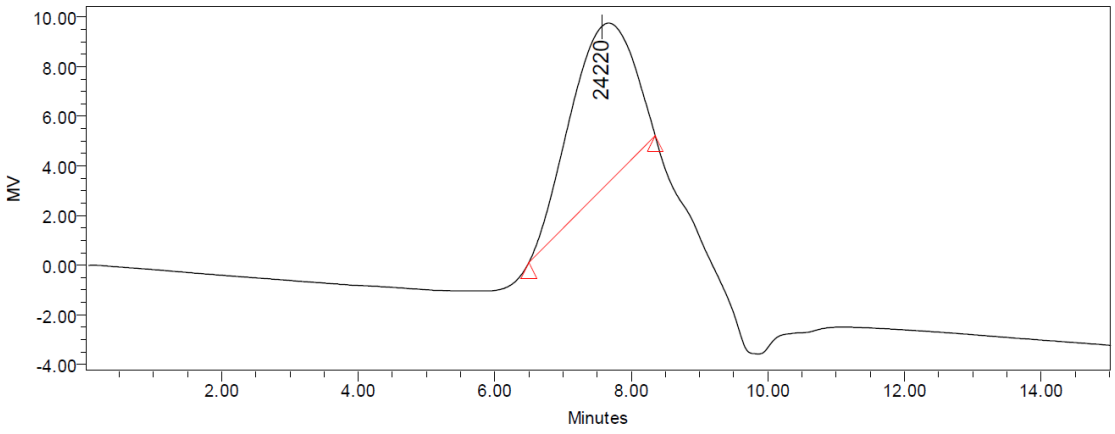

GPC Results

	Retention Time (min)	% Area	Mn	Mw	MP	Mz	Mz+1	Poly dispersity
1	7.567	100.00	22933	29321	24220	37353	45860	1.278543

Figure A2.7 GPC chromatogram of PFBT.

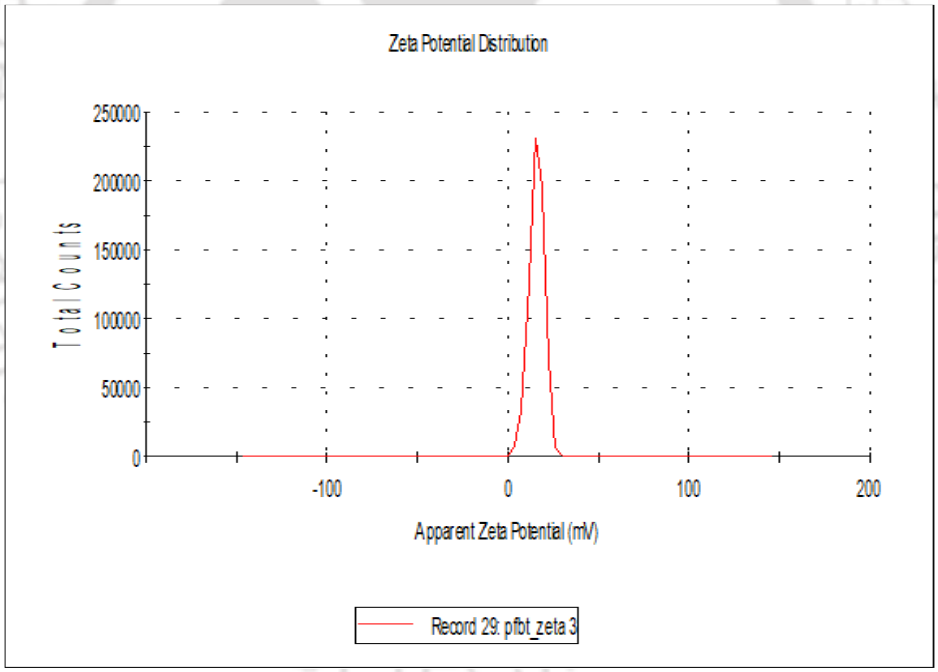

Figure A2.8 Zeta potential plot of PFBT-MI in aqueous solution.

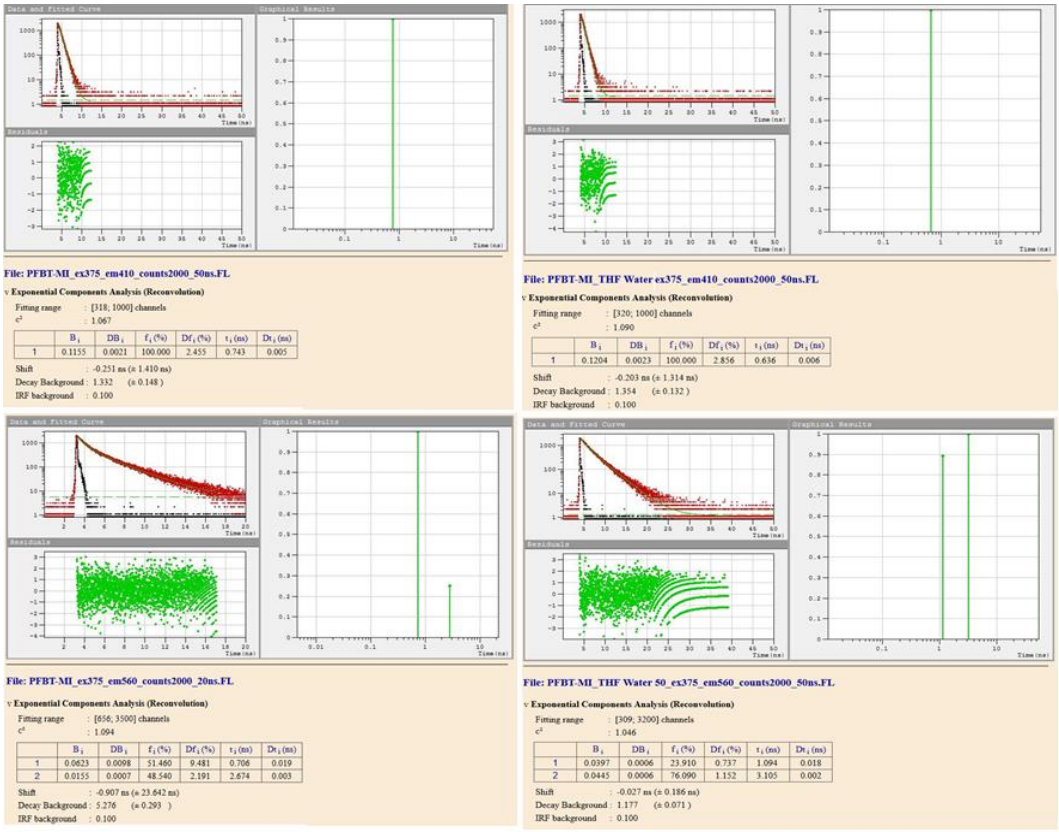

Figure A2.9 Fitting decay curves for PFBT-MI in water and water THF fraction monitored at 410 nm and 560 nm.

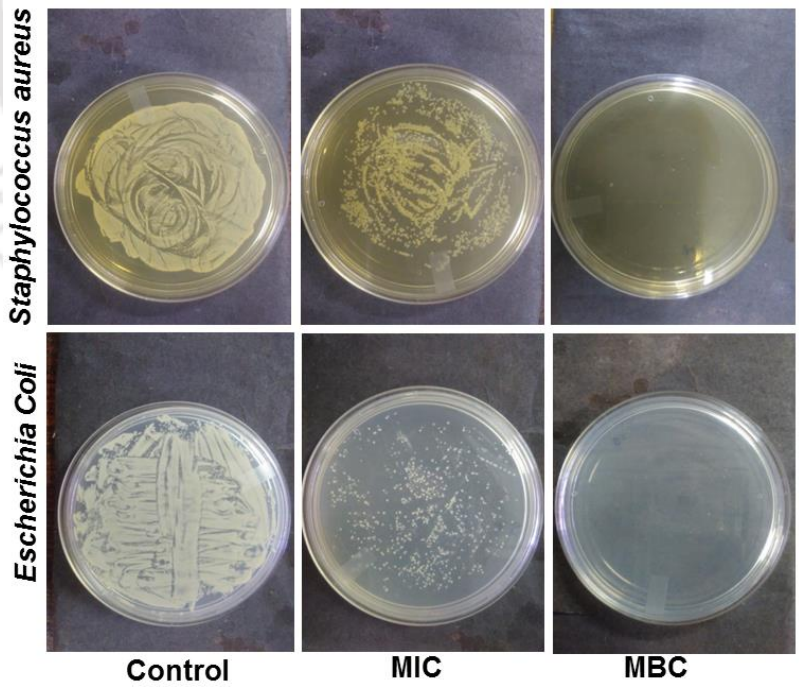

Figure A2.10 Plating images of *Staphylococcus aureus* (b) Plating images of *Escherichia coli* control, treated with MIC and MBC doses of PFBT-MI respectively.

Table A2.1: Comparative study of MIC values for reported polymer with antibacterial property.

S. No	Material	Bacteria	MIC (µg/mL)	Reference
1	**Non-β lactams antibiotics + PFP**	*E. coli*	128	*Angew. Chem. Int. Ed.* **2011,** *50, 9607*–9610.
2	**PTVan**	*S. aureus, E.coli*	1000 1000	J. Mater. Chem. B **2017**, *5, 8814*–8820.
3	**OP-PMOx-DDA**	*S. aureus* *E. coli*	40 1250	*Angew. Chem. Int. Ed*. **2014,** *53, 3830*–3834.
4	**TMC-g-EM, TMC-Q-g-EM, DMHC-g-EM, DMDC-Q-g-EM**	*S. aureus* *E. coli*	49-1600 98-3100	*Nat. Mater*.**2011**, *10,149*–156.
5	**PAMAM G2,** **PAMAM G3**	*E. coli*	157.2 >148.2	*Nat.Microbiol.* **2016**,*1*,16162.
6	**Poly(MMA-co-St)/Ag nanocomposite**	*E. coli*	300	*Colloid. Polym. Sci.* **2015,** *293,* 1997–2008.
7	**P1-P6**	*E. coli*	63-5000	*Biomacromolecules* **2017**, *18,* 1592−1599.
8	**Biopolymer,** **Quaternized biopolymer**	*E. coli*	>100 73	*J. Appl. Microbiol.* **2013**, *116,* 511—518**.**
9	**Poly-2(b-e)**	*S. aureus*	64-128	*ACS Macro Lett.* **2012,** ***1,*** 370−374.
10	**pDMAEMA Polymers**	*E. coli* *S. aureus*	64-512 50-100	*Biomacromolecules* **2011, *2,*** 443-453.
11	**PFBT-MI**	*S. aureus* *E. coli*	23.7 47.7	***Present Work***

Chapter 3

Conjugated Polymer-Based Electrical Sensor for Ultratrace Vapor-Phase Detection of Nerve Agent Mimics

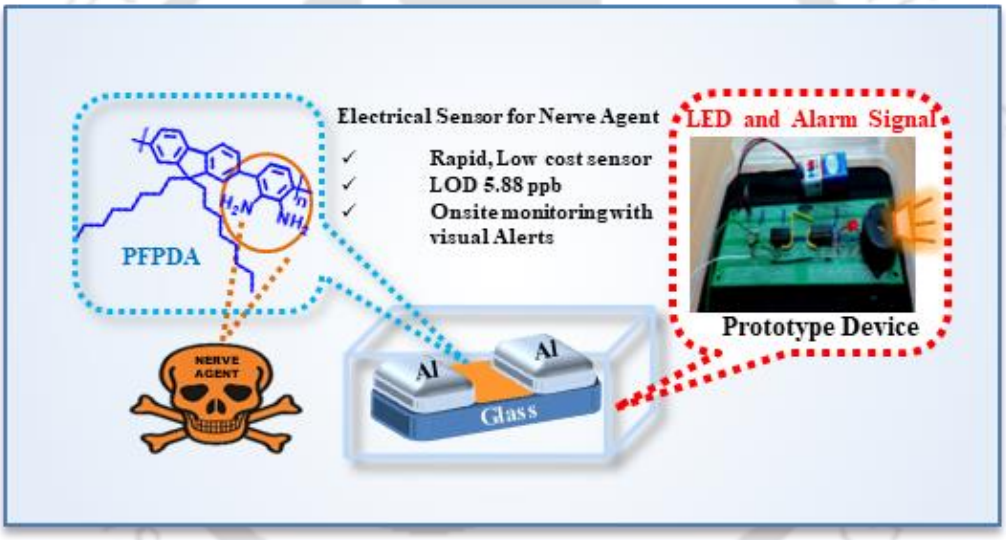

Zehra, N.; Kalita, A.; Malik, A. H.; Barman, U.; Afroz, M. A.; Iyer, P. K. Conjugated Polymer-Based Electrical Sensor for Ultratrace Vapor-Phase Detection of Nerve Agent Mimics *ACS Sens.* **2020**, *5*, 191–198.

.

Abstract

Considering the vital need to strengthen the national security emanating from chemical threats, a low-cost, portable ultra-sensitive electrical sensor for real-time monitoring of Diethylchlorophosphate (DCP) (nerve gas mimic) has been developed. The device consists of "simple to be fabricated" two-terminal resistor and an electronic combinational circuit for rapid onsite detection of lethal nerve gas vapors with high degree of accuracy in milliseconds. This device is an intelligent readout electronic model that detects ultra-trace DCP vapors by bright visual alerts from LED and loud alarm signal without the need for employing a sophisticated instrument. To obtain high sensitivity and discriminating response, a novel amine-functionalized conjugated polymer (CP) is designed as a sensory channel material for two-terminal sensor. The low-powered Poly(3-(9,9-dioctyl-9H-fluoren-2-yl)benzene-1,2-diamine) (PFPDA) fabricated two-terminal electrical sensor is tested at ambient conditions, which shows excellent sensitivity towards nerve gas mimic DCP, with rapid response in 3 sec and very low limit of detection (LOD) of 5.88 ppb. The amine moiety of PFPDA CP plays a vital role in redox interaction between the semiconductor CP and organophosphates, which ultimately leads to the amplified current signal. The redox interactions occurring among the organophosphate analytes and the amine functional group on the PFPDA backbone provided insights into the mechanism of sensing which formed the basis of the excellent sensitivity and discriminating ability of this sensor device. The newly designed PFPDA CP-based portable electrical sensor device demonstrates a key contribution in portable electronics for defense safety and environmental monitoring applications.

3.1 Introduction

Technological advances have significantly altered the use of weapons for mass destruction (WMD) across the globe. During World War II, chemical weapons are emerged as the cheapest tool to mortal and morbid the large mass.[1] Among the chemical warfare components, the nerve agent was accidentally discovered and deliberately used first against the unarmed civilians of Matsumoto.[2-5] Since then, the nerve agent has become a weapon of choice for rebellion as they are highly toxic, readily manufactured, colorless, odorless liquids that cannot be detected by human sensory receptors. Nerve agents are the derivatives of organophosphate family which can cause the death of the victim due to their irreversible binding with neurotransmitter cholinesterase enzyme.[6-8] Present criminal terrorism threats and non-availability of proper antidotes for such airborne toxic agents critically demand fast and reliable on-site detection in homeland security. Thus, there is an immense necessity to develop an effective detection system that should be portable, fast responsive, highly sensitive, accurate, operationally simple, and equipment free for real-time monitoring of the lethal nerve agents at remote locations.

Among the detection methods for highly toxic nerve agents, optical and spectrochemical techniques are counterproductive due to its expensive instrumentation, portability issues, and thus inappropriateness for practical application.[9-17] Electrical sensors have received significant attention owing to their inherent attributes of transforming physical or chemical events into the readily observable electrical signal. Among the electrical sensors, two-terminal resistors are best suited for the development of portable, low-cost advanced gas sensing systems as they are easy to assemble and economically fabricated. Over the past few years, various type of chemiresistor materials has been reported for nerve agent detection such as graphene oxide, metal-organic framework, metal oxide-based composites, small organic molecule, conducting polymers, etc.[18-23] Indeed inorganic based chemiresistors have their strengths; however, they have limited sensitivity, solution processibility, and high-temperature requirements, which disfavours their broad application.[24] Hybrid/composite materials of metal oxides and organic semiconductors have been utilized to rectify the high temperature and low sensitivity issues, but these modified structures make their fabrication and operation more multifaceted.

Organic semiconductors have been widely used active materials for thin-film devices due to their low cost, solution processibility, and room temperature operation. Among the organic semiconductor, conjugated polymer (CP) has emerged as an outstanding material

in various optoelectronic devices owing to its, intrinsic electrical properties, excellent thermal and mechanical stability, good film-forming ability, and are easier to introduce functional groups within the backbone or at the side chain of the CP for sensing application.[25-30] A key attribute of CPs is their ability to transform a single binding event into the amplified signal by the molecular wire effect from collective units; thus, they have great potential to develop cheap, low-powered, flexible advanced gas sensing systems. In this regard, a small number of conducting polymer-based electrical sensors for nerve agents have been reported with improved sensitivity, high stability, and prompt response. Additionally, nanomaterial engineering of conducting polymer has been carried out to enhance charge transport property and, ultimately, the sensitivity of the thin film-based sensor.[7,22] However, covalent structural engineering is another efficient method to get highly sensitive and high-performance sensors at ambient conditions.

Furthermore, due to their intrinsic property of organic semiconductor-based electrical sensors, they can be amenable to compact, lightweight, affordable and portable electronics.[31] A few wearable and wireless sensors for the detection of nerve gas have been developed, but their operation is very complex, requires specific enzymes or labelling and particular operating conditions to remain functional.[32,33] Thus, there is scope to establish newer low-cost portable electronics based on the smart organic semiconductor.

Herein, we report the synthesis and characterization of a novel CP poly(fluorene-co-phenylene) derivative via a straightforward synthetic route in good yields. The polar amine groups are strategically introduced directly on the CP backbone to increase the likelihood of redox interaction and to get the discriminating response among the organophosphate derivatives. Two-terminal sensor devices were fabricated (**Figure 3.1**) using PFPDA CP as a sensory layer, and the device showed remarkable sensitivity with rapid response within 3 seconds in the presence of DCP vapor at ambient conditions. Furthermore, the sensitivity of the PFPDA fabricated device is compared to Poly(9,9-dioctyl-2-phenyl-9H-fluorene)(P0) (without any amine groups) fabricated two-terminal sensor to confirm the role of amine functional group in PFPDA CP on sensing behavior. Finally, PFPDA fabricated sensor device is integrated with an electronic combinational circuit of Operational Amplifier (OPAMP) and logic AND gate for onsite detection of DCP vapor with bright visual alerts from LED and loud alarm sound signal. The designed electronic model produces rapid, precise and decisive output independent of human error and thus offers rapid onsite detection of nerve agent with high degrees of accuracy in milliseconds. This is the first report of using amine-functionalized CP for the development of low-cost

portable electronic model for the onsite-field detection nerve gas mimics and provides valuable mechanistic insight due to the presence of two amine groups on the CP backbone and their sensing as well as discrimination ability of organophosphates rapidly.

3.2 Experimental

3.2.1 Material and Instruments: Diethyl chlorophosphate (DCP), dimethyl methylphosphonate (DMMP), tributyl phosphate (TBP), triethyl phosphate (TEP), were procured from Merck (formerly Sigma-Aldrich). All other chemicals were obtained from Alfa Aesar, Merck, etc. ^{1}H NMR (600 MHz) and ^{13}C NMR (150 MHz) were recorded on a Bruker Ascend 600 MHz and Bruker 400 MHz spectrometers. GPC was recorded on Water Corporation USA. Q-TOF ESI-MS instrument (model HAB 273) was used to obtain Mass spectra. A Keithley 4200-SCS semiconductor parameter analyzer was used to perform all semiconductor device characterization. FT-IR spectra were recorded on a Perkin Elmer spectrometer with samples prepared as KBr pellets. Sigma Carl ZEISS field emission scanning electron microscope was used to obtain FE-SEM images. The ground state optimized structures were attained using the B3LYP function in the Gaussian 09 package. The 6-31G(d,p) basis set was used throughout the calculations.

3.2.2 Synthetic procedure

3.2.2a Synthesis of 4,5-Dibromo-1,2-benzenediamine (M1): The monomer M1 was synthesized according to previously established procedure.[34] To prepare M1, Dibromobenzothiadiazole (300 mg, 1.02 mmol) was first dissolved in 10 mL EtOH and then transferred into a two-necked round-bottom flask. The mixture was cooled to 0˚C for 10 min, $NaBH_4$ (386 mg, 10.2 mmol) added dropwise to the flask and stirred for 18h at room temperature. Once the reaction was over, confirmed by TLC test; solvent was removed under vacuum followed by extraction with diethyl ether and dried over Na_2SO_4. The extract was evaporated to dryness and the crude mixture was purified by neutral alumina column chromatography (EtOAc:Hexane=1/9) as an eluent. The title compound was obtained as a white solid. (246 mg, 91%). ^{1}H NMR (600 MHz, $CDCl_3$, δ ppm): 6.84 (s, 2H), 3.89 (s, 4H). ^{13}C (150 MHz, $CDCl_3$, δ ppm): 109.68, 123.21, 133.71. ESI-MS: $[M + H]^+$: calcd: 265.8877; found: 266.8980.

3.2.2b Synthesis of Poly(3-(9,9-dioctyl-9H-fluoren-2-yl)benzene-1,2-diamine) PFPDA and Poly(9,9-dioctyl-2-phenyl-9H-fluorene) P0: CP PFPDA and P0 were prepared using modified procedure.[35,36] In a 50 mL round bottom flask, 9,9-Dioctyl-9*H*-fluorene-2,7-

diboronic acid bis(pinacol) ester (150 mg, 0.27 mmol), 4,5-Dibromo-1,2-benzenediamine (71 mg, 0.27 mmol) and/or 1,4-Dibromobenzene (63.69 mg, 0.27 mmol), [$Pd(PPh_3)_4$] (15 mg, 0.014 mmol) and potassium carbonate (373 mg, 2.7 mmol) were taken under inert condition. A toluene:H_2O mixture (3:1) was introduced to the flask using a syringe and degassed thrice via freeze-thaw cycle. The reaction mixture was refluxed for 24h followed by the addition of iodobenzene and benzene boronic acid, added at an interval of 4h. The hot reaction mixture is allowed to cool and extracted with chloroform/water. The organic layer was vacuum dried and further purified by re-precipitation in methanol. **PFPDA:** Yield=90 mg, 77%. ^{1}H NMR (400 MHz, $CDCl_3$, δ ppm): 7.84-7.79 (b), 7.69-7.62 (b), 7.52-7.49 (b), 3.72 (b), 2.02 (b), 1.26-1.10 (b), 0.84-0.80 (b). GPC in THF, polystyrene standard: Mw = 32.5 ×10^3 g/mol, PDI- 1.66. FT-IR (KBr, cm^{-1}): 3422, 3339, 2925, 2855, 1742, 1611, 1457, 1258, 1089, 1018, 799, 723.

P0: Yield=100 mg, 80% ^{1}H NMR (400 MHz, $CDCl_3$, δ ppm): 7.85-7.78 (b), 7.70-7.61 (b), 7.60-7.53 (b), 2.08 (b), 1.64 (b), 1.23-1.09 (b), 0.81-0.78 (b). GPC in THF, polystyrene standard: Mw = 11.8 × 10^3 g/mol, PDI-1.6.

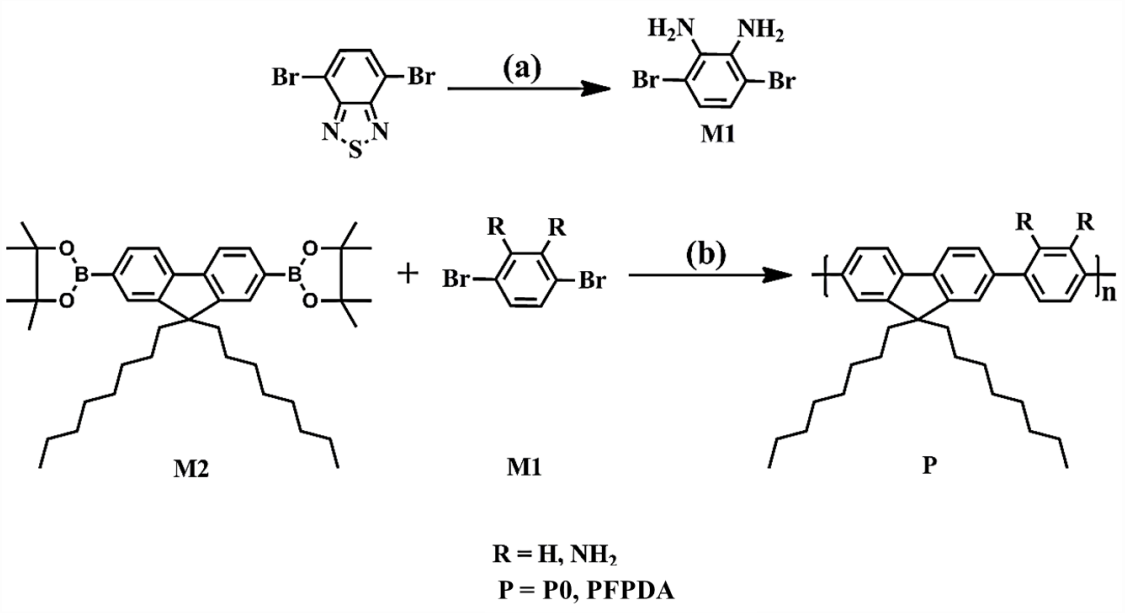

Scheme 3.1. (a) Sodium borohydride, EtOH rt (b) tetrakistriphenyl palladium, Toulene, 2M K_2CO_3, reflux, 85˚C.

3.2.3 Device assembly and electrical characterization: A cost-effective portable two-terminal sensor device was assembled using a glass slide as a substrate. At first, the microglass slide was cleaned with piranha solution (3:1 H_2SO_4:H_2O_2 mixture), deionized water followed by drying under vacuum at 100 °C for 1h. On the cleaned substrate, 100 nm

strips of Aluminium (Al) electrodes were deposited using the thermal deposition technique under vacuum (<10^{-6} mbar) using the mask for obtaining a channel with 30µm length (L) and 1500µm width (W). A 5µL PFPDA stock solution (10^{-3} M) (80nm thickness) was drop casted over the channel between the Al electrode pair. The solvent was allowed to evaporate by heating at 50 °C on a hotplate for 30min to form a thin film across the Al electrodes. Sensing studies were performed using a state-of-the-art setup connected to the two-electrode device (**Figure 3.1**). Keithley 4200-SCS semiconductor parameter analyzer was used to record all the electrical properties of the device under ambient conditions at room temperature.

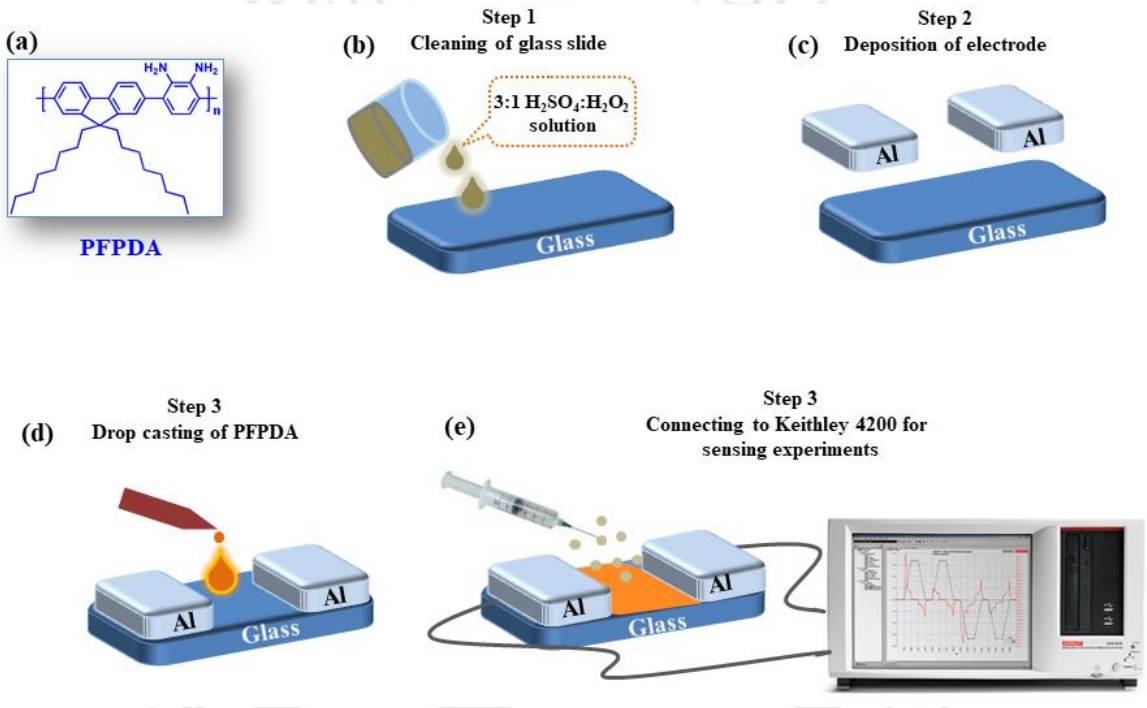

Figure 3.1: Fabrication steps of thin film electrical sensor device, (a) Structure of CP PFPDA, (b) cleaning of glass substrate using Piranha Solution, (c) thermal deposition of Aluminium (Al) electrodes on clean glass substrate, (d) deposition of PFPDA CP as a sensory channel material between the pair of Al electrode, (e) PFPDA fabricated device connected to Keithley 4200 for sensing experiments.

3.2.4 Vapor phase organophosphate detection: Various organophosphates were stored in an airtight glass vial for 2 days to accomplish full saturation over the vial headspace. For sensing experiment, organophosphate vapors were injected into the test chamber headspace at desired concentration after dilution using an airtight syringe. The

saturation concentration of organophosphate vapors was evaluated using the well-known equation.

Saturated Concentration (ppm) =Vapor Pressure (mmHg)/760 mmHg*10^6

3.2.5 Electronic Prototype: A state-of-the-art electronic prototype portable device was constructed using easily accessible, low-cost electronic component such as PCB, IC, resistors, battery, alarm buzzer, LED, etc. The presence of DCP changes the internal resistance of the device which is converted into amplified change in voltage at the output terminal of the Operational Amplifier (OPAMP) that sets the AND gate output HIGH, which in turn sets the LED as well as the loud alarm buzzer on for multiple signal output in presence of the analyte.

3.3 Result and discussion

3.3.1 Synthesis and characterization of polymer PFPDA

The synthetic strategy employed for the preparation of CPs PFPDA and P0 is illustrated in **Scheme 3.1**. The neutral CPs were prepared via Suzuki coupling polymerization in good yields. The polar amine group is incorporated in the CP backbone to provide a discriminating response to DCP. Moreover, it provides excellent solubility in polar organic solvents and thus extends its application in the solution processed fabrication of two terminal electrical sensor. The CP P0 is designed and easily synthesized as a control CP to scrutinize the strategic role of the amine group in sensing response of PFPDA fabricated sensor device. Detailed characterization spectra are included in the Supporting information file (**Figure A3.1-A3.8**).

3.3.2 Sensing and selectivity study

To demonstrate the efficient sensing ability two terminal devices is assembled using a thin film of CP PFPDA and P0 with the straightforward device configuration (**Figure 3.2a**). A two-terminal sensor device has a simple configuration and consists of thin films of drop cast CPs PFPDA and P0 over the channels between the pair of Al electrodes. The PFPDA and P0 layer of the sensor device functions as sensing element as well as conducting material that makes electrical contact with the thermally deposited Al electrode. The devices were placed in the control chamber and connected to a Keithley 4200 SCS semiconductor parameter analyzer to perform electrical measurements at ambient conditions.

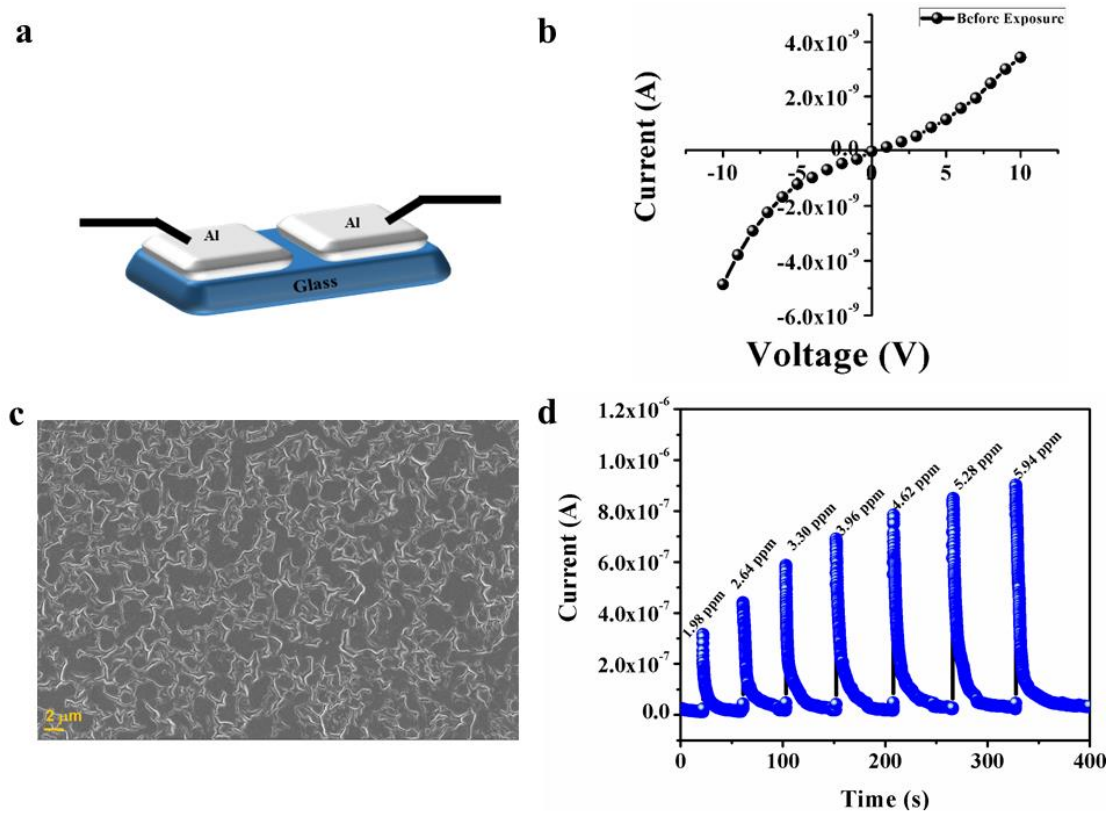

Figure 3.2. (a) Schematic representation of device architecture, (b) I-V characteristics of PFPDA fabricated device before exposure of DCP vapor, (c) FESEM image of PFPDA film (d) Sensing response of PFPDA fabricated device sensor upon subsequent addition of various concentrations of DCP vapors (From 1.98ppm to 5.94ppm).

To examine the nature of electrical contact, the I-V characteristics of CP PFPDA (**Figure 3.2b)** and P0 device sensor (**Figure A3.9**) are tested by sweeping voltage from -10V to +10V across the electrodes. I-V characteristics of both the devices (PFPDA & P0) thus obtained exhibit non-linear relationship between the current and voltage reflecting semiconductor behaviour of the CPs. Furthermore, the I-V curves reflect that CP PFPDA has a better conducting nature than the P0 as the current increment with respect to the applied voltage is more in case of PFPDA. This anomalous behaviour of PFPDA is due to the presence of the free amine groups that definitely enhances the electrical properties and sensing efficacy of PFPDA fabricated sensor device. The morphology formed by PFPDA (**Figure 3.2c)** and P0 film (**Figure A3.10**) is studied by FESEM analysis which shows even distribution of interconnected self-assembled structures that provides a high effective surface area for DCP binding and uniform flow of charge carriers.

Next, the efficacy of the CP-fabricated electrical device to detect DCP is examined by observing the change in the electrical signal. Concentrations of DCP ranging from 1.98 ppm to 5.94 ppm are subsequently introduced into the test chamber using an airtight syringe and real-time change in current intensity upon DCP exposure is monitored (**Figure 3.2d**). After exposure of 1.98 ppm DCP vapor, noteworthy increment in current intensity occurred which gets completely recovered back to its initial value on cutting off the DCP source. This remarkably reversible nature of PFPDA fabricated sensor device is also supported by I-V graphs of before (**Figure 3.2(b)** and after exposure (**Figure 3.3a**).

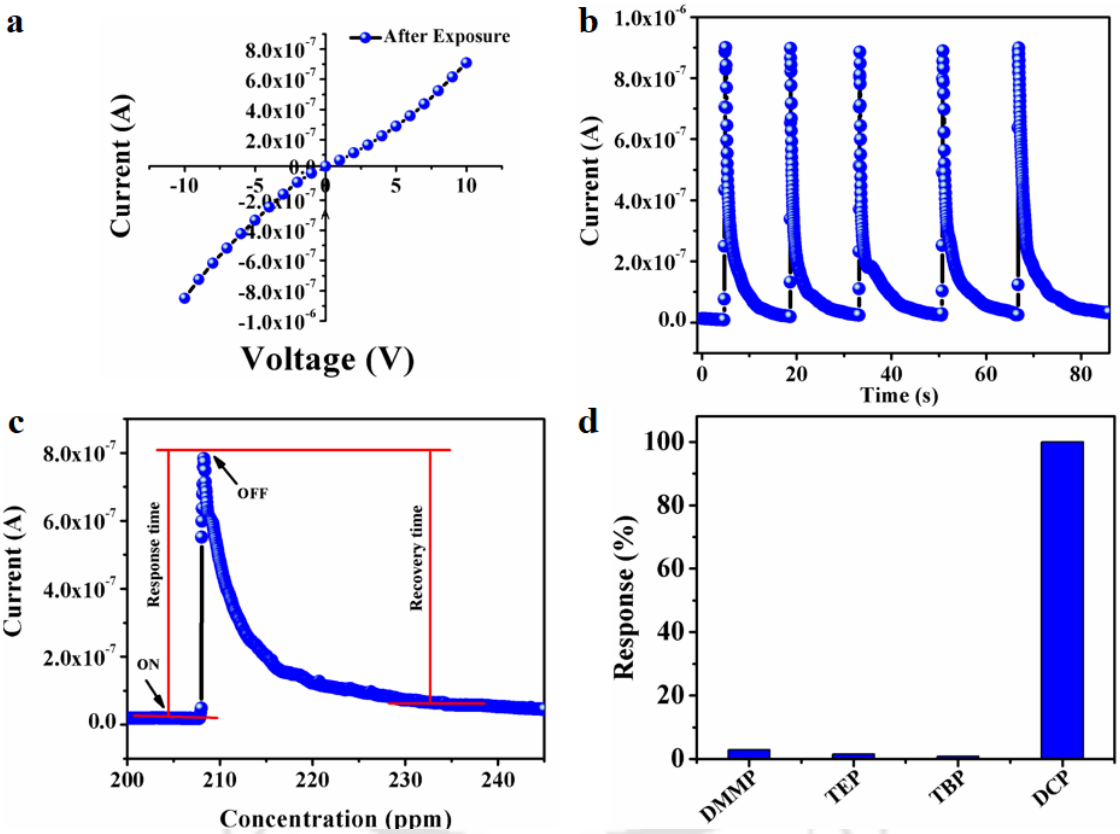

Figure 3.3 (a) I-V characteristics of PFPDA fabricated device after exposure of DCP vapor (b) Device response on periodical exposure of DCP vapor (5.94ppm). (c) Response and recovery time of PFPDA fabricated device sensor for DCP vapor (d) Selectivity studies of PFPDA fabricated sensor with vapors of other organophosphorus compounds.

Such instantaneous change in output current signal represents excellent sensitivity of sensor device towards DCP vapors. A similar sensing experiment is also performed using a control device i.e., P0 fabricated device. However, the P0 fabricated device failed to produce a significant electrical response after introducing DCP vapors of a much higher concentration of 52 ppm into the test chamber (**Figure A3.11**). Furthermore, the reproducibility of

sensing response for the sensor devices is analysed by exposing it with the same concentration (5.94 ppm) repetitively after a certain interval. The PFPDA fabricated device shows reproducible nature which makes the device feasible for real-time sensing of nerve gas agent (**Figure 3.3b**). The limit of detection (LOD) value is obtained from a linear calibration curve by deducing the maximum current intensity plotted against different DCP concentrations (**Figure A3.12**). The LOD value of 5.88 ppb calculated according to the standard reported method[37] is incredibility low compared to other reported literature documented in **Table A3.1**. Meanwhile, the response and recovery time are calculated as the time taken by gas sensing device to reach up to 90% of total current modification after introducing analyte vapors and the time needed to return back to 90% of initial current value on cutting off the analyte vapor source respectively. An average short response time of 3s and recovery time of 24s is observed for 4.62 ppm of DCP vapors (**Figure 3.3c)**.

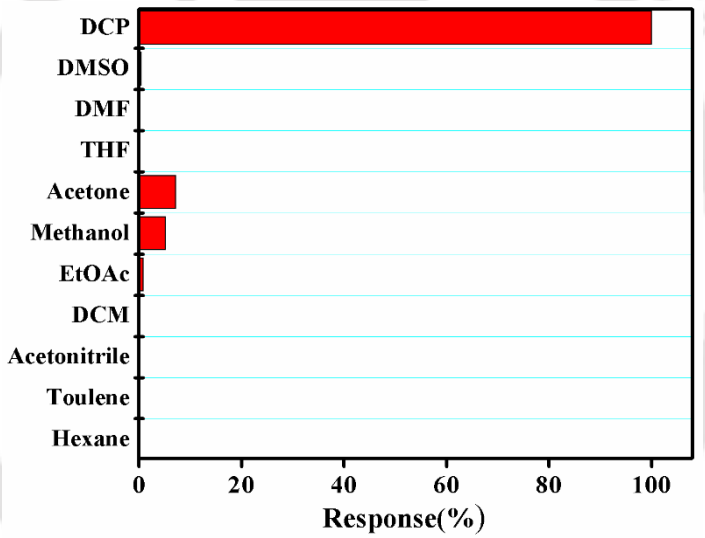

Figure 3.4: Sensing Response with other common organic solvents.

To gain more insight into the selective recognition by polymer film-based sensor device, vapor phase sensing experiment is carried out in parallel with other organophosphorus compounds viz. DMMP, TEP, and TBP and compared with DCP vapors. It is evident that other interfering analytes did not give significant device response even at higher concentrations (50 ppm) compared to a minuscule concentration of DCP vapors (5.94 ppm) (**Figure 3.3d)**, clearly demonstrating the unique discriminating ability for various organophosphates and the mechanistic role of free amines on the CP backbone. The selectivity of the device is verified in the presence of competing organic solvents but no notable responses are observed (**Figure 3.4**). Thus, such a fast response, remarkably selective and sensitive nature of PFPDA fabricated device towards the DCP vapor makes this protocol as a convenient onsite practical platform compared to other reported methods.

3.3.3 Effect of temperature and humidity on sensing

The effect of temperature on the sensing performance of the PFPDA fabricated device is investigated as shown in **Figure A3.13a-b**. The ambient condition of our laboratory was 25°C with Relative humidity of 45%. The temperature of the device was varied from 25°C to 50°C and the efficacy of the device was monitored after exposing the 4.62ppm of DCP vapor. At ambient temperature i.e., 25°C, the device shows the highest response and decreases by 26% on increasing the temperature up to 40°C and gets further reduced at 50°C by 15% compared to the ambient temperature. The decrease in performance of the device with the rise in temperature is consistent with the phenomenon of physisorption which is inversely proportional to temperature. Thus, at high temperatures, the number of DCP molecules getting adsorbed at the surface of PFPDA film is lesser which leads to a decrease in the efficacy of the device.

Similarly, the effect of humidity on performance of sensor device is examined at different humidity levels as shown in **Figure A3.14a-b**. At 0% relative humidity (vacuum) the device displayed highest response, which gets reduced by 22% at relative humidity of 45%. On further increasing the humidity of 85% the response gets decreased by 12% only. This anomalous behavior of the device is due to the fact that at high RH, there is strong competition between the DCP and water molecule for getting diffused or absorbed at the surface of PFPDA film. Thus, the sensor's performance is very promising at ambient conditions i.e., 25˚C and 45% RH, and can be deployed for real-time monitoring of chemical warfare attacks without imposing any specific experimental conditions.

3.3.4 Sensing mechanism

The sensing mechanism of the organic semiconductor-based sensor can be defined by the type of molecular interactions involved between the recognition element of the semiconductor and target analyte. Once the analyte gets diffused or adsorbed on the sensory layer, it undergoes different interactions such as dipole-dipole, acid-base, dipole-induced dipole, hydrogen bonding, covalent and ionic, etc. A key attribute of the CP-based sensor is its ability to transform a single binding event into an amplified signal by the "molecular wire effect" from its collective units. The amine functional groups are strategically incorporated in CP to boost the likelihood of complexation with organophosphates. On exposure to DCP vapor, the PFPDA fabricated device displays a reversible increment in the current signal, which gets back to its original position after the withdrawal of DCP vapors. The reversible nature of the current signal rules out the possibility of covalent

binding between the DCP and PFPDA CP and reflects the presence of other weak interactions. The PFPDA CP is a p-type material having liable lone pair at nitrogen atom of the amine group that promotes dipole-dipole interaction with polar organophosphates (electron deficient molecules). The magnitude of such interaction varies according to the dipole moment of the molecule adsorbed. The PFPDA fabricated sensor shows highest sensitivity towards DCP compared to other organophosphate derivatives viz, DMMP, TEP, TBP which can be supported by closely observing their dipole moment.[38] The dipole moment of organophosphates varies according to the order DCP>DMMP>TBP≈TEP as calculated from DFT calculations which is in line with the sensing response of PFPDA fabricated device **(Figure 3.5a)**. Moreover, organophosphates are also weak hydrogen bond acceptors and thus form H-bonding as confirmed by FTIR spectra of PFPDA CP before and after exposure to DCP vapors (**Figure 3.5b)**. The N-H stretching frequency of primary amine (3422, 3339 cm^{-1}) gets broadened and slightly shifted to higher energy (3429, 3348 cm^{-1}) after the DCP exposure that confirms hydrogen bond formation. The redox interactions (doping by DCP) at the surface of semiconductor PFPDA CP create local charge carriers that migrate throughout the conjugation length and thus give rise to the amplified current signal. The possible redox interaction between the DCP molecule and PFPDA CP is shown in **Figure 3.6**.

To gain more insight into sensing mechanism of PFPDA fabricated sensor and particularly the role of the amine moiety in the detection of DCP molecule, a similar sensing experiment was carried out with P0 CP (without amine groups) fabricated device (Control). Interestingly, the P0 fabricated sensor device does not produce any notable change in current signal on exposure to DCP vapor which clearly confirms that the presence of amine groups is vital for redox interaction between the semiconductor CP and organophosphates. Thus, by strategically incorporating the amine group into the CP backbone, high-performance two terminal toxic gas sensors are fabricated which can detect as well as distinguish various kinds of nerve gas mimics rapidly and provide mechanistic insights on the detection process of this device.

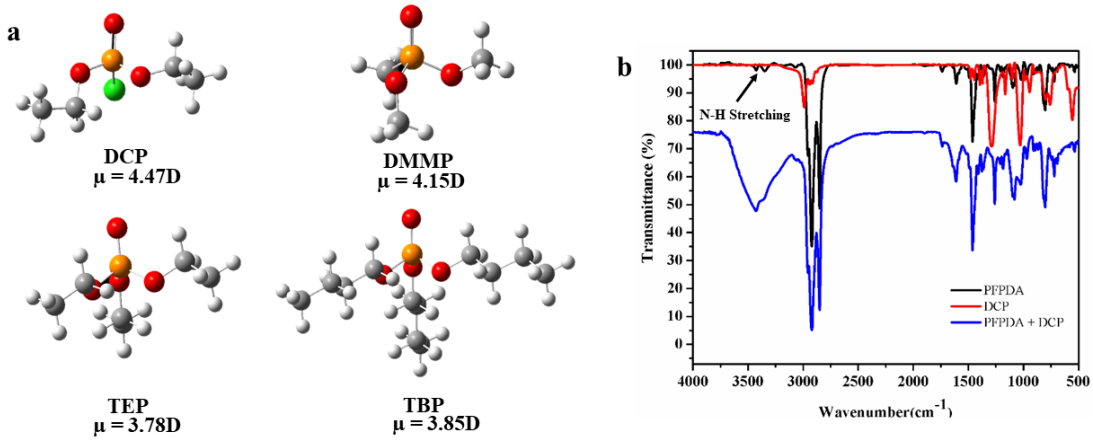

Figure 3.5: (a) Optimized structures of organophosphates and respective dipole moment as calculated by DFT calculation using B3LYP (6-31G*) function in Gaussian Program, (b) FT-IR spectra of PFPDA before and after exposing DCP vapors.

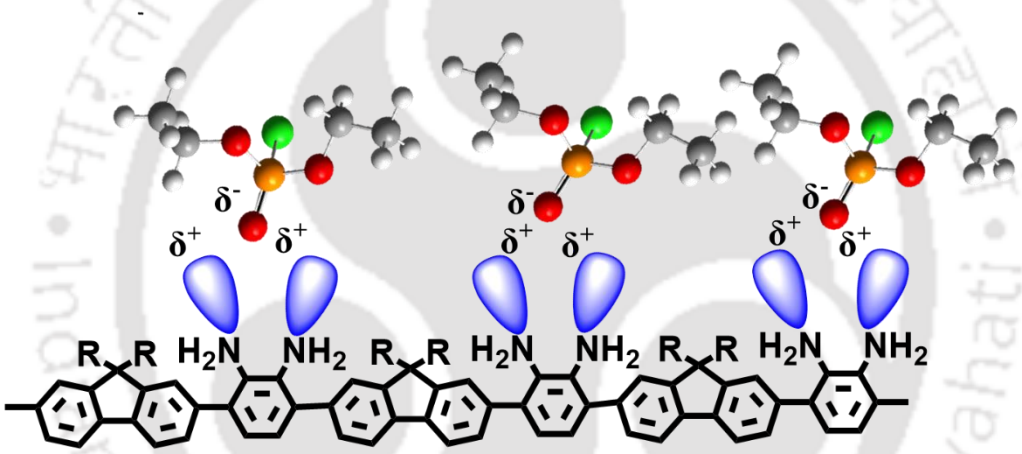

Figure 3.6: Possible Dipole-dipole Interaction between PFPDA CP and DCP molecule.

3.3.5 Development of electronic model for real time application

To check the viability of this PFPDA fabricated device for practical application, an electronic prototype version is deployed for the rapid and onsite detection of nerve gas vapors. The electronic prototype was assembled using low-cost easily accessible electronic components. The electronic circuit is made up of two main components i.e., the amplifier and logic gate (**Figure A3.15**).

Amplifier part is designed by means of non-inverting amplifier configuration of Operational Amplifier (OPAMP). LM324 IC has been used for this purpose. The logic gate part is made of AND gate (7408 IC) which detects the output from the OPAMP. The device for vapor phase detection of DCP is connected to the non-inverting input of the LM324 IC (OPAMP) via a potential divider configuration. The voltage at this input is amplified by

means of a combination of resistance at the inverting input of the IC. This amplification is necessary as the current flowing through the device is below the working limit of the circuit under normal applied bias because the device resistance is very high (of the order MΩ). In such a case, in order to detect even a small change in resistance of the prototype device due to the presence of DCP vapors with high precision using low-cost commercially available ICs, the amplification stage is a necessity. The change in device resistance (or conductance) due to the presence of DCP vapor is converted to change in voltage due to the presence of the potential divider circuit; which in turn changes the amplified voltage at the output terminal of OPAMP. Thus, a small change in resistance at the input is converted into a detectable large change in voltage at the output. On the other hand, one input of the AND gate is kept at logic 'HIGH' and the other input is fed from the output of the OPAMP.

The output of AND gate will be 'HIGH' (on) only when both the inputs of the gate are 'HIGH'. Otherwise, the output of AND gate remains at 'LOW' (off). The amplification value controlled by the combination of resistances at inverting input of OPAMP is set in such a way that its output remains at logic 'LOW' when DCP is not present on the device. Whereas, in the presence of DCP the output changes to logic "HIGH'. When this happens, the output of the AND gate gets to level 'HIGH', which sets the LED and the alarm buzzer on, thereby confirming the presence of DCP vapor in the system as shown in **Figure 3.7a-b**. Thus, it can be deployed for rapid detection of a nerve agent in crowded places and urban environment or even at remote locations and operated by a common man without any laboratory setup. Thus, a fast, cost-effective, portable and equipment free visual and sound output-based detection system is developed for real-time monitoring of the lethal nerve agent mimics.

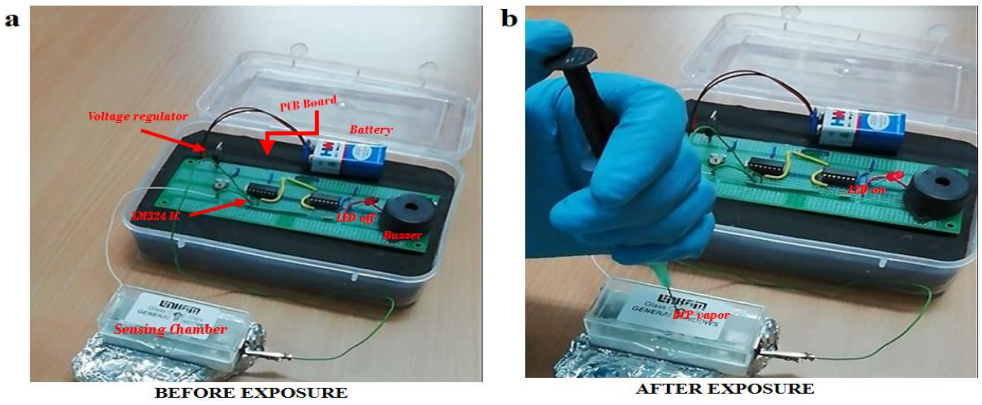

Figure 3.7. Visuals of operating electronic prototype device before (a) and after (b) DCP vapor exposure.

3.4 Conclusion

In summary, a simple configured, low-cost, portable sensor that can rapidly detect DCP vapor and distinguish it from other competing analytes has been developed with multiple output signals such as bright visual signals from LED and loud alarm buzzer. A highly sensitive and discriminating response is achieved by using newly designed PFPDA CP as a sensory layer of the two-terminal sensor. Mechanistic investigation suggested that the redox interactions between the organophosphates and amine functional moiety of PFPDA CP are responsible for its excellent sensitivity with a detection limit of 5.8 ppb. Moreover, the sensing response of the PFPDA CP fabricated sensor device is reversible and reproducible under similar exposure representing the feasibility of a device for repeated multiple uses. These excellent features of PFPDA CP fabricated electrical sensor demonstrates its enormous potential for on-site detection of nerve agent and thereby strengthen the homeland and national security from toxic chemical threats.

References

(1) Kim, H. J.; Lee, J. H.; Lee, H.; Lee, J. H.; Lee, J. H.; Jung, J. H.; Kim, J. S. A Mesoporous, Silica-Immobilized-Nanoparticle Colorimetric Chemosensor for the Detection of Nerve Agents. *Adv. Funct. Mater.* **2011**, *21*, 4035-4040.

(2) Kim, T. I.; Maity, S. B.; Bouffard, J.; Kim, Y. Molecular Rotors for the Detection of Chemical Warfare Agent Simulants. *Anal. Chem.* **2016**, *88*, 9259-9263.

(3) Wild, A.; Winter, A.; Hager, M. D.; Schubert, U. S. Fluorometric, Water-Based Sensors for the Detection of Nerve Gas G Mimics DMMP, DCP and DCNP. *Chem. Commun.* **2012**, *48*, 964-966.

(4) Stassen, I.; Bueken, B.; Reinsch, H.; Oudenhoven, J. F. M.; Wouters, D.; Hajek, J.; Speybroeck, V. V.; Stock, N.; Vereecken, P. M.; Schaijk, R. V.; Vos, D. D.; Ameloot, R. Towards Metal-Organic Framework based Field Effect Chemical Sensors: Uio-66-NH2 for Nerve Agent Detection. *Chem. Sci.* **2016**, *7*, 5827-5832.

(5) Lee, J.; Seo, S.; Kim, J. Colorimetric Detection of Warfare Gases by Polydiacetylenes Toward Equipment-Free Detection. *Adv. Funct. Mater.* **2012**, *22*, 1632-1638.

(6) Royo, S.; Manez, R. M.; Sancenon, F.; Costero, A. M.; Parra, M.; Gil, S. Chromogenic and Fluorogenic Reagents for Chemical Warfare Nerve Agents' Detection. *Chem. Commun.* **2007**, 4839-4847.

(7) Kwon, O. S.; Park, C. S.; Park, S. J.; Noh, S.; Kim, S.; Kong, H. J.; Bae, J.; Lee, C. S.; Yoon, H. Carboxylic Acid-Functionalized Conducting-Polymer Nanotubes as Highly Sensitive Nerve-Agent Chemiresistors. *Sci. Rep.* **2016**, *6*, 33724.DOI:10.1038/srep33724.

(8) Nourmohammadian, F.; Wu, T.; Branda, N. R. A 'Chemically-Gated' Photoresponsive Compound as a Visible Detector for Organophosphorus Nerve Agents. *Chem. Commun.* **2011**, *47*, 10954-10956.

(9) Xuan, W.; Cao, Y.; Zhou, J.; Wang, W. A FRET-based Ratiometric Fluorescent and Colorimetric Probe for the Facile Detection of Organophosphonate Nerve Agent Mimic DCP. *Chem. Commun.* **2013**, *49*, 10474-10476.

(10) Dale, T. J.; Rebek, J. Fluorescent Sensors for Organophosphorus Nerve Agent Mimics. *J. Am. Chem. Soc.* **2006**, *128*, 4500-4501.

(11) Rathfon, J. M.; Badri, Z. M. A; Shunmugam, R.; Berry, S. M.; Pabba, S.; Keynton, R. S.; Cohn, R. W.; Tew, G. N. Fluorimetric Nerve Gas Sensing Based on Pyrene Imines Incorporated into Films and Sub-Micrometer Fibers. *Adv. Funct. Mater.* **2009**, *19*, 689-695.

(12) Han, S.; Xue, Z.; Wang, Z.; Wen, T. B. Visual And Fluorogenic Detection of a Nerve Agent Simulant via a Lossen Rearrangement of Rhodamine-Hydroxamate. *Chem. Commun.* **2010**, *46*, 8413-8415.

(13) Wallace, K. J.; Fagbemi, R. I.; Andersen, F. J. F; Morey, J.; Lynth, V. M.; Anslyn, E. V. Detection of Chemical Warfare Simulants by Phosphorylation of a Coumarin Oximate. *Chem. Commun.* **2006**, 3886-3888.

(14) Climent, E.; Marti, A.; Royo, S.; Manez, R. M.; Marcos, M. D.; Sancenon, F.; Soto, J.; Costero, A. M.; Gil, S.; Parra, M. Chromogenic Detection of Nerve Agent Mimics by Mass Transport Control at the Surface of Bifunctionalized Silica Nanoparticles. *Angew. Chem. Int. Ed.* **2010**, *49*, 5945-5948.

(15) Rusu, A. D.; Moleavin, I. A.; Hurduc, N.; Hamel, M.; Rocha, L. Fluorescent Polymeric Aggregates for Selective Response to Sarin Surrogates. *Chem. Commun.* **2014**, *50*, 9965-9968.

(16) Jo, S.; Kim, D.; Son, S. H.; Kim, Y.; Lee, T. S. Conjugated Poly(fluorene-quinoxaline) for Fluorescence Imaging and Chemical Detection of Nerve Agents with Its Paper-Based Strip. *ACS Appl. Mater. Inter.* **2014**, *6*, 1330-1336.

(17) Balamurugan, A.; Lee, H. I. A Visible Light Responsive On-Off Polymeric Photoswitch for the Colorimetric Detection of Nerve Agent Mimics in Solution and in the Vapor Phase. *Macromolecules* **2016**, *49*, 2568-2574.

(18) Clavaguera, S.; Carella, A.; Caillier, L.; Celle, C.; Pecaut, J.; Lenfant, S.; Vuillaume, D.; Simonato, J. P. Sub-ppm Detection of Nerve Agents Using Chemically Functionalized Silicon Nanoribbon Field-Effect Transistors. *Angew. Chem. Int. Ed.* **2010**, *49*, 4063-4066.

(19) Hwang, H. M.; Hwang, E.; Kim, D.; Lee, H. Mesoporous Non-stacked Graphene-receptor Sensor for Detecting Nerve Agents. *Sci. Rep.* **2016**, 6.DOI:10.1038/srep33299.

(20) Lee, J.S.; Shin, D.H.; Jun, J.; Jang; J. Multidimensional Polypyrrole/Iron Oxyhydroxide Hybrid Nanoparticles for Chemical Nerve Gas Agent Sensing Application. *ACS Nano.* **2013**, *7*, 10139–10147.

(21) Taranekar, P.; Baba, A.; Park, J. Y.; Fulghum, T. M.; Advincula, R. Dendrimer Precursors for Nanomolar and Picomolar Real-Time Surface Plasmon Resonance/Potentiometric Chemical Nerve Agent Sensing Using Electrochemically Crosslinked Ultrathin Films. *Adv. Funct. Mater.* **2006**, *16*, 2000-2007.

(22) Kwon, O. S.; Park, S. J.; Lee, J. S.; Park, E.; Kim, T.; Park, H. W.; You, S. A.; Yoon, H.; Jang, J. Multidimensional Conducting Polymer Nanotubes for Ultrasensitive Chemical Nerve Agent Sensing. *Nano Lett* **2012**, *12*, 2797-2802.

(23) Wang, F.; Gu, H.; Swager, T. M. Carbon Nanotube/Polythiophene Chemiresistive Sensors for Chemical Warfare Agents. *J. Am. Chem. Soc.* **2008**, *130*, 5392-5393.

(24) Lee, J. S.; Kwon, O. S.; Park, S. J.; Park, E. Y.; You, S. A.; Yoon, H.; Jang, J. Fabrication of Ultrafine Metal-Oxide Decorated Carbon Nanofibers for DMMP Sensor Application. *ACS Nano* **2011**, *5*, 7992-8001.

(25) Das, D.; Gopikrishna, P.; Singh, A.; Dey, A.; Iyer, P. K. Efficient Blue and White Polymer Light Emitting Diodes based on a Well Charge Balanced, Core Modified Polyfluorene Derivative. *Phys. Chem. Chem. Phys.* **2016**, *18*, 7389-7394.

(26) Hussain, S.; Malik, A. H.; Afroz, M. A.; Iyer, P. K. Ultrasensitive Detection of Nitroexplosive - Picric Acid via a Conjugated Polyelectrolyte in Aqueous Media and Solid Support. *Chem. Commun.* **2015**, *51*, 7207-7210.

(27) Malik, A. H.; Hussain, S.; Kalita, A.; Iyer, P. K. Conjugated Polymer Nanoparticles for the Amplified Detection of Nitro-explosive Picric Acid on Multiple Platforms. *ACS Appl. Mater. Inter.* **2015**, *7*, 26968-26976.

(28) Tang, N.; Zhou, C.; Xu, L.; Jiang, Y.; Qu, H.; Duan, X. A Fully Integrated Wireless Flexible Ammonia Sensor Fabricated by Soft Nano-Lithography *ACS Sens.* **2019**, *4*, 726-732.

(29) Wang, X.; Li, S.; Zhang, P.; Lv, F.; Liu, L.; Li, L.; Wang, S. An Optical Nanoruler Based on a Conjugated Polymer−Silver Nanoprism Pair for Label-Free Protein Detection *Adv. Mater.* **2015**, *27*, 6040–6045.

(30) Zhu, S.; Wang, X.; Yang, Y.; Bai, H.; Cui, Q.; Sun, H.; Li, L.; Wang, S. Conjugated Polymer with Aggregation-Directed Intramolecular Förster Resonance Energy Transfer Enabling Efficient Discrimination and Killing of Microbial Pathogens *Chem. Mater.* **2018**, *30*, 3244-3253.

(31) Zhang, C.; Chen, P.; Hu, W. Organic Field-Effect Transistor-Based Gas Sensors. *Chem. Soc. Rev.* **2015**, *44*, 2087-2107.

(32) Mishra, R. K.; Hubble, L. J.; Martin, A.; Kumar, R.; Barfidokht, A.; Kim, J.; Musameh, M. M.; Kyratzis, I. L.; Wang, J. Wearable Flexible and Stretchable Glove Biosensor for On-Site Detection of Organophosphorus Chemical Threats. ACS Sensors 2017, 2, 553-561.

(33) Zhu, R.; Azzarelli, J. M.; Swager, T. M. Wireless Hazard Badges to Detect Nerve-Agent Simulants. *Angew. Chem. Int. Ed.* **2016**, *55*, 9662-9666.

(34) Lee, P. I.; Hsu, S. L. C.; Lin, P. White-Light-Emitting Diodes from Single Polymer Systems based on Polyfluorene Copolymers with Quinoxaline Derivatives. *Macromolecules* **2010**, *43*, 8051-8057.

(35) Yamaguchi, I.; Choi, B. J.; Koizumi, T. A.; Kubota, K.; Yamamoto, T. π-Conjugated Polyphenylenes with Diazaborole Side Chains Synthesized via 1,2-phenylenediamine Polymer. *Macromolecules* **2007**, *40*, 438-443.

(36) Giovanella, U.; Botta, C.; Galeotti, F.; Vercelli, B.; Battiato, S.; Pasini, M. Perfluorinated Polymer with Unexpectedly Efficient Deep Blue Electroluminescence for Full-Colour OLED Displays and Light Therapy Applications. *J. Mater. Chem. C* **2013**, *1*, 5322-5329.

(37) Kalita, A.; Hussain, S.; Malik, A. H.; Subbarao, N. V. V.; Iyer, P. K. Vapor Phase Sensing of Ammonia at the Sub-Ppm Level Using a Perylene Diimide Thin Film Device. *J. Mater. Chem. C* **2015**, *3*, 10767-10774.

(38) Snow, E. S.; Perkins, F. K.; Houser, E. J.; Badescu, S. C.; Reinecke, T. L. Chemical Detection with a Single-Walled Carbon Nanotube Capacitor. *Science* **2005**, *307*, 1942-1945.

Appendix

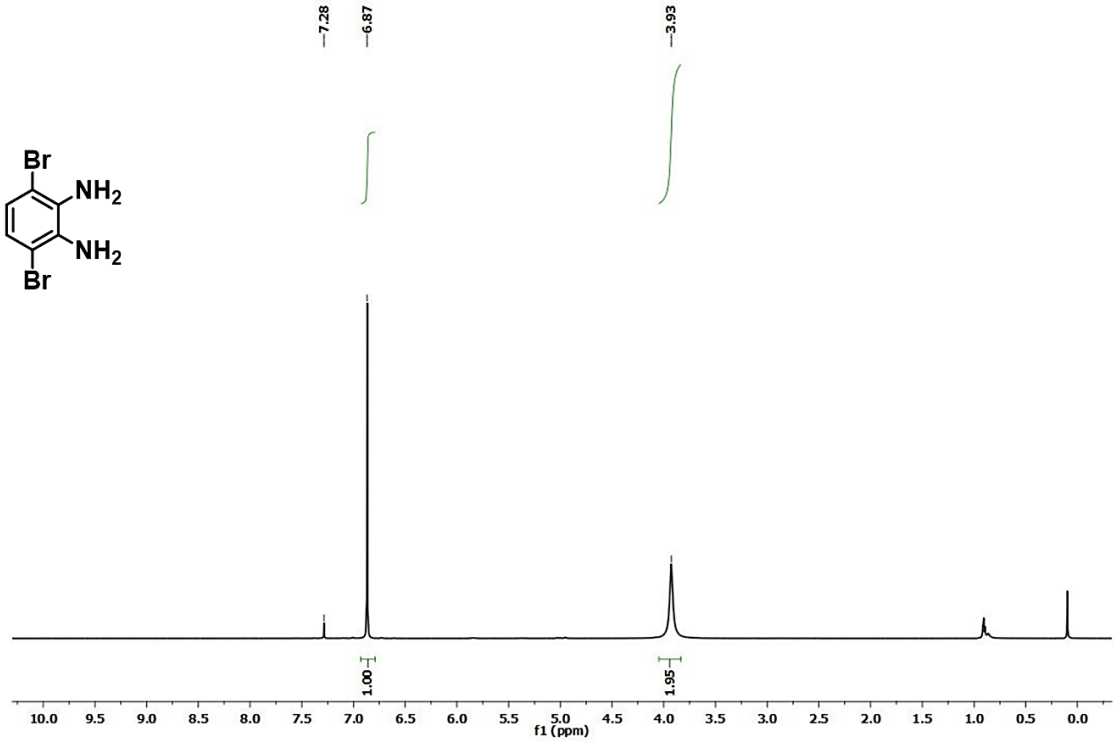

Figure A3.1. ^{1}H NMR (600 MHz, $CDCl_3$) of M1.

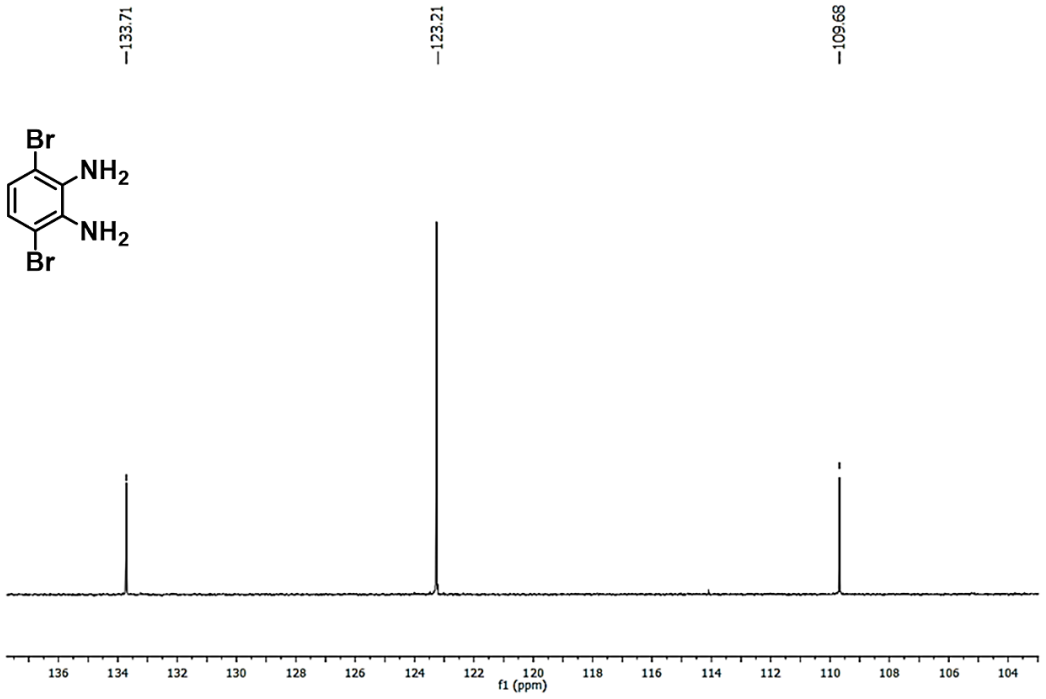

Figure A3.2. ^{13}C NMR (150MHz, $CDCl_3$) of M1.

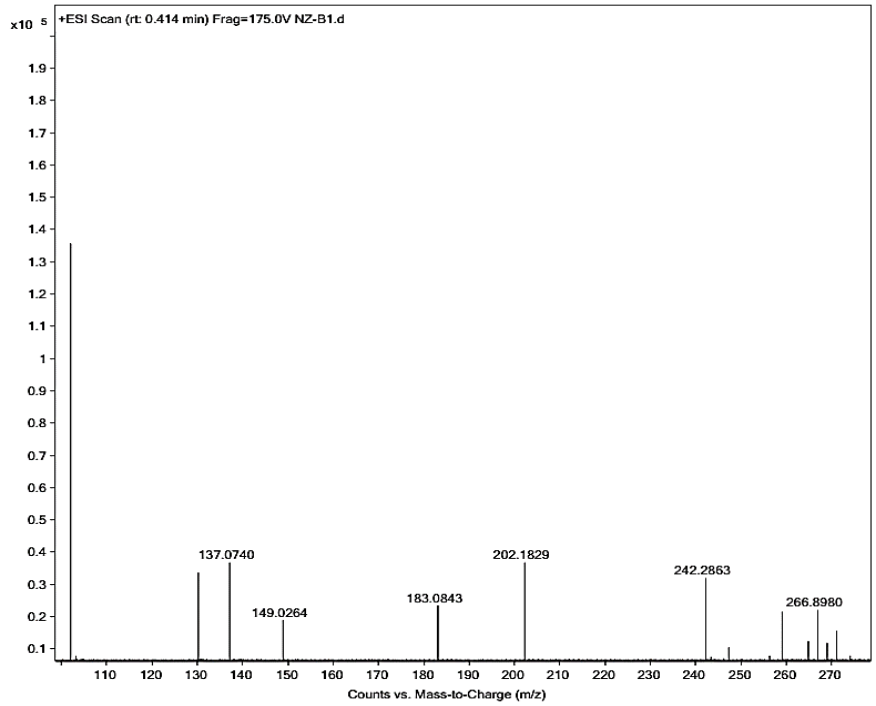

Figure A3.3. Mass spectra of M1.

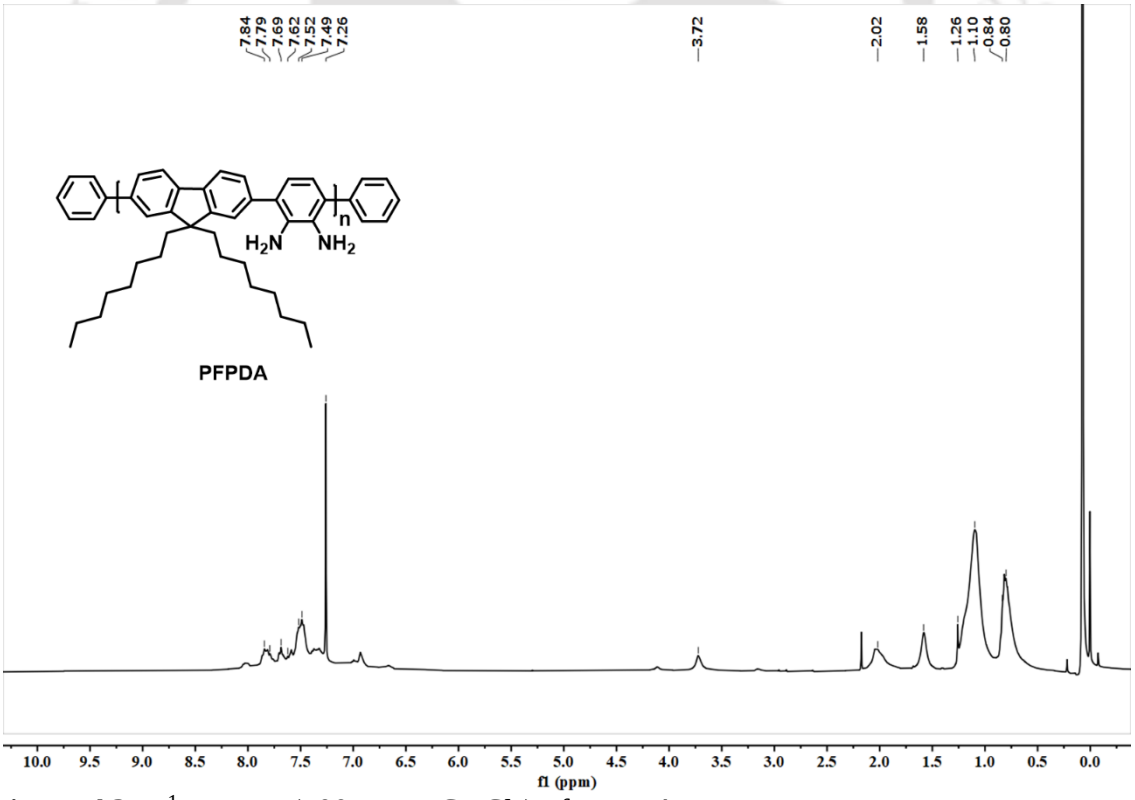

Figure A3.4. ^{1}H NMR (400 MHz, $CDCl_3$) of PFPDA.

GPC Results

	Retention Time (min)	% Area	Mn	Mw	MP	Mz	Mz+1	Polydispersity
1	7.667	100.00	19653	32575	21204	54654	81206	1.657525

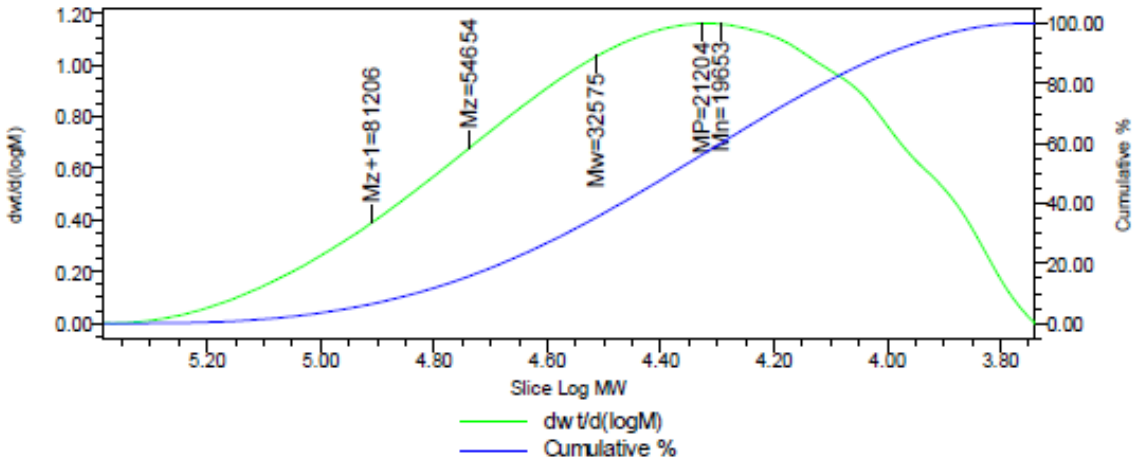

Figure A3.5. GPC chromatogram of polymer PFPDA.

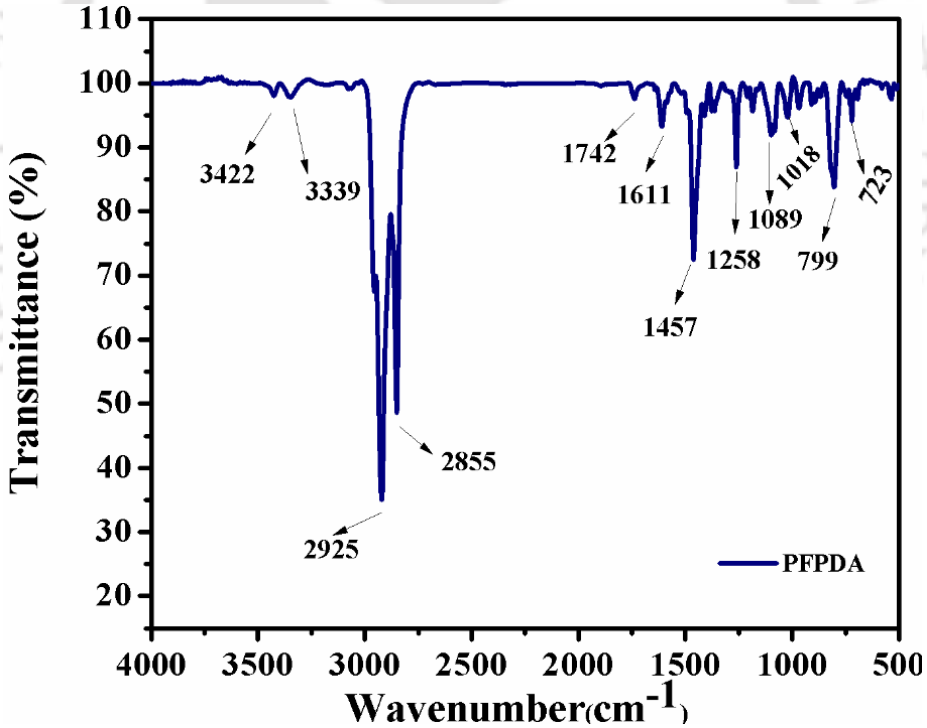

Figure A3.6. FT-IR spectra of PFPDA.

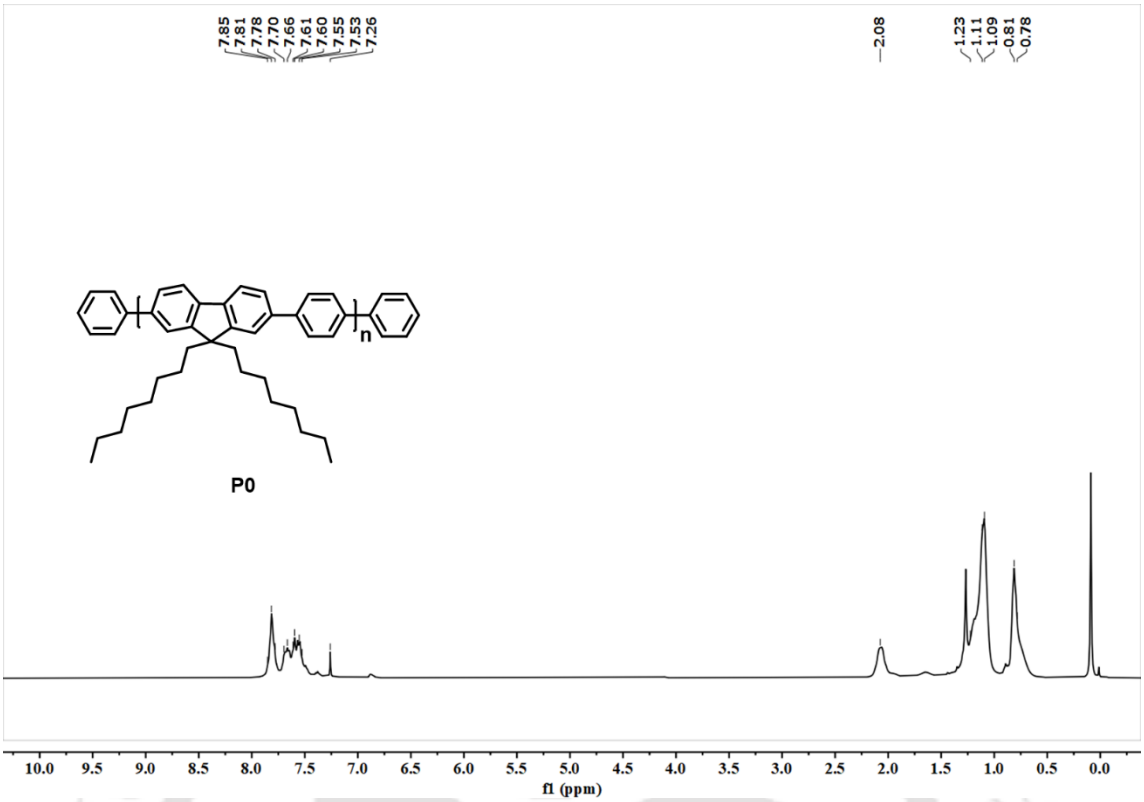

Figure A3.7. ^{1}H NMR (400 MHz, CDCl3) of P0.

GPC Results

	Retention Time (min)	% Area	Mn	Mw	MP	Mz	Mz+1	Poly dispersity
1	8.300	100.00	7594	11844	9133	17834	23828	1.559645

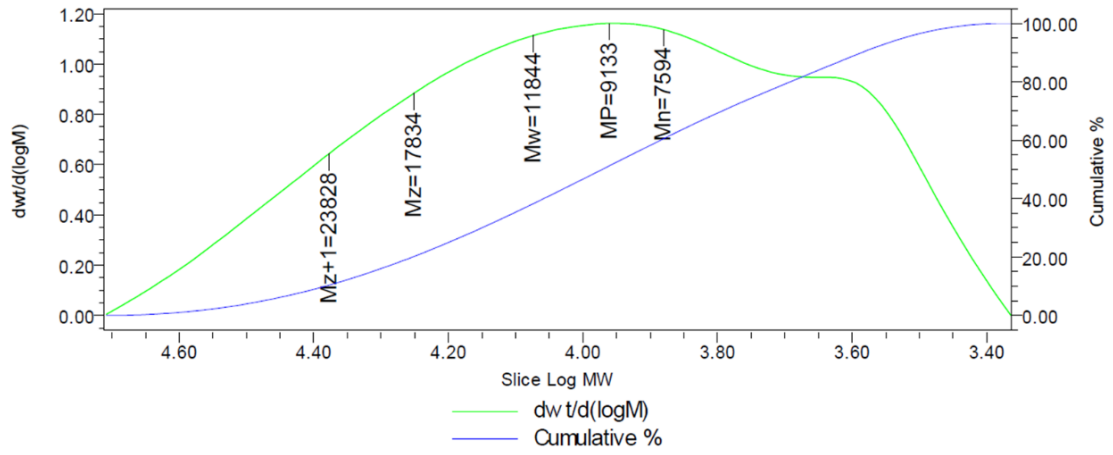

Figure A3.8. GPC chromatogram of polymer P0.

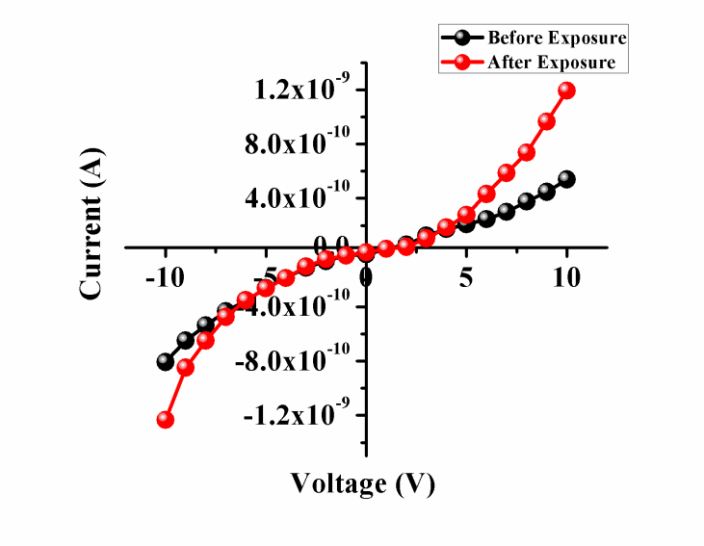

Figure A3.9. I-V graph of P0 before and after exposure of DCP vapor.

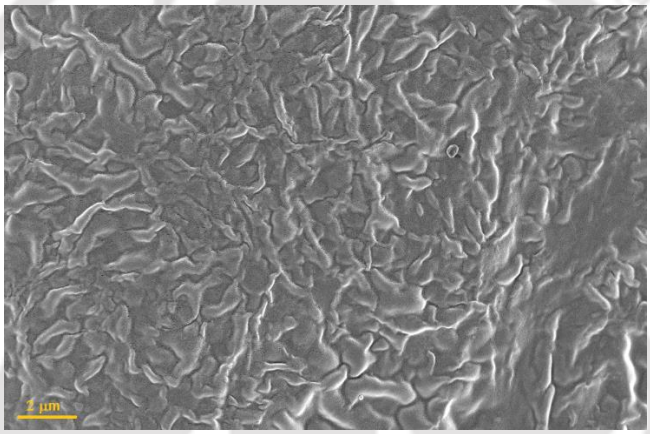

Figure A3.10: FESEM images of P0 thin film.

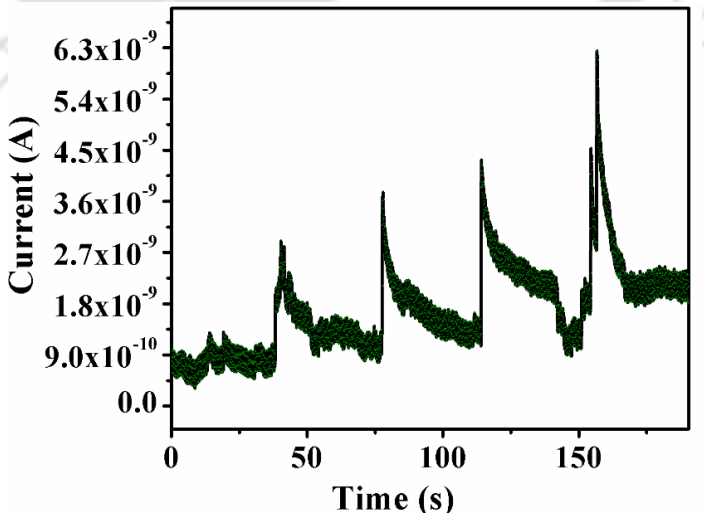

Figure A3.11: Sensing response of P0 after exposure of various concentration of DCP vapor.

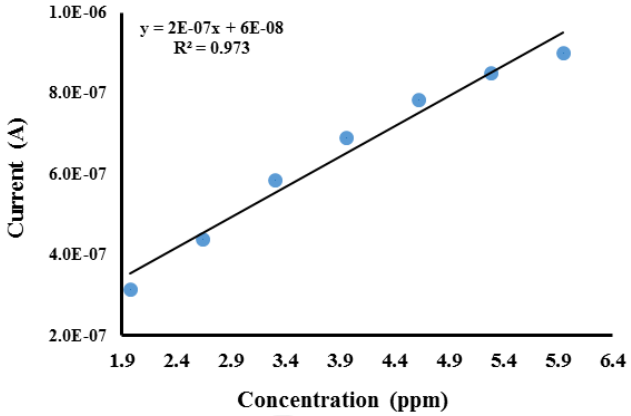

Figure A3.12: Detection limit plot of DCP in vapor phase (5.88 ppb).

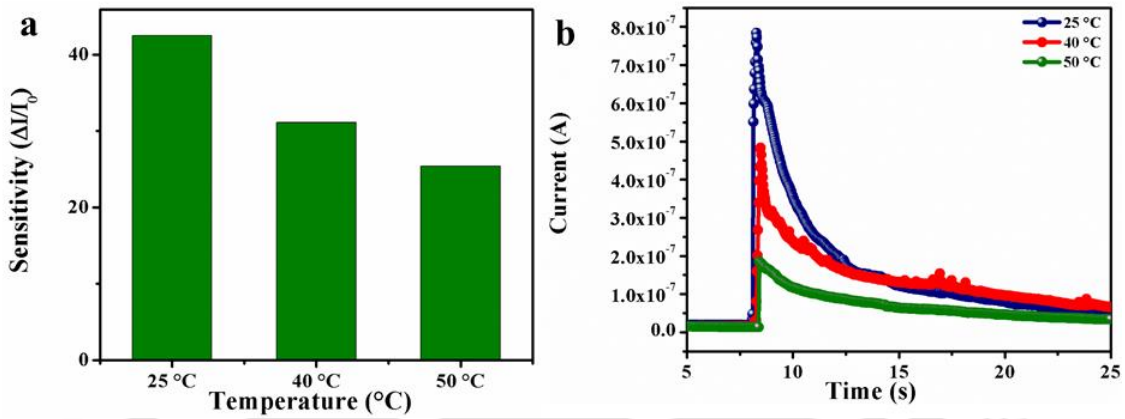

Figure A3.13: Effect of temperature on performance of PFPDA fabricated sensor device, (a) Sensitivity of PFPDA device at different temperature (25 °C to 50 °C), (b) Change in current response of the device at different temperature.

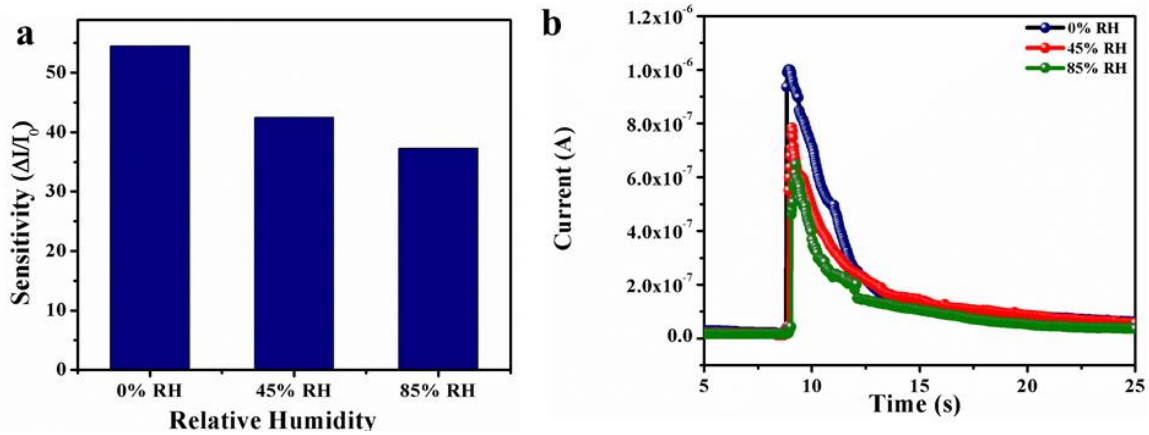

Figure A3.14: Effect of humidity on performance of PFPDA fabricated sensor device, (a) Sensitivity of PFPDA device at different relative humidity, (b) Change in current response of the device at different relative humidity.

Table A3.1: A comparative study of reported literature for Nerve agent detection with our work.

Publication	**Method**	**Material Used**	**LOD**	**Mode of Detection**
Present work	***Electrical***	***Conjuagted Polymer***	***5.88ppb***	***Vapor phase***
Macromolecules **2016**, 49, 2568-2574.	Colorimetric	poly(glycidyl methacrylate-co-dimethylacrylamide)	1.0 mM	Vapor phase
ACS Appl. Mater. Interfaces **2014**,*62*, 1330-1336.	Fluorometric	poly(fluorene-co-quinoxaline)	1.49×10^{-5} M	Solution phase
Angew. Chem. Int. Ed. **2017**, *56*, 9522 –9526.	Optical sensor	Meldrum's-acid-based conjugate acceptor	88ppb	Solution phase
Adv. Funct. Mater. **2006**, *16*, 2000–2007.	Surface plasmon resonance (SPR) and potentiometry	polyamidoamine (PAMAM) carbazole/Cu^{2+} dendrimer	10^{-5} M	Vapor phase
Adv. Funct. Mater. **2012**, *22*, 1632–1638.	Colorimetric	polydiacetylene	160 ppb	Solution phase
J. Am. Chem. Soc. **2017**, *139*,4635−4638.	Optical Sensor	Small molecule based Sensor	14ppb	Solution phase
Macromolecules **2017**, *50*, 6888−6895.	Fluorometric Sensor	poly-(glycidyl methacrylate-co-dimethylacrylamide) and pyrene derivative	0.1 mM	Solution and Vapor phase
Chem. Commun., **2014**, *50*, 9965—9968.	Fluorometric Sensor	polysiloxane	12 ppb	Solution phase
Chem. Commun., **2017**, *53*, 12954—12957.	Optical Sensor	ferrocenyl dye	0.15 mM	Solution and Vapor phase
Chem. Commun., **2014**, *50*, 8511—8513.	Fluorometric Sensor	Polynorbornene	25ppb	Solution and Vapor phase
ACS Macro Lett. **2015**, *4*, 138−142.	Colorimetric	Polythiophene fused tropone	6ppm	Solution and Vapor phase
Anal. Chem. **2002**, *74*, 4343-4352.	Ion Mobility Mass	Spectrometer	1ppm	Solution phase
Anal. Chem. ***2005***, *77*, 4792-4799.	Ion Mobility Mass	Spectrometer	10ppm	Solution phase
J. Phys. Chem. C **2010**, *114*, 7986–7994.	Impedance based Sensor	Doped sodium zeolite	20-100ppm	Vapor Phase
Anal. Chem. **2004**, *76*, 2689-2693.	Potentiometric	polysiloxane	NA	Solution phase
Anal. Chem. **2010**, *82*, 3191–3197.	Impedance based Sensor	Ferrocene-Lysine modified multiwalled carbon nanotubes	50µM	Solution phase
Angew. Chem. Int. Ed. **2010**, *49*, 4063 –4066.	Field-Effect Transistors	Functionalized Silicon Nanoribbon	500–800 ppb	Vapor phase

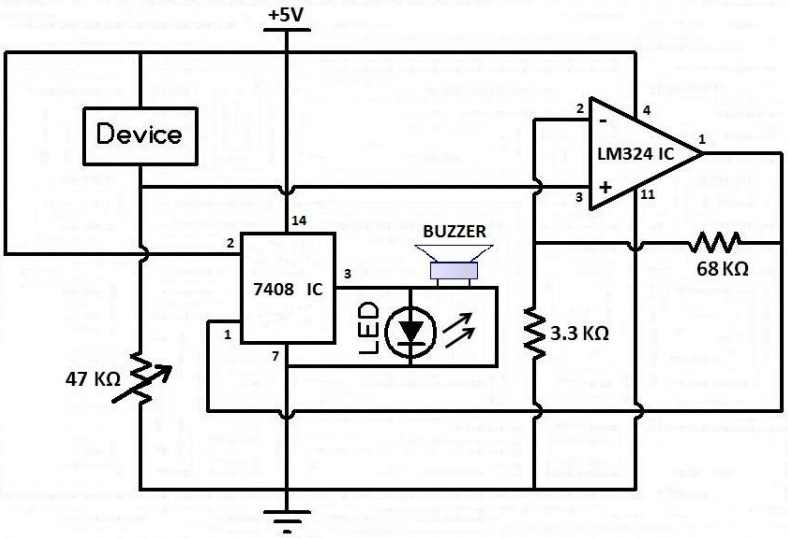

Figure A3.15: Circuit Diagram of electronic prototype for onsite detection of DCP vapor.

Chapter 4

A Portable Conjugated Polymer based Smartphone Platform for Sensitive Detection of Monoamine Neurotransmitter

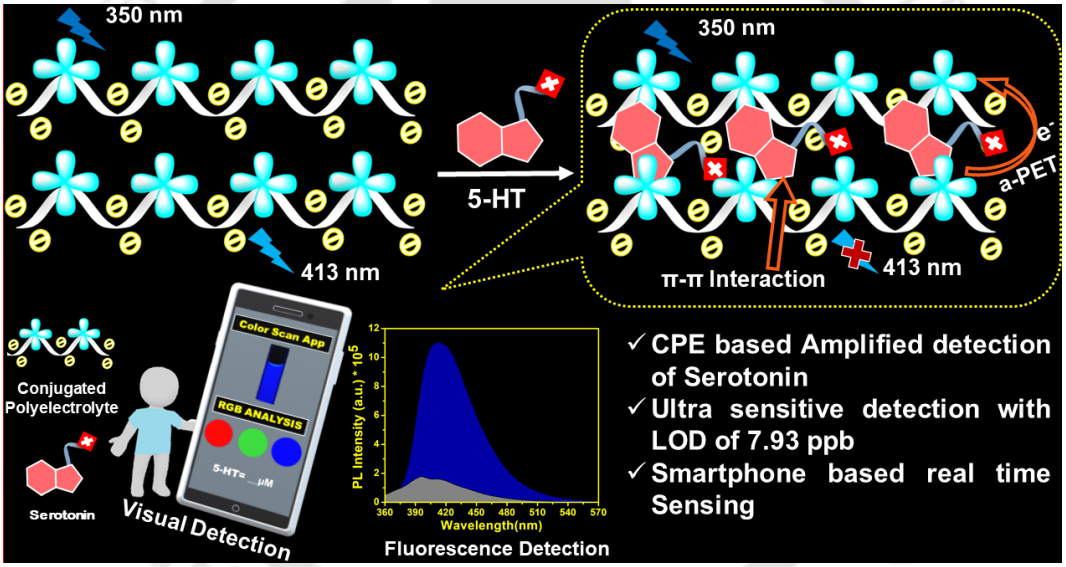

Zehra, N.; Malik, A. H.; Parui, R.; Hussain, S.; Iyer, P. K. A Portable Conjugated Polymer based Smartphone Platform for Sensitive Detection of Monoamine Neurotransmitter. (*Manuscript Communicated*)

Abstract

The precise and effective detection of neurotransmitters (NTs) is crucial for clinical investigation of neuronal processes, and timely monitoring of NT-related chronic diseases. However, sensitive detection of specific NT with unprecedented selectivity is highly challenging due to similarities in chemical and electronic structures of various interfering neurochemicals. Herein, an anionic conjugated polyelectrolyte Poly[(9,9-bis(4'-sulfonatobutyl)fluorene-co-alt-1,4-phenylene) sodium], PFPS is rationally designed and synthesized for amplified detection and point-of-care (POC) determination of monoamine neurotransmitter, serotonin (5-Hydroxy tryptamine or 5-HT, also diagnostic biomarker of carcinoid tumor) in human blood plasma. The PFPS displayed a remarkable sensing response with an exceptionally high fluorescence quenching constant of 1.14×10^5 M^{-1} and an ultralow detection limit of 7.65ppb, much below the clinical range (0.5-1.4μM). The excited-state electron transfer and aggregation caused π-π quenching governs the unparalleled sensitivity of PFPS for 5-HT even in the presence of other interfering neurochemicals. Furthermore, a smartphone-enabled portable platform is constructed for real-time onsite detection of 5-HT by quantification of visual fluorescence response of PFPS into RGB values using color recognizer android application. The smartphone platform could be readily applied for convenient, non-invasive POC testing of 5-HT levels in complex biological fluids accurately and is expected to revolutionize the clinical diagnosis and personalized health care devices.

4.1 Introduction

Neurotransmitters are endogenous chemicals that play a crucial role in transmitting the neuronal signal and are associated with brain development and functions. Among them, serotonin is one of the major monoamine neurotransmitter that regulates cognitive and behavioral functions, including mood regulation, appetite, sleep, and emotions.[1] In the brain, dysregulation of 5-HT neurotransmission has been linked to multiple neuropsychiatric diseases, including obsessive-compulsive disorder (OCD), schizophrenia, clinical depression, and autism. Surprisingly, 95% of body 5-HT is produced by enterochromaffin cells of the gut and is shuttled across the entire body where it participates in numerous physiological processes including platelet coagulation, tissue regeneration, hemostasis, and gastrointestinal tract motility.[2-6] Moreover, it has been reported that elevated 5-HT level is found in the blood plasma of patients afflicted with carcinoid tumor derived from enterchromaffin cells of small intestine.[7-11] Generally, excessively secreted 5-HT is inactivated or degraded by liver into its metabolite byproduct. However, during liver metastases, it escapes from hepatic degradation and releases into systemic circulation causing severe clinical syndrome symptoms.[12] Therefore, the rapid detection of such bioactive markers is of great importance for early diagnosis of metastasis tumors and neurological diseases.

Over the years, several techniques have been explored for 5-HT sensing that includes, mass spectrometry (MS), electrochemical assay, liquid chromatography (LC), and flow immunoassays.[1,13-17] However, most of the devised systems are either tedious or require complex instrumentation yet present lower selectivity and sensitivity than required.[18-21] For instance, selectivity of electrochemical assays is deterred by the presence of off-target neurochemicals such as ascorbic acid, dopamine, epinephrine and several other analogous molecules with similar redox potentials as that of 5-HT. In contrast, fluorescence technique represents a powerful sensing modality due to its simple operation, prompt response, superior sensitivity, and non-invasive nature. Additionally, it offers rapid and visual on-field detection simply using a UV light which facilitates the development of new generation smartphone-based point-of-care devices. In recent years, quite a few fluorescent probes have been explored for neurotransmitters detection based on small molecule probes, conjugated polymers and metal-organic frameworks.[18,22-26] However, most of these approaches seem to be trivial in terms of sensitivity, detection limit and portability. Moreover, it is often difficult to achieve high sensitivity for a specific neurotransmitter due

to their similar molecular and electronic structures. Therefore, the development of superior probes for rapid and point-of-care (PoC) measurement of 5-HT is important but remains immensely challenging.

Conjugated polyelectrolyte (CPE) has emerged as a highly renowned sensory material that consists of an electronically delocalized π-conjugated backbone and ionic moieties tethered with the conjugated main chain. CPEs have been explored with a great interest in the broad subject of sensing due to their excellent light-harvesting, signal amplification features, high quantum yield, and viability in aqueous biological systems.[27-33] The extended π-conjugated module of the CPE facilitates excitation energy transfer via the main chain to an electron or energy acceptor, accounts for its amplified sensitivity towards external stimuli.[34,35] Furthermore, the fluorescence of CPE is proficiently altered (quenched or enhanced) by the ultralow concentration of oppositely charged quencher resulting in the CPE chain aggregation with ultrafast inter/intra-chain exciton migration.[36,37] It is worth mentioning that despite their exceptional features, no constructive CP-based platform for ultrasensitive, instantaneous and onsite detection of 5-HT has been ever established, suggesting tremendous opportunities to explore.

Recently, smartphone based fluorescence strategy has emerged as a promising tool for on-field sensing and PoC testing due to its powerful data readout and processing functionality, portable and easy to operate features and thus, it has been widely used for detection of metal ions, volatile substances and diagnostic biomarkers.[38-40] For efficient performance of smartphone based devices, the recognition analyte or reagent should be highly sensitive to give visual information that would be transformed into quantitative data by android application. Herein we report a convenient, instrument free and portable smartphone-based platform for real time determination of 5-HT in 100% aqueous solution. As a sensing core, the anionic conjugated polyelectrolyte Poly[(9,9-bis(4'-sulfonatobutyl)fluorene-co-alt-1,4-phenylene) sodium], PFPS is designed and synthesized for rapid and amplified detection of 5-HT. The anionic sulphonate groups are strategically decorated at the side chain of the polymer framework to proximate the columbic interaction with positively charged 5-HT as well as to enhance its solubility in polar solvents. The PFPS displays an amplified turn-off response for 5-HT that can be recognized and converted into quantitative data by smartphone application with detection limit as low as 73 ppb. The mechanistic insights reveal that the excited-state electron transfer (a-PET), and electrostatic interaction driven aggregation caused π-π quenching is responsible for unparalleled sensitivity of PFPS towards 5-HT even in presence of other interfering neurochemicals. The present sensing

platform can be applied for PoC determination of 5-HT in blood plasma with high reliability for preliminary diagnosis of carcinoid tumors and other related medical complications.

4.2 Experimental

4.2.1 Material and Instruments: All chemicals and reagents, including Serotonin Hydrochloride (5-HT), Dopamine hydrochloride (DA), 5-hydroxy indole acetic acid (HIAA), Norepinephrine, Ascorbic acid, and Tryptophan, were purchased from Sigma-Aldrich. The ^{1}H NMR (600 and 500 MHz) and ^{13}C NMR (150 and 125 MHz) spectra were collected on Bruker Ascend 600 and Bruker Avance Neo 500 spectrometers, respectively. Absorbance and Fluorescence measurements were carried out using PerkinElmer Lambda-25 spectrophotometer and Horiba Fluoromax-4 spectrofluorometer, respectively. Cyclic Voltammetry was recorded on a CH Instruments Model 700D series electrochemical workstation. Time-resolved fluorescence studies were carried out using an Edinburgh Life Spec II instrument. FESEM images were obtained by a Sigma Carl ZEISS scanning electron microscope.

4.2.2 Synthetic procedure

4.2.2a Synthesis of 2,7-Dibromo-9,9-bis(4'-sulfonatobutyl)fluorene disodium, M: 2,7-dibromo fluorene (0.5 g, 1.5 mmol), tetrabutyl ammonium bromide (0.08g, 0.248 mmol) were transferred into a round bottom flask and degassed twice. Afterward, 1 mL of 50 wt% of sodium hydroxide solution was added. The reaction mixture was allowed to stir for 10 mins followed by successive addition of 1,4-butane sultone (0.49g, 3.6 mmol) dissolved in 9 mL DMSO solution. The reaction was stirred for 12 h at room temperature under an inert atmosphere.[41] The reaction mixture was then poured into 300 mL acetone, and the resulting precipitate was washed 3-4 times with acetone and methanol. The desired product was obtained by recrystallization in an acetone water mixture as a white crystal (0.55g, 55.7 %).

^{1}H NMR (600 MHz, D_2O, δ ppm): 7.55(s,2H), 7.55(d,2H), 7.44-7.41(d,2H), 2.45(m,4H), 1.93(m,4H), 1.33(m,4H), 0.48(m,4H).

^{13}C NMR (150 MHz, D_2O, δ ppm): 152.12, 139.02, 130.32, 126.48, 121.38, 121.23, 55.25, 50.72, 38.67, 24.14, 22.31.

4.2.2b Synthesis of Poly[(9,9-bis(4'-sulfonatobutyl)fluorene-co-alt-1,4-phenylene) sodium], PFPS: A mixture of monomer M1 (0.2g, 0.312 mmol), benzene 1,4-bisboronic acid (0.052 g, 0.318 mmol), and tetrakistriphenylphosphine palladium(0) (0.018g, 0.0156 mmol) were dissolved in DMF (8mL) and added to 50 mL two neck RB flask under inert

atmosphere. A 2M aq. K_2CO_3 (4 mL) was introduced into the flask. The reaction mixture was degassed three times via the freeze-thaw cycles. The reaction mixture was refluxed for 36h under an inert atmosphere. [42] The resulting reaction mixture was precipitated into 150 mL of acetone and purified using a dialysis membrane (molecular cut-off 2000 g/mole) for two days. The desired polymer was obtained by freeze-drying (0.18g, 81.1 %).

^{1}H NMR (500 MHz, DMSO-d6, δ ppm): 7.90-7.37 (m, 10H), 2.19 (b, 8H), 1.39 (b, 4H), 0.63 (b, 4H).

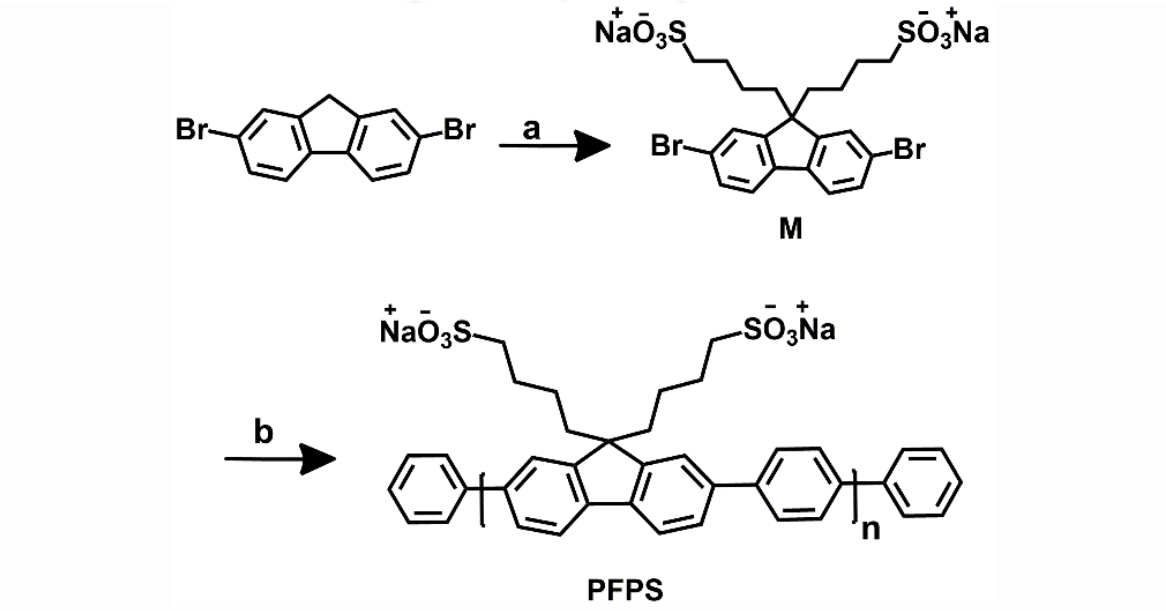

Scheme 4.1. Synthetic route to PFPS conjugated polyelectrolyte, (a) 1,4 butane sultone, NaOH, TBAB, DMSO: H_2O, RT, (b) benzene-1,4-bisboronic acid, tetrakistriphenylphosphine palladium (0), 2 M K_2CO_3 (aq.), DMF, reflux, 36h.

4.2.3 Preparation of Stock solutions and sensing studies of PFPS: The stock solution of PFPS was prepared in methanol at a concentration of 1mM. The stock solution of serotonin (5-HT) and other neurotransmitters viz. dopamine (DA), histamine (HA), epinephrine (EPI), 5-hydroxy indole acetic acid (5-HIAA) were prepared in aqueous solution (10 mM HEPES, buffer pH 7.4) at a concentration of 10mM. Similarly, the stock solution of other interfering analytes such as anions (F^-, Cl^-, Br^-, I^-, PO_4^{3-}, NO^{3-}, SO_4^{2-}, HCO_3^- CO_3^{2-}), metal ions (Na^+, K^+, NH_4^+, Al^{3+}, Fe^{2+}), amino acids (alanine, methionine, cystine, glutamic acid, arginine, tyrosine, phenylalanine, tryptophan) and biomolecules (glucose, creatine, creatinine, ascorbic acid, adenine diphosphate) were prepared at concentration of 10mM in aqueous solution (10 mM HEPES, buffer pH 7.4). The absorption and fluorescence studies of PFPS with different analytes were performed in a

3mL aqueous solution (10 mM HEPES, buffer pH 7.4) containing 5µM of PFPS in quartz cuvette.

4.2.4 Quantum yield calculations: The fluorescence quantum yield (Φs) of PFPS was determined by taking quinine sulfate (Φr = 0.52 in 0.1N H_2SO_4) as standard and using the following equation.

$$\Phi_s = \Phi_r\left(\frac{A_r F_s}{A_s F_r}\right)\left(\frac{\eta_s^2}{\eta_r^2}\right)$$

Where 's', 'r' denotes sample and reference, respectively. Φ, symbolize quantum yield, A represents absorbance, F indicates relative integrated fluorescence intensity, and η is the refractive index of the solvent.

4.2.5 Cyclic voltammetry: Electrochemical characterization was performed by using three electrode setup with glassy carbon as working electrode, saturated $Ag/AgNO_3$ electrode as reference electrode and a platinum wire as a counter electrode. The Fc^+/Fc couple was used as an internal reference, and the tetrabutylammoniumhexafluorophosphate (0.1 M) acetonitrile solution was taken as an electrolyte. All measurements were performed under an inert atmosphere at room temperature. A single oxidation peak was obtained for PFPS. The HOMO level (-5.7 eV) was determined from onset method [E_{HOMO} = -($E_{(onset,ox\ vs\ Fc+/Fc)}$ + 4.8) (eV)] while bandgap (3.02 eV) was calculated from onset UV-visible spectrum. The LUMO level (-2.68 eV) was obtained by subtracting HOMO from bandgap.

4.2.6 Development of portable smartphone sensing platform: To demonstrate the feasibility of the present system for onsite field detection, various concentration of 5-HT (0-30µM) were added to the fluorescent PFPS solution (5µM) and color change was imaged under 365nm UV light by smartphone (OnePlus 8T). The captured images were then processed into corresponding output RGB intensities using readily accessible Color Scanning Android Application (Color Picker App, from Google Play Store) to achieve visual quantitative detection. A calibration curve was setup by plotting the B values (Blue color Intensity) versus 5-HT concentration and LOD was interpreted linear fitting the resultant standard curve. For precise detection, the corresponding measurements were repeated 3 times.

4.2.7 Detection in real samples: The stock solution 5-HT (10mM) was prepared in fresh human blood plasma sample (diluted 20 times with HEPES, buffer pH 7.4)). Three spiked plasma samples of known concentration are then added to a cuvette containing PFPS 10 mM HEPES buffer (5µM) to record changes in fluorescence spectra and visual color change under 365 UV lamp. The concentration of 5-HT was calculated from both calibration curves obtained by fluorescence spectral change and smart phone based visual color method. Each measurement was carried out thrice and mean value was calculated.

4.3 Result and discussion

4.3.1 Synthesis and characterization of polymer PFPS

The anionic PFPS CPE was synthesized via Suzuki cross-coupling reaction with 81 % yield, (**Scheme 4.1**). The monomer and CPE PFPS are fully characterized before their use (**Figure A4.1-A4.3**). The sulphonate groups are appended on the polymer side chains to enhance its solubility in polar solvents such as methanol and DMSO as well as to interact with neurotransmitters efficiently via electrostatic/ H-bonding interactions between the sulphonate pendant group of the PFPS and multiple functional groups present on the various neurotransmitters. Such complexation facilitates polymer chain aggregation resulting in the amplified fluorescence quenching of the conjugated polyelectrolyte. As in this work, the fluorescence of PFPS is predominantly quenched by 5-HT, presumably via excited state electron transfer (a-PET) and aggregation-induced π-π interaction, facilitated by electrostatic interaction between the anionic PFPS polyelectrolyte and cationic 5-HT The anionic PFPS polyelectrolyte displayed absorption maxima at 350nm with an emission peak of 415nm in an aqueous solution. The fluorescence quantum yield of PFPS was found to be 51% in solution state.

4.3.2 Sensing study

To investigate the sensing behavior of PFPS towards neurotransmitters, fluorescence titrations were performed by successive addition of various analytes into PFPS solution. Surprisingly, among various neurotransmitters, only 5-HT had significantly influenced the emission of the PFPS. A fluorescence quenching of 23% was instantaneously observed by adding 3.3 µM of 5-HT, which further reached to 87% on total addition of 36.7 µM 5-HT (**Figure 4.1a**). However, other neurotransmitters viz DA, EPI, HA and 5-HIAA had reduced the PFPS fluorescence to a lesser extent. The disappearance of PFPS fluorescence in the presence of 5-HT was clearly remarked under UV light, demonstrating a simple low-cost-portable system for real-time detection of the neurotransmitter 5-HT (inset **Figure**

4.1a). The sensing efficiency is interpreted by linearly fitting the resultant statistics to the Stern–Volmer equation in lower concentrations range:

$$\frac{Io}{I} = 1 + Ksv[Q]$$

Where I_0 and I represent the emission intensity of PFPS before and after the addition of the quencher, [Q] is quencher's concentration, and K_{sv} is Stern Volmer constant. A K_{sv} of 1.14 * 10^5 M^{-1} was determined from S-V plot representing the ultra-sensitivity of PFPS towards 5-HT (**Figure 4.1b**). It is evident that K_{sv} plot rises exponentially at higher concentrations demonstrating amplified quenching via molecular wire effect or additional energy transfer mechanism (**Figure A4.4**). The detection limit calculated for 5-HT is 36 nM (7.65 ppb) based on the standard reported method (**Figure A4.5**). To the best of our knowledge, such incredibly low detection limit and very high K_{sv} are revealed for the first time using fluorescent CPE and is the best among all the previously reported method for 5-HT (**Table A4.1**).

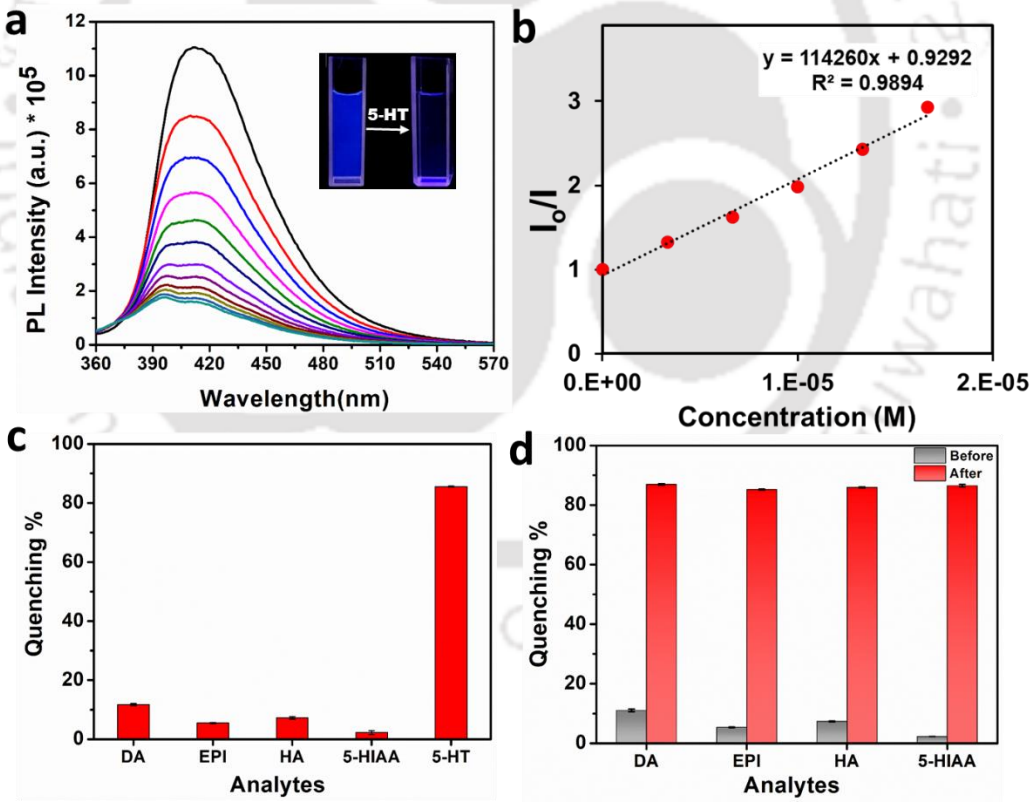

Figure 4.1. Fluorescence response of PFPS towards neurotransmitters in 10 mM HEPES, buffer pH 7.4, (a) Fluorescence spectra of PFPS (5 µM) with variable 5-HT concentration (0-33.7 µM), Inset color change of PFPS under UV light (irradiation at 365nm) before and after 5-HT addition (b) Stern Volmer Plot at lower concentration range (0-1.67 µM) of 5-HT (c) Bar diagram representing quenching percentage of PFPS for various

neurotransmitters, (d) Quenching percentage of PFPS before and after addition of various neurotransmitters (33.7 µM) followed by 5-HT addition (33.7 µM).

4.3.2 Selectivity study

The specific recognition of 5-HT is desirable and appealing for real-time practical applications. To investigate the selectivity of PFPS for 5-HT, a change in its fluorescence was monitored in the presence of various neurotransmitters under identical experimental conditions. The PFPS exhibited diverse signal responses for neutral and charged neurotransmitter molecules. **Figure 4.1c** demonstrates that 5-HT has the highest quenching percentage compared to other neurotransmitters and follows the decreasing order: cationic serotonin> cationic dopamine> neutral epinephrine> cationic histamine > anionic 5-HIAA.[43-46] This kind of sensing behavior suggests coulombic, as well as hydrophobic interaction, which modulates the quenching process. Furthermore, the discriminatory sensing response of PFPS is also investigated in a competing environment of neurotransmitters. Nevertheless, PFPS displayed remarkable selectivity towards 5-HT even in the presence of other interfering neurotransmitters (**Figure 4.1d**).

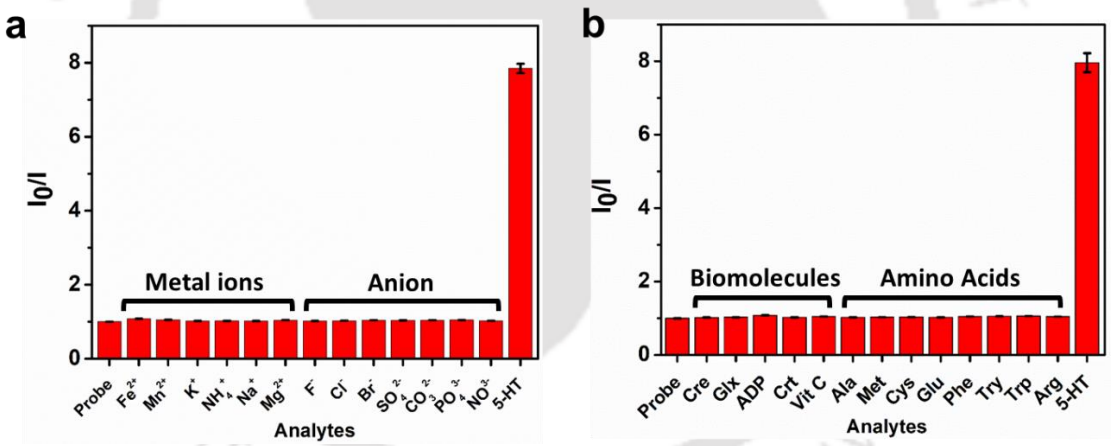

Figure 4.2: Emission response (I_0/I) of PFPS (5µM) with (a) various metal ions and anions, (b) various biomolecules and amino acids in HEPES buffer (10 mM pH 7.4).

Similar selectivity experiments were carried out with other interfering analytes such as anions (F^-, Cl^-, Br^-, I^-, PO_4^{3-}, NO^{3-}, SO_4^{2-}, HCO_3^- CO_3^{2-}), metal ions (Na^+, K^+, NH_4^+, Al^{3+}, Fe^{2+}), amino acids (alanine, methionine, cysteine, glutamic acid, arginine, tyrosine, phenylalanine, tryptophan) and biomolecules (glucose, creatine, creatinine, ascorbic acid, adenine diphosphate) as shown in **Figure 4.2a-b**. All these observations indicate that PFPS exhibits a selective response towards 5-HT even in the presence of various common interfering neurochemicals, demonstrating the practicability of this system for real-time sampling.

4.3.3 Sensing mechanism

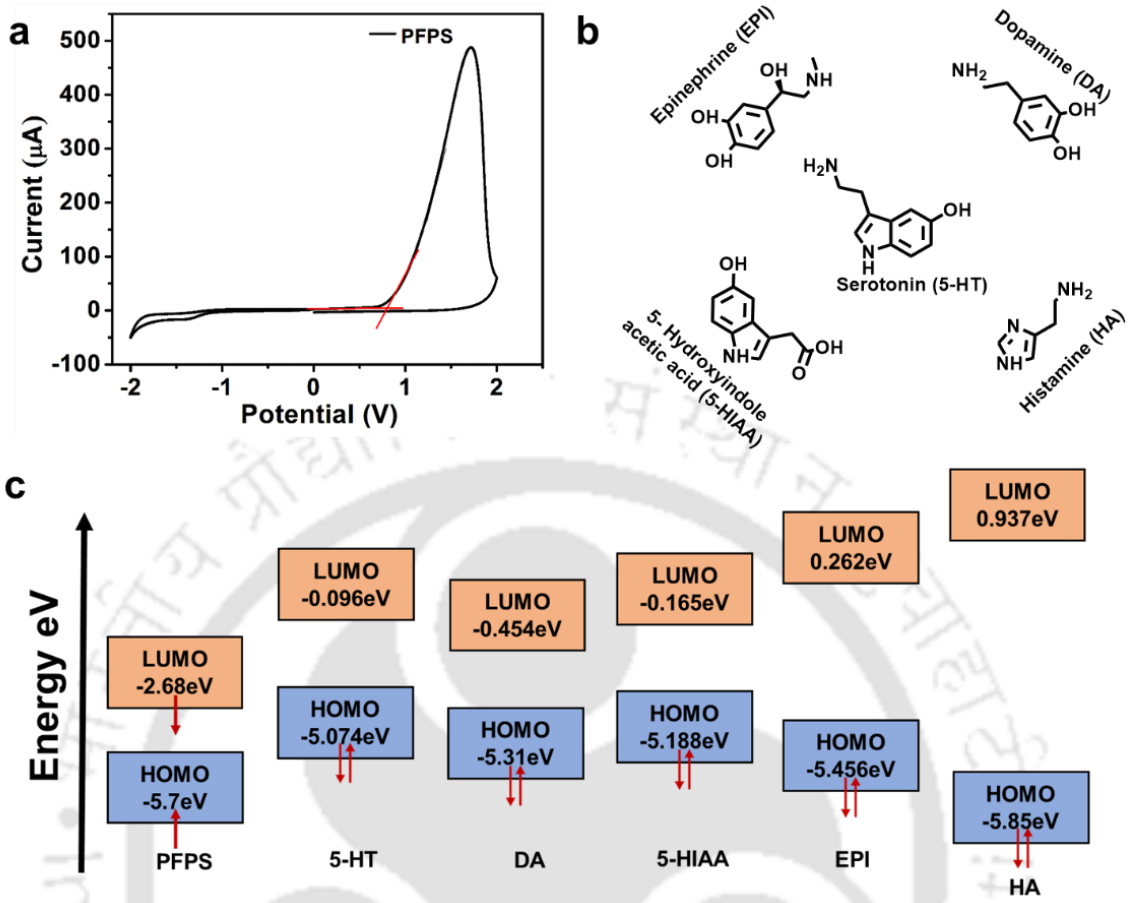

Figure 4.3. (a) Cyclic voltammogram of PFPS film measured at glassy carbon electrode with scan of 50 mV/s, (b) Molecular structures of various neurotransmitters, (c) Comparison of HOMO and LUMO energy level of PFPS with various neurotransmitters.

Generally, three primary mechanisms are associated with the amplified quenching of CPEs (i) electron transfer, (ii) resonance energy transfer (RET), and (iii) quencher-induced aggregation.[47] To comprehend the reason for the unparalleled fluorescence quenching of PFPS by 5-HT, all three possible mechanisms are investigated in detail. To validate the electron transfer as a sensing mechanism, the HOMO and LUMO energy level of PFPS CPE is determined by cyclic voltammetry (**Figure 4.3a**). There is a chance of a-PET (acceptor photoinduced electron transfer) from HOMO (-5.074eV) of 5-HT to the HOMO (-5.7eV) of PFPS, resulting in the fluorescence quenching of PFPS (**Figure 4.3b-c**, **Table A4.2**). [18,48-51] However, such excited state electron transfer is also favorable for other various neurotransmitters except HA suggesting parallel involvement of energy transfer or static mechanism. Since neurotransmitters do not have absorption in the range of PFPS polymer emission (360-650nm), it rules out the possibility of RET as a quenching

mechanism. Therefore, the additional quenching mechanism could be the formation of CPE co-aggregate structures favored by the electrostatic complexation between oppositely charged conjugated polyelectrolyte and the cationic neurotransmitter 5-HT.

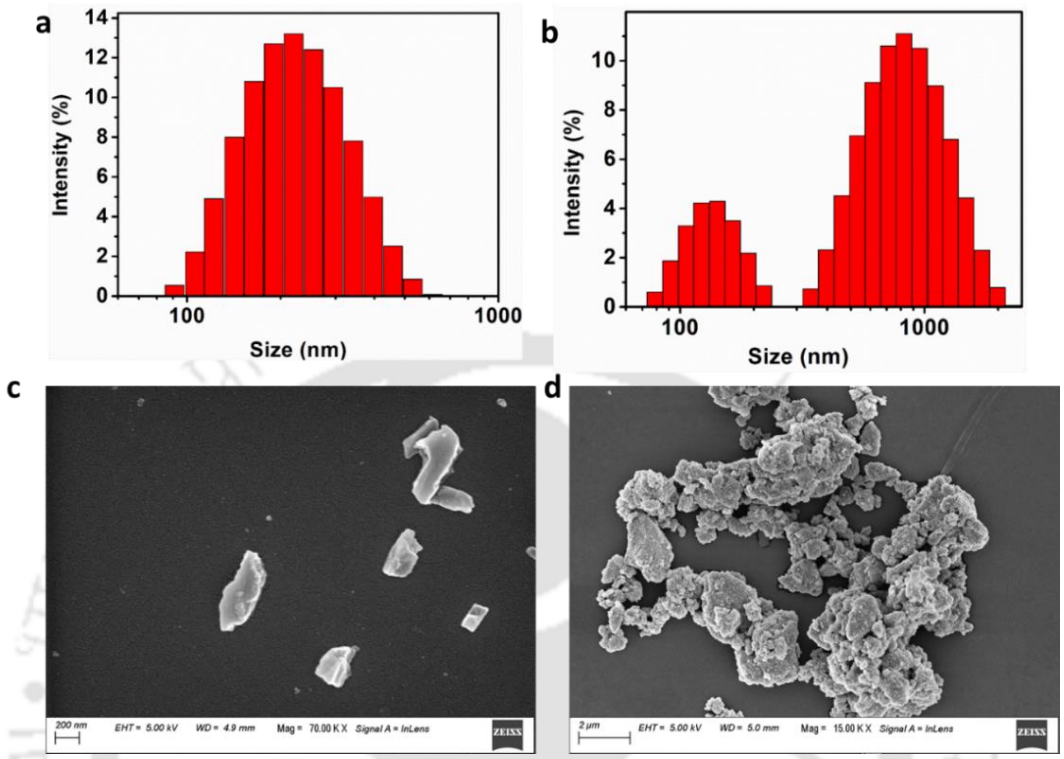

Figure 4.4. DLS spectra of PFPS before (a) and (b) after 5-HT addition, FESEM images showing change in the morphology of PFPS in absence (c) and presence (d) of 5-HT.

To verify the analyte induced polymer aggregation, particle size and morphological change of PFPS in the absence and presence of 5-HT were analyzed by DLS and FESEM analysis respectively (**Figure 4.4a-d**). The DLS measurement shows that the average particle size of PFPS (220 nm) was significantly increased after 5-HT addition (825nm) confirming strong aggregation of PFPS by 5-HT. This is also supported by FESEM analysis which reveals that PFPS exist as unsymmetrical nano-aggregate structures and transformed into large co-aggregates (micrometer size) upon 5-HT addition.

It is believed from the above experimental finding that specific secondary interactions are associated with PFPS/5-HT complex that force the polymer to form large aggregates. One possible secondary interaction could be the presence of aromatic π-π interaction between the indole moiety of 5-HT and polymer backbone to form interpolymer π-stacked co-aggregates driven by strong electrostatic interaction resulting in efficient fluorescence quenching of PFPS.[52-58] Moreover, despite of analogous structure of 5-HT and 5-HIAA

except the difference in function group on appendage chain, the least quenching by 5-HIAA validates that intermolecular π-π stacking is not favourable due to electrostatic repulsion between PFPS and 5-HIAA. Furthermore, the anomalous quenching behavior of PFPS towards cationic 5-HT compared to cationic DA and cationic HA is attributed the predominance intermolecular π-π interaction due to extra aromatic ring in 5-HT along with the involvement of excited state electron transfer. [59-61] Therefore, we have proposed that excited state electron transfer as well as electrostatic interaction driven aggregation induced π-π quenching establishes the basis for unprecedented sensitivity of PFPS towards 5-HT.

4.3.4 Smartphone-based visual detection

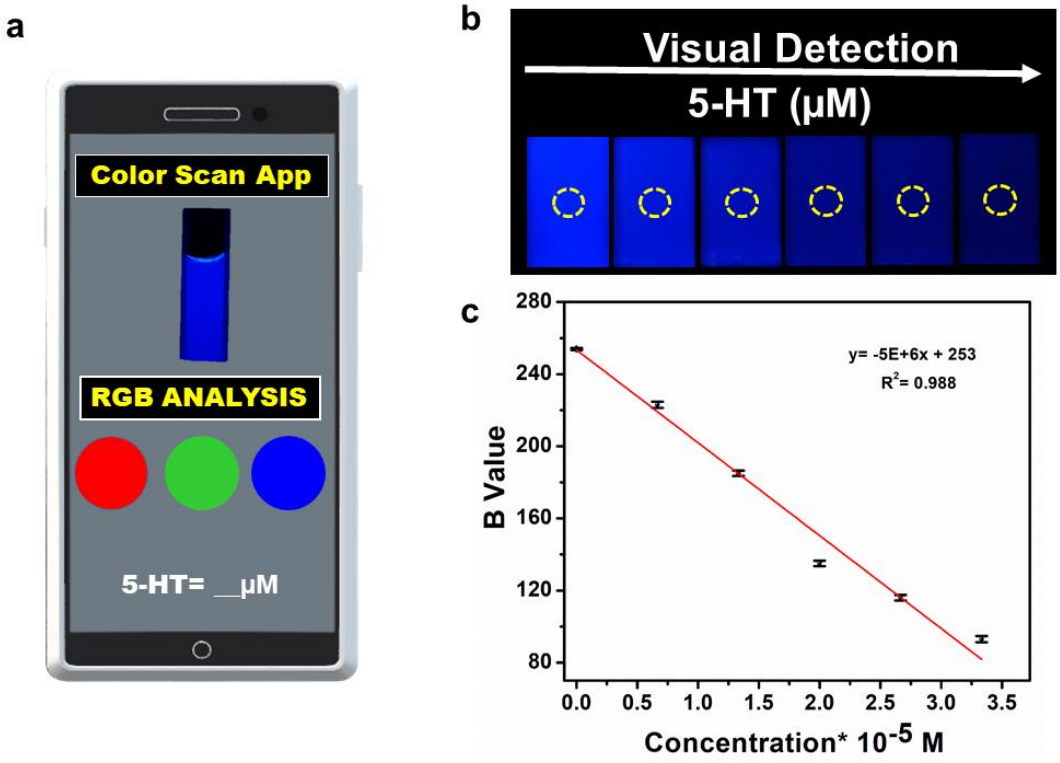

Figure 4.5. (a) Schematic representation of 5-HT detection using smartphone, (b) Captured images of PFPS solution under 365nm UV light with variable 5-HT concentration (0-33.7 µM), (c) Plot of B values versus various 5-HT concentration.

To assess the feasibility of the present method for instant onsite detection, a visual mode detection of 5-HT was carried out by a smartphone with user-friendly color scanning application (**Figure 4.5a**). The fluorescence titration was performed by successive addition of 5-HT to the PFPS solution and images were captured by smartphone under UV light (**Figure 4.5b**). The blue color intensity (B values) of fluorescent images can be extracted from the color recognizer android app. A calibration curve is setup using B values to calculate the LOD as shown in **Figure 4.5c**. The result displayed a good linear relationship

between B values and concentration of 5-HT, and the detection limit of 346 nM or 74 ppb is obtained, presenting a rapid and practical PoC platform for 5-HT estimation.

4.3.5 Real-time quantification in blood plasma

5-HT primarily regulates neurotransmission and several cognitive or behavioral functions, including mood, sleep, depression, appetite, and pain within the CNS.[2,4-6] Besides its involvement in the CNS, 5-HT performs crucial roles in several other human organ systems. Importantly, it has been outlined that elevated circulatory level of plasma 5-HT is associated with neuroendocrine tumors or carcinoid tumors.[7,12] For instance, the concentration of 5-HT in blood plasma of healthy individual ranges 0.5-1.4 µM, while critical concentration for patients with carcinoid tumor is 1.9 µM.[18] Therefore, detection of physiological concentration of 5-HT with superior sensitivity and high selectivity is crucial for basic pathophysiology research, as well as for diagnosis of chronic diseases and drug development. Prior to the real time testing, the stability and photostability of PFPS were monitored under day light and constant UV exposure considering the long-term utility for real world application. The PFPS emission signal was quite stable up to 5 days and decreased by only 11% under daylight. However, the emission signal perceived a slight change under continuous UV exposure endowing the 20.7% attenuation in the emission signal (**Figure A4.6a-b**). The practicability of the PFPS based approach for diagnostic application was evaluated by conducting the sensing experiment in fresh human blood plasma. The unspiked plasma samples does not affect the fluorescence and visual mode signal of PFPS probe. Next, a series of plasma samples were doped with known concentrations of 5-HT, and analysed using calibration curves of fluorescence and smart phone based visual detection methods (**Figure A4.7**, **Figure 4.5c, Table A4.3**). The recoveries of 5-HT based on fluorescence and visual mode using smartphone are found well in the range of 98-101% and 99-102% respectively demonstrating the effectiveness of the present method for instant, cost-effective, and reliable 5-HT determination in real biological samples.

4.4 Conclusion

A convenient and highly sensitive biosensor is constructed for selective detection of neurotransmitter 5-HT using rationally designed conjugated polyelectrolyte. The conjugated polyelectrolyte PFPS displayed fluorescence turn-off response upon successive addition of 5-HT with obvious visual color fading under 365 nm UV light resulting in the

on-site visual detection with LOD of 7.65 ppb. The unprecedented sensitive and highly selective response of PFPS for 5-HT is attributed to excited-state electron transfer (a-PET) and aggregation caused π-π quenching process. A portable smartphone-based platform is developed by analyzing the RGB values of the visual color response of PFPS using a color recognizer android app. Owing to the remarkable sensitivity and rapid onsite detection features, the designed sensing platform could be readily applied for point of care determination of 5-HT in the complex biological fluid such as blood plasma with good percent recoveries validating the reliability of the present system with great potential in the clinical investigation of neuronal processes and early diagnosis of chronic diseases.

References

(1) Shariatgorji, M.; Nilsson, A.; Fridjonsdottir, E.; Vallianatou, T.; Källback, P.; Katan, L.; Sävmarker, J.; Mantas, I.; Zhang, X.; Bezard, E.; Svenningsson, P.; Odell, L. R.; Andrén, P. E. Comprehensive Mapping of Neurotransmitter Networks by MALDI–MS Imaging. *Nat. Methods* **2019**, *16*, 1021-1028.

(2) Berger, M.; Gray, J. A.; Roth, B. L. The Expanded Biology of Serotonin. *Annu. Rev. Med*. **2009**. *60*, 355–66.

(3) Beyene, A. G.; Delevich, K.; Donnell, J. T. D. B-O.; Piekarski, D. J.; Lin, W. C.; Thomas, A. W.; Yang, S. J.; Kosillo, P.; Yang, D.; Prounis, G. S.; Wilbrecht, L.; Landry, M. P. Imaging Striatal Dopamine Release Using a Nongenetically Encoded Near Infrared Fluorescent Catecholamine. *Sci. Adv.* **2019**, *5*, eaaw3108.

(4) Jeong, S.; Yang, D.; Beyene, A. G.; Donnell, J. T. D. B-O.; Gest, A. M. M.; Navarro, N.; Xiaoqi Sun, X.; Landry, M. P. High-Throughput Evolution of Near-Infrared Serotonin. *Sci. Adv.* **2019**, 5, eaay3771.

(5) Shajib, M. S.; Baranov, A.; Khan, W. I. Diverse Effects of Gut-Derived Serotonin in Intestinal Inflammation. *ACS Chem. Neurosci.* **2017**, *8*, 920-931.

(6) Baganz, N. L.; Blakely, R. D. A Dialogue between the Immune System and Brain, Spoken in the Language of Serotonin. *ACS Chem. Neurosci.* **2013**, *4*, 48-63.

(7) Hofland, J.; Zandee, W.T.; Herder, W. W. de. Role of Biomarker Tests for Diagnosis of Neuroendocrine Tumours. *Nat. Rev. Endocrinol*. **2018**, *14*, 656–669.

(8) Li, Y-T.; Tang, L-N.; Ning, Y.; Shu, Q.; Liang, F-X.; Wang, H.; Zhang, G-J. In vivo Monitoring of Serotonin by Nanomaterial Functionalized Acupuncture Needle. *Sci. Rep.* **2016**, *6*, 28018.

(9) Graiti, W. A-.; Foroughi, J.; Liu, Y.; Chen, J. Hybrid Graphene/Conducting Polymer Strip Sensors for Sensitive and Selective Electrochemical Detection of Serotonin. *ACS Omega* **2019**, *4*, 22169−22177.

(10) Ran, G.; Chen, X.; Xia, Y. Electrochemical Detection of Serotonin Based on a Poly(Bromocresol Green) Film and Fe3O4 Nanoparticles in a Chitosan Matrix. *RSC Adv.* **2017**, *7*, 1847–1851.

(11) Sun, D.; Li, H.; Li, M.; Li, C.; Dai, H.; Sun, D.; Yang, B. Electrodeposition Synthesis of A NiO/CNT/PEDOT Composite for Simultaneous Detection of Dopamine, Serotonin, and Tryptophan. *Sens. Actuators B: Chem.* **2018**, *259*, 433–442.

(12) Brenner, B.; Harney, J. T.; Ahmed, B. A.; Jeffus, B. C.; Unal, R.; Mehta, J. L.; Kilic, F. Plasma Serotonin Levels and the Platelet Serotonin Transporter. *J. Neurochem.* **2007**, *102*, 206–215.

(13) Wu, S.; Lin, Y.; Liu, J.; Shi, W.; Yang, G.; Cheng. P. Rapid Detection of the Biomarkers for Carcinoid Tumors by a Water Stable Luminescent Lanthanide Metal–Organic Framework Sensor. *Adv. Funct. Mater.* **2018**, *28*, 707169.

(14) Choi, J.H.; Kim, T.H.; El-Said, W.A.; Lee, J.H.; Yang, L.; Conley, B.; Choi, J.W.; Lee, K. B. In Situ Detection of Neurotransmitters from Stem Cell-Derived Neural Interface at the Single-Cell Level via Graphene-Hybrid SERS Nanobiosensing. *Nano Lett.* **2020**, *20*, 7670-7679.

(15) Shaa, Q.; Sunb, B.; Yia, C.; Guana, R.; Feia, J.; Hua, Z.; Liua, B.; Liu, X. A Fluorescence Turn-On Biosensor Based on Transferrin Encapsulated Gold Nanoclusters for 5-Hydroxytryptamine Detection. *Sens. Actuators B: Chem.* **2019**, *294*, 177–184.

(16) Hashemi, P.; Dankoski, E.; Petrovic, J.; Keithley, R. B.; Wightman, R. M. Voltammetric Detection of 5-Hydroxytryptamine Release in the Rat Brain. *Anal. Chem.* **2009**, *81*, 9462–9471.

(17) Hettie, K. S.; Glass, T. E. Turn-On Near-Infrared Fluorescent Sensor for Selectively Imaging Serotonin. *ACS Chem. Neurosci*. **2016**, *7*, 21-25.

(18) Henke, A.; Kovalyova, Y.; Dunn, M.; Dreier, D.; Gubernator, N. G.; Dincheva, I.; Hwu, C.; Šebej, P.; Ansorge, M. S.; Sulzer, D.; Sames, D. T. Toward Serotonin Fluorescent False Neurotransmitters: Development of Fluorescent Dual Serotonin and Vesicular Monoamine Transporter Substrates for Visualizing Serotonin Neurons. *ACS Chem. Neurosci.* **2018**, *9*, 925-934.

(19) Kurniawan, D.; Jhang, R-C.; Ostrikov, K. K.; Chiang, W-H. Microplasma-Tunable Graphene Quantum Dots for Ultrasensitive and Selective Detection of Cancer and Neurotransmitter Biomarker. *ACS Appl. Mater. Interfaces* **2021**, *13*, 34572-34583.

(20) Klockow, J. L.; Hettie, K. S.; Glass, T. E. A Dual-Analyte Fluorescent Chemosensor for Visualizing Neurotransmitter Exocytosis. *ACS Chem. Neurosci.* **2013**, *4*, 1334-1338.

(21) Qian, C.G., Zhu, S., Feng, P.J., Chen, Y.L., Yu, J.C., Tang, X., Liu, Y. and Shen, Q.D., 2015. Conjugated Polymer Nanoparticles for Fluorescence Imaging and Sensing of Neurotransmitter Dopamine in Living Cells and the Brains of Zebrafish Larvae. *ACS Appl. Mater. Interfaces* **2015**, *7*, 18581-18589.

(22) Zhu, C.; Liu, L.; Yang, Q.; Lv, F.; Wang, S. Water-Soluble Conjugated Polymers for Imaging, Diagnosis, and Therapy. *Chem. Rev.* **2012**, *112*, 4687-4735.

(23) Malik, A.H.; Hussain, S.; Kalita, A.; Iyer, P. K. Conjugated Polymer Nanoparticles for the Amplified Detection of Nitro-explosive Picric Acid on Multiple Platforms. *ACS Appl. Mater. Interfaces* **2015**, *7*, 26968-26976.

(24) Malik, A.H.; Iyer, P. K. Conjugated Polyelectrolyte Based Sensitive Detection and Removal of Antibiotics Tetracycline from Water. *ACS Appl. Mater. Interfaces* **2017**, *9*, 4433-4439.

(25) Feng, L.; Liu, L.; Lv, F.; Bazan, G. C.; Wang, S. Preparation and Biofunctionalization of Multicolor Conjugated Polymer Nanoparticles for Imaging and Detection of Tumor Cells. *Adv. Mater.* **2014**, *26*, 3926–3930.

(26) Hussain, S.; Malik, A. H.; Afroz, M. A.; Iyer, P. K. Ultrasensitive Detection of Nitroexplosive – Picric Acid via a Conjugated Polyelectrolyte in Aqueous Media and Solid Support. *Chem. Commun.* **2015**, *51*, 7207-7210.

(27) Meher, N.; Iyer, P. K. Pendant Chain Engineering to Fine-Tune the Nanomorphologies and Solid State Luminescence of Naphthalimide AIEEgens: Application to Phenolic Nitro-Explosive Detection in Water. *Nanoscale* **2017**, *9*, 7674–7685.

(28) Traina, C. A.; Bakus II, R. C.; Bazan, G. C. Design and Synthesis of Monofunctionalized, Water-Soluble Conjugated Polymers for Biosensing and Imaging Applications. *J. Am. Chem. Soc.* **2011**, *133*, 12600–12607.

(29) Williams, A. K.; Tropp, J.; Crater, E. R.; Eedugurala, N.; Azoulay, J. D. Click Post-Polymerization Modification of a Fluorescent Conjugated Polymer for Parts-per-Billion Pyrophosphate Detection in Seawater. *ACS Appl. Polym. Mater.* **2019**, *1*, 309–314.

(30) Cao, A.; Tang, Y.; Liu, Y. Novel Fluorescent Biosensor for α Glucosidase Inhibitor Screening Based on Cationic Conjugated Polymers. *ACS Appl. Mater. Interfaces* **2012**, *4*, 3773-3778.

(31) Tan, C; Atas, E.; Mu¨ller, J. G.; Pinto, M. R.; Kleiman, V. D.; Schanze, K. S. Amplified Quenching of a Conjugated Polyelectrolyte by Cyanine Dyes. *J. Am. Chem. Soc.* **2004**, *126*, 13685-13694.

(32) Tanwar, A. S.; Adil, L. R.; Afroz, M. A.; Iyer, P. K. Inner Filter Effect and Resonance Energy Transfer Based Attogram Level Detection of Nitroexplosive Picric Acid Using Dual Emitting Cationic Conjugated Polyfluorene. *ACS Sens.* **2018**, *3*, 1451-1461.

(33) Zheng, Z.; Yu, H.; Geng, W-G.; Hu, X-Y.; Wang, Y-Y.; Li, Z.; Wang, Y.; Guo, D-S. *Nat. Commun.* **2019**, *10*, 5762.

(34) Yang, F.; Lin, D.; Pan, L.; Zhu, J.; Shen, J.; Yang, L.; Jiang, C. Portable Smartphone Platform Based on a Single Dual-Emissive Ratiometric Fluorescent Probe for Visual Detection of Isopropanol in Exhaled Breath. *Anal. Chem.* **2021**, *93*, 14506-14513.

(35) Chu, S.; Wang, H.; Du, Y.; Yang, F.; Yang, L.; Jiang, C. Portable Smartphone Platform Integrated with a Nanoprobe-Based Fluorescent Paper Strip: Visual Monitoring of Glutathione in Human Serum for Health Prognosis. *ACS Sustainable Chem. Eng.* **2020**, *8*, 8175-8183.

(36) Huang, F.; Wang, X.; Wang, D.; Yang, W.; Cao, Y. Synthesis and Properties of a Novel Water-Soluble Anionic Polyfluorenes for Highly Sensitive Biosensors. *Polymer* **2005**, *46*, 12010–12015.

(37) Lee, S.; Jang, C. H.; Nguyen, T. L.; Kim, S. H.; Lee, K. M.; Chang, K.; Choi, S. S.; Kwak, S. K.; Woo, H. Y.; and Song, M. H. Conjugated Polyelectrolytes as Multifunctional Passivating and Hole-Transporting Layers for Efficient Perovskite Light-Emitting Diodes. *Adv. Mater.* **2019**, *31*, 1900067.

(38) Pratuangdejkul, J.; Nosoongnoen, W.; Guerin, G.-A.; Loric, S.; Conti, M.; Launay, J.-M.; Manivet, P. Conformational Dependence of Serotonin Theoretical pKa Prediction. *Chem. Phys. Lett.* **2006**, 420, 538-544.

(39) Radu, D. R.; Lai, C.-Y.; Wiench, J. W.; Pruski, M.; Lin, V. S.-W. Gatekeeping Layer Effect: A Poly(lactic acid)-coated Mesoporous Silica Nanosphere-Based Fluorescence Probe for Detection of Amino-Containing Neurotransmitters. *J. Am. Chem. Soc.* **2004**, *126*, 1640-1641.

(40) Szeitz, A.; Bandiera, S. M. Analysis and Measurement of Serotonin. *Biomed. Chromatogr*. **2018**,*32*, e4135.

(41) Feng, X.; Liu, L.; Wang, S.; Zhu, D. Water-Soluble Fluorescent Conjugated Polymers and their Interactions with Biomacromolecules for Sensitive Biosensors. *Chem. Soc. Rev.* **2010**, *39*, 2411–2419.

(42) Tanaka, K.; Miura, T.; Umezawa, N.; Urano, Y.; Kikuchi, K.; Higuchi, T.; Nagano, T. Rational Design of Fluorescein-Based Fluorescence Probes. Mechanism-Based Design of a Maximum Fluorescence Probe for Singlet Oxygen. *J. Am. Chem. Soc.* **2001**, *123*, 2530 – 2536.

(43) Meher, N.; Iyer, P. K. Spontaneously Self-Assembled Naphthalimide Nanosheets: Aggregation-Induced Emission and Unveiling a-PET for Sensitive Detection of Organic Volatile Contaminants in Water.*Angew. Chem. Int. Ed.* **2018**, *57*, 8488 –8492.

(44) Ueno, T.; Urano, Y.; Setsukinai, K.; Takakusa, H.; Kojima, H.; Kikuchi, K.; Ohkubo, K.; Fukuzumi, S.; Nagano, T. Rational Principles for Modulating Fluorescence Properties of Fluorescein. *J. Am. Chem. Soc.* **2004**, *126*, 14079–14085.

(45) Li, Z.; Acharya, R.; Wang, S.; Schanze, K. S. Photophysics and Phosphate Fluorescence Sensing by Poly(Phenylene Ethynylene) Conjugated Polyelectrolytes with Branched Ammonium Side Groups. *J. Mater. Chem. C* **2018**, *6*, 3722.

(46) Zhao, Y.-J.; Miao, K.; Zhu, Z.; Fan, L-.J. Fluorescence Quenching of a Conjugated Polymer by Synergistic Amine-Carboxylic Acid and π-π Interactions for Selective Detection of Aromatic Amines in Aqueous Solution. *ACS Sens.* **2017**, *2*, 842-847.

(47) Wang, H.; He, F.; Yan, R.; Wang, X.; Zhu, X.; Li, L. Citrate-Induced Aggregation of Conjugated Polyelectrolytes for Al^{3+} Ion-Sensing Assays. *ACS Appl. Mater. Interfaces* **2013**, *5*, 8254-8259.

(48) Hussain, S.; Malik, A. H.; Iyer, P. K. Highly Precise Detection, Discrimination, and Removal of Anionic Surfactants Over the Full pH Range via Cationic Conjugated Polymer: an Efficient Strategy to Facilitate Illicit-Drug Analysis. *ACS Appl. Mater. Interfaces* **2015**, *7*, 3189-3198.

(49) Timothy M. Swager, T. M. The Molecular Wire Approach to Sensory Signal Amplification. *Acc. Chem. Res.* **1998**, *31*, 201-207.

(50) Thomas III, S. M.; Joly, G. D.; Swager, T. M. Chemical Sensors Based on Amplifying Fluorescent Conjugated Polymers. *Chem. Rev.* **2007**, *107*, 1339−1386.

(51) Chanu, M. A.; Mondal, S.; Zehra, N.; Tanwar, A. S.; Iyer, P. K. Conjugated Polymer Nanoparticles as a Fluorescence Probe for Amplified Detection of Human Serum Bilirubin. *ACS Appl. Polym. Mater.* **2022**, *4*, 3491-3497.

(52) Fan, C.; Hirasa, T.; Plaxco, K. W.; Heeger, A. J. Photoluminescence Quenching of Water-Soluble Conjugated Polymers by Viologen Derivatives: Effect of Hydrophobicity. *Langmuir* **2003**, *19*, 3554-3556.

(53) Xie, D.; Parthasarathy, A.; Schanze, K. S. Aggregation-Induced Amplified Quenching in Conjugated Polyelectrolytes with Interrupted Conjugation. *Langmuir* **2011**, *27*, 11732–11736.

Appendix

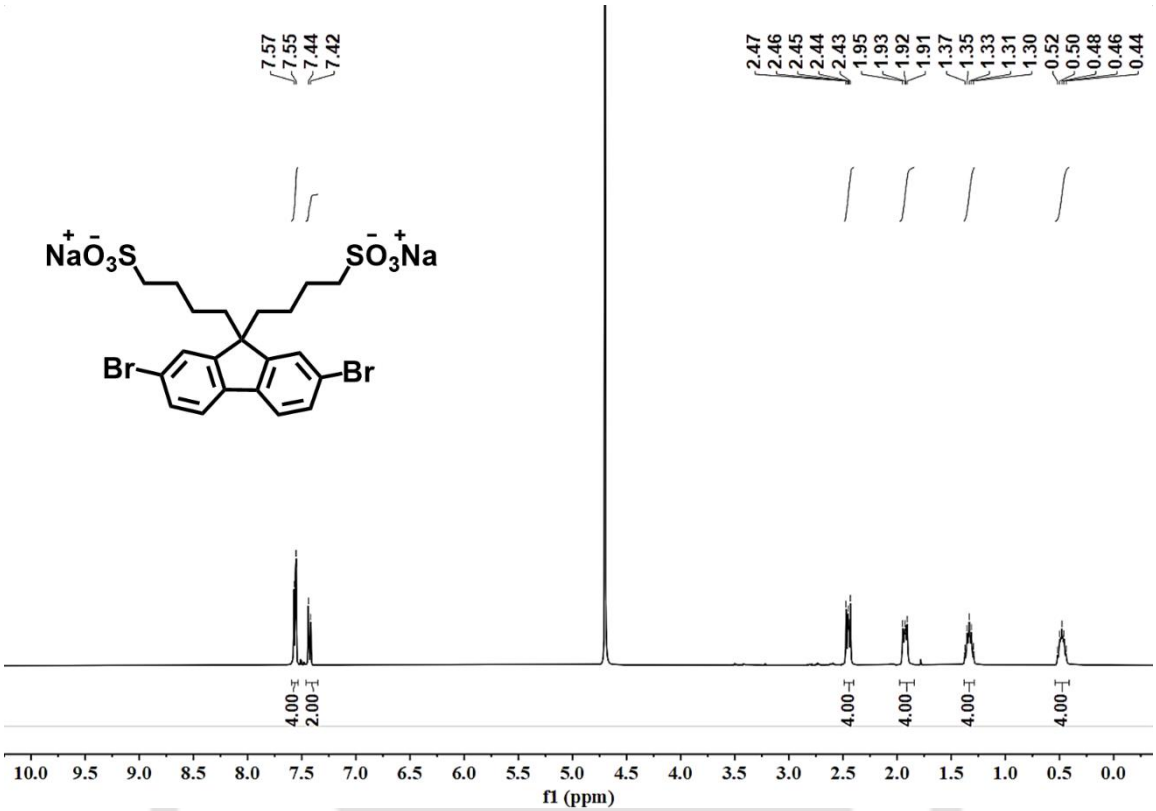

Figure A4.1. ^{1}H NMR of M.

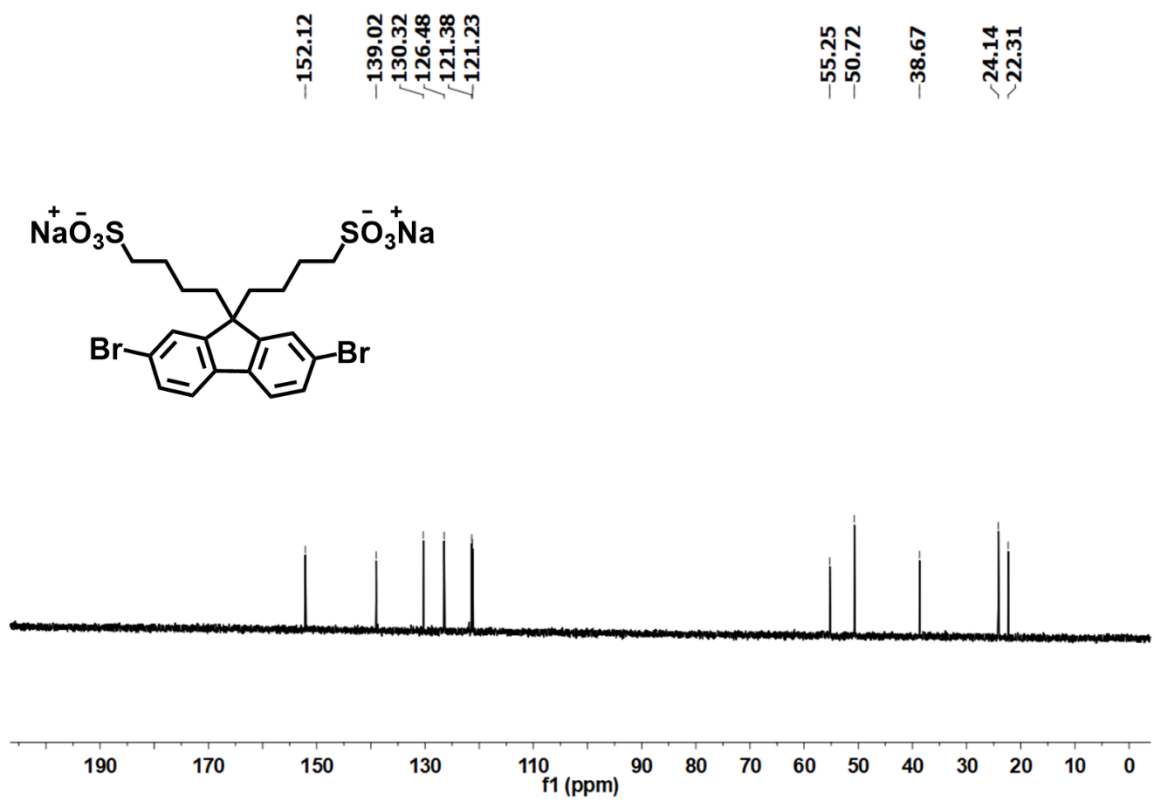

Figure A4.2. ^{13}C NMR of M.

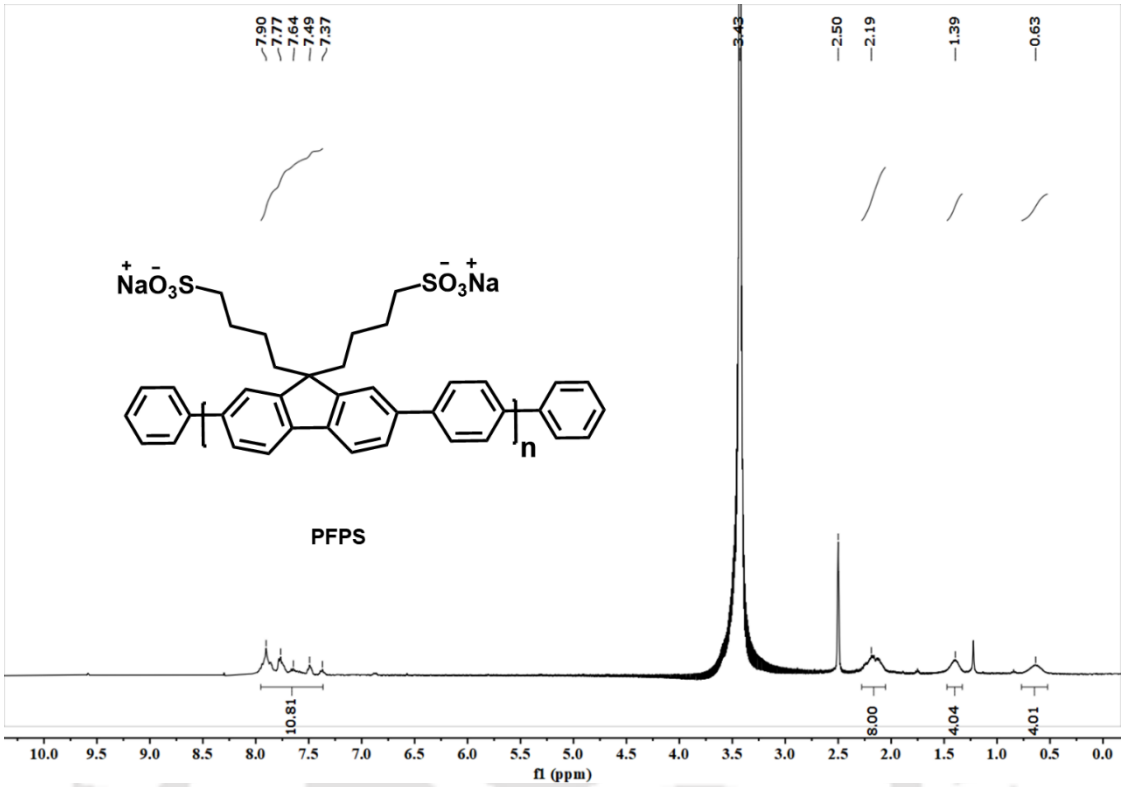

Figure A4.3. ^{1}H NMR of PFPS.

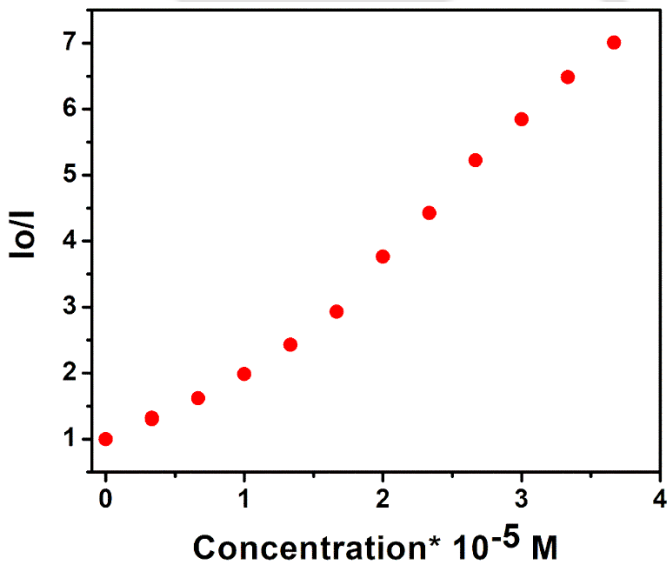

Figure A4.4. Stern-Volmer Plot of PFPS for serotonin in concentration range of (0-36.7 μM).

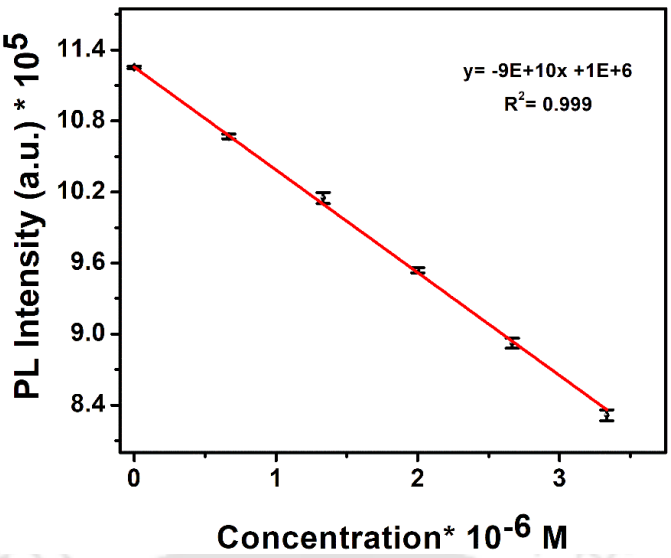

Figure A4.5. Fluorescence Intensity of PFPS (5 µM) in 10 mM HEPES, buffer pH 7.4 as a function of 5-HT concentration.

Table A4.1: Comparative study of LOD and K_{sv} values achieved by various system and material used for detection of serotonin.

Publication	**Material Used**	**Detection Method**	**LOD**	**Ksv**	**Medium Used**
Present Work	***Conjugated Polyelectrolyte***	***Fluorescence***	***7.65ppb/ 36 nM***	***1.14 * 10^5 M^{-1}***	***HEPES, buffer pH 7.4)***
Adv. Funct. Mater. **2018**, *28* 1707169.	Metal organic Framework	Fluorescence	0.66 * 10^{-6} M	7.1 × 10^3 M^{-1}	water
ACS Chem. Neurosci. **2016**, *7*, 21-25.	Small molecule probe	Fluorescence	NA	NA	Buffer (pH 5)
RSC Adv., **2017**, *7*, 1847–1851	Fe_3O4^- MWCNT–poly(BCG) composite	Electrochemical	80 nM	NA	phosphate buffer (pH 7.4)
Sci. Rep., **2016**, *6*, 28018	carbon nanotube	Electrochemical	50 nM	NA	NA
Sensing and Bio-Sensing Research **2017**, *13*, 17-27	GCE/MWCNT-NiO	Electrochemical	118 nM	NA	Phosphate buffer (pH 7)

ACS Omega, **2019**, *4*, 22169–22177	rGO–PEDOT/PSS nanocomposites	Electrochemical	0.1 µM	NA	Phosphate buffer (pH 7.4)
Sens. Actuators, B **2019**, *294*, 177–184	Transferrin-gold nanoclusters	Fluorescence	0.049 µM	NA	PBS buffer (pH 7.4)
Sens. Actuators, B **2018**, *259*, 433–442	NiO/CNT/PEDOT/GCE	Electrochemical	0.063 µM	NA	PBS buffer (pH 7)

Table A4.2: Energy levels of PFPS and various neurotransmitters.

Compound	HOMO (eV)	LUMO (eV)	Bandgap (eV)
PFPS	-5.7	-2.68	3.02
Serotonin (5-HT)	-5.07	-0.096	4.98
Dopamine (DA)	-5.31	-0.454	4.87
L(-)-Epinephrine (EPI)	-5.44	0.318	5.76
5-hydroxyindole acetic acid (5-HIAA)	-5.18	-0.165	5.02

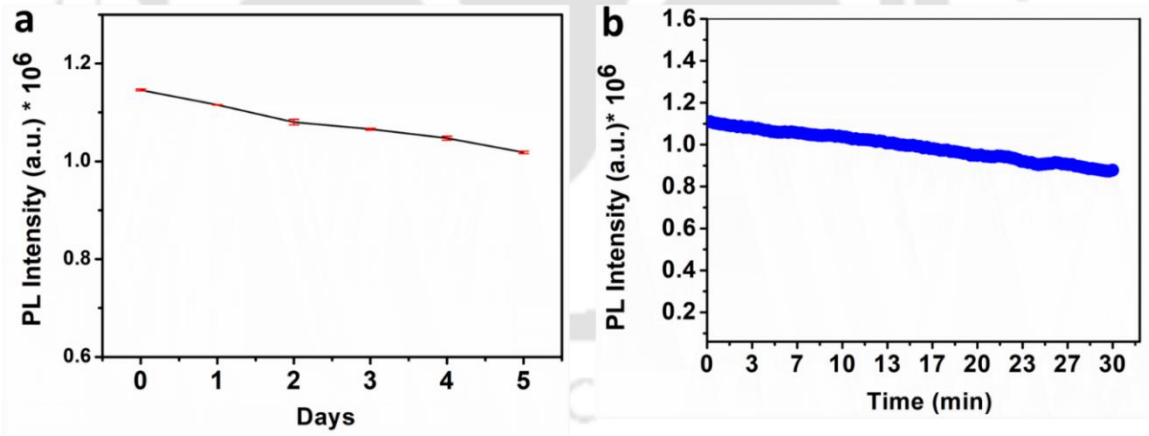

Figure A4.6: depicts (a) stability of the fluorescence of PFPS up to five days and (b) photostability of the fluorescence of PFPS under constant UV irradiation.

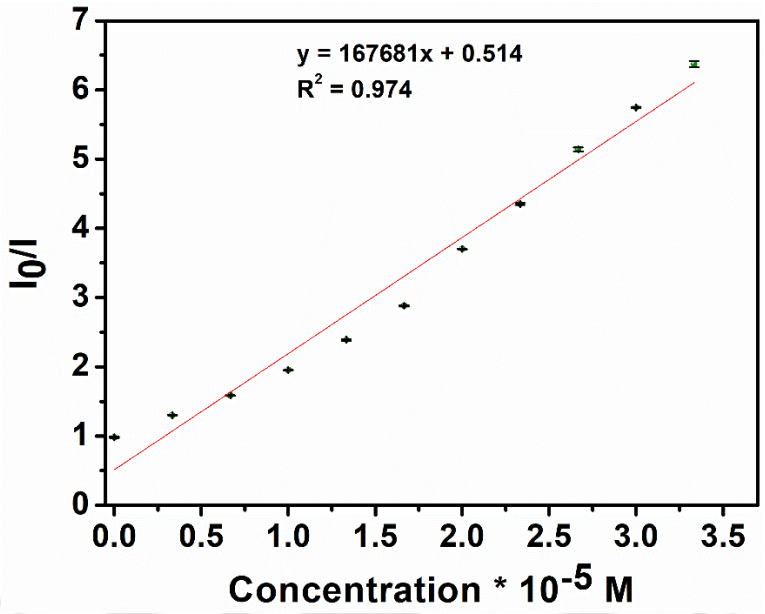

Figure A4.7. Calibration plot of PFPS fluorescence signal for 5-HT estimation.

Table A4.3: Detection of 5-HT in blood plasma samples based on fluorescence and visual mode signal of PFPS probe.

Spiked Sample	Spiked Concentration (µM)	Fluorescence Mode			Visual Mode		
		Found (µM)	Recovery (%)	RSD (%)	Found (µM)	Recovery (%)	RSD (%)
S1	11.6	11.65	99.7	0.26	11.73	100.3	0.54
S2	25	24.85	99.4	0.22	25.36	101.5	0.46
S3	18.33	18.38	100.3	0.53	18.15	99	2.31

Chapter 5

An AIEE active Conjugated Polyelectrolyte for Ultrasensitive Detection of Multicolor Artificial Food Dyes

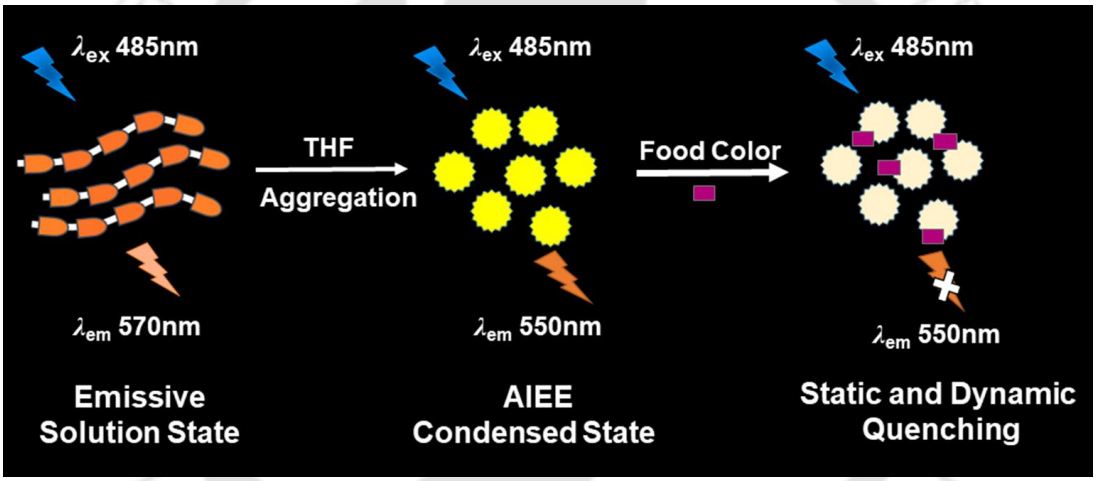

Zehra, N.; Parui, R.; Chanu, M. A.; Iyer, P. K. An AIEE active Conjugated Polyelectrolyte for Ultrasensitive Detection of Multicolor Artificial Food Dyes (*Manuscript Prepared*).

Abstract

A newly developed AIEE active conjugated polyelectrolyte PFTT-D is synthesized *via* Suzuki cross-coupling polymerization reaction and successfully applied for the rapid, highly sensitive detection of multicolor artificial food dyes in solution. The PFTT-D polymer forms a highly emissive macro-aggregate in THF/water fraction and unveils remarkable sensitivity towards various food color dyes with detection limits in the range of 5-7 nM. A very high quenching efficiency with Ksv value in the range of 6.4-4*10^5 M^{-1} is obtained for the first time which can be attributed to the Inner filter effect (IFE), ground state, and excited state complexation. Moreover, the PFTT-D probe is also applied for the rapid detection of food dyes in various processed food samples representing great potential application in screening dyes levels in various food products with high precision.

5.1 Introduction

Artificial food dyes (AFD) are phenyl azo or imine-containing organic compounds, extensively used in foodstuffs to restore color loss during processing and storage as well as to render food items look attractive and tempting for consumers without substantial addition to nutritional content. They are considered as economical substitutes for natural food colorants which are limited, less stable, and possess low tinctorial power.[1-4] According to the Food and Drug Administration (FDA) report, there has been a fivefold increase in AFDs consumption since 1955 as people's reliance has shifted toward processed food. Although most of the certified AFDs are water soluble, however, they release carcinogenic aromatic amine intermediates during chemical digestion.[2,5-9] In addition, the recent findings have reflected a correlation between the extensive consumption of permitted color additives with allergic reactions, and behavior change in children which led to the strict regulation of acceptable daily intake (ADI) for various AFDs by several international agencies.[10-12] Thus, to ensure the public health and food safety, it is necessary to develop an effective method for the determination of AFD levels in various food commodities.

An assortment of chromatographic methods such as high-performance liquid chromatography (HPLC), liquid chromatography coupled mass spectrometry (LC-MS), and Gas chromatography/mass spectrometry (GC-MS) has been largely established to determine the presence of AFDs in food commodities. In addition to the chromatographic techniques, capillary electrophoresis, electrochemical methods and surface-enhanced Raman spectroscopy (SERS) have also been recently explored.[13-19] Undoubtedly, these developed methods can generate promising and compelling results, however, they still have inevitable shortcomings of expensive instrumentation, tedious operation and complex measurement procedures which renders unsuitable for real-time and onsite operations. Therefore, the development of a simple and cost-effective detection platform that could provide fast, sensitive, and reliable on-field detection of AFDs at low concentrations is much more desirable.[1]

Fluorescence technique is considered as superior to various other detection methods due to its inherent multitude of features such as superior sensitivity, rapid response, easy operation, and on-field detection. In this context, conjugated polyelectrolytes (CPE) have been demonstrated as a useful functional material that inherits the excellent optical properties of conjugated backbone while their ionic side chains enhance aqueous solubility as well as make them prone to amphiphilic interaction with oppositely charged species.

Thus, CPEs have been widely used as a viable sensory platform to detect environmental organic pollutants, charged biomolecules and diseases biomarkers, etc. owing to its tunable broad absorption, strong emission brightness, excellent photostability, and ultrahigh sensitivity benefitted from molecular wire nature of conjugated backbone.[20-26] However, rigid planar CPE often gets aggregated in an aqueous environment resulting in the radiation less π-π quenching and reduction in emission signal or quantum yield which leads to erratic sensing results.[27,28] To enhance the emission brightness, Tang and co-worker discovered a new phenomenon of aggregation-induced emission in 2001. The AIEgens (AIE active molecules) are non-planar building block that shows weak emission in the dissolved state but exhibit boosted emission in aggregate or condensed state. By taking the distinct strengths of CPE and AIE luminogens in the polymer architecture, synergistic properties such as high quantum yield and amplified quenching via 3-dimensional exciton transport can be greatly achieved in the aggregated state.[29-34] In this regard, few AIE active conjugated polymers have been explored for the detection of metal ions and explosives.[35-39] However, to the best of our knowledge no AIE active CPE has ever been developed for the detection of artificial food dyes covering the entire visible color range till now.

Herein, we have designed a novel AIEE active CPE for sensitive label-free detection of artificial food dyes at the ppb level. The PFTT-D CPE forms a highly emissive micro-aggregate in water/THF fraction and demonstrates amplified quenching towards various multicolor AFDs with a very high quenching constant order of 10^{-5} M^{-1}. The sensing mechanism is attributed to the Inner filter effect (IFE) and specifically excited state complexation between polymer and AFDs. Furthermore, the PFTT-D-based sensing platform was successfully explored for the quantitative determination of AFDs in commercial food products with great precision.

5.2 Experimental

5.2.1 Material and instruments: All chemicals, including Fast Green FCF (FG), Allura red AC (AR), Sunset Yellow FCF (SY), and Brilliant Blue FCF (BB) were obtained from TCI India. Milli-Q water was used throughout the experiments. ^{1}H NMR (600 and 500 MHz) and ^{13}C NMR (150 and 125 MHz) spectra were collected on Bruker Ascend 600 and Bruker Avance Neo 500 spectrometers, respectively. GPC was recorded on Water Corporation USA. UV-visible and Fluorescence spectra were obtained on Agilent Cary 100 UV-VIS spectrophotometer and Horiba Fluoromax-4 spectrofluorometer, respectively.

Time-resolved fluorescence spectra were recorded on Edinburgh Life Spec II instrument. DLS measurement was performed on Malvern, Zetasizer Nano ZS90. FESEM analysis was carried out by using Sigma Carl ZEISS scanning electron microscopes.

5.2.2 Synthetic procedure

5.2.2a Synthesis of Monomer, M1 & M2:

The Monomer, M1 & M2 was synthesized according to the previously established procedure as illustrated in chapter 2.

5.2.2b Synthesis of Monomer, M3: A 100 ml two-neck RB flask was charged with 4-bromophenone (1 g, 3.9 mmol), Zinc dust (466 mg, 7.3 mmol) and was evacuated under vacuum and flushed with argon 2-3 times. Then 15mL anhydrous THF was injected. The reaction mixture was cooled to -5 ºC and treated with $TiCl_4$ (1 mL, 9 mmol) dropwise. The resulting reaction mixture was warmed to room temperature and then stirred and refluxed overnight. After reaction completion, the mixture was quenched by 10% aqueous potassium carbonate solution and extracted with chloroform. The organic layer was concentrated under reduced pressure and crude product was purified by column chromatography, using 4:1 hexane/chloroform solvent mixture to afford the M3 as white powder (1.2 g, 64%).[40]

^{1}H NMR (600 MHz, $CDCl_3$, δ ppm): 7.25-7.20 (m, 4H), 7.14-7.16 (m, 6H), 7-6.97 (m, 4H), 6.89-6.86 (m, 4H).

^{13}C NMR (150 MHz, $CDCl_3$, δ ppm): 142.97, 142.53, 140.43, 133.01, 131.36, 131.04, 128.16, 127.09, 120.80.

5.2.2c Synthesis of Poly[(E)-1-(4-(4-(2-(4-(9,9-bis(6-bromohexyl)-9H-fluoren-2-yl)phenyl)-1,2-diphenylvinyl)phenyl)-3-fluorothieno[3,4-b]thiophen-2-yl)-4 ethyloctan-1-one], PFTT: The monomer M2 (175 mg, 0.235 mmol), M3 (46 mg, 0.094 mmol), 2-ethylhexyl 4,6-dibromo-3-fluorothieno[3,4-b]thiophene-2-carboxylate, M4 (67 mg, 0.141 mmol), catalyst $Pd(PPh_3)_4$, (13.5 mg) and K_2CO_3 (2M) were added to 50ml RB under inert atmosphere. A THF: water (3:1) mixture was then introduced into the flask and followed by a three-time free thraw cycle to remove traces of dissolved oxygen. The mixture was stirred and refluxed at 80 ºC for 36 h. The resulting mixture was then cooled and washed with chloroform/water, followed by reprecipitation in methanol 3 times to get the orange solid product (200 mg, 75%).

^{1}H NMR (600 MHz, $CDCl_3$, δ ppm): 7.84 (b, 2H), 7.72-7.68 (b, 4H), 7.45-7.37 (b, 1.6H), 7.13-7.0 (b, 5.6H), 4.31(b, 1.2H), 3.28 (b, 4H), 2.14-2.08 (b, 4H), 1.75-1.68 (b, 4H), 1.50-1.37 (b, 8H), 1.25-1.12 (b, 7.6H), 0.98-0.95 (b, 4H), 0.77 (b, 3.6H).

GPC in THF, polystyrene standard: Mw= 2.39 × 10^4, PDI-1.67.

5.2.2d Synthesis of PFTT-D: The precursor polymer (100 mg, 0.09 mmol), and DABCO (96 mg, 1.76 mmol) were placed in a 25 ml round bottom flask and then dry DMF(3mL) was injected. The reaction mixture was maintained at 80 ºC overnight. Afterward, the mixture was poured in excess of diethyl ether in a 50 ml beaker to get the precipitate. The reddish-orange precipitate was redissolved in methanol and reprecipitated in chloroform three times to obtain the desired pure polymer PFTT-D (86 mg, 72%).

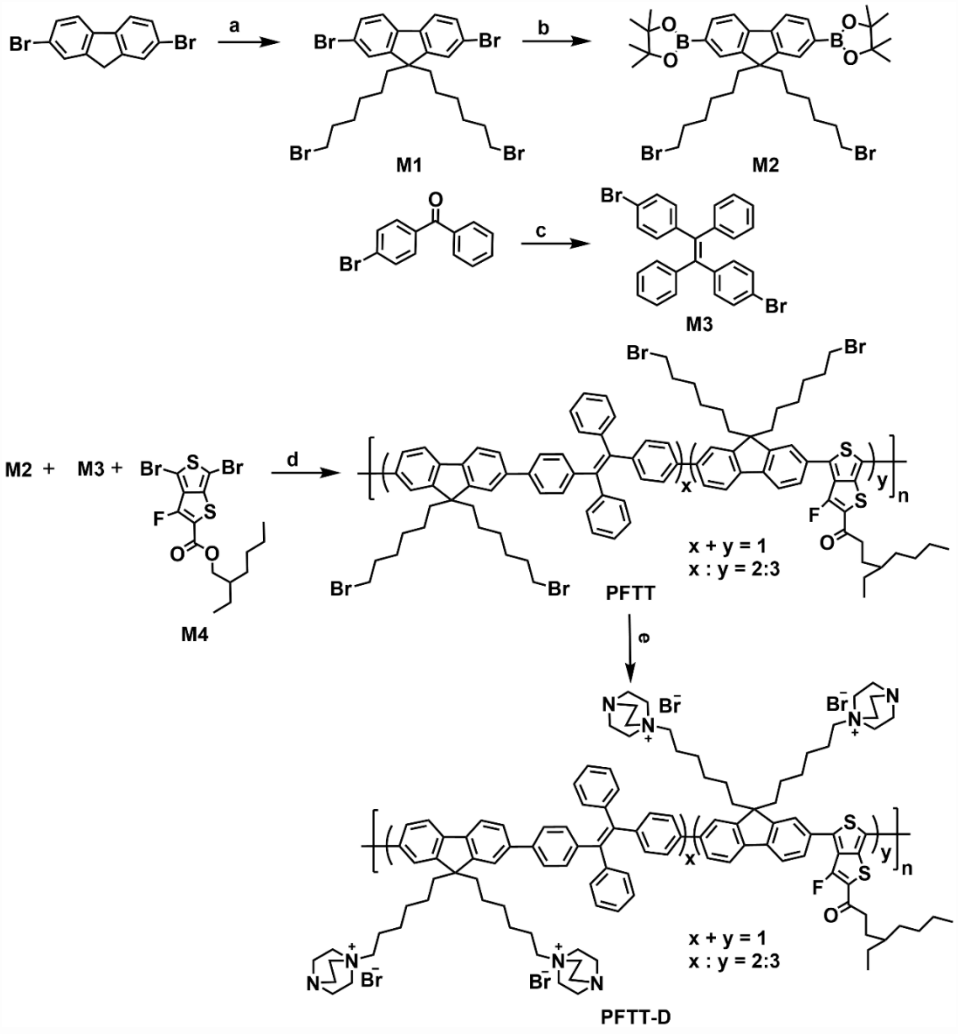

Scheme 5.1: Synthesis of PFTT-D (a) 1,6-Dibromohexane, TBAI, 50% aq. NaOH, 70 °C, 4 h; (b) bis(pinacolato)diborane, KOAc, [Pd(dppf)Cl_2], dioxane, 85°C, 24h; (c) Zn powder, $TiCl_4$, THF, 85 ºC, 24 h; (d) $Pd(PPh_3)_4$, 2M K_2CO_3 (aq.), THF, reflux, 36 h; (e) 1,4-diazabicyclo[2.2.2]octane, dry DMF, 80 ºC, 24 h.

^{1}H NMR (500 MHz, DMSO-d6, δ ppm): 8.13 (b, 2H), 7.93-7.78 (b, 4H), 7.63-7.03 (b, 7.5H), 4.29 (b, 1.2H), 3.16-2.94 (b, 23.4H), 2.17- 2.08 (b, 4H), 1.76-1.74 (b, 4H), 1.43-1.35 (b, 12H), 1.14-1.10 (b, 4H), 0.95-0.94 (b, 4H), 0.69 (b, 3.6H).

5.2.3 Preparation of stock solutions and sensing studies of PFTTD: The stock solution of PFTTD for photophysical studies was prepared in methanol at a concentration of 1 mM. The stock solution of various food dyes viz. Fast Green FCF (FG), Allura red AC (AR), Sunset Yellow FCF (SY), and Brilliant Blue FCF (BB) were prepared in Milli Q water at a concentration of 1mM. Similarly, the stock solution of other interfering natural food components such as natural compounds (D-glucose, D-fructose, vitamin C, aspartic acid, leucine), salts & food preservatives (NaCl, $NaNO_3$, $NaHCO_3$), and competing dyes (brilliant green, methyl red, Sudan II) were prepared at a concentration of 10mM in Milli Q water. The stock solution of PFTTD was diluted to 20 µM in 50% THF: water fraction for each titration in a 1 mL quartz cuvette. Various food dye stock solutions were introduced and PFTTD fluorescence intensity was monitored at room temperature.

5.2.4 TRPL studies: Lifetime decay profile of PFTTD (20 µM) in the absence and presence of various food dyes (0-10 µM) were recorded at an emission wavelength of 550nm using pulse excitation of 445 nm. Instrument response factor (IRF) was collected using solvent as a blank. The curves were fitted biexponentially and all decay parameters such as amplitude and lifetime of each component, and average lifetime are presented in (**Table A5.5**).

5.2.5 Inner filter effect correction: The IFE suppression effect on fluorescence intensity of PFTTD was calculated using the following equation for the cuvette of 1cm path length.

$$\frac{I_{corr}}{I_{obs}} = 10^{(A_{exc}+A_{em})/2}$$

Where 'I_{corr}' and 'I_{obs}' denote emission intensity with and without IFE correction while 'A_{exc}' and 'A_{em}' indicate the absorption value of PFTTD (fluorophore) at excitation and emission wavelength with various food dyes.

5.2.6 Quantification in real sample: The food products that are labeled with AFDs color codes were selected for this study. Liquid food products such as cold drinks and

energy drinks were used without any pretreatment. For solid food items such as candies or gems, a different protocol was designed and adapted. The semi-solid and solid food samples were grounded followed by washing with water. The resulting solution was then centrifuged and the supernatant was used as such for fluorescence measurement as AFDs are water soluble, hence it is present in the supernatant portion. The aliquots of food samples were added to the PFTT-D solution and the change in fluorescence signal was monitored. The amount of AFDs in food items was evaluated from standard calibration curves. For precise detection, three replicate measurements were recorded and the relative standard deviation was calculated.

5.3 Result and discussion

5.3.1 Synthesis and characterization of polymer PFTT-D

The synthetic procedure AIE active PFTT-D CPE is illustrated in **Scheme 5.1**. The neutral polymer PFTT was prepared via Suzuki cross-coupling polymerization using monomers M2, M3, and M4 in a molar ratio of 1:0.4:0.6. The side chain of PFTT is then decorated with 1,4-ethylenepiperazine to afford cationic conjugated polyelectrolyte PFTT-D. The monomers and polymers are well characterized before their final use (**Figure A5.1-A5.4)**. The molecular weight (M_w) of the polymer PFTT is 2.39×10^4 g/mol with PDI-n 1.67 determined by GPC analysis using polystyrene as standard (**Figure A5.5)**. The cationic piperazium group is harnessed at the polymer's side chains to serve as binding sites for various AFDs through multiple hydrophobic and hydrophilic interactions and bestow high solubility in polar organic solvents such as methanol and DMSO. The polymer PFTT-D displays two absorption peaks at 360nm and 485nm in aqueous solution as well in the aggregate state, corresponding to π-π transition and intramolecular charge transfer band respectively. The PFTT-D exhibits emission peaks at 570nm and 550nm in solution and aggregate state respectively (**Figure 5.1a)**.

To examine the aggregate characteristics of the PFTT-D polymer, fluorescence spectra were monitored in different water-THF fractions as shown in **Figure 5.1b-c**. The PFTT-D emits weakly at 570 nm when dissolved in pure water. However, on increasing THF fraction (f_{THF}) from 0-30%, the fluorescence intensity boosted sharply and the polymer starts aggregating resulting in the restriction of intramolecular motion of the tetraphenyl ethylene rotor group. At 50 % f_{THF} emission peak is a hypochromic shift to 550 nm (20 nm) with 6-fold enhancement fluorescence intensity which remains constant upto 80% f_{THF} showing a typical AIEE character. The aggregate formation was confirmed by FESEM

analysis which reveals that PFTT-D forms spherical-shaped microparticles with the average size of 1.386 µm at 50% THF: water fraction (**Figure 5.1d, inset 5.1d**). The PFTT-D micro aggregates were then subjected to sensing of various multicolor AFDs in solution.

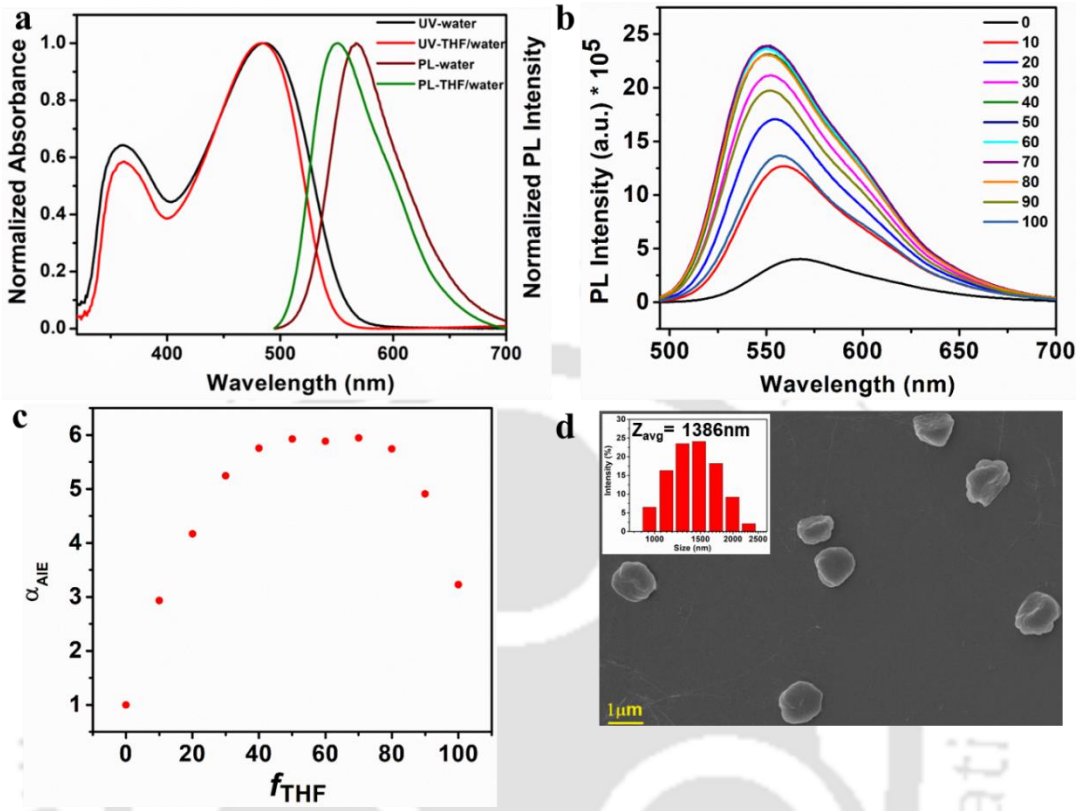

Figure 5.1. (a) UV-vis and fluorescence spectra of PFTT-D in water and THF: water mixture (1:1), (b) AIE study in different fractions of THF: water mixture, (c) α_{AIE} vs. f_{THF} plot of PFTT-D, (d) FESEM images of PFTT-D at 50% THF/water fraction and in inset DLS spectra of PFTT-D at 50% THF/water fraction.

5.3.2 Sensing studies

The AIEE active PFTT-D CPE is subjected to AFDs detection in the aggregated state owing to their broad absorption along with the presence of multiple ionic and hydrophobic aromatic functionalities, favorable for amplified quenching of PFTT-D via energy transfer or ion pair induced π-π quenching. **Figure A5.6** lists the structure of various artificial food dyes used in this work. The fluorescent aggregate of PFTT-D (20 µM) formed in THF-water 1:1 was considered for sensing experiments. To demonstrate the sensing ability of PFTT-D, fluorescence quenching studies are performed by gradual addition of multicolor artificial food dyes to PFTT-D solution. To our delight, all AFDs displayed significant responses on PFTT-D emission with the highest and lowest onset quenching of 31% and

24% observed for FG and SY respectively. Moreover, the addition of a total 0.5 equivalent of AFDs (10 µM) to PFTT-D solution results in nearly ~90% PL quenching with the disappearance of polymer yellow emission under UV lamp (**Figure 5.2a-b**, **Figure A5.7a-c**). The sensing efficiency of PFTT-D for multicolor AFDs is compared by linear fitting the obtained data at lower quencher concentration with the Stern-Volmer equation, as depicted in **Figure A5.8a-d**. The Stern-Volmer constant or quenching constant (K_{sv}) is found to be highest for FG (6.37 * 10^5 M^{-1}) and followed the decreasing order: FG > BB > AR> SY. Similarly, the detection limits (LOD) for multicolor AFDs are calculated using equation 3σ/k and listed in **Table 5.2c & Figure A5.9a-d**. The difference in quenching constant values among five AFDs suggests the difference in polymer-dye association driven by electrostatic interaction.

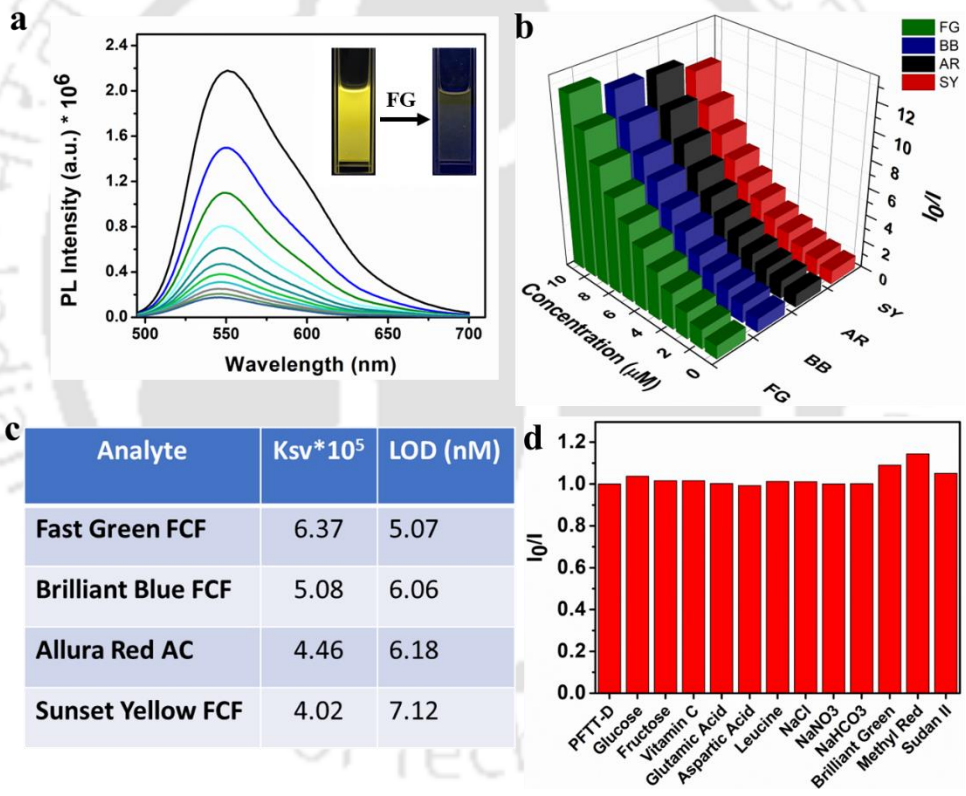

Analyte	Ksv*10^5	LOD (nM)
Fast Green FCF	6.37	5.07
Brilliant Blue FCF	5.08	6.06
Allura Red AC	4.46	6.18
Sunset Yellow FCF	4.02	7.12

Figure 5.2: Emission spectra of PFTT-D (20µM) with the subsequent addition of FG (0-10 µM) in THF: water mixture (1:1), (b) Stern-Volmer plots of PFTT-D with increasing concentration of various AFDs (0-10 µM) in THF: water mixture (1:1), Table (c) Stern-Volmer constant and LOD values obtained for various AFDs (d) Bar Diagram depicts the effect of various natural compounds, salts, preservatives and interfering dyes on the emission of PFTT-D.

To comprehend this hypothesis, the molecular structures and intermolecular interactions between the dyes and polymer are considered. First, all four AFDs carry a net -2 negative charge which gives rise to electrostatic interaction with positively charged polymer. Second, the presence of aromatic π-π interactions may also contribute to the quenching process. This seems to be operative, as FG and BB are consisting of the highest number of aromatic л cores and act as the most effective quenchers. The slight difference in Ksv values for FG and BB implies that the presence of the extra -OH group in FG stabilizes polymer-dye complexation via hydrogen bonding interactions.

5.3.3 Selectivity study

For real-time application, the selective detection of AFDs in food commodities is highly challenging yet desirable. To verify the selectivity of PFTT-D towards AFDs, various natural compounds (D-glucose, D-fructose, vitamin C, aspartic acid, leucine), salts & food preservatives (NaCl, $NaNO_3$, $NaHCO_3$) that are commonly present in food were analyzed and turned out to be ineffective towards fluorescence signal of PFTT-D. Moreover, the sensing response of PFTT-D is also examined with synthetic colorants other than AFDs such as brilliant green, methyl red, Sudan II, etc. However, negligible change in PFTT-D emission is observed indicating unparalleled selectivity and remarkable sensing response of PFTT-D towards AFDs (**Figure 5.2d**).

5.3.4 Sensing mechanism

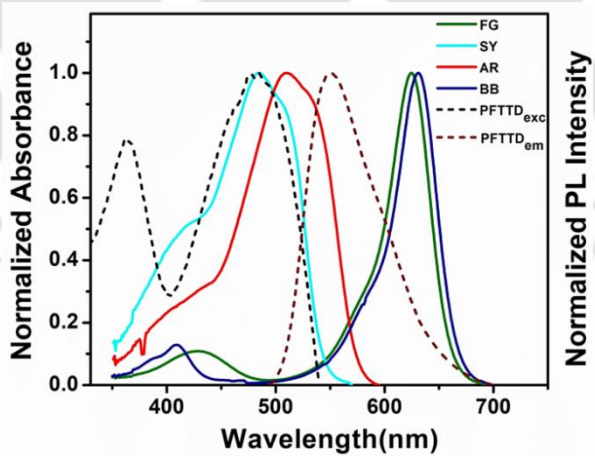

Figure 5.3: Spectral overlap between excitation and emission spectra of PFTT-D (20μM) with absorption spectra of various AFDs i.e., FG (10 μM), BB (10 μM), AR (10 μM), and SY (10 μM) in THF: water mixture (1:1).

The fluorescence quenching process can occur through a variety of mechanisms such as ground state complexation, collisional quenching, excited state reactions, and the Inner

Filter Effect (IFE). Since all four AFDs possess broad UV-vis absorbance spectra which overlap well with either excitation and/or emission spectra of the PFTT-D, there could be the possibility of an energy absorption process such as IFE or Resonance Energy Transfer (RET) as a sensing mechanism (**Figure 5.3**). [6,23-24] To confirm the presence of IFE in the system, the IFE correction factor is applied to the observed emission intensity of fluorophore (PFTT-D) up on successive addition of AFDs where the quenching efficiencies of PFTT-D are figured out before and after the IFE correction as shown in **Figure 5.4a-d**. It is observed that the suppression efficiency is 2-4% in the case of SY and AR while the rest of the two dyes viz FG and BB displayed an almost negligible change in quenching efficiency after IFE correction (**Table A5.1-5.4**). The difference in suppression efficiency of AFDs could be ascribed to a higher magnitude of spectral between the absorption band of AR and SY with both the excitation and emission spectra of PFTT-D compared to FG and BB. Since the overall IFE contribution was insignificant, it could not be accounted as a sole factor in this quenching process reflecting the involvement of additional quenching mechanisms.

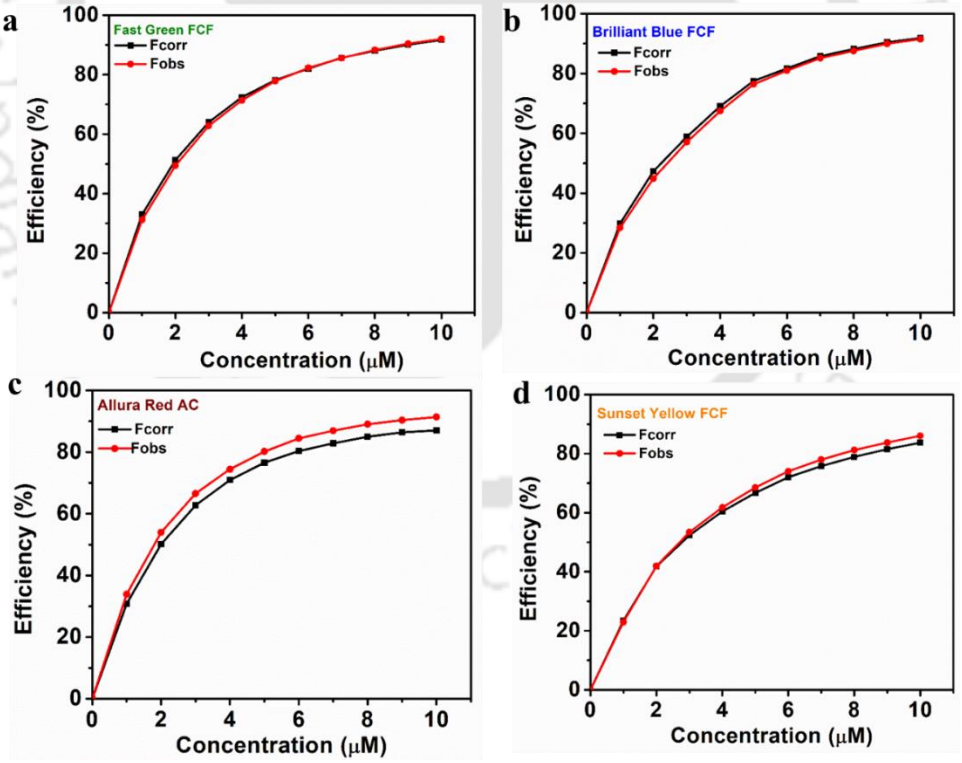

Figure 5.4: Suppression in quenching efficiency of corrected (red) and observed (black) emission intensity of PFTT-D (20 μM) with various concentrations of (a) FG (0-10 μM), (b) BB (0-10 μM), (c) AR (0-10 μM) and (d) SY (0-10 μM) in THF: water (1:1).

To check the possibility of a dynamic quenching process, time-resolved photoluminescence (TRPL) experiments are carried out. The change in fluorescence lifetime of PFTT-D is monitored in the absence and presence of AFDs using pulse excitation of 445nm, **Figure 5.5a-d & Table A5.5**. The average excited state lifetime of PFTT-D (0.90 ns) is found to increase significantly with addition of FG (1.41 ns), BB (1.38 ns), AR (1.15 ns), SY (1.11 ns), respectively, suggesting possibility of stable exciton formation via excited state complex (exciplex) between PFTT-D probe and dyes molecules.[41-44]

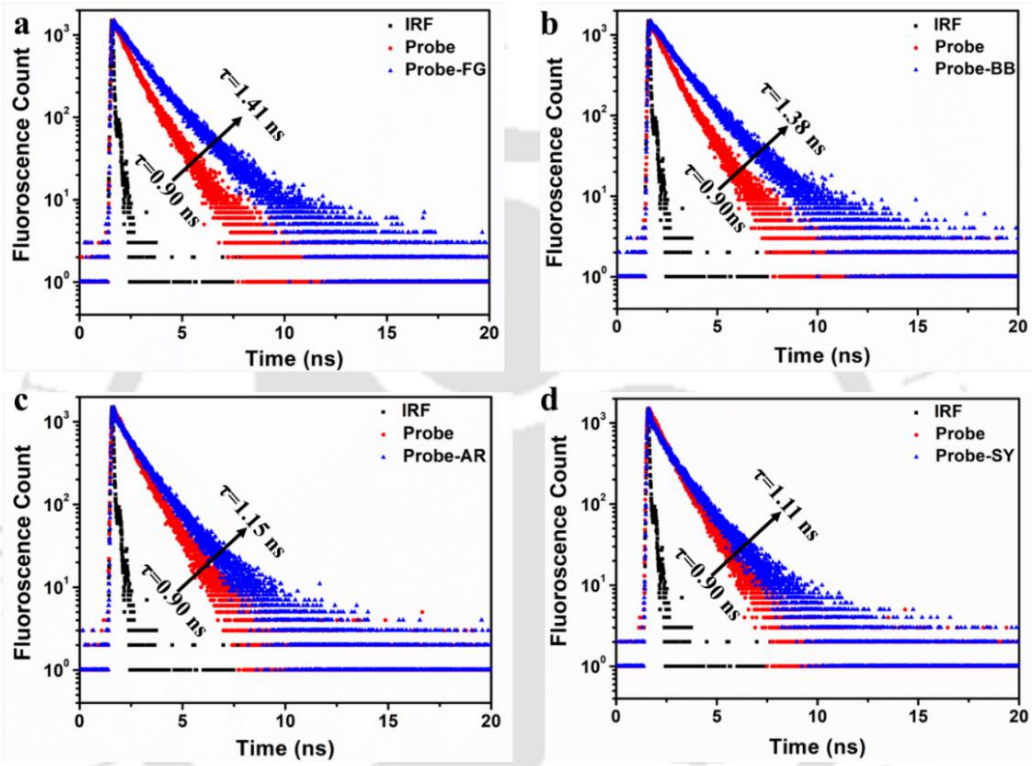

Figure 5.5: Fluorescence Lifetime of PFTT-D (20µM) before and after addition of (a) FG (10 µM), (b) BB (10 µM), (c) AR (10 µM) and (d) SY (10 µM) in THF: water mixture (1:1).

These observations are also in line with steady-state fluorescence of PFTT-D which displayed considerable quenching of emission peak at 550nm with appearance of very weak red shifted emission band centered at ~650nm after addition of FG and BB dyes as shown in **Figure 5.6a-b**. While, in case of AR and SY, although decrease in emission intensity of PFTT-D at 550nm is observed, however, no emission band at longer wavelength is noticed signifying very weak excited state complexation.[45] The lesser increment in average lifetime of PFTT-D with AR and SY compared to FG and BB also supports less stable excited state complex formation in the formers. Moreover, the AFDs alone does not exhibit any emission in the range 490-700 nm under identical condition (THF: Water mixture, λ_{exc} 480 nm) as

well as their fluorescence decay profile overlaps with instrument response function (IRF) indicating the AFDs are non-fluorescent **(Figure A5.10)**. Hence, based on above experimental observation and literature precedents it can be concluded that there could be formation of stable excited state complex between PFTT-D probe and AFDs molecules which leads to decrease in emission intensity of probe at 550 nm with appearance of structureless broad emission band ranges 600 nm-700 nm corresponds to exciplex peak. However, further mechanistic investigation is still under progress in our laboratory.

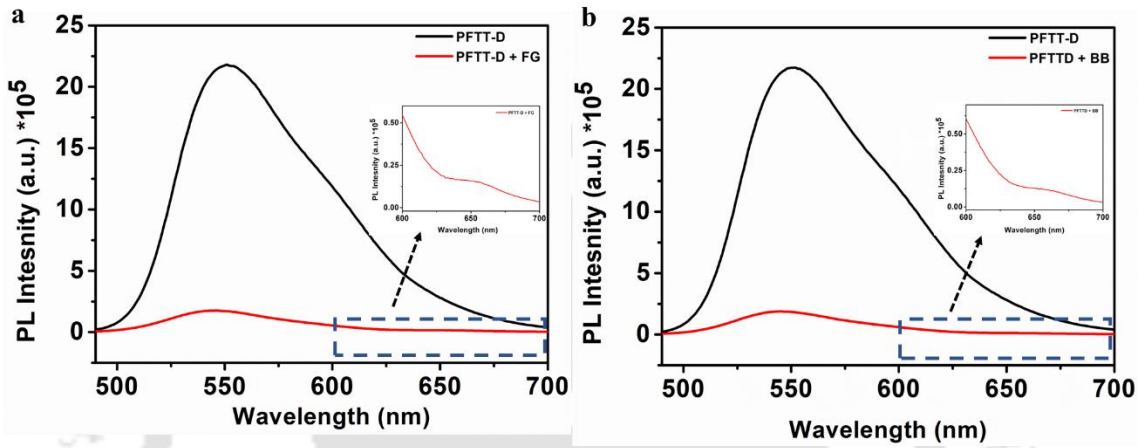

Figure 5.6: Emission spectra of PFTT-D (20µM) before and after addition of (a) FG (10 µM) and (b) BB (10 µM) in THF: water mixture (1:1). Inset: the magnified figure of PFTT-D spectra after addition of FG and BB respectively.

5.3.5 Determination in commercial food sample

To validate the feasibility of AIEE active PFTT-D as sensing probe for practical application, the detection of possible AFDs in various type processed food products are performed. The food products that are labeled with AFDs color codes are selected for this study. The liquid food products such as cold drinks and energy drinks are used as such without any pretreatment. For solid food items such as candies or gems, a different protocol is designed and adapted as mentioned in section 5.2.6. Fluorometric studies are carried out by adding aliquots of food samples to the PFTT-D solution and change in fluorescence signal is monitored. The amount of AFDs present in food items is evaluated from standard calibration curves (**Figure A5.11a-d**). For precise detection, three replicate measurements are recorded and relative standard deviation is calculated as present in **Table 5.1**.

Table 5.1: Determination of AFDs in commercial food products PFTT-D based method.

Food Type	Color Code	Dye Name	Concentration detected	RSD
Cold drink	110	Sunset Yellow FCF	3.41µM	1.47
Energy drink	129	Allura Red AC	2.75µM	1.11
Jam	110	Sunset Yellow FCF	2.41µM	0.84
Blue Gem	133	Brilliant Blue FCF	1.01µM	0.32
Green Gem	143	Fast Green FCF	0.67µM	0.82

5.4 Conclusion

In conclusion, AFDs detection is achieved at very low nanomolar range using newly developed AIEE active conjugated polyelectrolyte PFTT-D. The spherical-shaped micro aggregate structure of PFTT-D is utilized for AFDs detection which displayed amplified quenching with high Stern-Volmer constants varying un between $6.4*10^5$-$4*10^5$ M^{-1} in presence of various multicolor AFDs. The excellent signal response of PFTT-D is attributed to the ground state mechanism via IFE and formation of excited state complexes with AFDs. The present PFTT-D protocol is demonstrated for rapid and cost-effective quantification of AFDs in commercial food items to ensure public health and food safety.

References

(1) Sun, Z.; Du, J.; Yan, L.; Chen, S.; Yang, Z.; Jing, C. Multifunctional Fe_3O_4@SiO_2–Au Satellite Structured SERS Probe for Charge Selective Detection of Food Dyes. *ACS Appl. Mater. Interfaces* **2016**, *8*, 3056-3062.

(2) Nazim, M.; Kim, J. H.; Lee, H. Y.; Cho, S. K. Development of Three-Dimensional Nickel–Cobalt Oxide Nanoflowers for Superior Photocatalytic Degradation of Food Colorant Dyes: Catalyst Properties and Reaction Kinetic Study. *Langmuir* **2021**, *37*, 12929-12939.

(3) Denish, P. R.; Fenger, J. A.; Powers, R.; Sigurdson, G. T.; Grisanti, L.; Guggenheim, K. G.; Laporte, S., Li, J.; Kondo, T.; Magistrato, A.; Moloney, M. P. *Science advances* **2021**, *7*, p.eabe7871.

(4) Sharma, V.; McKone, H. T.; Markow, P. G. A Global Perspective on the History, Use, and Identification of Synthetic Food Dyes. *J. Chem. Educ.* **2011**, *88*, 24-28.

(5) Kobylewski, S.; Jacobson, M. F. Toxicology of Food Dyes. *Int. J. Occup. Med. Environ. Health* **2012**, *18*, 220-246.

(6) Wu, M.; Sun, L.; Miao, K.; Wu, Y.; Fan, L. J. Detection of Sudan Dyes Based on Inner-Filter Effect with Reusable Conjugated Polymer Fibrous Membranes. *ACS Appl. Mater. Interfaces* **2018**, *10*, 8287-8295.

(7) Amchova, P.; Kotolova, H.; Kucerova, J. R. Health Safety Issues of Synthetic Food Colorants. *Regul. Toxicol. Pharmacol.* **2015**, *73*, 914-922.

(8) Kuntzleman, T. S.; Corts, S.; Schmidt, A. At-Home Titration: Magnesium Hydroxide in Milk of Magnesia Using an Inexpensive Digital Balance and Natural Food Dye as Indicators. *J. Chem. Educ.* **2021**, *98*, 2592−2595.

(9) Chen, H.; Chen, M.; Wang, X.; Sun, R. Self-assembled Conjugated Polymer/Carboxymethyl Chitosan Grafted Poly(*P*-Dioxanone) Nanomicelles and their use in Functionalized Indicator Paper for Fast and Visual Detection of a Banned Food Dye. *Polymer Chemistry* **2014**, *5*, 4251-4258.

(10) Sharifpour, E.; Arabkhani, P.; Sadegh, F.; Mousavizadeh, A.; Asfaram, A. In-situ Hydrothermal Synthesis of CNT Decorated by Nano ZnS/CuO for Simultaneous Removal of Acid Food Dyes from Binary Water Samples. *Scientific Reports* **2022**, *12*, 1-20.

(11) Zhang, S.; Tan, Z.; Liu, J.; Xu, Z.; Du, Z. Determination of the Food Dye Indigotine in Cream by Near-Infrared Spectroscopy Technology Combined with Random Forest Model. *Spectrochim. Acta Part A* **2020,** *227*, 117551.

(12) Weiss, B. Synthetic Food Colors and Neurobehavioral Hazards: The View from Environmental Health Research. *Environ. Health Perspect.* **2012**, *120*, 1-5.

(13) Sannino, A.; Savini, S. A Fast and Simple Method for the Determination of 12 Synthetic Dyes in Spicy Foods by UHPLC-HRMS. *ACS Food Sci. Technol.* **2021**, *1*, 107-112.

(14) Shah, A. A Novel Electrochemical Nanosensor for the Simultaneous Sensing of Two Toxic Food Dyes. *ACS Omega* **2020**, *5*, 6187-6193.

(15) Brazeau, J. Identification and Quantitation of Water-Soluble Synthetic Colors in Foods by Liquid Chromatography/Ultraviolet–Visible Method Development and Validation. *ACS Omega* **2018**, *3*, 6577-6586.

(16) Malik, S.; Khan, A.; Rahman, G.; Ali, N.; Khan, H.; Khan, S.; Sotomayor, M. D. P. T. Core-shell Magnetic Molecularly Imprinted Polymer for Selective Recognition and Detection of Sunset Yellow in Aqueous Environment and Real Samples. *Environmental Research* **2022**, *212*,113209.

(17) Llanos, J. P.; Beltran, O. G.; Calderon, J. A.; Nagles, E.; Hurtado, J. J. Carbon Paste Composite with Co_3O_4 as a New Electrochemical Sensor for the Detection of Allura Red by Reduction. *Electroanalysis* **2019**, *31*,695-703.

(18) Huang, S. T.; Shi, Y.; Li, N. B.; Luo, H. Q. Sensitive Turn-on Fluorescent Detection of Tartrazine based on Fluorescence Resonance Energy Transfer. *Chem. Commun*. **2012**, *48*, 747-749.

(19) Damera, D. P.; Manimaran, R.; Venuganti, V. V. K.; Nag, A. Green Synthesis of Full-Color Fluorescent Carbon Nanoparticles from Eucalyptus Twigs for Sensing the Synthetic Food Colorant and Bioimaging. *ACS Omega* **2020**, *5*, 19905-19918.

(20) Pu, K. Y.; Liu, B. Conjugated Polyelectrolytes as Light-Up Macromolecular Probes for Heparin Sensing. *Adv. Funct. Mater.* **2009**, *19*, 277-284.

(21) Fan, Y.; Xing, C.; Yuan, H.; Chai, R.; Zhao, L.; Zhan, Y. Conjugated Polyelectrolyte-Based New Strategy for in Situ Detection of Carbon Dioxide. *ACS Appl. Mater. Interfaces* **2017**, *9*, 20313-20317.

(22) Hussain, S.; Chen, X.; Wang, C.; Hao, Y.; Tian, X.; He, Y.; Li, J.; Shahid, M.; Iyer, P. K. Gao, R. Aggregation and Binding-Directed FRET Modulation of Conjugated Polymer Materials for Selective and Point-of-Care Monitoring of Serum Albumins. *Anal. Chem.* **2022**, *94*, 10685-10694.

(23) Tropp, J.; Ihde, M. H.; Williams, A. K.; White, N. J.; Eedugurala, N.; Bell, N. C.; Azoulay, J. D.; Bonizzoni, M. A Sensor Array for the Discrimination of Polycyclic

Aromatic Hydrocarbons using Conjugated Polymers and the Inner Filter Effect. *Chem. Sci.* **2019**, *10*, 10247–10255.

(24) Tanwar, A. S.; Adil, L. R.; Afroz, M. A.; Iyer, P. K. Inner Filter Effect and Resonance Energy Transfer Based Attogram Level Detection of Nitroexplosive Picric Acid Using Dual Emitting Cationic Conjugated Polyfluorene. *ACS Sens.* **2018**, *3*, 1451-1461.

(25) Wen, Q.; Liu, L.; Yang, Q.; Lv, F.; Wang, S. Dopamine-Modified Cationic Conjugated Polymer as a New Platform for pH Sensing and Autophagy Imaging. *Adv. Funct. Mater.* **2013**, *23*, 764-769.

(26) Ozenler, S.; Yucel, M.; Tuncel, O.; Kaya, H.; Ozçelik, S.; Yildiz, U. H. Single Chain Cationic Polymer Dot as a Fluorescent Probe for Cell Imaging and Selective Determination of Hepatocellular Carcinoma Cells. *Anal. Chem.* **2019**, *91*, 10357-10360.

(27) Zhou, L.; Lv, F.; Liu, L.; Wang, S. Water-Soluble Conjugated Organic Molecules as Optical and Electrochemical Materials for Interdisciplinary Biological Applications. *Acc. Chem. Res.* **2019**, *52*, 3211-3222.

(28) Sun, K.; Chen, H.; Wang, L.; Yin, S.; Wang, H.; Xu, G.; Chen, D.; Zhang, X.; Wu, C.; Qin, W. Size-Dependent Property and Cell Labeling of Semiconducting Polymer Dots. *ACS Appl. Mater. Interfaces* **2014**, *6*, 10802-10812.

(29) Hu, R.; Leung, N. L. C.; Tang, B. Z. AIE Macromolecules: Syntheses, Structures and Functionalities. *Chem. Soc. Rev.* **2014**, *43*, 4494-4562.

(30) Cai, X.; Liu, B. Aggregation-Induced Emission: Recent Advances in Materials and Biomedical Applications. *Angew. Chem. Int. Ed.* **2020**, *59*, 9868-9886.

(31) Liu, S.; Ou, H.; Li, Y.; Zhang, H.; Liu, J.; Lu, X.; Kwok, R. T.; Lam, J. W.; Ding, D.; Tang, B. Z. Planar and Twisted Molecular Structure Leads to the High Brightness of Semiconducting Polymer Nanoparticles for NIR-IIa Fluorescence Imaging. *J. Am. Chem. Soc.* **2020**, *142*, 15146-15156.

(32) Xie, H.; Hu, W.; Zhang, F.; Zhao, C.; Peng, T.; Zhu, C.; Xu, J. AIE-active Polyelectrolyte based Photosensitizers: the Effects of Structure on Antibiotic-Resistant Bacterial Sensing and Killing and Pollutant Decomposition. *J. Mater. Chem. B* **2021**, 9, 5309-5317.

(33) Wang, Y.; Yao, H.; Zhuang, Z.; Yao, J.; Zhou, J.; Zhao, Z. Photostable and Biocompatible AIE-Active Conjugated Polyelectrolytes for Efficient Heparin Detection and Specific Lysosome Labelling. *J. Mater. Chem. B* **2018**, *6*, 6360-6364.

(34) Wang, Y.; Yao, H.; Zhou, J.; Hong, Y.; Chen, B.; Zhang, B.; Smith, T. A.; Wong, W. W. H.; Zhao, Z. A Water-Soluble, AIE-active Polyelectrolyte for Conventional and

Fluorescence Lifetime Imaging of Mouse Neuroblastoma Neuro-2A Cells. *J. Polym. Sci. A Polym. Chem.* **2018**, *56*, 672-680.

(35) Shyamal, M.; Mazumdar, P.; Maity, S.; Samanta, S.; Sahoo, G. P.; Misra, A. Highly Selective Turn-On Fluorogenic Chemosensor for Robust Quantification of Zn(II) Based on Aggregation Induced Emission Enhancement Feature. *ACS Sens.* **2016**, *1*, 739-747.

(36) Narayanaswamy, N.; Govindaraju, T. Aldazine-Based Colorimetric Sensors for Cu^{2+} and Fe^{3+}. *Sens. Actuators, B* **2012**, *161*, 304-310.

(37) Xu, Z.-H.; Wang, Y.; Wang, Y.; Li, J.-Y.; Luo, W.-F.; Wu, W.-N.; Fan, Y.-C. AIE Active Salicylaldehyde-Based Hydrazone: A Novel Single-Molecule Multianalyte (Al^{3+} or Cu^{2+}) Sensor in Different Solvents. *Spectrochim. Acta, Part A* **2019**, *212*, 146-154.

(38) Adil, L. R.; Gopikrishna, P.; Iyer, P. K. Receptor-Free Detection of Picric Acid: A New Structural Approach for Designing Aggregation-Induced Emission Probes. *ACS Appl. Mater. Interfaces* **2018**, *10*, 27260-27268.

(39) Dong, W.; Fei,T.; Candoa, A. P.; Scherf, U. Aggregation Induced Emission and Amplified Explosive Detection of Tetraphenylethylene-Substituted Polycarbazoles. *Polym. Chem.* **2014**, *5*, 4048-4053.

(40) Hong, Y.; Chen, S.; Leung, C. W. T.; Lam, J. W. Y.; Liu, J.; Tseng, N. W.; Kwok, R. T .K.; Yu, Y.; Wang, Z.; Tang, B. Z. Fluorogenic Zn(II) and Chromogenic Fe(II) Sensors Based on Terpyridine-Substituted Tetraphenylethenes with Aggregation-Induced Emission Characteristics. *ACS Appl. Mater. Interfaces* **2011**, *3*, 3411-3418.

(41) Tanwar, A. S.; Adil, L. R.; Afroz, M. A.; Iyer, P. K. Inner Filter Effect and Resonance Energy Transfer Based Attogram Level Detection of Nitroexplosive Picric Acid Using Dual Emitting Cationic Conjugated Polyfluorene. *ACS Sens.* **2018**, *3*, 1451-1461.

(42) Castella, M.; Millie, P.; Piuzzi, F.; Caillet, J.; Langlet, J.; Claverie, P.; Tramer, A. Molecular Complexes with Interacting van der Waals and Ionic Excited States. 2. Electronic Spectra of Jet-Cooled Complexes. *J. Phys. Chem.* **1989**, *93*, 3949-3957.

(43) Hirota, J.; Usui, K.; Fuchi, Y.; Sakuma, M.; Matsumoto, S.; Hagihara, R.; Karasawa, S. Fluorescence Properties and Exciplex Formation of Emissive Naphthyridine Derivatives: Application as Sensors for Amines. *Chem. Eur. J.* **2019**, *25*, 14943-14952.

(44) Guzauskas, M.; Volyniuk, D.; Tomkeviciene, A.; Pidluzhna, A.; Lazauskas, A.; Grazulevicius, J. V. Dual Nature of Exciplexes: Exciplex-Forming Properties of Carbazole and Fluorene Hybrid Trimers. *J. Mater. Chem. C* **2019**, *7*, 25-32.

(45) Tan, C.; Atas, E.; Muller, J. G.; Pinto, M. R.; Kleiman, V. D.; Schanze, K. S. Amplified Quenching of a Conjugated Polyelectrolyte by Cyanine Dyes. *J. Am. Chem. Soc.* **2004**, *126*, 13685-13694.

Appendix

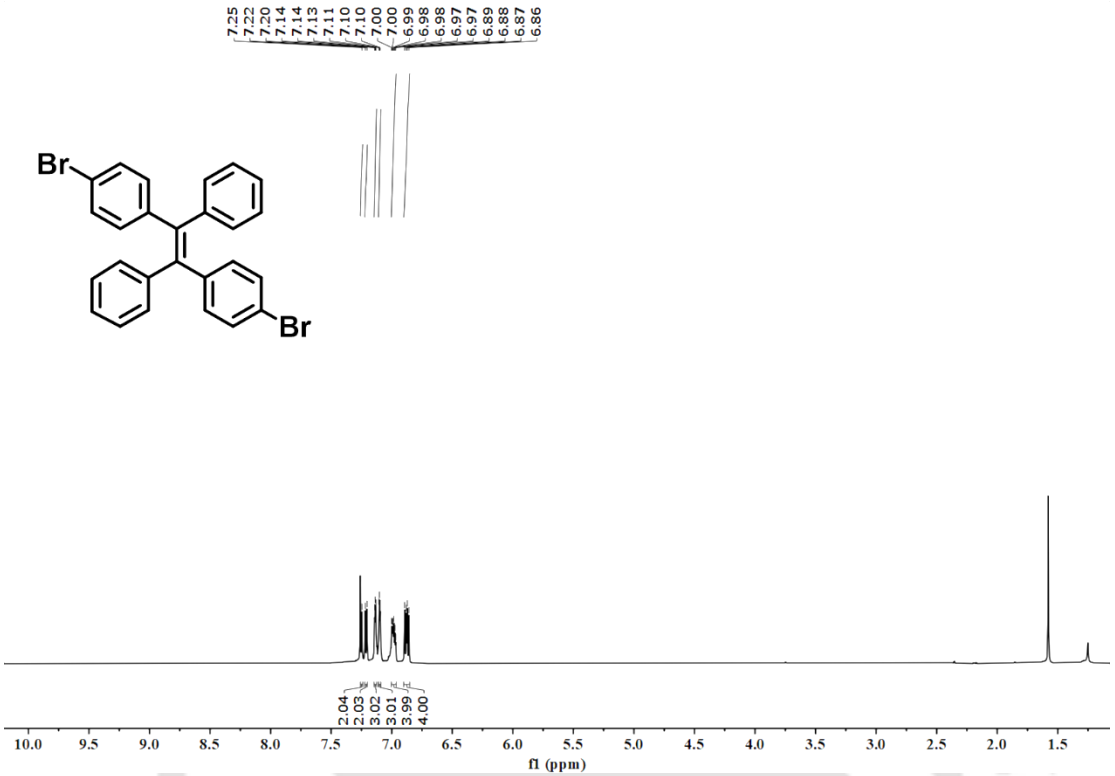

Figure A5.1 ^{1}H NMR spectra of M3.

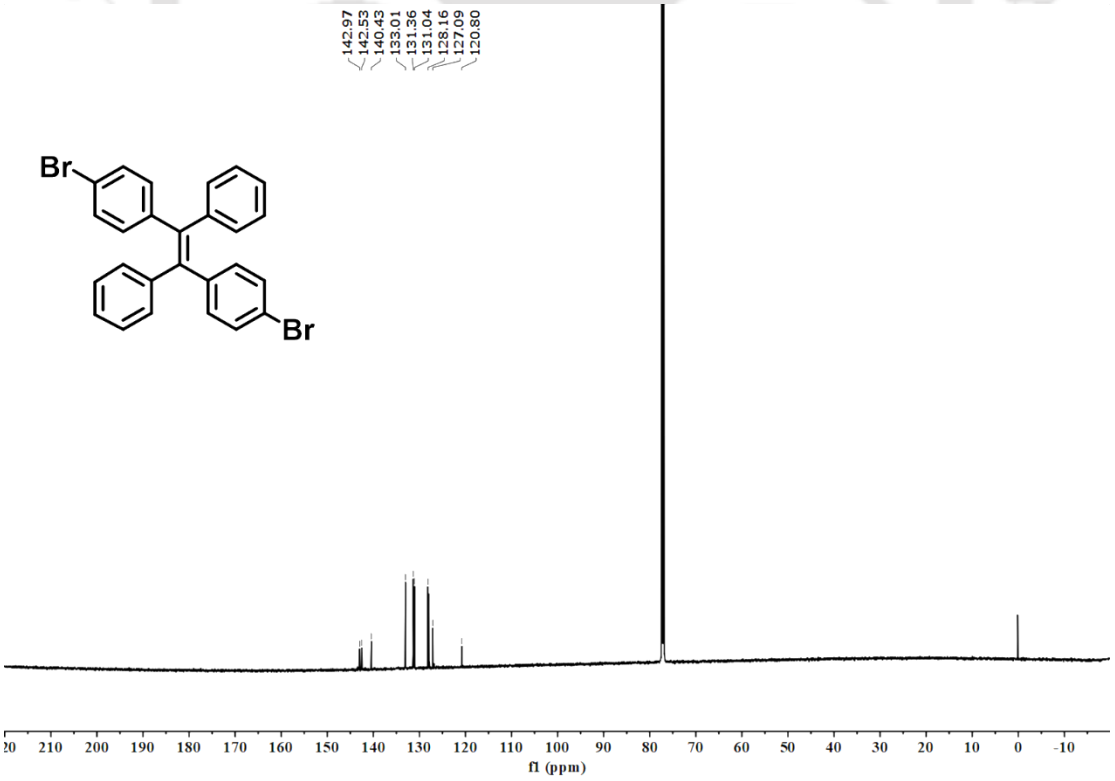

Figure A5.2 ^{13}C NMR spectra of M3.

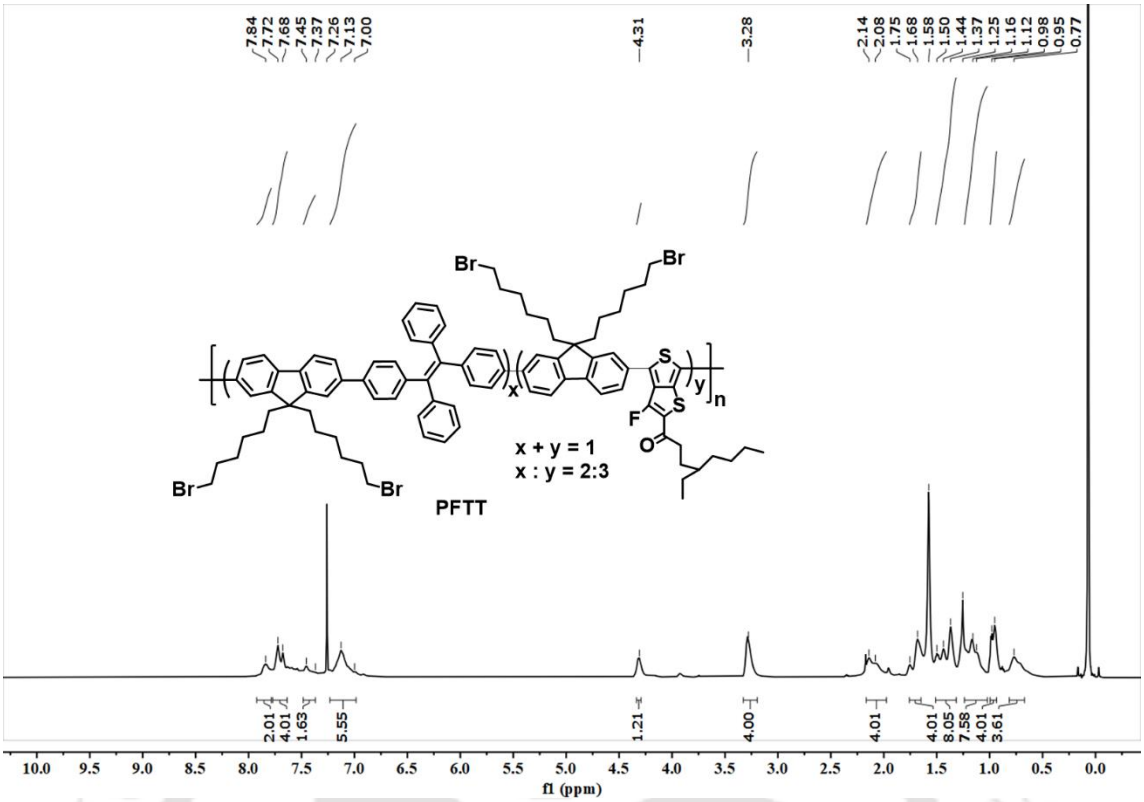

Figure A5.3 ^{1}H NMR spectra of PFTT.

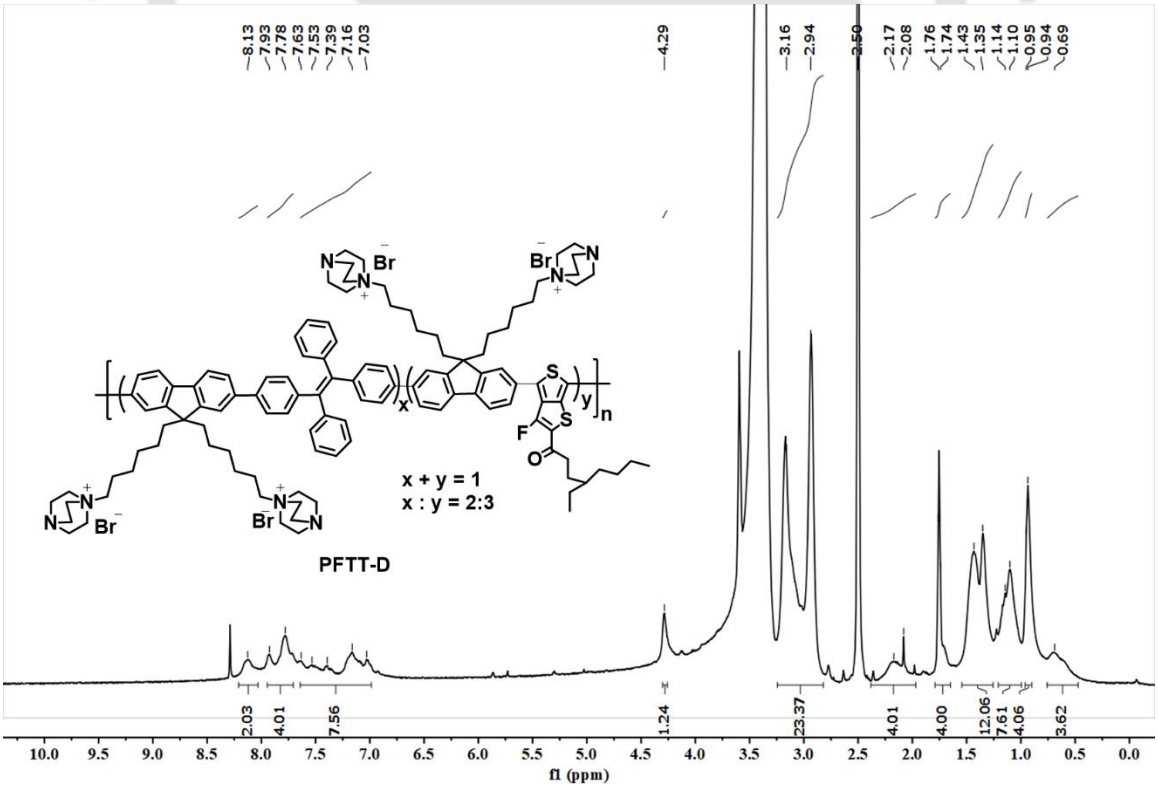

Figure A5.4 ^{1}H NMR spectra of PFTT-D.

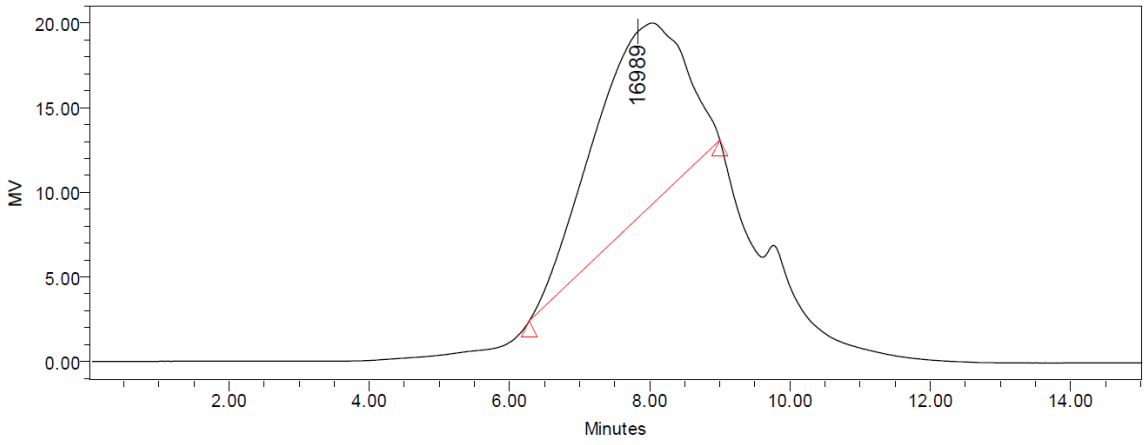

GPC Results

	Retention Time (min)	% Area	Mn	Mw	MP	Mz	Mz+1	Poly dispersity
1	7.833	100.00	14338	23976	16989	38837	54941	1.672266

Figure A5.5 GPC chromatogram of PFTT.

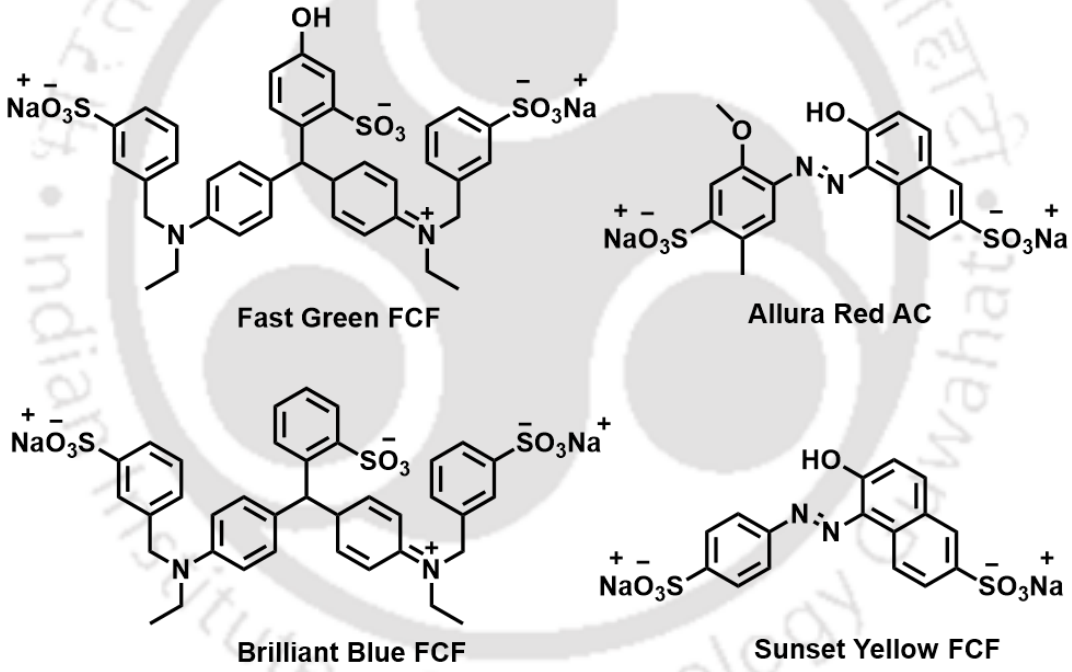

Figure A5.6 Structure of various food dyes used in this work.

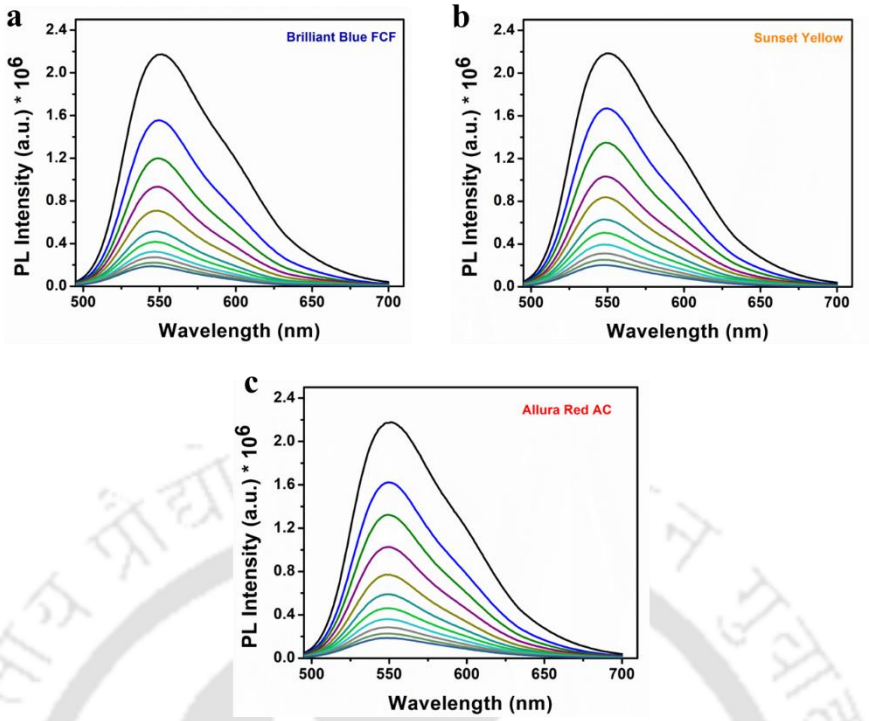

Figure A5.7 Fluorescence spectra of PFTT-D (20 µM)) with subsequent addition of (a) BB (0-10 µM), AR (0-10 µM), and (c) SY (0-10 µM) in THF: water mixture (1:1).

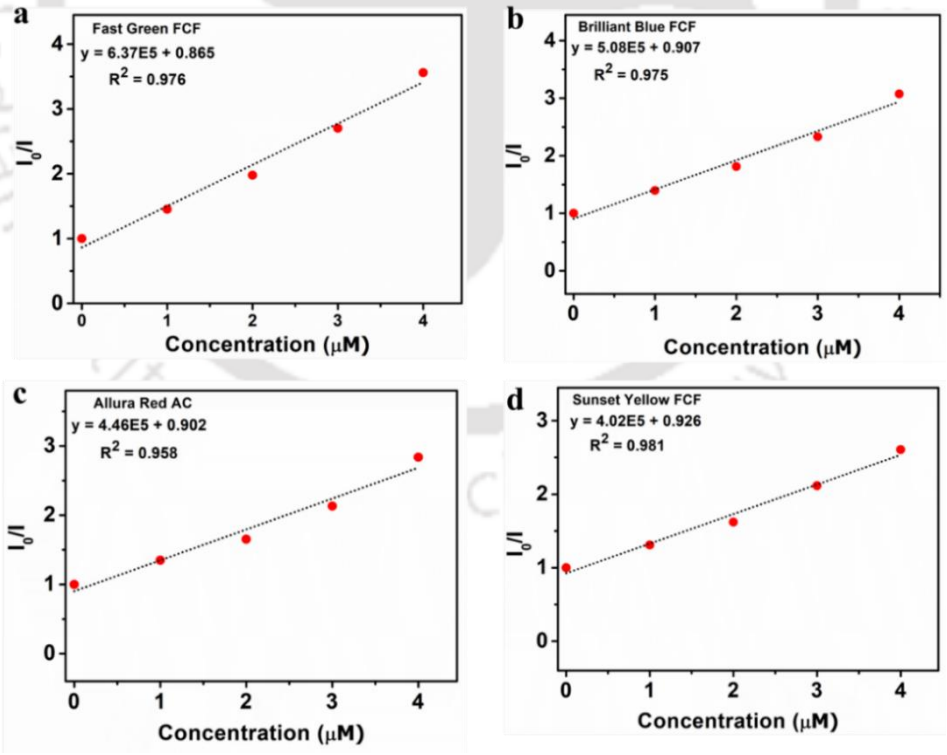

Figure A5.8 Stern−Volmer plot of PFTT-D (20 µM) with increasing concentration of (a) FG, (b) BB (0-4 µM), (c) AR (0-4 µM), and (d) SY (0-4 µM) in THF: water mixture (1:1).

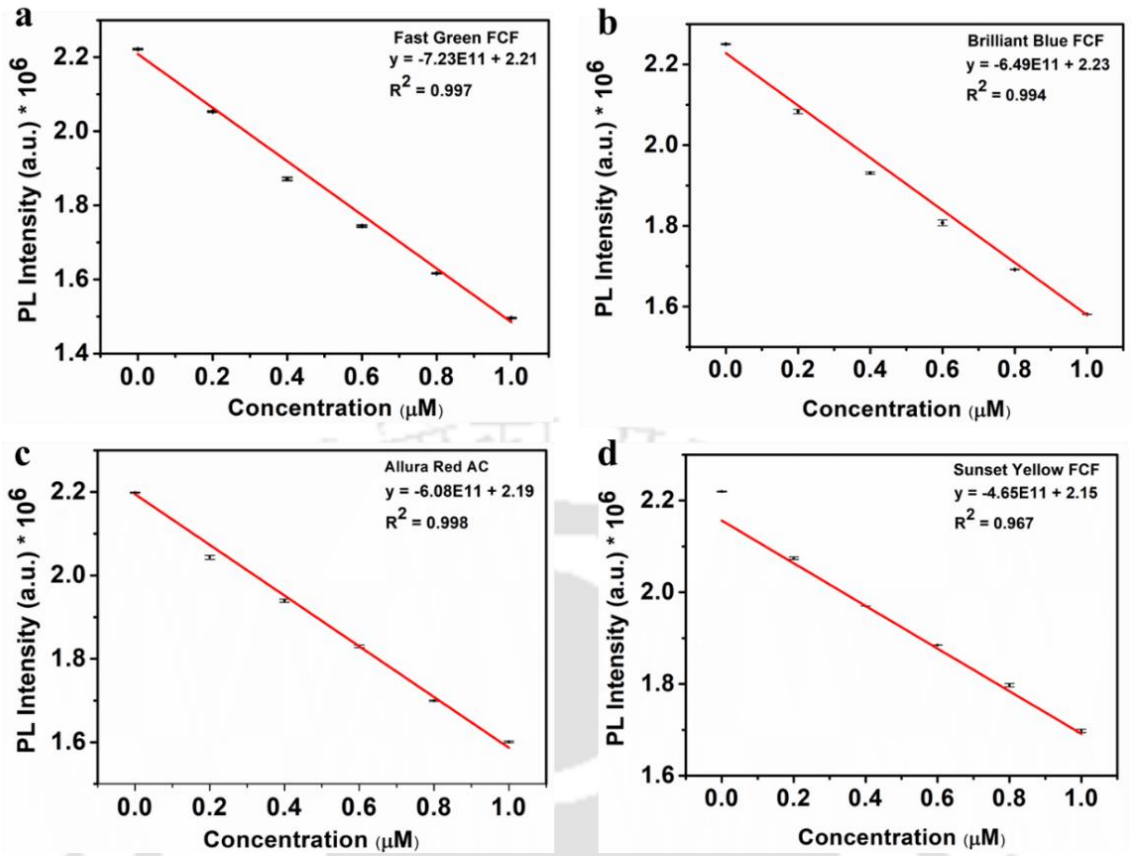

Figure A5.9 Fluorescence intensity of PFTT-D (20 μM) in THF: water mixture (1:1) as a function of (a) FG, (b) BB (0-1 μM), (c) AR (0-1 μM), and (d) SY (0-1 μM) concentrations respectively.

Table A5.1: IFE of FG on fluorescence intensity of PFTT-D.

FG μM	A_{ex}	A_{em}	I_{obs}	I_{corr}	I_{corr}/I_{obs} correction factor	E_{obs}	E_{corr}
0	0.704367	0.022550	2175660	5023995.1	2.309182	0	0
1	0.683200	0.021032	1496920	3367555.7	2.249656	31.19697	32.97056
2	0.665627	0.028746	1100420	2447627.5	2.224267	49.42133	51.28125
3	0.662048	0.035895	808934	1806691.7	2.233424	62.81893	64.03875
4	0.657111	0.036338	622894	1384008.8	2.221900	71.36987	72.45203
5	0.661754	0.053153	482043	1097840.2	2.277474	77.84383	78.14806
6	0.668532	0.068096	385973	901303.59	2.335146	82.2595	82.06002
7	0.653781	0.067217	313266	718474.94	2.293501	85.60136	85.69913
8	0.662042	0.082468	254912	600682.78	2.356432	88.28346	88.04372
9	0.661293	0.095731	208168	497653.4	2.390630	90.43195	90.09447
10	0.655820	0.099867	174073	415502.71	2.386950	91.99909	91.72964

Table A5.2: IFE of BB on fluorescence intensity of PFTT-D.

BB µM	A_{ex}	A_{em}	I_{obs}	I_{corr}	I_{corr}/I_{obs} correction factor	E_{obs}	E_{corr}
0	0.676335	0.094305	2171860	5274142.377	2.428399	0	0
1	0.663769	0.089434	1555130	3701420.939	2.380136	28.3964	29.81947
2	0.649772	0.082192	1197390	2781105.826	2.322640	44.86799	47.26904
3	0.646290	0.088428	931839.059	2171200.071	2.330016	57.09488	58.83312
4	0.637102	0.088960	706644.0422	1630166.675	2.306913	67.46365	69.09134
5	0.633818	0.095714	511756.0383	1185301.525	2.316146	76.43697	77.52618
6	0.633595	0.104854	412176.2648	964511.8187	2.340047	81.02197	81.71244
7	0.625428	0.106995	321942.3395	748152.0134	2.323870	85.17665	85.81472
8	0.616127	0.109687	269570.3619	621697.2149	2.306252	87.58804	88.21235
9	0.612208	0.118432	217729.938	504938.3391	2.319104	89.97496	90.42615
10	0.608024	0.124756	183970.8304	427699.7495	2.324824	91.52934	91.89063

Table A5.3: IFE of AR on fluorescence intensity of PFTT-D.

AR µM	A_{ex}	A_{em}	I_{obs}	I_{corr}	I_{corr}/I_{obs} correction factor	E_{obs}	E_{corr}
0	0.682772	0.024154	2187530	4936477.234	2.256644	0	0
1	0.700551	0.046110	1446470	3416960.487	2.362275	33.87656	30.7814
2	0.711657	0.064695	1007350	2462386.941	2.444420	53.95035	50.11854
3	0.722606	0.077851	731573	1838595.432	2.513210	66.55714	62.75491
4	0.729243	0.088864	559274	1434426.897	2.564800	74.43353	70.9423
5	0.743484	0.108923	433028	1155365.525	2.668108	80.20471	76.59534
6	0.767767	0.142334	340199	970027.0639	2.851353	84.44826	80.34981
7	0.783115	0.159364	285552	845131.6892	2.959644	86.94638	82.87986
8	0.801808	0.179144	239719	741614.2903	3.093685	89.04158	84.97685
9	0.813543	0.194448	210516	671861.5078	3.191505	90.37656	86.38986
10	0.842389	0.218255	188484	639141.2367	3.390955	91.3837	87.05269

Table A5.4: IFE of SY on fluorescence intensity of PFTT-D.

SY µM	A_{ex}	A_{em}	I_{obs}	I_{corr}	I_{corr}/I_{obs} correction factor	E_{obs}	E_{corr}
0	0.696791	0.045333	2177730	5117596.52	2.349968	0	0
1	0.697558	0.039400	1677890	3919604.92	2.336032	22.95234	23.40926
2	0.704320	0.039251	1265100	2977904.64	2.353889	41.9074	41.81048
3	0.715654	0.046312	1014830	2439924.5	2.404269	53.39964	52.32284
4	0.723843	0.048016	832399.5	2024236.57	2.431809	61.77674	60.44556
5	0.736859	0.054180	685504.8	1704238.41	2.486107	68.52205	66.69846
6	0.747408	0.059347	565863.5	1432481.17	2.531496	74.0159	72.00871
7	0.759322	0.064937	479307.7	1238065.49	2.583029	77.99049	75.80768
8	0.771358	0.070931	409036.4	1078713.74	2.637207	81.21731	78.92148
9	0.779212	0.074152	354030.7	945633.704	2.671050	83.74313	81.52192
10	0.791769	0.083538	304163.2	833220.798	2.739387	86.03302	83.71851

Table A5.5: Fitting parameters of fluorescence lifetime decay of PFTT-D before and after addition of AFDs.

Sample	τ_1	%	τ_2	%	χ^2	τ_{avg}
PFTT-D	0.590	47.131	1.177	52.869	1.091	90.03
PFTT-D + FG	1.014	59.412	1.998	40.588	1.019	141.33
PFTT-D	0.553	43.673	1.167	56.327	1.012	89.88
PFTT-D + BB	1.001	60.387	1.982	39.613	1.027	138.96
PFTT-D	0.535	42.280	1.159	57.720	1.030	89.52
PFTT-D + AR	0.491	28.543	1.410	71.457	1.009	114.77
PFTT-D	0.587	46.289	1.177	53.711	1.074	90.39
PFTT-D + SY	0.208	19.093	1.317	80.907	1.043	110.53

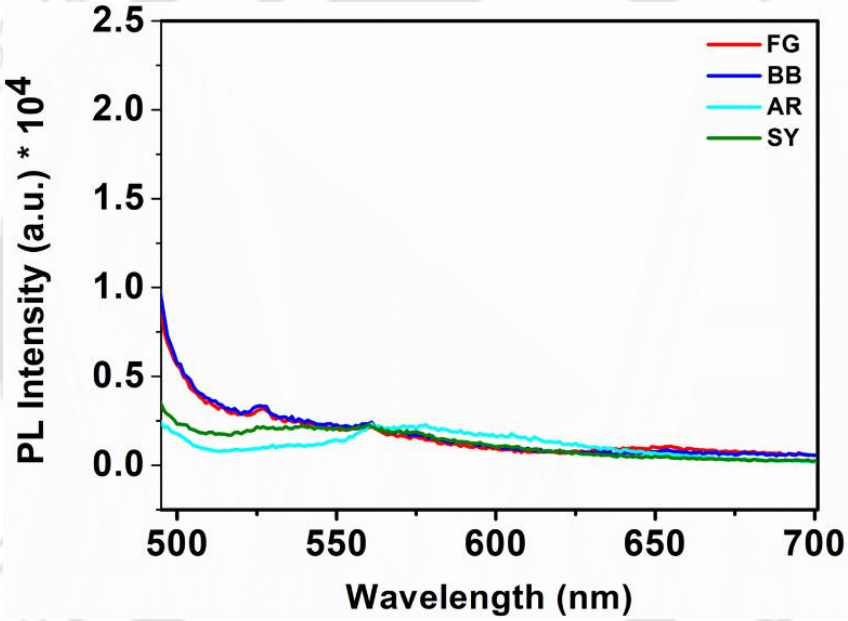

Figure A5.10 Fluorescence spectra of (a) FG, (b) BB, (c) AR and (d) SY in THF: water mixture (1:1)

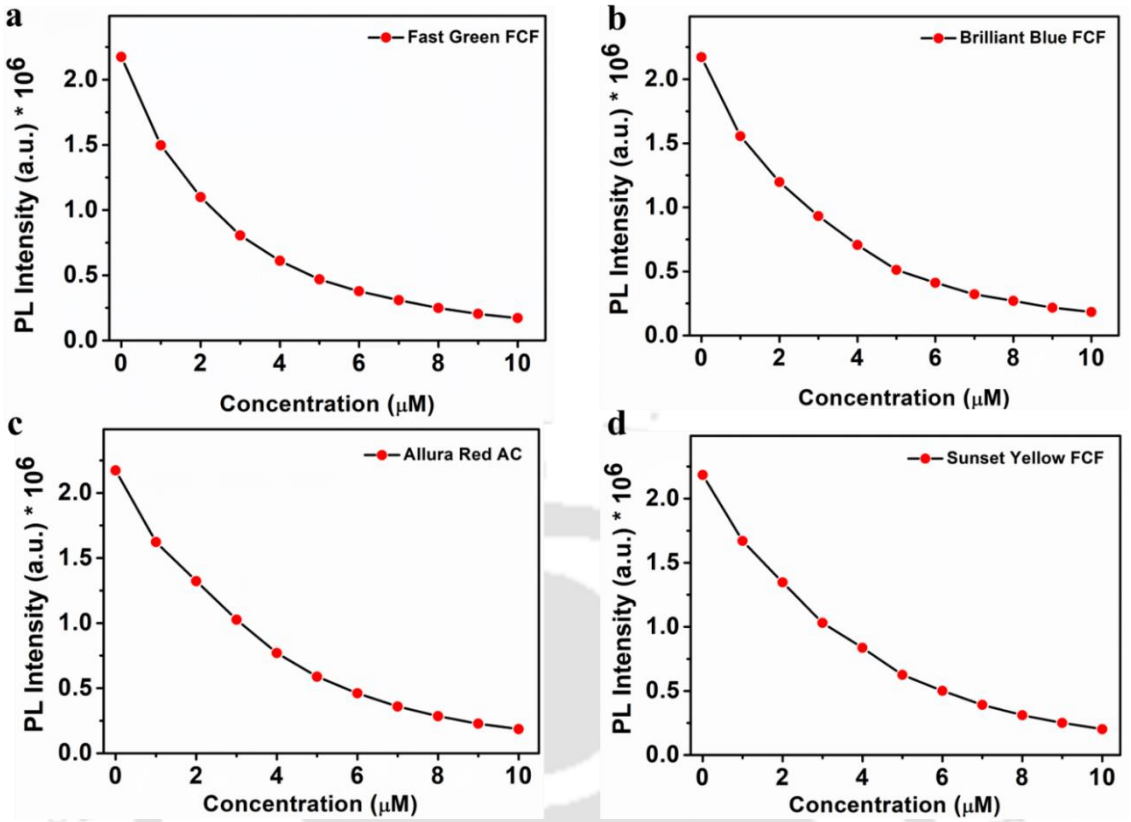

Figure A5.11 Calibration curves obtained for the determination of (a) FG, (b) BB, (c) AR, (d) SY in commercial food samples.

Thesis Overview and Future Perspective

Sensor acts as a communication link between human and their environment. Over the period of evolution, human body has developed five basic set of sensors i.e., eyes, skin, nose, tongue and ear which helps in perceiving external signal. Inspired by nature, researchers around the globe have been focusing on creating synthetic chemical sensors which can selectively detect environmental and biological molecules. Among various molecular probes, conjugated polymers as transducers have received significant research interest due to their outstanding sensitivity, excellent light-harvesting and conducting properties, thermal/photostability, and biocompatibility. The property that makes the conjugated polymer a unique technological material includes its efficient intra/intermolecular charge or energy transfer resulting in large signal amplification compared to various other molecular probes. Moreover, the conjugated polymer framework can be easily tailored to specific applications such as optimal emission or electronic properties, and water solubility via altering electron donating or accepting repeating units and appending ionic side chains or inserting sterically demanding groups. While designing conjugated polymer as a transducer, several molecular designing parameters including choice of the receptor, chemical processing, orientation, and packing of polymer chains should be considered to achieve a stable and high-performance sensing platform.

Due to the growing demand for personal health monitoring devices, and highly efficient systems for chemical threat assessments, this thesis entitled " **Design and Development of Optical and Electrical Transducers based on π-Conjugated Polymers"** primarily focuses on the designing and development of highly efficient, rapid, and portable systems based on conjugated polymers for on-field detection of various biological and environmental important analytes with the major aim of overcoming the problem and challenges associated with existing sensing systems. To serve this purpose several co-polyfluorene derivatives with suitable donor/acceptor repeating units, hydrophilic side chains, and appended functional groups have been designed and synthesized to get optimal electrical or fluorescence signal, chemical processing, high sensitivity, and selectivity towards specific analytes. The as-designed CPs are then successfully integrated into the low-cost, and portable handheld devices for real-time monitoring of pathogens, toxic gases, disease biomarkers, food additives, etc.

To proof the concept of self-signal amplifying biosensors, a dual-emissive, water-soluble conjugated polyelectrolyte for bacterial imaging and bacterial susceptibility has been

developed via Suzuki cross-coupling polymerization in good yield (***Chapter II***). To overcome the issue of instrumental and environmental interventions associated with single-wavelength probes, the dual emissive or ratiometric CP-based biosensor (PFBT-MI) is strategically designed by incorporating fluorene as a donor and benzothiadiazole as an acceptor in the conjugated backbone. Moreover, the pendant imidazolium group is appended onto the polymer side chains to enhance hydrophilic and hydrophobic interactions with the negatively charged bacterial membrane as well as to endow water solubility. The dual emissive PFBT-MI CP displays a rapid color change response from blue to yellow in the presence of bacteria and also offers wash-free bacterial imaging without any background emission. The fluorescence color change response of polyelectrolyte is due to the polymer chain aggregation caused by electrostatic and hydrophobic interactions with negatively charged bacteria membrane which results in intermolecular FRET from fluorene donor to locally increased benzothiazole acceptor.

Similarly, for environmental and chemical threat monitoring emanating from chemical warfare agents, a novel semiconducting polyfluorene derivative PFPDA is designed and synthesized using fluorene and phenylene diamine as a repeating unit (***Chapter III***). The amine group is strategically introduced into the backbone framework to increase the likelihood of redox interaction and to get the discriminating electrical response among the nerve agent mimics (organophosphates derivatives). A cost-effective two-terminal chemiresistive sensor is constructed using amine-functionalized CP as a sensory layer over the channel between the pair of thermally deposited metal electrodes. The PFPDA CP fabricated sensor displays a rapid and discriminatory response towards diethylchlorophosphate (DCP) vapors exposure at ambient conditions with a very low detection limit in ppb level. The PFPDA fabricated sensor is then successfully integrated with an electronic combinational circuit that generates bright visual alerts such as a light-emitting diode (LED) and loud alarm sound signal in presence of DCP demonstrating on-field portable electronics for national security and environmental monitoring applications.

The aim of developing a user-friendly portable healthcare device is further extended to the carcinoid tumor biomarker, serotonin detection (***Chapter IV***). A Polyfluorene-co-phenylene polyelectrolyte, PFPS having anionic sulphonate group appendage on side chains is prepared for this purpose. The PFPS showed a fluorescence turn-off response with remarkably high fluorescence quenching efficiency toward serotonin even in presence of other interfering analytes. The highly sensitive and discriminatory response of PFPS CPE is due to the excited state electron transfer (a-PET) from the HOMO of the serotonin to the

HOMO of PFPS and also electrostatic interaction-assisted polymer aggregation. The PFPS CPE sensor is further transformed into a cost-effective, user-friendly portable smartphone-based fluorescence sensing platform to measure the 5-HT levels in blood samples via quantifying fluorescence color change (RGB value variation) of PFPS under UV light by color-scanning android application.

The development of an amplified CP-based sensor is further expanded to include artificial food color detection for ensuring public health security (***Chapter V).*** In this regard, a novel AIEE active conjugated polyelectrolyte, PFTT-D including fluorene as a donor, tetraphenylene ethylene as rotor, and 2-ethylhexyl 3-fluorothieno[3,4-b]thiophene-2-carboxylate as an acceptor at its backbone is designed and synthesized via Suzuki cross-coupling reaction. The PFTT-D polyelectrolyte forms a highly emissive macro-aggregate in aggregated state and is exposed to various artificial food dyes (AFD) ranging from blue to red. The PFTT-D polyelectrolyte displays remarkable sensitivity towards various food color dyes with detection limits in the nanomolar range enabling the quality check of AFD adulteration in food commodities even in minute traces. Moreover, the PFTT-D probe is also applied to rapidly detect food dyes in various processed food samples, representing great potential application in screening dyes levels in different food products with high precision.

Future Directions

The present thesis describes the synthesis and characterization of several conjugated polymers and their development as optical and electrical transducers for specific applications encompassing bacterial detection and antibacterial susceptibility, chemical warfare sensing, carcinoid biomarker serotonin detection, and health-risk-associated artificial food dye sensing. However, some of the topics covered in this thesis are worthy of future investigation. For example, bacterial detection using PFBT-MI could be extended to in-vitro and mixed bacterial cultures. Similarly, the PFTT-D CP-based artificial food dye detection could be made into advanced portable smartphone-based platforms with on-field features. Overall, the future direction of developing CP-based sensors could be focused on array-based sensing, ratiometric detection using dual-wavelength emissive CP, and establishing more sophisticated receptors. In addition, future research on CP should not be limited to simply detection but should include the development of user-friendly smartphone-based platforms or wireless sensor tags with real-time monitoring features.

Publications

1. **Zehra, N.;** Parui, R.; Chanu, M. A.; Iyer, P. K. An AIEE active Conjugated Polyelectrolyte for Ultrasensitive Detection of Multicolor Artificial Food Dyes. (Manuscript Prepared)
2. **Zehra, N.**; Malik, A. H.; Parui, R.; Hussain, S.; Iyer, P. K. A Portable Conjugated Polymer based Smartphone Platform for Sensitive Detection of Monoamine Neurotransmitter. (Manuscript Communicated)
3. Chanu, M.A.; Mondal, S.; **Zehra, N.**; Tanwar, A. S.; Iyer, P. K. Conjugated Polymer Nanoparticles as a Fluorescence Probe for Amplified Detection of Human Serum Bilirubin. *ACS Appl. Polym. Mater.* **2022,** *4*, 3491-3497.
4. Barman, D.; Narang, K.; Parui, R.; **Zehra, N.;** Khatun, N.; M.; Adil, L.; R.; Iyer, P. K. Review on Recent Trends and Prospects in π-Conjugated Luminescent Aggregates for Biomedical Applications. *Aggregate* **2022**, *e172*, 1-33.
5. **Zehra, N.**; Tanwar, A. S.; Khatun, N.; M.; Adil, L. R.; Iyer, P. K. AIE active Polymers for Biological Applications. In *Advances in Aggregation Induced Emission Materials in Biosensing and Imaging for Biomedical Applications - Part B*; Bhosale, R. S.; Singh, V. Eds.; Progress in Molecular Biology and Translational Science, Vol. 185; Elsevier, **2021**; 137-177.
6. **Zehra, N.**; Adil, L. R.; Tanwar, A. S.; Mondal, S.; Iyer, P. K. Thin-film Devices for Chemical, Biological, and Diagnostic Applications. In *Chemical Solution Synthesis for Materials Design and Thin Film Device Applications*, 1st ed.; Elsevier, **2021**; 365-405.
7. Mondal, S.; **Zehra, N.**; Choudhury, A.; Iyer, P.K. Wearable Sensing Devices for Point of Care Diagnostics. *ACS Appl. Bio Mater.* **2021**, *4*, 47–70.
8. **Zehra, N.**; Kalita, A.; Malik, A. H.; Barman, U.; Afroz, M. A.; Iyer, P. K. Conjugated Polymer-Based Electrical Sensor for Ultratrace Vapor-Phase Detection of Nerve Agent Mimics *ACS Sens.* **2020**, *5*, 191–198.
9. Malik, A.H.; **Zehra, N.**; Ahmad, M.; Parui, R.; Iyer, P.K. Advances in Conjugated Polymers for Visualization of Latent Fingerprints: a Critical Perspective. *New J. Chem.* **2020**, *44*, 19423-19439.
10. **Zehra, N.**; Dutta, D.; Malik, A. H.; Ghosh, S. S.; Iyer, P. K. Fluorescence Resonance Energy Transfer-Based Wash-Free Bacterial Imaging and Antibacterial Application Using a Cationic Conjugated Polyelectrolyte *ACS Appl. Mater. Interfaces* **2018**, *10*, 27603-27611.

Conferences & Seminars

1. Delivered an **Oral Presentation** *at* 7th International Conference for Nanotechnology, organized by Centre for Nanotechnology, IIT Guwahati during 14th – 17th December 2021.
2. Delivered an **Oral Presentation** at 30th Annual Meeting of Material Research Society of Japan, during 9th – 11th December 2020 held online.
3. Presented a **Poster** in 6th International Conference on Advanced Nanomaterials and Nanotechnology**,** organized by Centre for Nanotechnology, IIT Guwahati during 18th – 21th December 2019.
4. Presented a **Poster** at Research Conclave'19, organized by Student Academic Board (SAB), IIT Guwahati during 14th –17th March 2019. (**Best Poster**)
5. Participated 4th National Workshop on NEMS/MEMS and Theranostics Devices organized by Centre for Nanotechnology, held at IIT Guwahati from 21th – 23th February 2019.
6. Presented a **Poster** at 15th International Conference on Polymer Science and Technology SPSI-Macro 2018, organized by IISER Pune during 19th –21th December 2018.
7. Participated 5th International Conference for Nanotechnology, organized by Centre for Nanotechnology, IIT Guwahati from 18th –21th Dec 2017.
8. Participated 3rd National Workshop on NEMS/MEMS and Theranostics Devices organized by Centre for Nanotechnology, held at IIT Guwahati from 21th – 23th Feb 2017**.**
9. **Attended** the full agenda of **ACS on Campus 2017 (**An initiative American Chemical Society) at IIT Guwahati on 16 Jan 2017.

ELSEVIER LICENSE
TERMS AND CONDITIONS

Oct 12, 2022

This Agreement between NEHAL ZEHRA ("You") and Elsevier ("Elsevier") consists of your license details and the terms and conditions provided by Elsevier and Copyright Clearance Center.

License Number	5406440245994
License date	Oct 12, 2022
Licensed Content Publisher	Elsevier
Licensed Content Publication	Coordination Chemistry Reviews
Licensed Content Title	Fluorescent conjugated polymer molecular wire chemosensors for transition metal ion recognition and signaling
Licensed Content Author	Li-Juan Fan,Yan Zhang,Clifford B. Murphy,Sarah E. Angell,Matthew F.L. Parker,Brendan R. Flynn,Wayne E. Jones
Licensed Content Date	Feb 1, 2009
Licensed Content Volume	253
Licensed Content Issue	3-4
Licensed Content Pages	13
Start Page	410
End Page	422
Type of Use	reuse in a thesis/dissertation